

**STRATIFYING OF LIQUID-LIQUID TWO
PHASE FLOWS THROUGH SUDDEN
EXPANSION**

NAZRUL HIZAM YUSOFF, BSc.

**Thesis submitted to the University of Nottingham for
the degree of Doctor of Philosophy**

December 2012

ABSTRACT

The transport and separation of oil and water is an essential process to the oil and chemical industries. Although transporting the mixtures is often necessary due to few reasons, it is generally beneficial to separate out the phases in order to reduce installation and maintenance costs, at the same time, avoiding safety problems. Thus, separation of liquid-liquid flows is a necessary part of many industrial processes. Hence, knowledge of two-phase flow dynamics is important for the design optimisation of separators. Therefore, the aim of this research is to investigate the feasibility of a sudden pipe expansion to be used as phase separator because it compact in design and capable for converting dispersed flow to stratified flow.

In the test section, spatial distribution of the liquid-liquid phases in a dynamics flow system was visualised for the first time for by means of capacitance Wire Mesh Sensor (CapWMS), providing instantaneous information about the interface shapes, waves and phase layer evolution of oil-water flow. Visual assessment and analysis of the WMS data showed three distinct layers: an oil layer at the pipe top; a water layer at the pipe bottom and a mixed layer between them. The interfaces that form between the separated phases (oil or water) and the mixed layer were classified as oil interface or water interface. Results showed interface shapes were initially concave or convex near to the inlet of the test section and became flat further downstream the expansion, especially for water interfaces. There were no waves observed for horizontal and downward pipe orientations at all flow conditions and axial position downstream of the expansion. As for the upward inclined pipe orientation, waves were found, and they formed at position close to the inlet at all input oil volume fraction except at 0.2

OVF. The amplitude of the waves was: $\sim 0.29D$ for 0.8 OVF; $\sim 0.22D$ for 0.6 OVF and $\sim 0.26D$ for 0.4 OVF. The higher the input oil volume fraction, the larger the waves become. In conclusion, the WMS results demonstrated that spatial distributions are strongly dependent on the mixture velocity, input oil fraction and inclination angles for the far position.

In this present work, droplets were found to be larger near the interface. Drops were large nearer to the interface at the near position (10D) for all pipe orientations and throughout the test section for horizontal flow. The drops size decreased when the distance from the interface increased for these pipe configurations. As for the furthest position from the expansion for upward and downward inclined pipe orientation, larger droplets could also be seen at distance away from the interface and vice versa.

The gravity or buoyant force is one of the contributing factors to the settling of the droplets. These forces are acting simultaneously on the droplets i.e. if the buoyant force which tends to spread the droplets throughout the pipe cross-section, is not large enough to overcome the settling tendency of gravity settling of the droplets occurs. Hence, the droplets that are non-uniformly scattered within the continuous phase begin to coalesce as they flow further downstream the pipe, producing larger drops. In addition, as the distance from expansion increased, the mixed layer becomes narrow and more drops begin to coalesce to form large drop due to increased droplet-droplet collision. Owing to these factors, results indicate that the mechanisms of coalescence occurred faster at the bottom, for water droplets and at the top, for oil droplets than the other locations in a pipe cross-section. For a better separation design, the coalescence process should occur at the aforementioned (bottom for water and top for oil) locations within the expansion pipe. However, at

higher mixture velocities the mixed layer would be responsible for the smaller droplet size for horizontal and both inclinations of pipe orientation. The mixed layer dominated almost entirely in the pipe cross-section.

ACKNOWLEDGEMENTS

It has been a pleasure and a privilege to work with both my supervisors Prof. Barry Azzopardi and Dr Buddhika Hewakandamby, and to study at the Nottingham University. It has been a great learning and enjoyable experience. I am extremely grateful to Prof. Azzopardi for his informality, patience, and above all guidance in every stage of this thesis. My utmost gratitude also to Dr Buddhi for his unfailing help, support and encouragement, that keep me striving towards this success. It was a great honour to work with them.

There are many other people whom I can't thank them enough for their help and support: Bayou, Mohammed, Lokman, Safa, Peter, Mukhtar, Mayowa, Abolore and Aime who have rendered their expertise to ensure that every task is within reach. They have always been very supportive throughout the good and hard times. Apologies to anyone unintentionally not mentioned here.

In addition, I wish to express my gratitude to the technical staffs, in particular Phill Bennett, Mick Fletcher, Reg, Terry, Paul, Jim, Marion Bryce, Fred Anderson, Sue Richard and Phill Perry for their invaluable technical contribution. Special thanks to Mel. We achieved a great deal when we put our efforts together.

The biggest thanks I reserved to my wife, Siti Nadira; my two lovely daughters, Nurin and Nissa who have given me constant love, support and patience throughout my time here in Nottingham. My Mum for the never ending prays. Words cannot express my gratitude for their encouragement. Above all, I thank God for granting me the will to achieve this accomplishment. All the glory belongs to Him.

I wish to dedicate this thesis to my late Father...

3 Jamadilakhir 1429H

7th June 2008

Al-Fatihah

TABLE OF CONTENTS

ABSTRACT	i
ACKNOWLEDGEMENT	iv
TABLE OF CONTENTS	vi
LIST OF FIGURES	xi
LIST OF TABLES	xxiv
NOMENCLATURE	xxv
CHAPTER 1: INTRODUCTION	1
1.1 Background.....	2
1.2 Motivations.....	5
1.3 Research aims and objectives	6
1.4 Structure of the thesis.....	7
CHAPTER 2: LITERATURE REVIEW	9
2.1 Background.....	10
2.2 Flow pattern and Flow pattern maps.....	13
2.2.1 Flow patterns for liquid-liquid flows	14
2.2.1.1 Flow pattern in horizontal pipes	16
2.2.1.2 Flow pattern in inclined pipes	25
2.2.2 Flow pattern maps	31
2.3 Liquid-liquid dispersion	35
2.3.1 Drop breakage and coalescence in dispersion	36
2.3.2 Models for drop breakage and coalescence	38

2.4 Drop size distribution.....	43
2.4.1 Measurement techniques for drop size distribution	49
2.4.1.1 Laser backscatter technique	49
2.4.2 Estimating particle size.....	50
2.5 Oil volume fraction	54
CHAPTER 3:INSTRUMENTS AND EXPERIMENTAL METHODS.....	62
3.1 The liquid-liquid flow facility	63
3.2 Test section.....	64
3.3 The separator and liquid storage tanks.....	67
3.4 Metering and control system	68
3.5 Properties of fluids	70
3.6 Experimental approaches	70
3.7 Instrumentation	74
3.7.1 Rotameter.....	74
3.7.2 Differential pressure flow meter	75
3.7.3 Laser backscatter equipment.....	76
3.7.3.1 Principle of Lasentec FBRM M500P	77
3.7.3.2 Verification of Lasentec FBRM M500P	78
3.7.3.3 Measurement of drop size	81
3.7.4 Capacitance wire mesh sensor (CapWMS)	82
3.7.4.1 Design of capacitance wire mesh sensor (CapWMS).....	85
3.7.4.2 Principle of capacitance wire mesh sensor (CapWMS).....	86
3.7.4.3 Calibration and validation of CapWMS	87
3.7.4.4 Determination of oil volume fraction	88

CHAPTER 4: WMS RESULTS AND FIRST INTERPRETATIONS	89
4.1 Wire mesh sensor results.....	91
4.2 Experimental design.....	91
4.3 Experiment results and discussions	95
4.3.1 WMS results for horizontal pipe expansion	96
4.3.1.1 Interface Shapes and Waves – Horizontal pipe orientation	100
4.3.2 WMS results for an upward inclined pipe expansion	104
4.3.2.1 Interface Shapes and Waves – Upward pipe orientation	108
4.3.3 WMS results for an downward inclined pipe expansion.....	111
4.3.3.1 Interface Shapes and Waves – Downward pipe orientation.....	115
4.3.4 Comparison between different angles of inclination.....	117
CHAPTER 5: EVOLUTION OF INTERFACE.....	122
5.1 Flow pattern evolution	123
5.2 Experimental design.....	124
5.3 Experimental results and discussions.....	124
5.3.1 Flow pattern evolution in horizontal pipe expansion	125
5.3.2 Flow pattern evolution in an upward inclined pipe expansion	128
5.3.3 Flow pattern evolution in downward inclined pipe expansion	132
5.4 Comparison between different angles of inclination	135

CHAPTER 6: DROP SIZES DOWNSTREAM OF PIPE EXPANSION	139
6.1 Drop size distribution.....	139
6.2 Experimental design.....	141
6.3 Results and discussions	143
6.3.1 SMD of drop size distribution in mixed and interface layer	144
6.3.2 SMD of drop size distribution in horizontal expansion	146
6.3.2.1 SMD of drop size distribution - Effect of the volume fraction	147
6.3.2.2 SMD of drop size distribution - Effect of the mixture velocity	150
6.3.2.3 SMD of drop size distribution - Probe position	155
6.3.2.4 Development of drops size - Cross sectional of horizontally pipe expansion	158
6.3.3 SMD of drop size distribution in an upward inclined expansion.....	160
6.3.3.1 SMD of drop size distribution - Effect of the volume fraction	161
6.3.3.2 SMD of drop size distribution - Effect of the mixture velocity	165
6.3.3.3 SMD of drop size distribution - Probe position	170
6.3.3.4 Development of drops size - Cross sectional of upward inclined pipe expansion	175
6.3.4 SMD of drop size distribution in downward inclined expansion	179
6.3.4.1 SMD of drop size distribution - Effect of the volume fraction	180
6.3.4.2 SMD of drop size distribution - Effect of the mixture velocity	183
6.3.4.3 SMD of drop size distribution - Probe position.....	187
6.3.4.4 Development of drops size - Cross sectional of downward inclined pipe expansion.....	192
6.3.5 Comparison between different angles of inclination.....	195

CHAPTER 7: PRELIMINARY INVESTIGATION ON INFLUENCE OF SURFACETENSION ON DROP SIZE	199
7.1 Influence of interfacial tension on drop size	200
7.1.1 Interfacial tension – static flow	200
7.1.1.1 Drop weight method	201
7.1.1.2 High speed camera (CCD)	203
7.1.1.3 Interfacial tension results - Static flow results	204
7.1.2 Interfacial tension – mixing flow	205
7.1.2.1 Experimental conditions	206
7.1.2.2 Interfacial tension results - Mixing flow results.....	207
CHAPTER 8: CONCLUSIONS AND RECOMMENDATIONS	216
8.1 Contributions to knowledge	217
8.2 Evolution of interface.....	217
8.3 Flow patterns	219
8.4 Drop size distributions	220
8.5 Recommendations for future work	222
BIBLIOGRAPHY	226
APPENDIX 2A	244
APPENDIX 2B.....	249
APPENDIX 3A	253
APPENDIX 7A	254

LIST OF FIGURES

CHAPTER 2

Figure 2.1: Pipe configurations	11
Figure 2.2: Pipe fittings.....	12
Figure 2.3: Conical diffuser	12
Figure 2.4: Drawing prepared from photographs showing transition from mixed flow, through stratified flow, to bubble flow for fixed water superficial velocity 1.07 m/s and varying oil input fraction, R_v (Russell <i>et al.</i> , 1959).....	18
Figure 2.5: Flow patterns defined by Arirachakaran <i>et al.</i> , (1989).....	20
Figure 2.6: Horizontal oil-water flow pattern sketches (Trallero <i>et al.</i> , 1997).....	21
Figure 2.7: Flow patterns for oil-water system in a horizontal pipe (Nädler and Mewes, 1997).....	24
Figure 2.8: Flow regimes in 15° upward inclined pipes (Scott, 1985) (a) Rolling wavy counter current flow (b) Rolling wavy co-current flow (c) Bubble flow stratified (d) Bubble flow massive	26
Figure 2.9: Schematic representations of vertical oil-water flow patterns by Flores <i>et al.</i> , (1997).	30
Figure 2.10: Schematic representation of upward inclined oil-water flow patterns by Flores <i>et al.</i> , (1997).....	31
Figure 2.11: A typical flow pattern map for oil-water horizontal flow (Trallero, 1996).....	32
Figure 2.12: The Sauter mean diameter (D_{32}) measured by the backscatter technique for horizontal flow in Simmons and Azzopardi (2001).....	47
Figure 2.13: Measurement principle and schematic drawing of the FBRM probe	50

CHAPTER 3

Figure 3.1: Schematic diagram B09/ R123 Multiphase flow inclined liquid- liquid test facility (68mm)	63
Figure 3.2: Photograph, B09/ R123 Multiphase flow inclined liquid-liquid test facility (68mm).....	64

Figure 3.3: Cross-section and photograph of sudden pipe expansion	65
Figure 3.4: Test section mounted on a tubular steel frame hinged at one end, which permitted the small angle of inclination by $\pm 7^\circ$ to the horizontal	65
Figure 3.5: Plan view of multi-holes orifice plate { 18 holes (5 mm) = 32% orifice open area}	65
Figure 3.6: Cross-section of Lasentec FBRM pipe test section	66
Figure 3.7: The capacitance wire mesh sensor (CapWMS) unit on experimental rig.....	67
Figure 3.8: Diagram of separator vessel	68
Figure 3.9: Components of the control system.....	69
Figure 3.10: The calibration of water and silicone oil flowrates.	74
Figure 3.11: Schematic of differential pressure (D_p) flow meters engaged on the flow facility	75
Figure 3.12: Calibration of mixtures flow rates with differential pressure flow meter	76
Figure 3.13: Typical diagram of laser backscatter system (Mettler Toledo)	77
Figure 3.14: Focused Beam Reflectance Measurement, FBRM (Lasentec, 2007)	78
Figure 3.15: PVC Reference procedure set up (Lasentec, 2007)	80
Figure 3.16: PVC reference calibration	81
Figure 3.17: Example of the (a) CLD and (b) DDD graphs	82
Figure 3.18: Electrical schematic of capacitance WMS (Da Silva et al., 2007)	85
Figure 3.19: Capacitance wire mesh sensor 24 x 24 (Left) Sketch of wire mesh sensor (Right)	86
Figure 3.20: Tomographic images of water-oil in horizontal pipe. (a) water only, (b) silicone oil only and (c) oil volume fraction 0.4 (d) oil volume fraction 0.6	88

CHAPTER 4

Figure 4.1: Mixture velocities after orifice (U_{smo}) and mixture velocities downstream (U_{sme}) of flow pattern encountered within the rig and possible operational limits plotted on flow pattern map of Trallero <i>et</i> <i>al.</i> , (1997).....	92
---	----

Figure 4.2: U_{smo} and U_{sme} of flow pattern transition through the sudden expansion and WMS images plotted on horizontal liquid-liquid flow pattern map of Trallero <i>et al.</i> , (1997)	92
Figure 4.3: The capacitance wire mesh sensor (CapWMS) system on experimental rig.....	94
Figure 4.4: Oil volume fraction and phase distributions in a pipe cross section for distance from expansion $10D$, mixture velocity 0.20 m/s and horizontal flow, at different input oil fractions	96
Figure 4.5: Oil volume fraction and phase distribution in a pipe cross section for distance from expansion $34D$, mixture velocity 0.20 m/s and horizontal flow, at different input oil fractions	97
Figure 4.6: Oil volume fraction in a pipe cross section for distance from expansion $34D$, input oil fraction 0.2 and horizontal flow, at different mixture velocities.	98
Figure 4.7: Oil volume fraction in a pipe cross section for distance from expansion $34D$, input oil fraction 0.4 and horizontal flow, at different mixture velocities	98
Figure 4.8: Oil volume fraction in a pipe cross section for distance from expansion $34D$, input oil fraction 0.6 and horizontal flow, at different mixture velocities	99
Figure 4.9: Oil volume fraction in a pipe cross section for distance from expansion $34D$, input oil fraction 0.8 and horizontal flow, at different mixture velocities.....	99
Figure 4.10: Oil volume fraction in a pipe cross section for mixture velocity 0.20 m/s, input oil fraction 0.2 and horizontal flow, at different distances from expansion.	100
Figure 4.11: Interface shape for distance from expansion $10D$, mixture velocity 0.2 m/s and horizontal flow, at different input oil fractions	101
Figure 4.12: Interface shape for distance from expansion $20D$, mixture velocity 0.2 m/s and horizontal flow, at different input oil fractions	102
Figure 4.13: Interface shape for distance from expansion $34D$, mixture velocity 0.2 m/s and horizontal flow, at different input oil fractions	102

Figure 4.14: Spatial distribution for distance from expansion $10D$, mixture velocity 0.2 m/s and horizontal flow: (a) 0.2 OVF (b) 0.4 OVF (c) 0.6 OVF (d) 0.8 OVF.....	103
Figure 4.15: Spatial distribution for distance from expansion $34D$, mixture velocity 0.2 m/s and horizontal flow: (a) 0.2 OVF (b) 0.4 OVF (c) 0.6 OVF (d) 0.8 OVF.....	104
Figure 4.16: Oil volume fraction in a pipe cross section for distance from expansion $34D$, mixture velocity 0.2 m/s and +6 degree flow, at different input oil fractions	105
Figure 4.17: Oil volume fraction in a pipe cross section for distance from expansion $34D$, input oil fraction 0.2 and +6 degree flow, at different mixture velocities	105
Figure 4.18: Oil volume fraction in a pipe cross section for distance from expansion $34D$, input oil fraction 0.8 and +6 degree flow, at different mixture velocities	106
Figure 4.19: Oil volume fraction and phase distribution in a pipe cross section for mixture velocity 0.20 m/s, input oil fraction 0.2 and +6 degree flow, at different distances from expansion	107
Figure 4.20: Oil volume fraction and phase distribution in a pipe cross section for mixture velocity 0.20 m/s, input oil fraction 0.8 and +6 degree flow, at different distances from expansion	107
Figure 4.21: Interface shape for distance from expansion $10D$, mixture velocity 0.2 m/s and +6° upward flow, at different input oil fractions	108
Figure 4.22: Interface shape for distance from expansion $20D$, mixture velocity 0.2 m/s and +6° upward flow, at different input oil fractions	109
Figure 4.23: Interface shape for distance from expansion $34D$, mixture velocity 0.2 m/s and +6° upward flow, at different input oil fractions	109
Figure 4.24: Spatial distribution for distance from expansion $10D$, mixture velocity 0.2 m/s and +6° upward flow: (a) 0.2 OVF (b) 0.4 OVF (c) 0.6 OVF (d) 0.8 OVF.....	110
Figure 4.25: Spatial distribution for distance from expansion $34D$, mixture velocity 0.2 m/s and +6° upward flow, (a) 0.2 OVF (b) 0.4 OVF (c) 0.6 OVF (d) 0.8 OVF.....	110

Figure 4.26: Oil volume fraction in a pipe cross section for distance from expansion $34D$, mixture velocity 0.2 m/s and -6° flow, at different input oil fractions.	111
Figure 4.27: Oil volume fraction in a pipe cross section for distance from expansion $34D$, mixture velocity 0.20 m/s and -3° flow, at different input oil fractions	112
Figure 4.28: Oil volume fraction in a pipe cross section for distance from expansion $34D$, input oil fraction 0.2 and -6° flow, at different mixture velocities	113
Figure 4.29: Oil volume fraction in a pipe cross section for distance from expansion $34D$, input oil fraction 0.8 and -6° flow, at different mixture velocities	114
Figure 4.30: Oil volume fraction in a pipe cross section for mixture velocity 0.20 m/s, input oil fraction 0.2 and -6° flow, at different distances from expansion.....	114
Figure 4.31: Oil volume fraction in a pipe cross section for mixture velocity 0.20 m/s, input oil fraction 0.8 and -6° flow, at different distances from expansion.....	115
Figure 4.32: Interface shape for distance from expansion $10D$, mixture velocity 0.2 m/s and -6° downward flow, at different input oil fractions	115
Figure 4.33: Interface shape for distance from expansion $20D$, mixture velocity 0.2 m/s and -6° downward flow, at different input oil fractions	116
Figure 4.34: Interface shape for distance from expansion $34D$, mixture velocity 0.2 m/s and -6° downward flow, at different input oil fractions	116
Figure 4.35: Spatial distribution for distance from expansion $34D$, mixture velocity 0.2 m/s and -6° downward flow: (a) 0.2 OVF (b) 0.4 OVF (c) 0.6 OVF (d) 0.8 OVF	117
Figure 4.36: Phase distribution in a pipe cross-section for distance from expansion $10D$, mixture velocity 0.20 m/s, input oil fraction 0.2 at different angles of inclination	118
Figure 4.37: Phase distribution in a pipe cross-section for distance from expansion $34D$, mixture velocity 0.20 m/s, input oil fraction 0.2 at different angles of inclination	118

Figure 4.38: Phase distribution in a pipe cross-section for distance from expansion $10D$, mixture velocity 0.20 m/s, input oil fraction 0.8 at different angles of inclination	119
Figure 4.39: Phase distribution in a pipe cross-section for distance from expansion $34D$, mixture velocity 0.20 m/s, input oil fraction 0.8 at different angles of inclination	119
Figure 4.40: Phase distribution in a pipe cross-section for distance from expansion $24D$, mixture velocity 0.2 m/s and horizontal flow, at different input oil fractions (Hasan, 2006).....	120
Figure 4.41: Phase distribution in a pipe cross-section for distance from expansion $24D$, mixture velocity 0.2 m/s and -4 degree flow, at different input oil fractions (Hasan, 2006).....	120
Figure 4.42: Spatial distribution for distance from expansion $10D$, mixture velocity 0.2 m/s and 0.8 input oil volume fractions at different angles of inclination	121

CHAPTER 5

Figure 5.1: Phase layer evolution downstream of the pipe expansion at U_{sme} 0.20 m/s, oil volume fraction 0.5 for horizontal pipe orientation plotted with Yang (2003).....	125
Figure 5.2: Analysis of the cross section for the three flow pattern observed by Vedapuri (1999).	125
Figure 5.3: Effect of the oil volume fraction on the phase layer evolution downstream of the horizontally pipe expansion at U_{sme} 0.20 m/s.....	126
Figure 5.4: Effect of the oil volume fraction on the phase layer evolution downstream of the horizontally pipe expansion at U_{sme} 0.30 m/s.....	127
Figure 5.5: Effect of the oil volume fraction on the phase layer evolution downstream of the horizontally pipe expansion at U_{mse} 0.35 m/s.....	128
Figure 5.6: Prediction of interfacial level for stratified flow with the model of Taitel and Dukler, 1976 by Yang (2003).....	129
Figure 5.7: Effect of the oil volume fraction on the phase layer evolution downstream of the $+3^\circ$ upward inclined pipe expansion at U_{mse} 0.20 m/s.....	130

Figure 5.8: Effect of the oil volume fraction on the phase layer evolution downstream of the $+6^\circ$ upward inclined pipe expansion at U_{me} 0.20 m/s.....	131
Figure 5.9: Effect of the oil volume fraction on the phase layer evolution downstream of the $+3^\circ$ upward inclined pipe expansion at U_{me} 0.35 m/s.....	131
Figure 5.10: Effect of the oil volume fraction on the phase layer evolution downstream of the $+6^\circ$ upward inclined pipe expansion at U_{sme} 0.35 m/s.....	132
Figure 5.11: Effect of the oil volume fraction on the phase layer evolution downstream of the -3° downward inclined pipe expansion at U_{sme} 0.20 m/s.....	133
Figure 5.12: Effect of the oil volume fraction on the phase layer evolution downstream of the -6° downward inclined pipe expansion at U_{sme} 0.20 m/s.....	133
Figure 5.13: Effect of the oil volume fraction on the phase layer evolution downstream of the -3° downward inclined pipe expansion at U_{sme} 0.35 m/s.....	134
Figure 5.14: Effect of the oil volume fraction on the phase layer evolution downstream of the -6° downward inclined pipe expansion at U_{sme} 0.35 m/s.....	135
Figure 5.15: Effect of the angles inclination on the phase layer evolution downstream of the pipe expansion for 0.2 OVF at downstream mixture velocity, $U_{sme} = 0.20$ m/s.	136
Figure 5.16: Effect of the angles inclination on the phase layer evolution downstream of the pipe expansion for 0.8 OVF at downstream mixture velocity, $U_{sme} = 0.20$ m/s.	137
Figure 5.17: Effect of the angles inclination on the phase layer evolution downstream of the pipe expansion for 0.8 OVF at downstream mixture velocity, $U_{sme} = 0.30$ m/s.	138

CHAPTER 6

- Figure 6.1: Locations of probe positions downstream of the expansion and in a pipe cross-section with height from the bottom of the pipe. **141**
- Figure 6.2: D_{32} of water droplets for downstream mixture velocity, $U_{me} = 0.20$ m/s, within test distance in horizontally pipe orientation at oil volume fraction system, $OVF = 0.8$, at different probe position. **146**
- Figure 6.3: Interface mapping along the axial length of the pipe. The lower line indicates the interface between water and the mixture whilst the upper line shows the interface between oil and the mixture at downstream of the horizontal pipe expansion at $U_{sme} 0.20$ m/s, $OVF = 0.8$ **146**
- Figure 6.4: Orifice and downstream mixture velocities of flow pattern transition through the sudden expansion plotted on the flow pattern maps of Trallero *et al.*, (1997)..... **147**
- Figure 6.5: Sauter mean diameter for downstream mixture velocity, $U_{sme} 0.20$ m/s, within test distance in horizontally pipe orientation, probe position 17 mm from bottom at different oil volume fraction, OVF **148**
- Figure 6.6: Sauter mean diameter for downstream mixture velocity, $U_{sme} 0.20$ m/s, within test distance in horizontally pipe orientation, probe position 34 mm from bottom at different oil volume fraction, OVF **149**
- Figure 6.7: Sauter mean diameter for downstream mixture velocity, $U_{sme} 0.20$ m/s, within test distance in horizontally pipe orientation, probe position 51 mm from bottom at different oil volume fraction, OVF . .. **150**
- Figure 6.8: D_{32} of oil droplets for 0.2 oil volume fraction system, within test distance in horizontally pipe orientation, probe position 51 mm from bottom at different downstream mixture velocity, U_{sme} **151**
- Figure 6.9: D_{32} of oil droplets for 0.4 oil volume fraction system, within test distance in horizontally pipe orientation, probe position 34 mm from bottom at different downstream mixture velocity, U_{sme} **152**
- Figure 6.10: D_{32} of water droplets for 0.6 oil volume fraction system, within test distance in horizontally pipe orientation, probe position 34 mm from bottom at different downstream mixture velocity, U_{sme} **153**

Figure 6.11: D_{32} of water droplets for 0.8 oil volume fraction system, within test distance in horizontally pipe orientation, probe position 17 mm from bottom at different downstream mixture velocity, U_{sme}	153
Figure 6.12: D_{32} of oil droplets for downstream mixture velocity, $U_{mse} = 0.20$ m/s, within test distance in horizontally pipe orientation at oil volume fraction system, $OVF = 0.2$, at different probe position	155
Figure 6.13: D_{32} of oil droplets for downstream mixture velocity, $U_{sme} = 0.20$ m/s, within test distance in horizontally pipe orientation at oil volume fraction system, $OVF = 0.4$, at different probe position	156
Figure 6.14: D_{32} of water droplets for downstream mixture velocity, $U_{sme} = 0.20$ m/s, within test distance in horizontally pipe orientation at oil volume fraction system, $OVF = 0.6$, at different probe position.	157
Figure 6.15: D_{32} of water droplets for downstream mixture velocity, $U_{sme} = 0.20$ m/s, within test distance in horizontally pipe orientation at oil volume fraction system, $OVF = 0.8$, at different probe position	158
Figure 6.16: Sauter mean diameter as a function of the distance from $ Z $ at $U_{sme} 0.20$ m/s of horizontal pipe orientation flow, 10D downstream the expansion	159
Figure 6.17: Sauter mean diameter as a function of the distance from $ Z $ at $U_{sme} 0.20$ m/s of horizontal pipe orientation flow, 34D downstream the expansion.	160
Figure 6.18: Sauter mean diameter for downstream mixture velocity, $U_{sme} 0.20$ m/s, within test distance in upward 6° pipe orientation, probe position 17 mm from bottom at different oil volume fraction, $OVF \dots$	163
Figure 6.19: Sauter mean diameter for downstream mixture velocity, $U_{sme} 0.20$ m/s, within test distance in upward 6° pipe orientation, probe position 34 mm from bottom at different oil volume fraction, $OVF \dots$	164
Figure 6.20: Sauter mean diameter for downstream mixture velocity, $U_{sme} 0.20$ m/s, within test distance in upward 6° pipe orientation, probe position 51 mm from bottom at different oil volume fraction, $OVF. \dots$	165
Figure 6.21: D_{32} of water droplets for 0.8 oil volume fraction system, within test distance in upward 6° pipe orientation, probe position 17 mm from bottom at different downstream mixture velocity, U_{sme}	166

Figure 6.22: D_{32} of water droplets for 0.8 oil volume fraction system, within test distance in upward 6° pipe orientation, probe position 34 mm from bottom at different downstream mixture velocity, U_{sme}	167
Figure 6.23: D_{32} of water droplets for 0.8 oil volume fraction system, within test distance in upward 3° pipe orientation, probe position 17 mm from bottom at different downstream mixture velocity, U_{sme}	169
Figure 6.24: D_{32} of water droplets for 0.8 oil volume fraction system, within test distance in upward 3° pipe orientation, probe position 34 mm from bottom at different downstream mixture velocity, U_{sme}	169
Figure 6.25: D_{32} of oil droplets for downstream mixture velocity, $U_{sme} = 0.20$ m/s, within test distance in upward 6° pipe orientation at oil volume fraction system, $OVF = 0.2$, at different probe position	171
Figure 6.26: D_{32} of water droplets for downstream mixture velocity, $U_{sme} = 0.20$ m/s, within test distance in upward 6° pipe orientation at oil volume fraction system, $OVF = 0.8$, at different probe position	172
Figure 6.27: D_{32} of water droplets for downstream mixture velocity, $U_{sme} = 0.35$ m/s, within test distance in upward 6° pipe orientation at oil volume fraction system, $OVF = 0.8$, at different probe position	173
Figure 6.28: D_{32} of water droplets for downstream mixture velocity, $U_{sme} = 0.20$ m/s, within test distance in upward 3° pipe orientation at oil volume fraction system, $OVF = 0.8$, at different probe position	174
Figure 6.29: D_{32} of water droplets for downstream mixture velocity, $U_{sme} = 0.35$ m/s, within test distance in upward 3° pipe orientation at oil volume fraction system, $OVF = 0.8$, at different probe position	175
Figure 6.30: Sauter mean diameter as a function of the distance from $ Z $ at $U_{sme} = 0.20$ m/s of $+6^\circ$ upward inclined pipe orientation flow, 10D downstream the expansion	176
Figure 6.31: Sauter mean diameter as a function of the distance from $ Z $ at $U_{sme} = 0.20$ m/s of $+6^\circ$ upward inclined pipe orientation flow, 34D downstream the expansion	177
Figure 6.32: Sauter mean diameter as a function of the distance from $ Z $ at $U_{sme} = 0.20$ m/s of $+3^\circ$ upward inclined pipe orientation flow, 10D downstream the expansion	178

- Figure 6.33: Sauter mean diameter as a function of the distance from $|Z|$ at U_{sme} 0.20 m/s of $+3^\circ$ upward inclined pipe orientation flow, 34D downstream the expansion..... **179**
- Figure 6.34: Sauter mean diameter for downstream mixture velocity, U_{sme} 0.20 m/s, within test distance in downward 6° pipe orientation, probe position 17 mm from bottom at different oil volume fraction, OVF... **181**
- Figure 6.35: Sauter mean diameter for downstream mixture velocity, U_{sme} 0.20 m/s, within test distance in downward 6° pipe orientation, probe position 34 mm from bottom at different oil volume fraction, OVF... **182**
- Figure 6.36: Sauter mean diameter for downstream mixture velocity, U_{sme} 0.20 m/s, within test distance in downward 3° pipe orientation, probe position 17 mm from bottom at different oil volume fraction, OVF... **183**
- Figure 6.37: Sauter mean diameter for downstream mixture velocity, U_{sme} 0.20 m/s, within test distance in downward 3° pipe orientation, probe position 34 mm from bottom at different oil volume fraction, OVF... **183**
- Figure 6.38: D_{32} of oil droplets for 0.2 oil volume fraction system, within test distance in downward 6° pipe orientation, probe position 17 mm from bottom at different downstream mixture velocity, U_{sme} **184**
- Figure 6.39: D_{32} of water droplets for 0.8 oil volume fraction system, within test distance in downward 6° pipe orientation, probe position 17 mm from bottom at different downstream mixture velocity, U_{sme} **185**
- Figure 6.40: D_{32} of water droplets for 0.8 oil volume fraction system, within test distance in downward 6° pipe orientation, probe position 34 mm from bottom at different downstream mixture velocity, U_{sme} **186**
- Figure 6.41: D_{32} of water droplets for 0.8 oil volume fraction system, within test distance in downward 6° pipe orientation, probe position 51 mm from bottom at different downstream mixture velocity, U_{sme} **187**
- Figure 6.42: D_{32} of oil droplets for downstream mixture velocity, $U_{sme} = 0.20$ m/s, within test distance in downward 6° pipe orientation at oil volume fraction system, $OVF = 0.2$, at different probe position. **188**
- Figure 6.43: D_{32} of water droplets for downstream mixture velocity, $U_{sme} = 0.20$ m/s, within test distance in downward 6° pipe orientation at oil volume fraction system, $OVF = 0.8$, at different probe position **188**

- Figure 6.44: D_{32} of oil droplets for downstream mixture velocity, $U_{sme} = 0.35$ m/s, within test distance in downward 6° pipe orientation at oil volume fraction system, $OVF = 0.2$, at different probe position **189**
- Figure 6.45: D_{32} of water droplets for downstream mixture velocity, $U_{sme} = 0.35$ m/s, within test distance in downward 6° pipe orientation at oil volume fraction system, $OVF = 0.8$, at different probe position. **190**
- Figure 6.46: D_{32} of water droplets for downstream mixture velocity, $U_{sme} = 0.20$ m/s, within test distance in downward 3° pipe orientation at oil volume fraction system, $OVF = 0.8$, at different probe position... **191**
- Figure 6.47: D_{32} of water droplets for downstream mixture velocity, $U_{sme} = 0.35$ m/s, within test distance in downward 3° pipe orientation at oil volume fraction system, $OVF = 0.8$, at different probe position. **192**
- Figure 6.48: Sauter mean diameter as a function of the distance from $|Z|$ at U_{sme} 0.20 m/s of -6° downward inclined pipe orientation flow, 10D downstream the expansion. **193**
- Figure 6.49: Sauter mean diameter as a function of the distance from $|Z|$ at U_{sme} 0.20 m/s of -6° downward inclined pipe orientation flow, 34D downstream the expansion. **194**
- Figure 6.50: D_{32} of oil droplets for downstream mixture velocity, $U_{sme} = 0.20$ m/s, oil volume fraction system, $OVF = 0.2$, at 17 mm probe position from bottom, along test section distance for different pipe orientation. **195**
- Figure 6.51: D_{32} of oil droplets for downstream mixture velocity, $U_{sme} = 0.35$ m/s, oil volume fraction system, $OVF = 0.2$, at 17 mm probe position from bottom, along test section distance for different pipe orientation. **196**
- Figure 6.52: D_{32} of oil droplets for downstream mixture velocity, $U_{sme} = 0.35$ m/s, oil volume fraction system, $OVF = 0.2$, at 51 mm probe position from bottom, along test section distance for different pipe orientation **196**
- Figure 6.53: D_{32} of water droplets for downstream mixture velocity, $U_{sme} = 0.20$ m/s, oil volume fraction system, $OVF = 0.8$, at 17 mm probe position from bottom, along test section distance for different pipe orientation. **197**

Figure 6.54: D_{32} of water droplets for downstream mixture velocity, $U_{sme} = 0.35$ m/s, oil volume fraction system, $OVF = 0.8$, at 17 mm probe position from bottom, along test section distance for different pipe orientation.	198
--	------------

CHAPTER 7

Figure 7.1: Correction factors (F) for the drop weight method (Harkins and Brown, 1919)	203
Figure 7.2: Effect of surfactant on interfacial tension	204
Figure 7.3: Interfacial tension for different surfactant CMC	205
Figure 7.4: Effect of surfactant CMC concentration on droplet size.....	205
Figure 7.5: The effect of mixing time for 0.5 OVF at $N_{Re}=10000$	207
Figure 7.6: The effect of IFT on drop size distribution for 0.8 OVF at $N_{Re}=10000$	208
Figure 7.7: The effect of IFT on drop size distribution for 0.6 OVF at $N_{Re}= 10000$	209
Figure 7.8: The effect of IFT on drop size distribution for 0.5 OVF at $N_{Re}= 10000$	209
Figure 7.9: The effect of IFT on drop size distribution for 0.4 OVF at $N_{Re}= 10000$	210
Figure 7.10: The effect of IFT on drop size distribution for 0.15 OVF at $N_{Re}= 10000$	201
Figure 7.11: The effect of the impeller Reynolds number (impeller speed) on drop size distribution for $\varnothing = 0.8$ system with IFT 44mN/m	211
Figure 7.12: The effect of the impeller Reynolds number (impeller speed) on drop size distribution for $\varnothing = 0.8$ systems with IFT 17mN/m.....	212
Figure 7.13: The effect of the impeller Reynolds number (impeller speed) on drop size distribution for 0.15 OVF systems with IFT 44mN/m.	213
Figure 7.14: The effect of the impeller Reynolds number (impeller speed) on drop size distribution for 15 OVF systems with IFT 17mN/m	213
Figure 7.15: The effect of the impeller Reynolds number (impeller speed) on drop size distribution for 0.8 OVF systems with IFT 6mN/m	214
Figure 7.16: The effect of the impeller Reynolds number (impeller speed) on drop size distribution for 0.15 OVF systems with IFT	214

LIST OF TABLES

Table 2.1: Pertinent experimental flow pattern maps for oil-water flow in horizontal pipelines	17
Table 2.2: Summary of some studies on liquid-liquid dispersion in mechanically agitated contractors.....	41
Table 3.1: Physical properties of fluids at 25°C.....	70
Table 4.1: Summary of experimental conditions	94

NOMENCLATURE

Symbol	Description	Dimension
<u>Roman letters</u>		
$A(h_o)$	Function in Table 2.2	(-)
a	interfacial area per unit volume	(-)
C	Capacitance	(F)
C_D	Drag coefficient	(-)
D	pipe diameter	(m)
D_i	diameter of impeller	(m)
d	drop diameter	(μm)
d_i	the drop i in a drop distribution	(-)
D_{32}	Sauter mean drop diameter	(mm)
d_{max}	maximum drop diameter	(mm)
d_{min}	minimum drop diameter	(mm)
E_a	energy of adhesion between two drops	(Joule)
f	Friction factor	(-)
F	turbulent force	(N/m^3)
f_{col}	frequency of collision	(-)
$f(h)$	Attraction forces per unit area between two finite parallel surfaces separated by distance h	(N/m^2)
g	gravitational acceleration	(m/s^2)
h	distance	(m)
H	distance from bottom of the pipe cross-section	(mm)
N_{vi}	viscosity group	(-)
N_d	number of drops	(-)
N	impeller speed	(m/s)
n_i	drop number in the i^{th} size range	(-)
OVF	input oil volume fraction	(m^3)
P_i	probability of obtaining i^{th} chord size	(-)
N_{Re}	Reynolds number	(-)

u_o	oil average in-situ velocity	(m/s)
u_w	water average in-situ velocity	(m/s)
U	velocity	(m/s)
U_m	Mixture velocity	(m/s)
U_c	velocity of continuous phase	(m/s)
U_{os}	oil superficial velocity	(m/s)
U_{ws}	water superficial velocity	(m/s)
U_{smo}	superficial mixture velocity at orifice	(m/s)
U_{sme}	superficial mixture velocity after expansion	(m/s)
V_{cum}	cumulative volume fraction	(-)
v_{coal}	frequency of coalescence	(-)
V	volume	(m ³ /s)
We	Weber Number	(-)
We'_{crit}	Critical Weber Number	(-)
N_{Re}	Reynolds number	(-)
W_{cut}	water cut	(-)

Greek symbols

ϕ	Volume fraction of dispersed phase	(-)
ϕ_d	concentration of dispersed phase	(-)
μ_w	Water viscosity	(cP or mPa·s)
μ_o	Oil viscosity	(cP or mPa·s)
σ	Interfacial tension	(dyne/cm or N/m)
ε	Energy dissipation	(m ² /s ²)
ε_r	relative permittivity	(F/m)
ε_{mat}	permittivity of material	(F/m)
ε_o	average in-situ volume fraction of oil	(-)
ε_w	average in-situ volume fraction of water	(-)
μ	Viscosity	(cP or mPa s)
ρ	Density	(kg/m ³)
ρ_w	Water density	(kg/m ³)
ρ_o	oil density	(kg/m ³)

ρ_c	density of continuous phases	(kg/m ³)
θ	Inclination angle from horizontal	(degree)

Subscripts

c	Continuous
cut	Cut
coal	coalescence
col	collision
cum	cumulative
d	dispersed
drain	drainage
e	expansion
m	mixture
M	mean
max	maximum
min	minimum
o	oil
s	superficial
t	total
w	water

CHAPTER 1

INTRODUCTION

Multiphase flow involves in a wide range of applications and widely encountered in the chemical and petroleum industries. In the latter, it is important in both the upstream and downstream. An examination of the flows in many pieces of equipment from these industries would reveal that many flows involve more than one phases. It occurs in as relatively simple equipment as pipelines to as complex geometries such as heat exchangers, reactors and separators.

The term multiphase flow can be defined as a simultaneous fluid flow which contains of two or more phases. In many cases, the two phases are gas and liquid. There are, however, other possible combinations - two immiscible liquids (oil/water), solid/gas (fluidized beds, pneumatic conveying), solid/liquid (hydraulic conveying), and occasionally more than two phases (gas/oil/water). This thesis concentrates on two immiscible liquids systems (oil/water).

In oil fields producing hydrocarbon (upstream industry), multiphase flows can consist of water, gas, hydrocarbon liquids and solids (sands). They are lifted to the surface through a drilled well connected to a reservoir. As there is no gain in transporting water and sands, these phases then need to be separated for further downstream processing. Conventionally, a separator such as a vessel or cyclone is

employed to accomplish this. However, such separators involve high capital and installation costs and at the same time, safety measures are extremely restricted. One way to remove this economic and safety problem is to use smaller but more efficient process vessels or to invent novel techniques (separation in pipe) to separate components of the mixture while still being transported within the pipes. Thus, by introducing the use of an expansion pipe as an alternative method for efficient separation of the mixture is the subject of this thesis. This chapter serves as an introduction to the scope of this thesis; that is, the subject of stratification of liquid-liquid two phase flows through sudden pipe expansion with respect to hydrodynamics properties is presented. Motivations that have led to select those areas within the research field are included. It also reviews the aims of this study and outlines the details of the structure of this thesis.

1.1 Background

The multiphase flow of two immiscible liquids is encountered in a variety of industrial processes such as liquid-liquid extraction and most importantly petroleum transportation. The flow characteristics of the immiscible liquids and their configuration in the pipe are of fundamental as well as of practical interest. In contrast, gas-liquid flows have received more attention than the other forms of two-phase flow. This includes massive of experimental data and has resulted in many predictive models being developed. However, for liquid-liquid flow there is much less experimental data despite the importance in the hydrodynamic process. Particularly, there is still a lack of understanding on how drop size distributions and interaction of droplets within the phases affect the phase separation in liquid-liquid two-phase flow. These phases need to be transported to the downstream processing

plant and therefore, one possible solution is through pipelines. The uses of pipelines have become more prevalent in recent years due to the exploitation of marginal fields some of which are in deep water. Generally, multiphase flowing through pipelines involves dynamic flow characteristics which are important in applications such as the designing of downstream equipment. The standard separator is a large cylindrical vessel with axis horizontal. These are expensive, particularly for high pressure operation. There are of very significant weight which is unwelcome for platform applications. Most recently, high aspect ratio liquid-liquid separators have been investigated as possible replacements. These are essentially pipes which are employed for converting dispersed flow to stratified flow. To understand how this occurs is a challenge.

Hence, research in the field of liquid-liquid multiphase flow is of high importance from engineering and economical point of view, to improve safety, reliability, sustainability, efficiency and a significant decreasing maintenance frequency of multiphase flow applications. The present project has been planned to gather information in a particular geometry. But the understanding gained will be useful for the understanding of pipeline flows. The information obtained from the experiment of separation process of oil-water in a pipe expansion will give confidence to the potential users of the novel technique to separate components of the mixture while still being transported within a pipe work system and would meet the essential requirements which are economic, safe to use, smaller than standard process vessel separator.

Furthermore, oil-water flow behaviour is also important in arriving at the correct interpretation of the response of production logging instruments. The performances of separation facilities and multiphase pumps are all a strong function of upstream flow pattern and droplet size. The developments of the pipeline separator for gas-liquid flow have been successfully demonstrated by many researchers (e.g. Wren, 2001 and Baker, 2003) and have now been extended to liquid-liquid flow (Yang *et al.*, 2001, 2003; Liu, 2005 and Hasan, 2006).

Research at Nottingham has indicated that a cheaper and safer alternative for the gas/liquid separation process may be pipe junctions as investigated by Roberts (1994), Wren (2001) and Baker (2003). However, the introduction of a T-junction is quite successful only for gas-liquid flow, leaving liquid-liquid flow inexplicable. There is therefore a need to develop a new approach for liquid-liquid separation which could overcome the problems that troubled the industries, and one possibility is by using an expansion pipe. Accordingly, results showed that an expansion pipe can reduce the mixture velocity of two-phase flow and hence can convert the dispersed flows to the stratified flow patterns which can be easily separated later (Yang *et al.*, 2003 and Liu, 2005). Yang *et al.* (2003) showed that, if the flow approaching the T-junction with a horizontal pipe and a vertical side arm was stratified, good separation of liquids could be obtained.

1.2 Motivations

Research into multiphase flow has been prompted by industrial problems. Among the critical problems are high construction costs and safety measures are extremely restricted. For example, current separators used on offshore platforms are large and the bulk of these separators means that they are costly, both to manufacture and to install. Moreover, they contain a large flammable inventory and as safety is a major concern on offshore platforms this is not good news. Furthermore, evidence has indicated that incidents which occur on oil production platforms are caused by human factors associated with large equipment size (separator vessels) which contain this flammable inventory.

On 6 July 1988, the disaster on the Piper Alpha, the worst offshore oil disaster in terms of lives lost and industry impact, killing 167 men, with only 61 survivors. The disaster on this oil production platform at the UK North Sea continental shelf became a turning point as Cullen (1990) recommended that inventories of flammable fluid on the platforms should be minimised to curtail hazards. It is therefore essential to find possible ways to improve the design and performance of separation processes, with the ultimate goal of saving capital costs at a time of ever tightening environmental regulations and to enhance the safety of the working environment. Thus the motivation of this project is to examine more closely the relationships between the properties of liquids and an expansion pipe designed to produce stratified flow upon the performance of the separator.

1.3 Research aims and objectives

The information available for the phase separation of liquid-liquid two-phase flow in an expansion pipe is limited. This research program was, therefore undertaken to study the stratification process of two immiscible liquid-liquid flows in such geometry. The purpose to monitor the effects of flow conditions approaching sudden expansion in terms of microscopic level and phase distributions resulting.

This program of research global objective is to provide data of two immiscible liquids' flow in an expansion pipe to optimise the operational conditions for the phase separation. Due to the importance of liquid-liquid flows in the petroleum industry, resemblance of the industry liquids which are silicone oil and deionised water were chosen as test fluids. The main objectives of this research programme are:

- To investigate the effect of different input oil volume fractions, downstream mixture velocity and inclination angle on drop size distributions at downstream expansion.
- To investigate the drop size evolution, vertically in the pipe cross section and axially downstream of the pipe expansion for different experimental conditions.
- To visualise the liquid-liquid two phase flow pattern boundaries of transition and to determine the phase distributions for different operating conditions with the use of capacitance Wire Mesh Sensor (CapWMS).
- To investigate the phase evolution and identify the flow pattern development downstream expansion pipe for different experiment conditions.

- To carry out preliminary investigations into the effect of impurities on drop size distributions in a liquid/liquid flow containing a surfactant in a stirred vessel and to examine the rate of separation when the stirring speed is decreased.

1.4 Structure of the thesis

The project is primarily experimental in nature. Henceforth, a comprehensive series of literature reviews were conducted to provide supportive background and a foundation on which to base resultant research study. The following gives a concise breakdown of the major conclusions drawn from the research investigations identified by these literature surveys and contents of chapter in this thesis.

A brief background and the rationale for carrying out this work were discussed in Chapter 1. Chapter 2 gives a brief review of published work on two-phase flows in industrial pipelines. Particular attention is focused on physical configurations and operational conditions of the system. Chapter 3 describes the apparatus and methodology used to performed experiments on liquid-liquid flow through the sudden pipe expansion, as well as the instruments calibration and validations of the experimental measurements. The results obtained from the Wire Mesh Sensor instrumentation downstream of an expansion pipe are presented and discussed in Chapter 4. Subsequently, in Chapter 5, further analysis on WMS data was made and discussion on evolution and stratification that results when dispersed flow passes through a sudden expansion is illustrated. Findings on mean drop size and drop size distribution over the cross section of the pipe downstream of an expansion are presented in Chapter 6. Chapter 7 discussed the results of preliminary investigations on effect of impurities (surfactant) on drop size distributions and characterise the

drop size distribution of the dispersed mixed flows. Finally, summary of the main findings drawn from this research project and recommendations for further work are presented in the final chapter, Chapter 8.

CHAPTER 2

LITERATURE REVIEW

In reality most of the practical oil-water flows in the petroleum and chemical industries are to some extent dispersed. The flow characteristics of the immiscible liquids and their configuration in the pipe are of the fundamental as well as of practical interest. An extensive literature of published research related to liquid-liquid flow was conducted with the most relevant results demonstrated in this chapter. However, the flow pattern, drop size distribution and oil volume fraction have been addressed in a number of the articles but these are mainly for stirred vessels and mixing tanks only. These studies related to pipes were limited to liquid-liquid flow in either horizontal or vertical straight pipes. Less than a handful of papers have had significant data pertinent to the current work.

Knowledge on transformation processes of the dispersed flow to the segregated flow is crucial to the use of pipe expansion as phase separators. There is a need to examine more closely the relationships between the flow and drop characteristics on liquid-liquid flow, together with pipe configurations upon the possibilities of uses the sudden expansion as separator. Once a greater understanding of the processes taking place is found, then it will be possible to suggest ways to improving design and performance, at the same time eliminating the economic and safety problems. The

reviews are intended to provide background and context to the results presented later in the thesis.

2.1 Background

Of the work on multiphase flows, studies on gas-liquid flows have the most attention than other forms of two phase flows. Investigations on gas-liquid flows have and still increase in volume, generating a large amount of data. Hence, many predictive models being developed, improving the understanding of the physical phenomena involved. In contrary, investigations on liquid-liquid two phase flows are much less compared to gas-liquid. Despite of their importance in many engineering applications, liquid-liquid two phase flows have not been explored to the same extent as gas-liquid flows i.e. study of two immiscible liquids flowing in a pipeline.

While many forms of transportation are used to move products from production field to marketplace, pipelines remain the safest, most efficient and economical way to move this natural resource. However, in many applications, pumping of dispersions or emulsions through pipelines and pipe fittings is required. Consequently, some of the parameters are changed, especially when the liquids flow through pipe configurations and fittings. Furthermore, despite their widespread use, there is at present, a severe lack of information concerning liquid-liquid flow behaviour through these pipe configurations and fittings.

In practice, most of the pipes are mounted horizontally or vertically but there are some cases where the pipeline is slightly inclined. The angle of inclination from horizontal can be divided into two types, positive values of θ indicate upward flow

and negative values indicate downward flow (Scott, 1985; Kurban, 1997; Vedapuri *et al.*, 1997; Alkaya, 2000; Lum *et al.*, 2002, 2004, 2006 and Yang *et al.*, 2003). In contrast, the angle, θ of deviation of pipes from the vertical have been reported by Vigneaux *et al.* (1988), Zavareh *et al.* (1988) and Flores *et al.* (1997). These configurations are schematically shown in Figure 2.1.

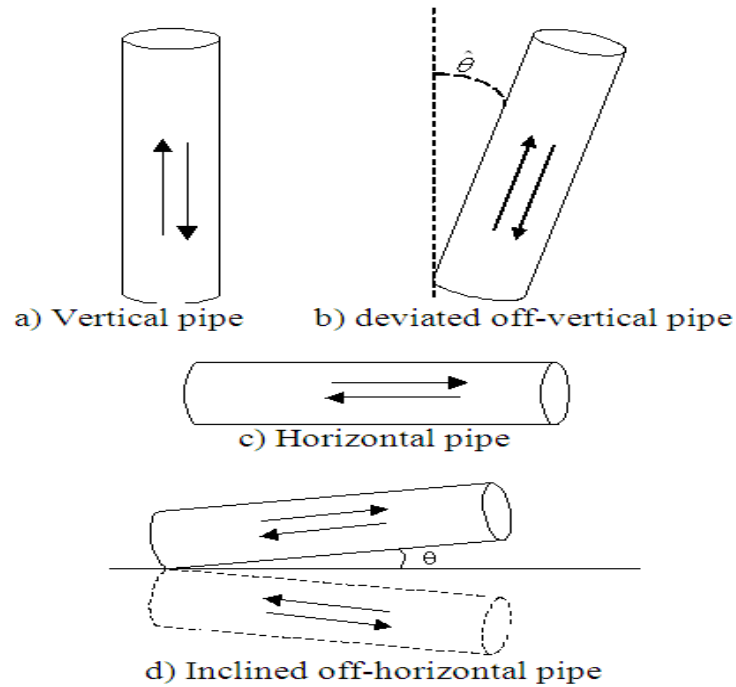


Figure 2.1: Pipe configurations

Although the two-phase flow in straight pipes has been the subject of a number of investigations (Simmons *et al.*, 2000; Angeli, 1996; Lovick and Angeli, 2004a; Rodriguez and Oliemans, 2006; Lum *et al.*, 2006), the flow through pipe fittings (as shown in Figure 2.2) has remained largely unaddressed in particular for liquid-liquid flow.

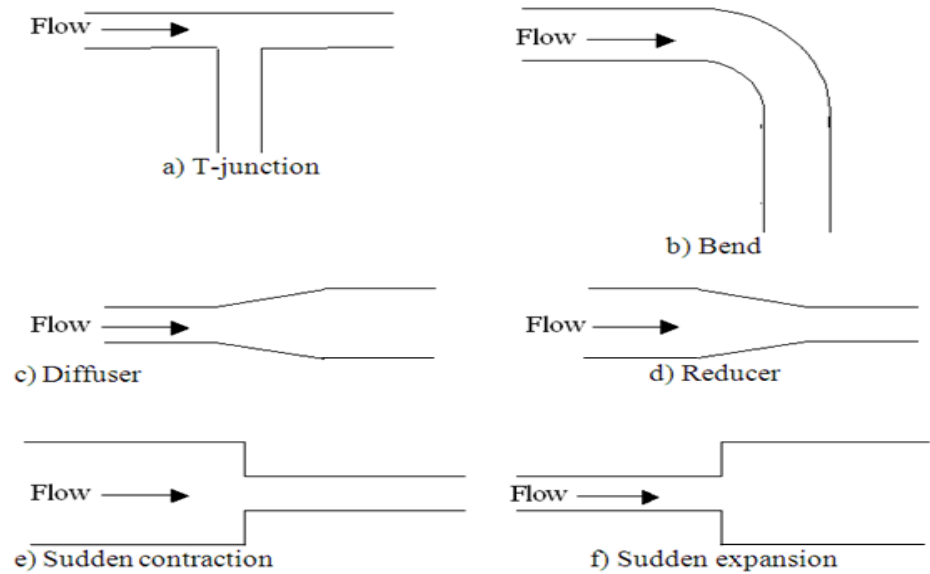


Figure 2.2: Pipe fittings

When flowing through a pipe fitting, the diameter changed. Hence, the friction losses become higher than they would have been in a straight pipe. The Bernoulli energy equation tells us that when the velocity is reduced, such as in a diffuser as shown in Figure 2.3, some of the kinetic energy is transformed to pressure energy. If the flow had been lossless, the pressure change for incompressible flow in a diffuser would be:

$$p_{out} - p_{in} = \frac{\rho v_{in}^2}{2} - \frac{\rho v_{out}^2}{2} = \left[1 - \left(\frac{d_{in}}{d_{out}} \right)^4 \right] \frac{\rho v_{in}^2}{2}$$

2.1

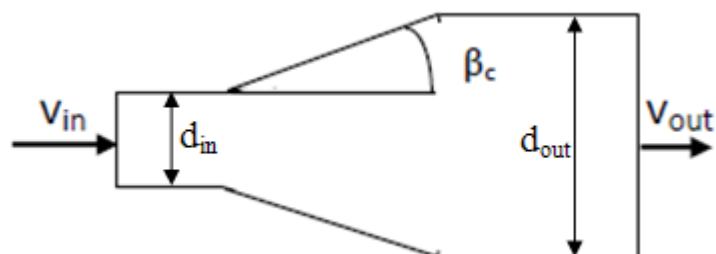


Figure 2.3: Conical diffuser

Since $d_{out} > d_{in}$, clearly $p_{out} > p_{in}$, as expected. Furthermore, in general, very small angles β_c lead to a smooth flow with relatively small losses, and the flow follows the conical geometry without separating from the wall. Increasing β beyond a certain point leads to separation, and the losses increase. At exactly which angle separation starts depends on both Re , d_{in}/d_{out} and any upstream disturbances. Measurements carried out by Idelchik (1992) indicate that if $\beta_c \leq 2^\circ$, no separation occurs under any circumstances, and losses are kept to a minimum. For relatively large β_c , separation becomes so dominant that the conical section has no effect, and one may as well use an abrupt diameter step ($\beta_c = 90^\circ$).

It is noticeably demonstrated that the pipe configuration and fittings play an important role in determining the pattern of liquid-liquid flow, as reported by Nädler and Mewes (1997), Flores *et al.* (1997) and Yang *et al.* (2001; 2003).

Hence, having the fundamental knowledge of flow patterns and flow pattern maps is certainly a great advantage in understanding the separation process of liquid-liquid two-phase flow.

2.2 Flow pattern and flow pattern maps

In the pipe flow of two fluids with different properties flowing simultaneously, the interface between the phases can appear in quite different topological or morphological configurations. The flows with similar interfacial shapes and spatial distributions can be classified as being one *flow regime* or *flow pattern*. Each individual flow pattern refers to its unique hydrodynamics properties. In two-phase flow, the fluid phases within the pipe is distributed in several fundamentally different

flow patterns or flow regimes, depending primarily on these properties, e.g. mixture velocity, input phase ratio, pipe orientation, pipe geometry and other interfacial properties. All flow patterns are usually delineated in terms of areas on a graph with two independent axes, giving the flow pattern maps. Many different names have been given to these various patterns, with as many as 84 having been reported in the literature (Rouhani *et al.*, 1983). Nevertheless, the interest on the flow pattern maps lies on the fact that in each regime, the flow has certain hydrodynamic characteristics. When flow patterns are taken into account, not only can a better model be developed but also the operational conditions can be optimised (Yang, 2003).

2.2.1 Flow patterns for liquid-liquid flows

In liquid-liquid flows, a flow pattern is defined as a characteristic geometrical flow configuration or physical geometry exhibited by a multiphase flow in a conduit. Each individual flow pattern has its unique hydrodynamics properties.

However, as in gas/liquid flow a number of names have been put forward for flow pattern for liquid-liquid flows. Each paper have classified oil-water flow patterns based on their own investigations, e.g., Guzhov (1973), Laflin (1976), Oglesby (1979), Cox (1985), Scott (1985), Arirachakaran *et al.* (1989), Nadler and Mewes (1995), Trallero (1996), Angeli (1996), Simmons (1998), Fairuzov *et al.* (2000) and Munaweera *et al.* (2002). In general, these variations pattern names is due to the subjective nature of flow pattern definitions and others are the variety of names given to what are essentially the same geometric flow patterns. However, for the oil-water flow in the petroleum industry, these classifications can be reduced to four main flow

patterns. These flow patterns that have been observed can be classified as dispersed flow, annular flow, stratified flow and stratified flow with mixed layer at the interface.

Segregated flow is defined as the flow pattern where there is continuity of both phases (liquids) in the axial direction. The two liquids flow tends to stratify when flowing together in a pipe due to their different densities. These separate layers which are segregated flows can be classified as *stratified flow* (ST) and *stratified flow with mixed layer at the interface* (ST&MI). Details of SI and SI & MI flow patterns are discussed in the following sub-section.

In general, dispersed flow is characterized by the flow where one phase is dispersed in the other continuous phase. The dispersed phase often present in the form of small droplets that are non-uniformly scattered within the continuous phase in two immiscible liquids. According to the size of the drops and their distribution in the continuous medium, several subdivisions of this flow pattern can be observed. The dispersed flow can either be water dominated or oil dominated. Further detail will be presented later on in this thesis.

Furthermore, annular flow is characterized by the presence of a liquid film flowing on the channel wall (in a round channel this film is annulus-shaped which gives the name to this type of flow). In liquid-liquid flows, the lighter fluid flows in the centre of the pipe, and the heavier fluid is contained in a thin film on the pipe wall. The lighter fluid may be a mist or an emulsion. Annular flow occurs at high velocities of the lighter fluid, and is observed in both vertical and horizontal wells. As the velocity

increases, the film may disappear, leading to mist flow or emulsion flow. When the interface between the fluids is irregular, the term wavy annular flow may be used (Russell and Charles, 1959).

2.2.1.1 Flow pattern in horizontal pipes

Flow patterns of oil-water systems in horizontal pipes have been extensively studied by several authors. A summary of the pertinent research published for oil-water flow in horizontal pipes is listed in chronologically in Table 2.1.

The earliest experiment of the flow patterns in a horizontal pipeline was reported by Russell *et al.* (1959) by varying the input ratio of water and oil in a 0.8m long and 25.4mm internal diameter test section. Three flow patterns of water and white mineral oil (density = 834 kg/m^3 , viscosity = 18 cP) were observed based on visualisation as bubble (B), stratified (S) and mixed (M) flow. Their sketch of the respective flow patterns is shown in Figure 2.4.

Table 2.1 Pertinent experimental flow pattern maps for oil-water flow in horizontal pipelines.

Author	Pipe Diameter, D (cm)	Velocity range U _w U _{os} (m/s)	Viscosity μ_w μ_o (cP)	Density ρ_w ρ_o (kg/m ³)	σ (dyne/cm)	Observed flow patterns
Russell <i>et al.</i> (1959)	2.03	0.04 - 1.08	0.894 18	999.2 833.3	N.R	ST & MI; Do/w & w; o/w
Charles <i>et al.</i> (1961)	2.50		1 6.29, 16.8, 65	$\rho_o/\rho_w = 1$	N.R	w/o; w/o; annular
Guzhov <i>et al.</i> (1973)	3.94	U _m = 0.20-1.70	1 21.8	998 896	44.8	ST; ST & MI; Do/w & w; o/w; Dw/o & Do/w; w/o
Lafin & Oglesby (1976)	3.84	0.17 - 1.16 0.17 - 1.16	1.2 4.94	998 828	22.3	ST & MI; Do/w & w; o/w; Dw/o & Do/w; w/o
Oglesby (1979)	4.10	0.07 - 2.71 0.03 - 3.19	1.0 33, 61, 167	998 857, 861, 868	30.1, 29.4, 35.4	Do/w & w; o/w; Dw/o & Do/w; w/o
Cox (1985)	5.08	0.05 - 0.64 0.05 - 0.64	0.894 1.380	998 754	N.R	ST; Do/w & w; o/w
Scott (1985)	5.08	0.05 - 0.64 0.05 - 0.64	0.894 1.380	998 754	N.R	ST; Do/w & w; o/w
Stapelberg and Mewes (1990)	2.38, 5.90	0.06 - 1.20 0.04 - 0.65	1.0 30	998 850	50.0	ST & MI; Do/w & w; Dw/o & Do/w
Nadler and Mewes (1995)	5.90	0.0078 - 1.48 0.0143 - 1.44	0.9 16.2 - 31.5	997 845	N.R	ST; ST & MI; Do/w & w; o/w; Dw/o & Do/w; Dw/o & w; w/o
Valle and Kvandal (1995)	3.75	0.20 - 1.20 0.25 - 1.15	1.02 2.30	1002.3 794.	37.3	ST; ST & MI; Do/w & w; Dw/o & Do/w
Trallero <i>et al.</i> (1997)	5.01	U _m = 0.2 - 1.6	0.97 28.8	1037 884	36.0	ST; ST & MI; Do/w & w; o/w; Dw/o & Do/w; w/o

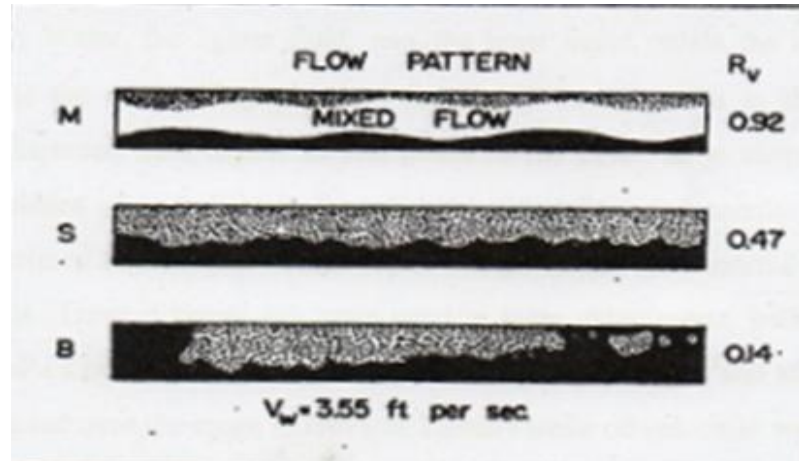


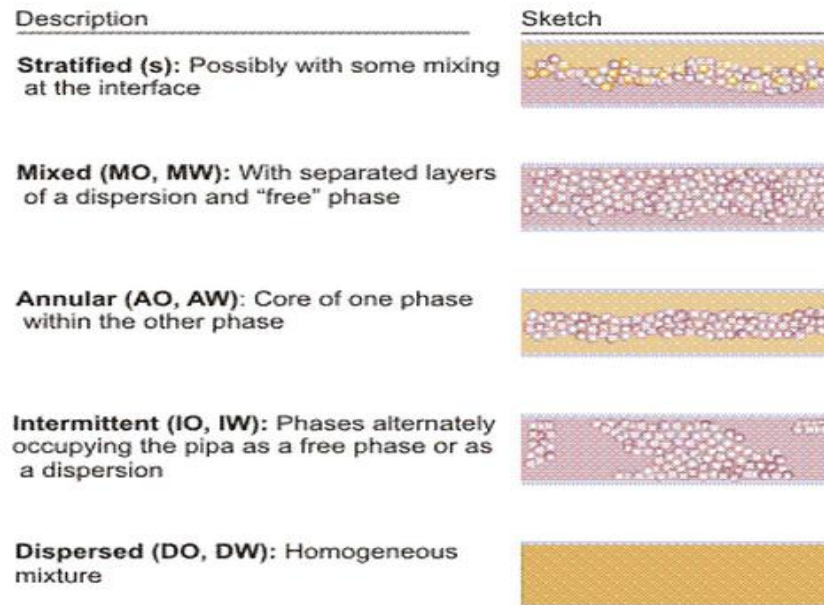
Figure 2.4: Drawing prepared from photographs showing transition from mixed flow, through stratified flow, to bubble flow for fixed water superficial velocity 1.07 m/s and varying oil input fraction, R_v (Russell *et al*, 1959).

Subsequently, Charles *et al.* (1961) defined four flow patterns in their equal density oil/water flow in a 25 mm internal diameter pipe using a photography technique. These flow patterns are water droplets in oil, concentric water with oil flowing in the core, oil slugs in water and oil bubble in water. Three different types of Newtonian oils were used with viscosities of 6.29, 16.8 and 65 mPa's and tap water. The flow patterns observed were mostly independent of the oil viscosities, even though the oil used has equal density to the water.

Oglesby (1979) conducted 422 experimental studies on horizontal oil-water pipe flow and reported up to fourteen flow patterns. Three refined oil with viscosities of 32, 61 and 167 cP were used. In general, flow regimes from segregated to homogeneous were observed with an increase in mixture velocity. Their results demonstrated that the stratified flow is dominant in the pipe at a low velocity whereby the liquid flow is in two distinct layers with no mixing at the interface. However, an increase of the mixture velocity, some mixing occurs at the interface and this pattern is called semi-stratified flow.

A semi-stratified flow pattern characterized by a thick water layer at the bottom and thick oil layer at the top of the pipe, with a thin mixed layer at the centre (Vedapuri, 1999). With further increase in mixture velocity, more mixing occurs at the interface and the thickness of the mixed layer increased in such the oil-water dispersion (mixed layer) occupies more than half of the pipe and this pattern is corresponds to the semi-mixed flow. At a subsequently higher mixture velocity lead to the mixed layer occupied major cross section of the pipe and thin oil and water layer were observed, this flow pattern is termed as semi-dispersed flow. Further promoting the mixture velocity to the system, the flow patterns become a fully dispersed/homogeneous flow. There is a steep concentration gradient in semi-dispersed flow while homogeneous flow has no appreciable change in concentration. It is interesting to note that annular flow pattern with the core of water rather than oil has been reported by Oglesby (1979) which was not discovered in Charles *et al.* (1961).

An experiment of oil-water flow using six oil viscosities for two different pipe diameters was performed by Arirachakaran *et al.* (1989). The flow pattern for range velocities of 0.45 - 3.65 m/s with an input oil fraction from 10 to 95% was investigated (Figure 2.5). The results showed that the flow pattern disappeared for lower oil viscosity and the oil-annulus annular flow pattern diminished in size as the oil viscosity decreased. It can be concluded from the attained data that, in general, the oil viscosity has little effect on the flow behaviour when water is the continuous phase.

Figure 2.5: Flow patterns defined by Arirachakaran *et al.* (1989)

Trallero (1996) has divided the oil-water flow pattern into two major categories: Segregated Flow and Dispersed Flow. As for these two categories, six different flow patterns for oil-water flow in pipes have been characterised. A sketch of the flow patterns and abbreviated names are shown in Figure 2.6 (Trallero *et al.*, 1997). Based on his own experiments and the results of previous investigators for horizontal flow, Trallero (1996) identified and reclassified the flow pattern nomenclature and defined the six flow patterns as the following:

Segregated flows:

- Stratified flow (ST)
- Stratified flow with mixed layer at the interface (ST & MI)

Dispersed flows:

Water dominated

- Dispersion of oil in water and water (Do/w & w)
- Oil in water emulsion (o/w)

Oil dominated

- Dispersion of water in oil and oil in water (Dw/o & Do/w)
- Water in oil emulsion (w/o)

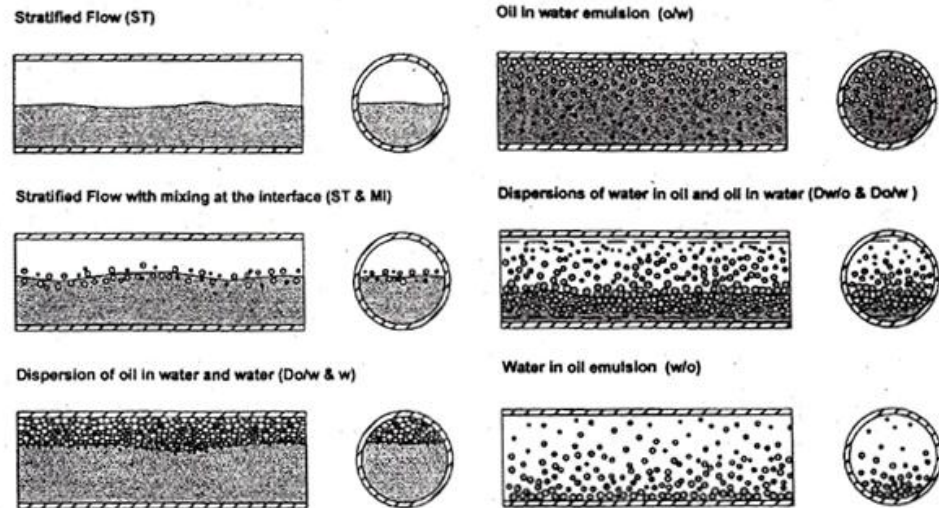


Figure 2.6: Horizontal oil-water flow pattern sketches (Trallero *et al.*, 1997)

Segregated flow is defined as the flow pattern where there is continuity of both phases (liquids) in the axial direction. The two liquids flow tends to stratify when flowing together in a pipe due to their different densities. These separate layers which are segregated flows can be classified as *stratified flow* (ST) and *stratified flow with mixed layer at the interface* (ST&MI). The stratified flow (ST) is identified when the smooth interface exists. As the velocities of the phases increase, the interface becomes more disturbed or wavy and drops of the two liquids may also appear. At that time the flow pattern shifts to the stratified flow with a mixed layer at the interface (ST&MI). There exist water droplets in the oil and oil droplets in the water layer. Both kinds of droplets remain close to the interface. In this case, dynamic and buoyant forces are acting simultaneously on the droplets. The former, which tends to spread the droplets throughout the pipe cross-section, is not large enough to overcome the settling tendency of the counteracting gravity force (Brauner and Maron, 1989; Arirachakaran *et al.* 1989; Vedapuri *et al.*, 1997; Kurban, 1997).

As continuity of both phases (liquids) in the axial direction defined segregated flow, dispersed flow on the other hand is identified when the continuity is lost in either or both phases. In general, dispersed flow is characterized by the flow where one phase is dispersed in the other continuous phase. The dispersed phase often present in the form of small droplets that are non-uniformly scattered within the continuous phase in two immiscible liquids. According to the size of the drops and their distribution in the continuous medium, several subdivisions of this flow pattern can be observed. The dispersed flow can either be water dominated or oil dominated. As for water-dominated flows, the water is always the continuous (dominant) phase and vice versa. A dispersion of oil in water over a water layer ($D_{o/w}$ & w) and emulsion of oil in water (o/w) are dispersed flow patterns where water is the dominant phase. On the other hand, an emulsion of water in oil (w/o) and the coexistence of both type of dispersions ($D_{w/o}$ & $D_{o/w}$) are oil dominated flow patterns (Hinze, 1955; Karabelas, 1978; Trallero, 1996; Angeli and Hewitt, 2000b). Interestingly, dual continuous dispersed flow namely oil continuous and water continuous, have been experimentally identified by Jayawardena *et al.*, 2000 and Lovick and Angeli 2003, 2004a.

Beretta *et al.* (1997) studied the flow patterns of oil-water flow in a 3 mm small diameter tube for three oil viscosities using a stroboscope and a photography technique. They found that most flow patterns for gas-liquid also occur in liquid-liquid horizontal flow in a small diameter tube.

In general, two immiscible liquids of different densities tend to stratify when flowing together in a pipe. The greater the density difference, the more nearly complete is the

stratification. Nädler and Mewes (1997) presented the flow patterns with axes of the mixture velocity and the input oil volume fraction for oil-water flow in a 59 mm internal diameter Perspex pipe. The conductivity measurement in their oil-water horizontal flow was utilised to generate seven flow patterns. Basically, those patterns are similar to that of Trallero's which is based on the stratified flow or dispersed flow. However, they precisely added them into sub-patterns as a combination from those flow patterns, as sketched in Figure 2.7.

Angeli and Hewitt (2000b) implemented two methods for the flow pattern identification, namely high speed video recording and determination of the local phase fractions with a high frequency impedance probe, while the continuous phase in dispersed flows was recognised with a conductivity needle probe. The effect of wall material on the flow pattern was investigated. Over this range of conditions, many different flow patterns were observed, ranging from stratified to fully mix, however, annular flow did not appear. The flow patterns observed had substantial differences in that the propensity for dispersion was greatly increased in the steel pipe, whereas the oil tends to be the continuous phase for a wider range of flow in the acrylic pipe than in the steel pipe. In certain ranges of conditions the distribution of the phases differed dramatically between the stainless steel and the acrylic pipes. They also found the intermediate regime, which they named the Three Layer (3L) flow, in which a mixed layer occurred between the kerosene and water layers in a manner similar to that described by Vedapuri *et al.* (1997).

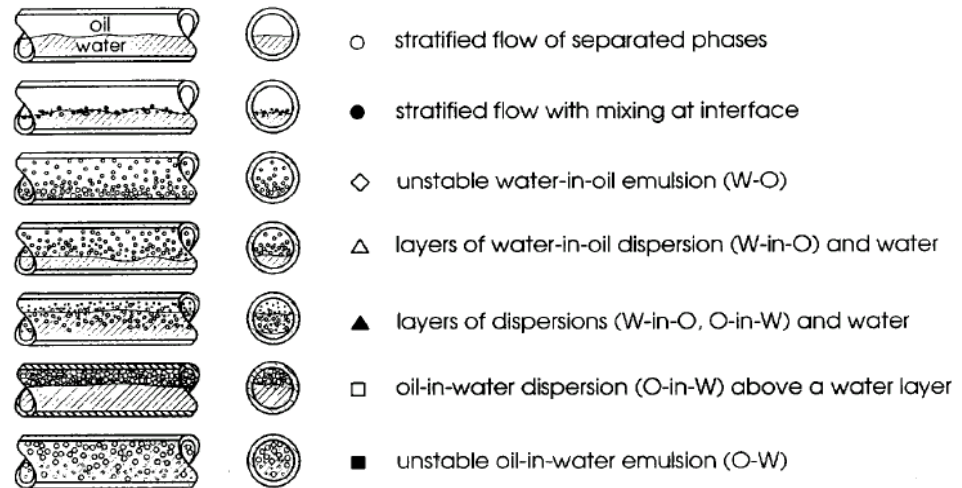


Figure 2.7: Flow patterns for oil-water system in a horizontal pipe (Nädler and Mewes, 1997)

Yang (2003) observed the flow patterns of oil-water flow which were confined to stratified wavy flows approaching the T-junction. The flow patterns were observed with the naked eye and recorded using a high-speed video camera. They found that the different flow patterns depend on the superficial velocity used in a range of studies. At low superficial velocities for both phases, the stratified (ST) flow pattern was observed. By increasing either phase velocity, the flow pattern transits to stratified flow with mixed layer at the interface (ST&MI). The thickness of the mixed layer increases as the velocity increased and the flow pattern transit to a dispersed flow. Generally, the flow patterns observed by Yang (2003) are very similar to that given by Trallero *et al.* (1997). The difference is that the area of the segregated regimes observed by Yang (2003) is slightly larger and the area of dispersion of oil in water above water layer (Do/w & w) is also slightly broader.

2.2.1.2 Flow pattern in inclined pipes

Two phase flow occurrences in industry are ubiquitous, whether it was in horizontal, vertical or inclined pipelines. Even though it occurs in all of the pipe orientations, horizontal and vertical pipe orientations received the most attention. Therefore, there is little flow patterns data of the oil-water system available for inclined pipe orientation. Nevertheless, researchers have reported flow patterns for inclinations from the horizontal, such as Scott (1985), Cox (1985), Vigneaux *et al.* (1988); Kurban (1997), Vedapuri *et al.* (1997), Alkaya (2000), Lum *et al.* (2002; 2004; 2006), Yang *et al.* (2003) and Rodriguez and Oliemans (2006).

Scott (1985) studied the flow of a mixture water and mineral oil in upward inclined pipes. The physical phenomenon studied were flow regime occurrence and hold-up, as a function of flow rate and pipe inclination. Interestingly, the effect of the flow patterns on the inclination angle was first investigated by him. He applied the upward angle from $+5^\circ$ to $+30^\circ$ and concluded that the effect of inclination on the transition to dispersed flow was influenced by the mixture composition. In addition, the appearance of local backflow or recirculation cells within the angles studied was also observed. Figure 2.8 shows the flow pattern observed by Scott (1985) in inclined pipes.

At the same time, Cox (1985) has conducted experiments of horizontal and downhill two-phase oil-water flow. He concludes that at low oil-water flow rate ratios, stratified flow is naturally unstable. The parallel gravity component drives the instability, causing a wavy interface. An increase in the oil superficial velocity stabilizes the oil, and both phases flow as continuous layer even though the interface

is still wavy with some mixing (ST&MI). Further increase in the flow rates disperses the oil (Do/w & w). Finally, for the highest velocities, the oil becomes emulsified in the water (o/w). He also found that the departure from stratified wavy flow and onset of droplet formation at the interface was marked by a decrease in the interfacial wave amplitude.

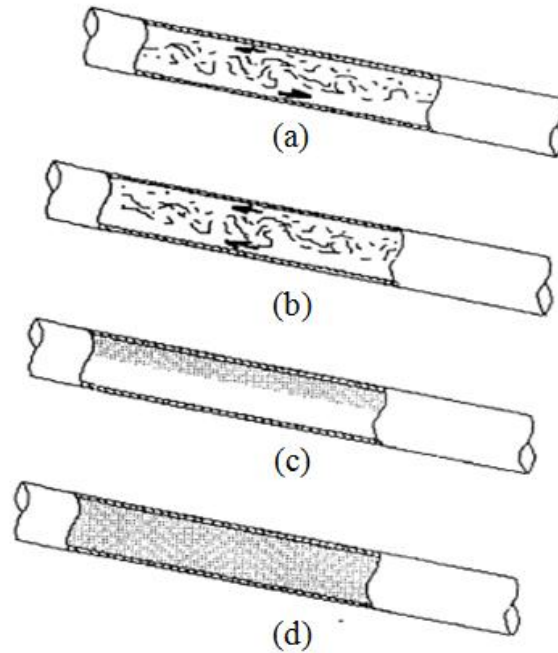


Figure 2.8: Flow regimes in 15° upward inclined pipes (Scott, 1985)
 (a) Rolling wavy counter current flow (b) Rolling wavy co-current flow
 (c) Bubble flow stratified (d) Bubble flow massive

The influence of oil viscosity (2 and 90 cP) on the flow pattern for the velocity between 0.1 and 2.0 m/s were examined in a 100 mm internal diameter pipe by Vedapuri *et al.* (1997). They revealed that a great improvement of mixing is observed at the interface for low viscosity compared to high viscosity oil, whereby a homogeneous mixture was formed at much lower mixture velocities at an inclination angle of 2° .

Meanwhile, Alkaya (2000) who applied horizontal and four inclination angles of $\pm 5^\circ$, and found that the inclination did not have a significant effect on the transition boundaries of dispersed regimes as compared to a horizontal position, except for the appearance of a dispersion of water-in-oil under an oil layer ($D_{w/o}$ and o) at the highest oil fraction. Alkaya (2000) also reported that the velocity ratio at low mixture velocities increased with increasing upward inclination, indicating that the water tended to stay back.

Lum *et al.* (2002; 2004) investigated the effect of a small inclination angle (0° & $+5^\circ$) on flow patterns using a visual identification and an impedance probe. They used an experimental set-up as described in detail by Lovick and Angeli (2001). They exhibited that three flow patterns as follows: stratified wavy flow, Three-Layer (3L) flow and fully dispersed, which is similar to those seen in the horizontal flows. However, the three-layer pattern predominated in flows at small inclination, lower mixture velocity and at an intermediate oil fraction. Besides, three-layers were also reported to have appeared at lower mixture velocity for the oil-in-water dispersions and at high mixture velocity for the water-in-oil dispersions, due to the increase of dispersion present that favours drag reduction in inclined flow.

In addition, Lum *et al.* (2006) who initially used the same experimental facility as reported in Lum *et al.* (2002; 2004) but added two other inclination angles (-5° & $+10^\circ$) in his studies found a new flow pattern called oil plug flow at both $+5^\circ$ and $+10^\circ$ of inclination angles. This was not reported by Scott (1985) and Alkaya (2000). However, this pattern was not seen in downward flow but is in accordance with other investigators (Vedapuri *et al.*, 1997 and Alkaya, 2000). The stratified wavy flow was

observed to become wavier as the upward inclination angle is increased but disappeared completely in downward flow. In general, four flow patterns in upward flow and two flow patterns in downward flow were recorded by Lum *et al.* (2006).

Furthermore, Yang (2003) studied the small inclination angle between -7° and $+6^\circ$ from the horizontal downstream of a pipe expansion. For upward inclination, he found that large waves occur at the interface between the water and mixed layer. The larger the upward inclined angle, the larger the waves become and the shorter the distance downstream of the singularity at which the waves occur. Conversely, for downward inclinations, as the angle of inclinations increased, the amplitude of the waves severely decreases. The waves dissipated quickly with very thin water layer and at -7° the waves and the thin water layer also dissipated.

Recently, Rodriguez and Oliemans (2006) conducted an experimental study on oil-water flow in horizontal and slightly inclined pipes in a 82.8 mm internal diameter steel pipe at the inclination angles of -5° , -2° , -1.5° , $+1^\circ$, $+2^\circ$, $+5^\circ$ and horizontal flow. Basically, seven flow patterns were observed for horizontal, upward and downward inclined flow, and are reasonably well described by the Trallero's flow pattern map. They observed a stratified smooth flow pattern appears in most horizontal flow; however, this pattern disappeared with inclination and is replaced by the stratified wavy (SW) flow pattern in downward and upward flow.

Most recently, Hasan (2006) performed experiment on phase separation of the oil-water flows downstream of sudden expansion with an internal diameter of 63 mm inlet and 100 mm outlet, which can be inclined. The test fluids used were oil and

purified water at operating conditions for mixture velocities 0.2, 0.3 and 0.4 m/s, input oil fraction from 20 to 70% and pipe orientations at angles of +6°, +3°, 0°, -4° and -7° to the horizontal. He concludes that the mechanisms of coalescence occurred faster at the top than the other locations in a pipe cross-section. Furthermore, Hasan (2006) also observed 3 different interface shapes for the stratified oil-water flow; plane horizontal interface, concave interface and convex interface. The concave interfaces were observed for horizontal and downward flow, and the convex interfaces were identified only for an upward inclination.

Moreover, the experiments at an upward deviation angle off vertical were conducted by Vigneaux *et al.* (1988), Zavareh *et al.* (1988) and Flores *et al.* (1997). Vigneaux *et al.* (1988) have conducted experiments on kerosene-water for inclinations between 5° and 65° from the vertical in 100 mm and 200 mm ID pipes for a mixture velocity ranges from 0.1 to 0.5 m/s. Most of the studies concentrated on the effect of inclination and mixture velocity on the slip velocity (oil-water) and on water volume fraction radial gradient. They found that in inclined pipes, the gradient of the water volume fraction is very large in the centre part of the pipe. Whereas the upper part of the pipe section is almost occupied only by oil and the lower section by water. They also observed that the fast-moving droplet swarms occurred at the deviation angle above 10° and the concentration of oil remains very small outside the swarms.

Oil-water flow behaviour in vertical and large deviated incline pipe to characterize flow pattern flow in a transparent pipe of 50 mm internal diameter was investigated by Flores *et al.* (1997). The conductance probes were employed at various points in a pipe cross-section and the oil-water flow patterns in vertical and large deviated

incline pipe were identified as illustrated in Figure 2.9 and Figure 2.10, respectively. They demonstrated that the flow pattern transition in dispersed oil-water flows in vertical pipe seem to be governed by the mechanisms of droplet breakage and coalescence. As for flow patterns in deviated inclined pipe, at low to moderate superficial oil and water velocities, a dispersed oil in water counter-current flow was observed. Furthermore, segregated flow did not appear for inclinations above 33° from horizontal, as it was obviously reported in the true horizontal (Trallero *et al.*, 1997; Nadler and Mewes, 1997 and Vedapuri *et al.*, 1997) and in a small inclination flow (Lum *et al.*, 2002; 2004; 2006; Yang, 2003 and Rodriguez and Oliemans, 2006). The disappearance of segregated flow above 33° is due to the existence of a gravitational component to the flow direction in conjunction with pressure and viscous forces that generated the unique hydrodynamics characteristic.

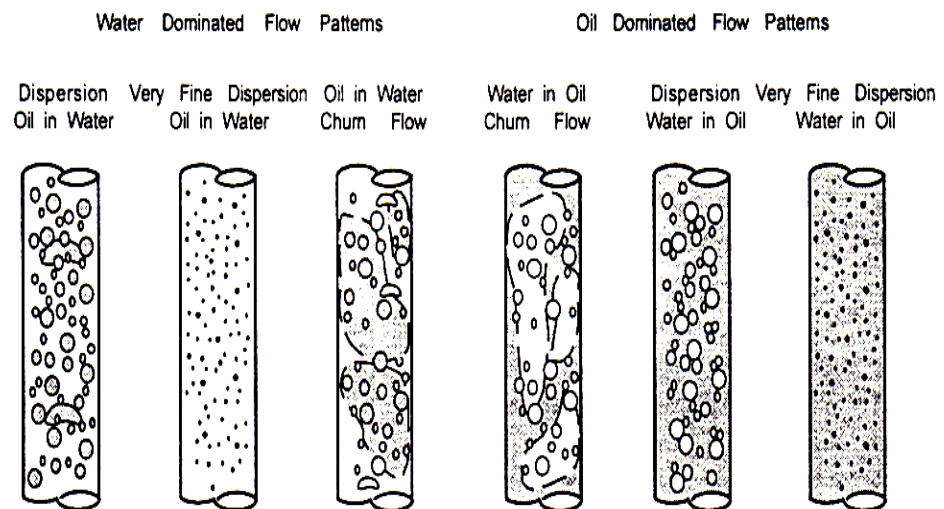


Figure 2.9: Schematic representations of vertical oil-water flow patterns by Flores *et al.* (1997)

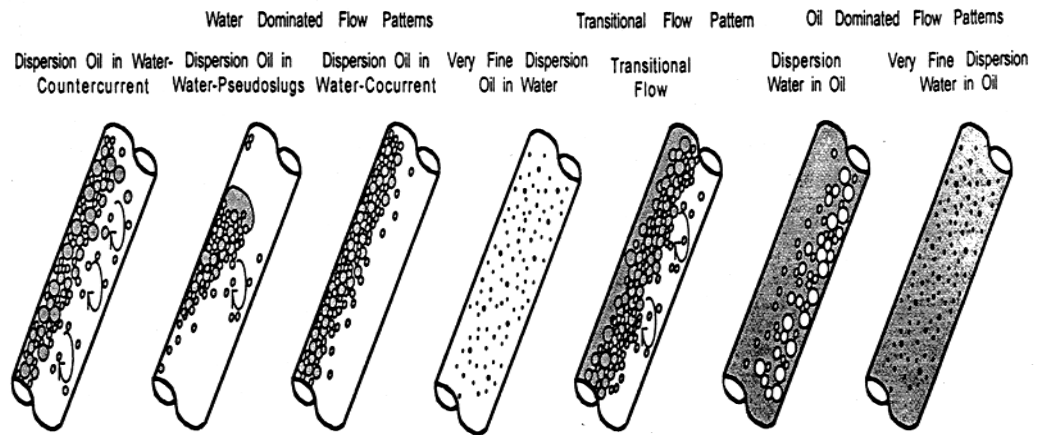


Figure 2.10: Schematic representation of upward inclined oil-water flow patterns by Flores *et al.* (1997)

2.2.2 Flow pattern maps

Flow pattern data are often represented on a two dimensional diagram in terms of system variables. There are two types of graphs used to present the flow data; mixture velocity versus water cut, and superficial velocity of one phase versus the other. The most common variables used in liquid-liquid system are the oil and water superficial velocities (volumetric flow rate/cross sectional area of the pipe). The works on the flow pattern maps in oil-water systems have been attempted by many researchers either in horizontal, vertical or transition between configurations. Charles *et al.* (1961) were the first to draw a flow pattern maps based on superficial oil and water velocities. Later on several investigators have classified oil-water flow patterns based on their own investigations. Flow patterns of some of the investigators, Russell *et al* (1959), Guzhov (1973), Oglesby (1979), Cox (1985), and Nadler and Mewes (1995) were shown in Appendix 2A. An example of typical flow pattern map for oil-water in horizontally flow measured by Trallero (1996) is shown in Figure 2.11.

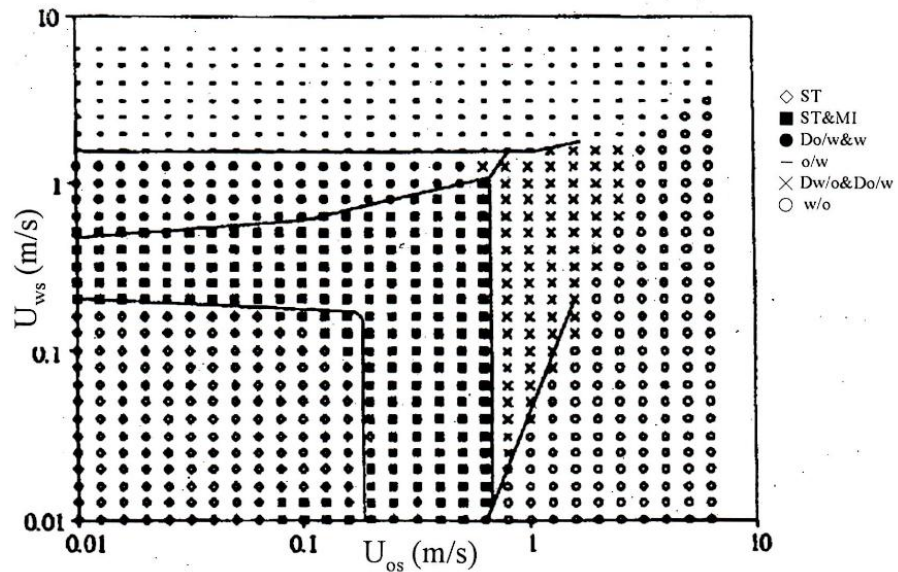


Figure 2.11: A typical flow pattern map for oil-water horizontal flow (Trallero, 1996)

Furthermore, several total flow rates and phase input ratios were independently investigated by Guzhov *et al.* (1973) and Arirachakaran *et al.* (1989) but demonstrated similar flow pattern maps. Nonetheless, eight types of flow pattern were presented in the map by Arirachakaran *et al.* (1989) including the annular flow which was not reported by Guzhov *et al.* (1973).

Moreover, Zavareh *et al.* (1988) studied the flow behaviour of 5° and 15° deviation angles and plotted the flow pattern maps for each angle respectively. These maps were then compared with the model predictions maps of gas-liquid in a horizontal flow from Taitel and Duckler (1976), and it was found that the model had failed to properly predict flow pattern transitions in oil-water flow patterns. This can be explained by the great difference in the relative magnitude of buoyant and interfacial forces between oil-water flow and gas-liquid flow. A second comparison was done with the model developed by McQuillan and Whalley (1985) for true vertical flow pattern maps of a gas-liquid system. Both model predictions were very different for the true vertical and deviation angle, especially at the transition boundary between

bubbly flow and dispersed flow. Nevertheless, it did come closer than the gas-liquid flow maps in predicting the correct boundary.

Meanwhile, an experiment of stratified flow oil-water had been undertaken by Valle and Kvandal (1995). The dispersed region was found at the bottom when oil superficial velocity is greater than water superficial velocity, in contrast the opposite true for water dispersed oil zone in the upper region of pipe. On the other hand, a major conclusion cannot be done due to the fact that the experiment range was too small compared to predicted results. As a consequence, most of the flow patterns that appeared were stratified flows with negligible droplet entrainment and dispersed flow regions.

On the other hand, the flow pattern map of a Newtonian and low-viscosity oil-water system in a horizontal pipe was developed by Trallero (1996), as shown in Figure 2.11. A video camera coupled with a still camera was used to record the flow patterns and their structure. Consequently, the map showed that the segregated flow region was dominant at low and intermediate superficial velocities while the water or oil could be the dominant phase at a high superficial velocity and was not previously mentioned by Charles *et al.* (1961).

Additionally, the effect of the mixture velocity and phase input ratio on the flow pattern map was explored by Nadler and Mewes (1997) and the conductivity technique was used to distinguish different flow patterns. The continuous layers of both phases occurred simultaneously in the water-in-oil and oil-in-water dispersion

zones. A drag reduction was also observed in these zones appearing between the water continuous dispersed flow and the oil continuous dispersed flow.

In the same year, Flores *et al.* (1997) developed four flow pattern maps for upward inclination flows of 45° , 60° and 75° from horizontal and vertical upward flow respectively. The flow pattern map for vertical flow was completely different to that of horizontal flow, as described elsewhere (Trallero, 1996; 1997). They argued that the dispersed oil-in-water was the most predominant area wherein a slightly churning flow occurred at high oil velocity. Nevertheless, the dispersed areas were divided into oil-in-water-Pseudo slugs and oil-in-water counter current as the deviation angle was increased (45°). They established that stratified flow and stratified flow with some mixing at the interface, which were previously reported in horizontal and near horizontal flows no longer exists for inclination above 33° from horizontal. This revealed that the inclination angle significantly affected the flow pattern map.

Simmons (1998) developed a flow pattern map from the experiment of oil-water mixed aqueous in a 63 mm horizontal pipe and used video footage for the flow pattern determination. The boundaries of the flow pattern map obtained from that study showed an excellent agreement with the theoretical flow boundaries predicted by Brauner and Moalem Maron (1992a).

Undoubtedly, the deviation or inclination angles have maximal effect to the flow pattern maps produced and this is possibly due to the presence of droplet sizes in oil-water flowing at appropriated pipe configurations. Thus further investigation on

droplet size distributions would be valuable in order to understand the behaviour of the flow present in the pipeline.

2.3 Liquid-liquid dispersion

Outside the ST and ST&MI regions, the liquids are dispersed in different ways, contingent upon which one is dominant. A dispersion of two immiscible liquids, where one of the liquids forms a continuous phase and the other is dispersed in it, is a flow pattern often observed in liquid-liquid systems. In some conditions, each phase can be dispersed as drops into the other phase in different layers, e.g., dual dispersions. Dispersions will always form in motions of two immiscible liquids which are sufficiently intense, where the disperse forces are due to the turbulent energy dissipation. The formation of dispersions is generally governed by two competing processes; drop break-up and drop coalescence (Sajjadi *et al*, 2001). The drop breakage rate dominates the drop coalescence rate in the initial stage, which causes the drop sizes to decrease with time (Narishman, Ramkrihna, & Gupta, 1980). However with time, the drop breakage rate decreases while drop coalescence rate increases. Ultimately, a steady state is reached where the rate of both processes become equal, and a steady-state drop size distribution is established.

Therefore, without a shred of doubt, behaviour of the dispersion depends strongly on hydrodynamic interaction of drops which includes drop breakage, drop coalescence and drop sedimentation or settling. These events results in changes in the drop sizes, drop size distribution and drop size distribution profile across the pipe section, as well as layer separation of the two phases.

2.3.1 Drop breakage and coalescence in dispersion.

There are three factors that acting on drops in dispersion; turbulences, coagulating and gravity/buoyancy. The first is the factor of turbulences of the continuous phase which arise to breaks the drops or to prevent the coalescence of the drops. The turbulence of the continuous phase can be considered to be the inertial force and viscous shear force analysed by Kolmogoroff (1949), Hinze (1955), Taylor (1934) and Shinnar (1961). The second factor is the coagulating of the dispersed phased which make the drops coalesce or prevents the drops from breaking up. The coagulating of the dispersed phase are the forces of interfacial tension, viscous friction and inner agglutination of the drops (Shinnar, 1961 and Thomas, 1981). The third is the gravity or buoyant force which is the main contribution to the settling of the drops.

In dispersion, the drop size and drop size distribution mainly depend on the equilibrium balance between the turbulence forces and the coagulating forces. Size distribution of the disperse phase affects the overall performance efficiency. Smaller droplets provide larger interfacial area per unit volume and contrariwise. The sizes distribution of the drops depend on several factors as mentioned earlier. In order to understand the dispersive process better, it is important that drop break-up and coalescence be investigated.

In dispersed flow, drop break-up usually occurs when large droplets break into smaller ones. For a dispersed phase with low viscosity, the viscous friction forces can be neglected. Therefore, interfacial tension and agglutination of the drops are the two main coagulating forces. If the turbulence forces overcome the interfacial tension, the

drops deformed and break up, by turbulence inertial force and turbulence shear force. If the turbulence forces overcome the agglutination of the drops and then prevent coalescence of drops, coalescence blocked by turbulence inertial force and by turbulence shear force.

According to the observation of Ali *et al* (1981), the breakage processes of the drops for the two breaks up mechanisms are different. For the drop break up by turbulence inertial force, the drop is lashed by inertial force and smashed into a cloud of smaller drops and then these smaller drops separate. For the drop break up by viscous shear force, the drop firstly deforms and prolongs and the ruptures to form smaller drops. There is other mechanism for drop breakage, i.e., accelerated drops (Cohen, 1991; Brauner, 2002). For accelerated drops, drops deform and break due to rapid acceleration of drops bursting into a stream of a second fluid, which is the main mechanism for pneumatic atomisation.

Hence, a wide range of concepts has been developed from the studies of drop breakage by many investigators (Kolmogoroff, 1949; Hinze, 1955; Taylor, 1934; Shinnar, 1961; Sleicher, 1962; Sprow, 1967; Hughmark, 1971; Kubie and Gradner, 1977; Karabelas, 1978 and Noik *et al.*, 2002).

In most cases, investigators have not reported on drop coalescence probably because they were observing single drops in a turbulent flow field or working with dilute dispersions. Whereas, in dense dispersions, droplets coalescence and additional factors introduced when a swarm of droplets interact must be taken into account (Jeelani, 1993 and Wagner, 1997).

In turbulent dispersion, coalescence results when smaller droplets tend to form large ones. Coalescence phenomenon is more complex since it involves the approach of two drops collides, trapping a small amount of liquid between them. Then the drainage of the liquid film separating the drops until it reaches a critical values and eventual rupture of the intervening liquid film resulting in coalescence. Therefore the physical properties of the fluids and interfaces play an important role in drops coalescence. For example, coalescence in dispersion is usually reduced considerably by the combined action of a protective colloid and turbulent agitation. Hence, there is not as many concepts have been developed as for drop breakage. Among the few that involved in studies of drop coalescence are Sleicher (1961), Levich (1962), Howarth (1964), Coualoglou and Tavlarides (1977) and Thomas (1981).

What's more, sedimentation or settling in liquid-liquid system has scarcely been studied. Mostly, the sedimentation has been studied in liquid-solids systems (Coulson and Richardson, 1991).

2.3.2 Models for drop breakage and coalescence

The possibility of predicting fluid particle (drops or bubbles) size distributions is very important for determining interfacial areas and heat- and mass-transfer rates when designing and scaling up equipment such as chemical reactors and separators. Population balances can be used to describe changes in the fluid particle size distributions and other dispersion properties, and are usually the result of dynamic fluid particle breakage and coalescence processes.

In models of drops breakage and coalescence in the literature, owing to continuous breakage and coalescence, a distribution of drop sizes is observed. Therefore, to get an overall picture of the quality of dispersion, characteristics of dispersion are usually expressed in typical minimum drop diameter (d_{\min}), maximum stable drop diameter (d_{\max}) and/or Sauter mean diameter (D_{32}). In many instances, direct proportionality between the two representative drop diameters (D_{32} and d_{\max}) has been reported (Brown and Pitt, 1972; Calabrese *et al.*, 1986; Nishikawa *et al.*, 1987). Therefore, correlation for either of the representative diameters can be used to compute the other representative diameter. However, for the mass transfer processes in a dispersion, the Sauter mean diameter, D_{32} , is preferred due to the fact that its link to the specific interfacial area as:

$$a = \frac{6\phi}{D_{32}} \quad 2.2$$

$$D_{32} = \frac{\sum_{j=1}^k n_i d_i^3}{\sum_{j=1}^k n_i d_i^2} \quad 2.3$$

Where a is the interfacial area per unit volume and ϕ is the dispersed phase volume fraction; d_i and n_i are, respectively, the drop size and drop number in the i^{th} size range.

Immense industrial importance of liquid–liquid dispersions has led to studies on experimental measurements of drop size in liquid–liquid dispersions, whether in batch vessels or continuous flow stirred tanks as reported in many literatures. Some of these studies are summarized in Table 2.2. In most of the cases, the experimental

data have been correlated using the functional form developed by Hinze (1955) and modified by subsequent researchers (Shinnar and Church, 1960; Doulah, 1975). In some cases, altogether different functional forms are reported (Wienstein and Treybal, 1973; Quadros and Baptista, 2003).

Table 2.2 Summary of some studies on liquid-liquid dispersion in mechanically agitated contractors.

Reference	Experimental	Correlations
Vermeulen (1955)	Several systems both A/O and O/A were studied in batch experiments. Holdup values were between 0.1 and 0.4. Drop size measurement was done using light transmission technique.	$\frac{N^2 d^{5/3} D^{4/3} \rho_m}{\sigma f_\phi^{5/3}} = 0.016$ $f_\phi = \frac{d}{d_{\phi=0.1}}$ $\rho_m = 0.6\rho_d + 0.4\rho_c$
Wienstein and Treybal (1973)	Eight different systems, O/A and A/O were studied. Both batch and continuous experiments were done. Holdup varied between 0.08–0.6. Light transmission method was used for drop size measurement.	$d_{32} = 10^{(-2.316+0.672\phi)} v_c^{0.0722} \varepsilon^{-0.194} \left(\frac{\sigma}{\rho_c}\right)^{0.196}$ $d_{32} = 10^{(-2.066+0.732\phi)} v_c^{0.047} \varepsilon^{-0.204} \left(\frac{\sigma}{\rho_c}\right)^{0.274}$
Brown and Pitt (1974)	Three O/A systems with MIBK, kerosene, n-butanol as dispersed phase and water as continuous phase were investigated. Holdup was equal to 0.05. Photoelectric probe was used for drop size measurement.	$\left(d_{32}^{5/3} \frac{\rho}{\sigma} \varepsilon^{2/3}\right) \left(\frac{\varepsilon^{1/3} t_c}{T^{2/3}}\right) = c$ $Nt_c \left(\frac{W}{T}\right) \left(\frac{D}{T}\right)^{8/3} = 0.0122$
Calabrese <i>et al.</i> (1986)	Study was aimed at finding effect of dispersed phase viscosity on drop size. Five different grades of silicone oil in water were used to obtain dispersed phases of varied viscosity. Hold up was 0.0015. Batch experiments were done with direct photography as drop size measuring technique.	$\frac{d_{32}}{d_0} = \left[1 + 11.5 \left(\frac{\rho_c}{\rho_d}\right)^{1/2} \frac{\mu_d \varepsilon^{1/3} d_{32}^{1/3}}{\sigma}\right]^{5/3}$ $\frac{d_{32}}{D} = 2.1 \left(\frac{\mu_d}{\mu_c}\right)^{3/8} \left(\frac{\rho_c N D^2}{\mu_c}\right)^{-3/4}$ $d_{32} = 0.6d_{\max}$ $d_{32} = 0.5d_{\max}$

Wang and Calabrese (1986)	Objective of the study was to establish relative importance of dispersed phase viscosity and interfacial tension on drop size. Silicone oils were dispersed in water, methanol and their solution. Batch experiments were done with holdup was less than 0.002. Direct photography was used for drop size measurement.	$\frac{d_{32}}{D} = 0.066We_1^{-0.66} \left[1 + 13.8V_i^{0.82} \left(\frac{d_{32}}{D} \right)^{0.33} \right]^{0.59}$ $V_i = \frac{\mu_d ND}{\sigma} \left(\frac{\rho_c}{\rho_d} \right)^{1/2}$
Zhou and Kresta (1998)	Batch experiments with water as the continuous and silicone oil as the dispersed phase. Holdup was 0.0003. PDPA (Phase Doppler Particle Analyzer) was used for drop size measurement.	$d_{32} = 118.6(\varepsilon_{\max} ND^2)^{-0.270}$
Pacek <i>et al.</i> (1999)	Batch experiments were done with water as the continuous phase and chlorobenzene or sunflower oil as the dispersed phase. Measurements were done by direct photography near the tank wall. Dispersed phase holdup ranged between 0.01to 0.05.	$d_{32} \propto \varepsilon^b$
Quadros and Baptista (2003)	Experiments to determine interfacial area in continuous flow stirred tank with di-isobutylene diluted with benzene as the dispersed and sulfuric acid as the aqueous phase. A chemical method was used to determine overall interfacial area under different operating conditions. Hold up values ranged between 0.061–0.166.	$d_{32} = 6\phi \left\{ 1 + \left(\frac{c_1}{We_1\phi} \right)^2 \right\} (c_2\phi^2 + c_3\phi)$ $\frac{d_{32}}{D} = 0.0336We_1^{-0.6}(1 + 13.76\phi)$ $\frac{d_{32}}{D} = 0.0286We_1^{-0.6}(1 + 13.24\phi)$
Sechremeli <i>et al.</i> (2006)	Batch experiments were done. Distilled water was used as continuous and kerosene as the dispersed phase. Direct photography was used to measure drop size. Holdup values ranged between 0.01–0.1.	$d_{32} \propto N^{-a}$

2.4 Drop size distribution

Knowledge of drop size and distribution would improve understanding of dispersed system and contribute to better design and modelling of many industrial processes as well as oil production and transportation. The size of the dispersed phase is important when interfacial mass and/or heat transfer involved, while it will affect phase separation at the end of the process. Drop size, drop size distribution and dynamics of their evolution are significant factors that determine the rheology and stability of dispersions. Hence, knowledge of the parameters would enhance and optimised the energy consumption and pumping requirements of the system.

Experimental studies of drop sizes in liquid-liquid flow have mainly been carried out in stirred tanks or agitated vessels. While information on the drop size during pipe flow is almost entirely limited to low dispersed phase concentrations (Sleicher, 1962; Ward and Knudsen, 1967; Collins and Knudsen, 1970; Kubie and Gardner, 1976; Karabelas, 1978; El-Hamouz and Stewart, 1996; Simmons and Azzopardi, 2001 and Hasan, 2006). In addition, most models are based on the fundamental theory developed by Kolmogorov (1949) and/or Hinze (1955) for drop break-up in isotropic turbulence with improvements to account for increasing dispersed phase fraction.

Drop size distributions during the pipe flow of two immiscible liquids have been given by a few researchers. Among early studies, Ward and Knudsen (1967) present an investigation to obtain information on drop size and drop size distribution of liquid-liquids dispersions in turbulent flow. They investigated the distribution of oil drops in water fraction up to 47% for downward vertical flow in dispersions formed in stirred vessels before entering the test section. The photography technique was

used to capture photos of droplets in the dispersions. Over 1000 photographs of dispersions were obtained and from these photos, the Sauter mean diameters (D_{32}) of the well-defined droplets were measured. The Sauter mean drop diameter, D_{32} was found to augment when dispersed phase fraction increases. Interestingly, it was observed that D_{32} initially increases and then decreases with increasing velocity. The decrease in size at high velocities agreed with the model suggested by Sleicher (1962) while the initial increase confirmed the theory proposed by Howarth (1964) whereby an increase in velocity causes an increase in coalescence frequency.

Collins and Knudsen (1970) conducted an experimental program to characterise the drop size distributions formed when liquid-liquid dispersion was exposed to turbulent pipe flow. They used photography technique to study the effect of pipe turbulence on drops formed by injecting an organic phase at low concentrations (0.6 – 10%) into the vertical downward flowing aqueous. The observed distributions are two superimposed distributions; the initial distribution formed at the injecting nozzle and the distribution produced by the turbulence of the flowing stream. Increasing the dispersed phase viscosity seemed to delay drop deformation and break-up, while drop break-up appeared to be much more probable near the pipe wall rather than in the turbulent core. The authors presented a model for the evolution of drop size distribution along the pipe, which its experimental data is in agreement with the maximum stable drop size (d_{\max}) as predicted by Sleicher's correlation.

Kubie and Gardner (1977) conducted experiments in a 4m long, 17.2 mm diameter horizontal glass tube and in helical coils to get information on the equilibrium drop size distribution, especially on the d_{\max} occurring in the flow of two liquids. They

used four different injectors for the disperse phase and found that the various methods of disperse phase injection had little effect on the drop size distributions. In fact, suggesting that the steady-state distribution was probably independent of the initial distribution. The droplet size distribution obtained by photography through the pipe wall became narrower with increasing continuous phase velocity as maximum drop size (d_{\max}) decreased at a greater rate than minimum drop size (d_{\min}). For drops smaller than the size of the energy-containing eddies, the model suggested by Hinze (1955) predicted satisfactorily maximum drop size (d_{\max}) but for larger drops an alternative model was suggested.

Karabelas (1978) performed an experiment using an encapsulation technique concurrently with photography technique to study drop size distributions formed by turbulence when oil was injected at low concentrations (0.2%) into flowing water in horizontal pipes. The resulting distribution can be well represented by either Rosin-Rammler or the upper limit log-normal function, while maximum drop diameter (d_{\max}) was found to satisfy Kolmogorov/Hinze model.

Kurban *et al.* (1995) used photography and needle conductivity probe to measure local droplet size of oil-water flow in a horizontal acrylic pipe and have attained significant differences between the two results. Their results showed that Sauter mean diameters of 678 μm for the photographic technique and 206 μm for the conductivity techniques were reported at the same flow conditions. However, the conductance technique did have some disadvantages, like the fact that it is only suitable for water volume fractions below 4% due to the conductive properties of water.

Furthermore, El-Hamouz and Stewart (1996) utilised a laser back-scatter technique to measure chord length distributions formed downstream of a static mixer in horizontal flow system. The droplets were formed in the static mixer before entering the 25.4 mm internal diameter pipe test section. The mean chord length increased with the distance from the mixer, suggesting that the distributions were influenced by drop coalescence in the test section rather than turbulent drop break-up.

Subsequently, the laser backscattering technique was employed, together with laser diffraction technique by Simmons and Azzopardi (2001) to examine drop size distribution in a dispersed vertically and horizontally pipe flow. Both measurement techniques have been found to be limited to different concentration ranges. The laser diffraction technique was suitable at dispersed phase concentrations less than 3%, while the backscatter technique was suitable at concentrations greater than 5% by volume. The Sauter means diameter (D_{32}) measured by the backscatter technique for horizontal flow in Simmons and Azzopardi (2001) was shown in Figure 2.12. The D_{32} detected were small at higher measurement positions at low velocities, conversely at higher velocities, the value converge at around 350 μm . Stratification of droplets was observed at low mixtures velocities for horizontal flow. This showed that D_{32} decreased with increasing mixture velocity until it reached certain value. However, for vertical up-flow, homogeneous dispersions were obtained and no stratification was observed. The drop sizes for dispersed phase volume fraction up to 42.3%, acquired by the laser backscatter technique were generally fitted by an upper limit log-normal distribution (ULLN). Although the authors demonstrated that the maximum drop size, d_{max} , at low concentration of the dispersed phase could be described by the Hinze (1955) model. Nevertheless, for the minimum drop size, d_{min} ,

which could be possibly inferred for high concentration, could not be fitted using Hinze's model.

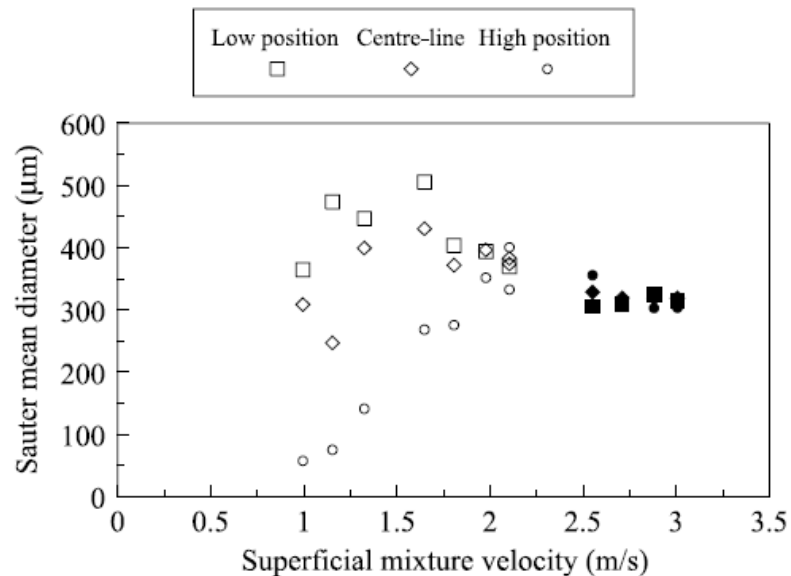


Figure 2.12: The Sauter mean diameter (D_{32}) measured by the backscatter technique for horizontal flow in Simmons and Azzopardi (2001)

Angeli and Hewitt (2000a) was the pioneer that used video recording techniques implementing an endoscope to study drop size distribution attained from different positions inside a pipe for oil-water flow. The use of endoscope allows the visual observation of the flow anywhere within the pipe and not only from the region near the wall, as is the case with other photographic methods. They found that the velocity and nature of the continuous phase affected the drop size distribution, with drops sizes were found to decrease with increasing continuous phase velocity, and water drops in oil continuous flow were smaller than oil drops in water continuous flow in both pipe. Interestingly, the channel wall material also affected the drop size distribution with small drops forming in the steel than in the acrylic test section under the same flow conditions.

The droplet size and vertical distribution of drops of dual continuous flow in a stainless steel pipe were investigated by Lovick and Angeli (2004b). A dual sensor impedance probe was used in the investigation to allow drop chord length measurement at different locations vertically of the pipe cross section. The size and number of drops dispersed in the respective continuous phases was found to decrease as the distance from the interface increased. They asserted that in dual continuous flow mixture velocity does not have a clear effect on the drop size. Instead, they proclaimed that a decrease in mixture velocity decreases the number of drops entrained from one phase into the opposite and causes greater vertical concentration gradient, vice versa for increasing mixture velocity. Moreover, Rosin-Rammler distribution was used to describe their experimental data and they found Rosin-Rammler's model fit satisfactorily the chord length distribution.

Hasan (2006) performed an investigation on the feasibility of a sudden pipe expansion towards stratification of liquid-liquid dispersion in horizontal and inclined horizontal pipe flow. Drop size distributions were measured using a laser back-scatter technique, which measured chord length distributions at several locations vertically and axially of the test section. According to Hasan (2006), at the same axial position of the test section, large drops were initially detected at the top of the pipe cross-section. Therefore, assumptions were made that the mechanisms of coalescence occurred faster at the top than the other locations in a pipe cross-section. Furthermore, log-normal distribution and Rosin-Rammler function were found to fit satisfactorily the experiment on chord length distributions at all regions except in the interface between mixed and kerosene regions.

2.4.1 Measurement techniques for drop size distribution

Dispersion of one phase in the other can occur at the interface of a stratified flow, and is a common phenomenon in several flow patterns, specifically dispersed and annular flow. When the flow pattern of liquid-liquid two phase flow is in dispersed flows, drop size and drop size distribution will become an important characteristic of the flow. These parameters not only affect the mass or heat transfer between the two phases, but also it may affect the flow performance in the pipe. A significant body of work has been published measuring drop sizes for liquid-liquid systems. Furthermore, there are many drop size measurement methods in the literature. However, for the liquid-liquid flow in pipelines, especially for the high ratio of dispersed phase, the measuring of drop size is very difficult. Hence, there are fewer suitable methods could be applied due to the natural drops break up and coalescence of the dispersed phase. Measurement techniques used are generally optically based and were described in this chapter.

2.4.1.1 Laser backscatter technique

In a two immiscible liquid-liquid flow in a pipe, continuous process of measuring drop sizes and drop size distribution requires an in-line measurement technology. One of the most frequently used for in-line drop size measurement is the focussed beam reflectance measurement (FBRM). In this work, FBRM M500P was utilised for measuring drop size. FBRM was developed by Lasentec and is basically a method of obtaining particle chord distribution from back-scattered laser light. A beam from a laser diode is focused to a very small spot, which produces high light density at the focal point. This beam is passed through an eccentric spinning lens that produces a circular rotating beam, normal to the motion of the liquid (Figure 2.13).

When the spot intercepts the particle, enough light is back scattered to be detected by the photodiode. The detected light is converted into electrical pulses, classified by time, which are recorded by computer. As time of detection and angular velocity of the spinning beam are known, dividing these quantities yields the chord size of each particle detected. Details of the FBRM M500P were further discussed in Chapter 3.

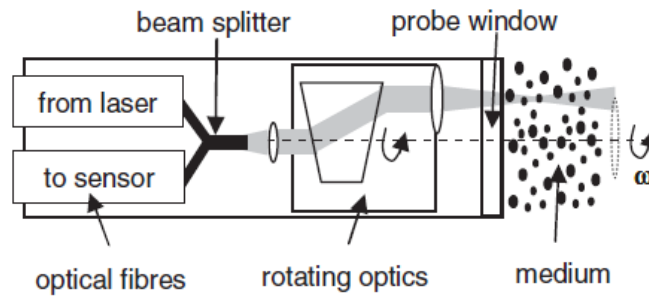


Figure 2.13: Measurement principle and schematic drawing of the FBRM probe.

This chord data is not directly useful for comparison as most techniques measure droplet diameter. It is therefore necessary to convert this chord distribution to a meaningful distribution and that is diameter distribution. So that the results is comparable with data obtained from other sources.

Recently, some investigators have studied methods for converting a chord distribution to a drop size distribution. The matter of converting and estimating drop size distribution from chord measurements is detailed further in the next section in this chapter.

2.4.2 Estimating particle size

The size distribution of liquid droplets present is a valuable design parameter in order to create efficient and cost-effective equipment, for example, in storage, conveying, reaction and separation processes. Several different techniques have been developed

by many researchers to obtain such particle size data. Examples of methods, which have been applied to gas–liquid and liquid–liquid systems, are photography, conductivity probes and droplet encapsulation. An advantage of the majority of the techniques that have been employed is that the droplet diameter distribution is measured directly or can be obtained by simple analysis. However, these methods can only obtain useful data from dilute systems whereas within the oil industry, concentrated oil–water dispersions frequently occur. Hence, it is necessary to measure drop sizes for such systems. Therefore, FBRM M500P instrument, developed by Lasentec, is one of very few techniques suitable for this task. However, the FBRM produces distributions of droplet chord lengths (CLD) whereas most other techniques produce diameter distributions directly. It is therefore necessary to process the CLD to give diameter distributions so that the present data could be compared with data obtained from other sources. The process of transformation from CLD to diameter distribution is known as estimating particle size.

As chord length is neither directly useful nor unique even for a perfectly spherical particle, though spheres can be uniquely defined by the diameter. Herringe and Davis (1976) and Clark and Turton (1988) presented probabilistic techniques to solve this problem. However, the output is very dependent upon the shape of the particles and can suffer problems with very irregular distributions.

Consequently, Liu and Clark (1995) further revised the works by Clark and Turton (1988) and considered that the bubble sizes are represented in two geometric shapes, i.e. an ellipsoidal shape and a truncated ellipsoidal shape. In these cases, they found

that the means and standard deviations of chord lengths and bubble sizes are related but are not dependent on the nature of their distributions.

In 1991 Hobbel *et al.*, described a method of calculating diameter distribution from chord measurements assuming random sphere cuts. In this circumstance, the largest chord size is assumed to be the largest diameter and the chord distribution from this diameter is subtracted from the total chord size distribution. This is basically a ‘peeling method’ and it should be noted that this method was successively only for smaller diameters. Conversely, this method is too sensitive to “noise” in the population of the largest sizes.

Meanwhile, Liu *et al.* (1998) have considered the probability relationships in obtaining representative overall bubble size distribution by inferring the bubble size density from local chord measurements in a heterogeneous bubbling system. They showed that the accuracy of information transformed by a numerical approach using Monte-Carlo simulation was increased as the number of partitions in the bubble size range increased.

In order to create an ideal chord size distribution from a known particle diameter distribution, Simmons *et al.* (1999) emphasized that it is necessary to make some assumptions. For spherical particle in dilute systems, where there are no interactions between particles, the probability of the beam taking a cut through any part of the projected area of the sphere is equal. Thus, probability apportioning method (PAM) described a method of calculating diameter distribution from chord randomly sphere cuts measurements using equation 2.4. This method assumes the diameter bands are

known, where $P\{x_1, x_2\}$ is the probability of obtaining a chord size between x_1 and x_2 for a sphere of diameter D .

$$P\{x_1, x_2\} = \frac{\sqrt{D^2 - x_1^2} - \sqrt{D^2 - x_2^2}}{D} \quad 2.4$$

Hence for a known diameter distribution, range of chord lengths for each diameter band can be calculated using equation 2.4. Full details of the derivation of equation 2.4 are shown in Simmons *et al* (1999) and Langston *et al.* (2001).

Unfortunately, PAM was inaccurate and has shown poor results for unknown diameters distributions because it did not use the collective information from the data set. Therefore, Langston *et al.* (2001) revised this method; which they incorporated the Bayes' theorem (Equation 2.5) for combining conditional probabilities and included an iterative procedure that can approach the true diameter distribution. This revised method was named probability apportioning method version 2.0 (PAM2).

$$P(A_i / B) = \frac{P(B / A_i)P(A_i)}{\sum_{k=1}^N P(B / A_k)P(A_k)} \quad i = 1, 2, \dots, N \quad 2.5$$

Even though, Hasan (2006) found that the results of the transformation of chord lengths using PAM2 were shown unsatisfactorily. In this present work the computational coding for the PAM2 has been updated and upgraded (see Appendix 2B), allowing the measured chord length distribution to be transformed into a drop size distribution successively. Since PAM2 (newer version – version 2.1) methods were found to successfully convert a chord length distribution to a drop diameter distribution, the latter were then analysed further to obtain Sauter mean diameter (SMD). This SMD of the drop diameter distribution were then used in the results, discussion and comparisons between different conditions.

2.5 Oil volume fraction

In most of process and industrial plants, pipeline is universally used as transportation of their raw material and products from one place to the other. Pipelines are generally the safest, most efficient and most economical way to transport large quantities of these material or products. In petroleum industry for instance, increased of offshore oil and gas exploration have resulted in transportation of well fluids in pipelines over relatively long distances. Often the fluid delivered by the wells contains water, which is already present within the stratum. Over period of time, maturing oil wells produce more and more amount of free water, due to naturally presence of water in the old wells or injection of water into the wells for a better oil exploration. The presence and amount of free water phase in contact with pipe wall could cause corrosion and in some cases, blockage in the pipe. Wicks *et al* (1975) found that corrosion in pipelines was usually dominant in areas where the possible accumulation of water in the pipe.

Recently, researchers have come up with an important method to curb this corrosion problem, by introducing corrosion inhibitors. However, the effectiveness of the inhibitors depends on the pipeline material, the inhibitor composition and the type of flow (Vedapuri, 1999). Therefore, it is necessary to introduce the inhibitor into the appropriate phase that in contact with the pipe wall. This can be accomplished only if the flow pattern and the phase distributions under different conditions are known. Therefore, optimisation of pipeline operations for transport of these fluids requires the knowledge of the several parameters. One of the major parameters is the knowledge of the volume ratio of each phase over the total volume also known as volume fraction.

Oil volume fraction (OVF) is a dimensionless quantity that varies from 0 to 1, or is sometimes expressed as a percentage between 0 - 100%, which indicates of a geometry or temporal domain occupied by the oil in a two-phase oil-water flow. There are many typical methods of measurement for oil volume fraction, including irradiation methods (x-ray and γ -ray), quick-closing valve (QCV) method, ultrasonic method and electrical methods (electrical tomography and conductance probe). Besides, there are some other methods, such as optical probe method, observation method, etc.

In industrial applications, the studies that include imaging of phase distribution in process pipelines have becoming important. Process imaging techniques allow us to investigate inside complex structures such as the oil volume fraction of liquid-liquid mixtures. Today, a number of techniques to measure the dispersed phase volume fraction or hold-up have been attempted. These techniques employed non-intrusive or intrusive measurement sensors. Examples of some non-intrusive techniques are x-ray tomography, gamma-densitometry tomography, ultrasonic system, electrical capacitance tomography, electrical resistance tomography and impedance tomography. While, for intrusive measurement sensors such as needle-contact probe and parallel wire probe, are also popular. However, in the recent years, much attention has been focused to a newly developed intrusive method namely the wire-mesh sensor (WMS) method.

Vigneaux *et al.* (1988) reported results of systematic volume fraction profile measurements obtained using a local high-frequency probe in vertically inclined pipe orientation (0° to 65°) of a liquid-liquid flow. High frequency impedance probe was

used to measure mean water volume fraction because of large dielectric constant contrast between the two liquids used. The effect of pipe orientation with water flow rate fraction ranging from 30 to 100% and mean velocity between 0.027 and 0.35 m/s was investigated. They demonstrated that the input oil fraction was dependent on the mean volume composition of mixture and the deviation angle but was minimally affected by the total flow rate (in the range studied).

Two different measurement techniques, a high frequency probe (impedance probe) and a gamma densitometer system were applied by Soleimani *et al.* (1999a) for measuring volume fraction distribution across the tube. Interestingly, the results of the oil volume fraction from the two systems showed an agreement for all mixture velocities used in the range studied. The results exhibited that oil encapsulation by water, especially at low mixture velocity. This phenomenon could probably be explained the wetting of the surface, viscous instability and waves spreading in the water layer due to a high shear stress from the oil layer. In the meantime, in the dispersed flow regime (high mixture velocity) oil droplets were concentrated at the centre of the tube. Thus, they suggested that three mechanisms are responsible for droplet rearrangement in the turbulent dispersed flow regime; the droplets had the same diffusivity as the continuous phase, the lift force in the boundary layer pushed the droplets towards the core region and the distribution of droplets was influenced by gravity.

Oddie *et al* (2003) measured water holdup in two- and three-phase flows using 3 different methods which were quick-closing valve (QCV), electrical conductivity probe and gamma densitometer. The effects of the flow rates of the different phases

and pipe deviation on holdup were evaluated. They concluded that deviation angle had minimum effect to the hold-up at higher oil-water flow rates and the opposite was true for the very flow rates. They also found that steady-state holdups from nuclear measurements were in reasonably close agreement with QCV's measurements. However as for probe data, even though can provide transient and steady-state holdup profiles along the length of the pipe, the accuracy of the probes was not as high as that of the nuclear densitometer or QCV measurements (Oddie *et al.*, 2003). Further, they concluded that deviation angle had minimum effect to the hold-up at higher oil-water flow rates and the opposite was true for the very flow rates.

In the meantime, Yang (2003) used a direct observation method to study the spatial distribution of oil-water flow in a downstream expansion pipe for mixture velocities of 0.2, 0.3 & 0.4 m/s for water cut of 30, 50 & 80%, and horizontal and small inclination angles of $\pm 7^\circ$. The results demonstrated that the stratifying liquid-liquid flow is most rapidly obtained for a horizontal pipe, lower downstream velocities and higher water cuts. However, the water phase is entirely dominating at downstream expansion for the same configurations but with high mixture velocities. In general, Yang (2003) concludes that horizontal is the best pipe position for a dispersed flow to evolve quickly to a segregated flow through the sudden expansion within a short distance. Both, upward and downward inclinations tend to increase the mixed layer and slow down the evolution process.

A spatial distribution of dual continuous liquid-liquid flow has been studied by Lovick and Angeli (2004a) using an impedance probe. The comparison of average

oil volume fraction between the impedance probe and the use of quick closing valves (QCVs) was obtained at less than 5.8% for all conditions. Moreover, the velocity ratio increased during dual continuous flow to above 1 as the oil input fraction increased. At high input oil fractions, however, the velocity ratio decreased again to values below 1 as the mixture velocity increased. These could possibly be explained by the change of interface shape and thus interestingly if the cross section of this shape can be real-time imaged.

Subsequently, Liu (2005) used the same pipe test section as initially described by Yang *et al.* (2003), but employed the sampling method to measure the oil volume fraction across the section of pipe at middle expansion. The mixture velocities and input oil fractions are also the same as the ones applied by Yang's. Liu's results confirmed the phase profiles by Yang's at downstream expansion. Furthermore, the dispersed flow actually dominated over a pipe cross-section at downstream expansion for low input oil fractions and high mixture velocities which was not been mentioned by Yang *et al.* (2003).

Meanwhile, Lum *et al.* (2006) investigated the phase distribution of oil-water flow at $\pm 5^\circ$ (from horizontal) and horizontal flow using similar liquid-liquid flow rig, mixture velocities and oil volume fractions to Lovick and Angeli (2004a). The results of phase distribution in a pipe cross-section showed that the convex interface shapes were obtained in downward flow at a high input oil fraction and high mixture velocity, whereas the shape of interface is replaced by concave interface shape at low mixture velocity even though high input oil fraction is applied. It is clearly showed that the mixture velocity plays a major role in determining the shape of interface in a

pipe cross-section for downward flow. Meanwhile, the shape obtained in an upward flow is similar to those in a horizontal flow as concluded by other investigators (Soleimani *et al.*, 1999a; Angeli and Hewitt, 2000b; Lovick and Angeli, 2004a).

In 2006, Hasan used electrical capacitance tomography (ECT) method to study the spatial distribution of oil-water flow, downstream of an expansion pipe. In this technique, the continuous measurement of dispersed phase volume fraction exploits the differences in electrical permittivity of the two liquid phases to obtain images (Xie *et al.*, 1995; Williams and Beck, 1995; Reinecke and Mewes, 1996; Dyakowski, 1996 and Isaksen, 1996). The effect of pipe orientation (horizontal and small inclination angles of $\pm 7^\circ$) with input oil fraction of 20, 50, & 70% and mixture velocities 0.2, 0.3 and 0.4 m/s was investigated. Hasan (2006) proclaimed that the obtained results clearly indicate the images are satisfactorily agreed well with two methods (Yang, 2003 and Liu, 2005) and could then be used to substantiate the flow patterns as predicted in the Trallero map. The results of phase distribution in the pipe cross-section showed that the concave interfaces were present for horizontal and downward flow, whereas convex interfaces were observed only for upward inclination flow at high input oil fraction and mixture velocity.

Most recently, new technology to generate images of the phase fraction distribution and investigate the flow of fluids in a pipe called Wire Mesh Sensor (WMS) has been developed. The wire-mesh sensor is an intrusive imaging device which provides flow images at high spatial and temporal resolutions (Da Silva *et al.*, 2010) and it has been accepted as an alternative technique for multiphase flow tomographic imaging. The use of tomographic imaging for the investigation of two-phase flows has been

reported in a few review papers (Chaouki *et al.*, 1997, Prasser, 2008, Mudde, 2010) and a book (Williams and Beck, 1995). There are two variants of the WMS, which are conductance and capacitance WMS, often abbreviated in this thesis as CondWMS/ CapWMS.

A wire-mesh sensor for measuring the volumetric fraction of water in crude oil was first described by Johnson (1987). This consisted of a crude device that had two planes of wire grids are placed into the flow in a short distance from each other. However, sensor developed by Johnson (1987) contained no imaging capability.

A wire-mesh device that performs tomographic imaging was presented by Reinecke *et al.* (1996), who proposed a three plane sensor of 29 thin wires each of 0.1 mm diameter. However, the sensor had several limitations and the main disadvantage is that the transformation into the image has to be performed by applying tomographic image reconstruction algorithms (Prasser *et al.*, 1988).

Further development of the WMS was made by Prasser *et al.* (1988). He developed a two plane conductivity (conductance) wire mesh sensor which is a fast tomographic imaging without the need of time consuming and inaccurate image reconstruction procedures. Further, special emphasis was given to a stable sensor design for hostile conditions in industrial facilities.

Up till now, conductance wire-mesh sensors have been applied in many gas-liquid flows (Prasser 2008, Da Silva *et al.*, 2010, Szalinski *et al.*, 2010). However, with increased of interest in two-phase liquid-liquid flows, mostly from the petroleum

industry where, for instance, oil (non-conducting) and water are often produced and transported together. The conductive WMS could not be used in such applications. Therefore, a new WMS was developed by Da Silva *et al.* (2007) based on the measurement of the electrical permittivity (capacitance), to extend the sensor's capabilities to the detection of the non-conducting fluids.

In this thesis focused are on CapWMS since working fluids are oil and water. Great details of the principle and application of CapWMS in determine the volume fraction of multiphase system of two immiscible liquids is discussed in Chapter 3.

CHAPTER 3

INSTRUMENTS AND EXPERIMENTAL METHODS

The literature review in the previous chapter gave an overview of published research related to liquid-liquid flow. The focus of most studies were on drop size distribution, oil volume fraction and flow pattern, especially studies or research conducted in stirred vessels, mixing tanks and pipes. Furthermore, most of these studies were limited to liquid-liquid flow in either horizontal or vertical straight pipe. Up to date, there is no previous studies have had significant data pertinent to the current work which concentrates on sudden expansions.

This chapter discusses the apparatus and methodology used to perform experiments on liquid-liquid flow through a sudden expansion in a pipe. A liquid-liquid flow facility has been built for the purpose of these studies. The physical properties of the system, the criteria of experimental design and the operational principle of each instrument are explained. The experimental processes of drop size measurements and determination of phase layer evolution completed on the flow facility were discussed briefly in Chapter 2.

3.1 The liquid-liquid flow facility

In response to the need for better understanding of the flow pattern, drop size distribution and oil volume fraction in liquid-liquid flow through a sudden expansion, an experimental liquid-liquid flow facility has been designed, constructed and commissioned at the laboratory of the Department of Chemical and Environmental Engineering, the University of Nottingham. This facility is shown schematically in Figure 3.1. The flow facility consisted of a test section, separator, liquid storage tanks and a metering and control system. A photograph of the rig is presented in Figure 3.2. Details of each part are described in the following subsections.

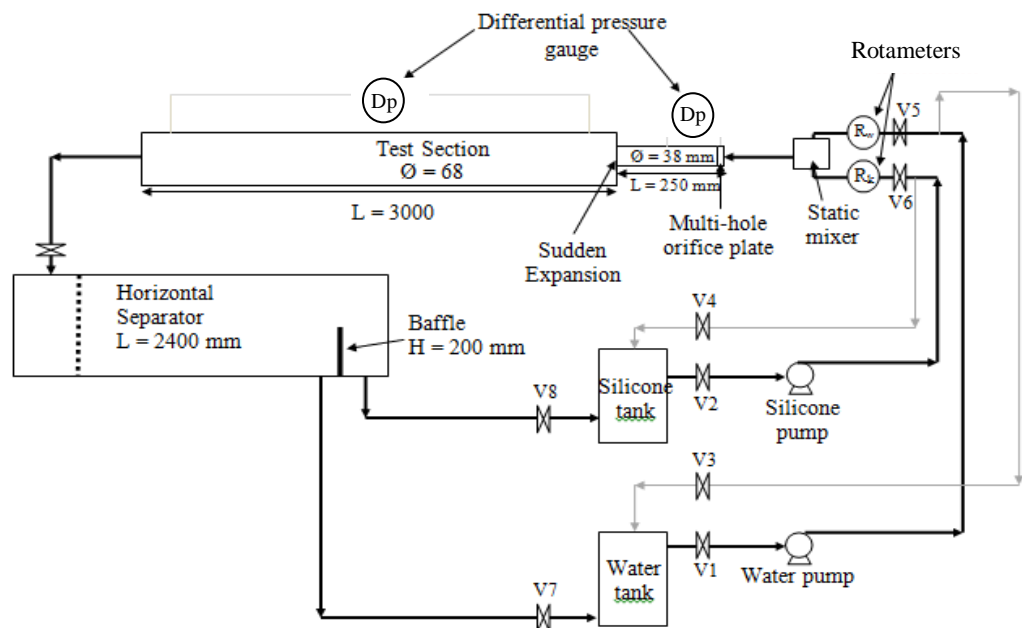


Figure 3.1: Schematic diagram B09/ R123 Multiphase flow inclined liquid-liquid test facility (68mm)

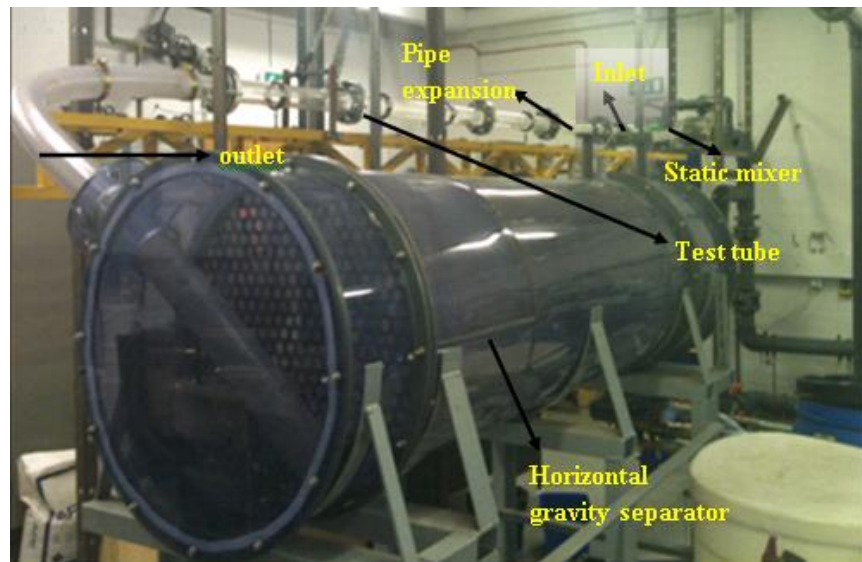


Figure 3.2: Photograph, B09/ R123 Multiphase flow inclined liquid-liquid test facility (68mm)

3.2 Test sections

A diagram and photograph of the test section are shown in Figure 3.3. All section of the test section was manufactured from transparent acrylic pipe. This permitted the flow to be observed. These observations enabled the flow pattern and the transitions from dispersed to stratified with mixing interface or stratified flow to be determined. In addition, the observation section was a useful means of comparing the flows behaviour.

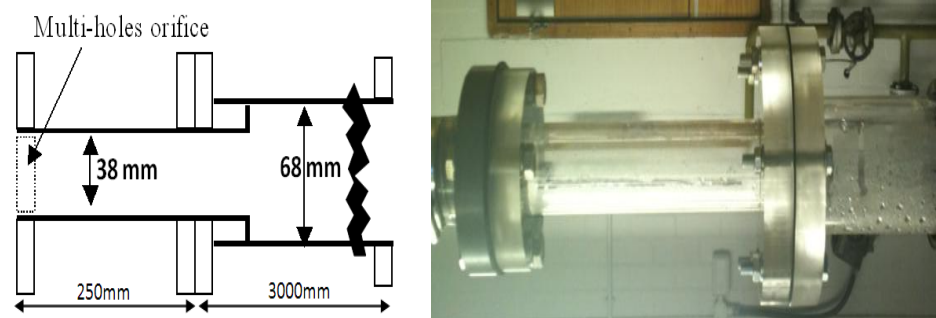


Figure 3.3: Cross-section and photograph of sudden pipe expansion

The test section consisted of a sudden pipe expansion from an internal diameter of 38 mm to 68 mm at the outlet. The total length of the test section was 3250 mm. It was mounted on a tubular steel frame hinged at one end, which permitted the small angles

of inclination maximum by $\pm 7^\circ$ to the horizontal. See Figure 3.4. These sections were joined with flanges with a rubber gasket providing a seal. A multi-hole orifice plate is positioned 250 mm upstream of the expansion to provide further mixing by accelerating of the flow through the orifice. Orifice plate with 32% open area was used in the present work. Made up of 18 holes of 5 mm diameter positioned as in Figure 3.5.



Figure 3.4: Test section mounted on a tubular steel frame hinged at one end, which permitted the small angle of inclination by $\pm 7^\circ$ to the horizontal

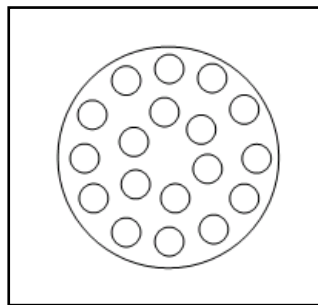


Figure 3.5: Plan view of multi-holes orifice plate { 18 holes (5 mm) = 32% orifice open area }

The oil volume fraction and drop size distributions were measured in special sections. A section of pipe was designed to allow the insertion of the Focused Beam Reflectance Measurement (FBRM) probe at 45° to the oncoming flow as shown in Figure 3.6.

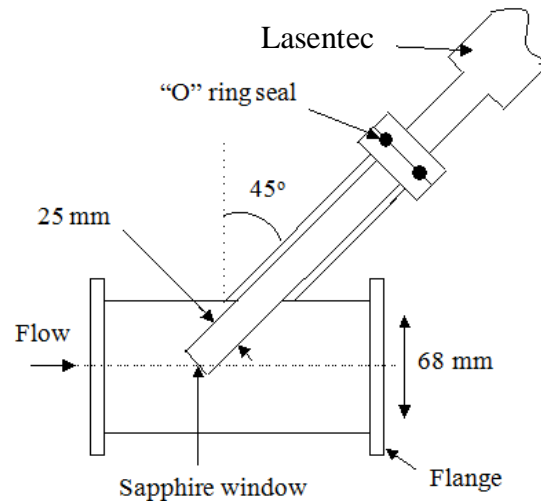


Figure 3.6: Cross-section of Lasentec FBRM pipe test section

This arrangement is necessary in order to minimise eddies near to the probe window which could cause the particles to stream past the window without being detected. This configuration was also designed to minimise droplet breakage at the point of measurement. With this design, any disturbance to the flow occurs after the detection point, downstream of the probe. The position of the FBRM was also adjustable. It could be positioned either on the centre-line, above or below which permitted coverage of the entire test section.

A tomographic technique, the Wire Mesh Sensor (WMS) was used to produce cross-sectional or ‘slice images’ illustrating the spatial variation in a one or more physical parameter based on sets of boundary measurements. Wire mesh sensor is chosen among them because it is a fast method for imaging the process dynamics. Though much used for gas/liquid flows the WMS has hardly been used for liquid-liquid two-phase flow. The WMS probe was installed at numerous positions along the test section by utilizing a special flange section made for the system. A photograph of WMS mounted on the test section was shown in Figure 3.7.

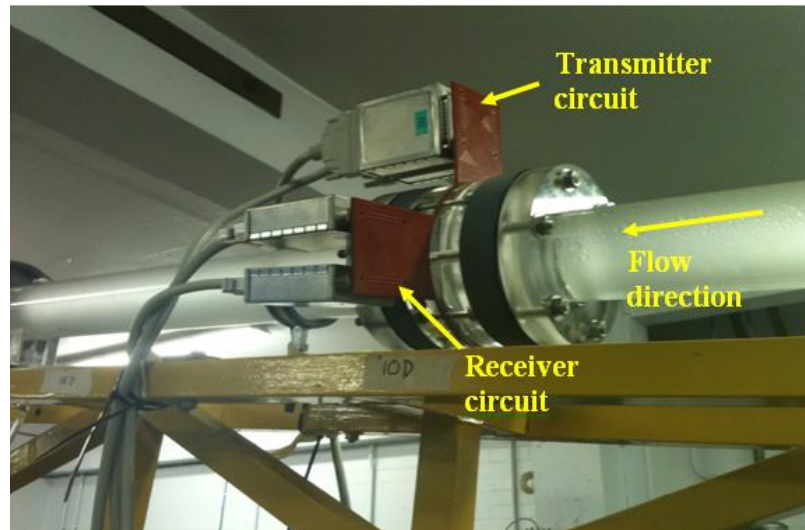


Figure 3.7: The capacitance wire mesh sensor (CapWMS) unit on experimental rig.

3.3 The separator and liquid storage tanks

The separator employed in this flow facility is a horizontal gravitational cylindrical vessel (internal diameter, 600 mm and length 2500 mm). The arrangements can be seen in Figure 3.8. The vessel was manufactured from clear uPVC and a perforated baffle was fitted at the inlet of the separator vessel to attempt to smooth the flow through the vessel. A weir of height 220 mm was placed at the outlet end of the vessel to retain the heavier liquid. Therefore, it's providing enough time for the heavier liquid to further settled and be fully separated. By manipulating the valve for each liquid, located at the bottom end of the separator, each phase was finally returned to respective storage tanks.

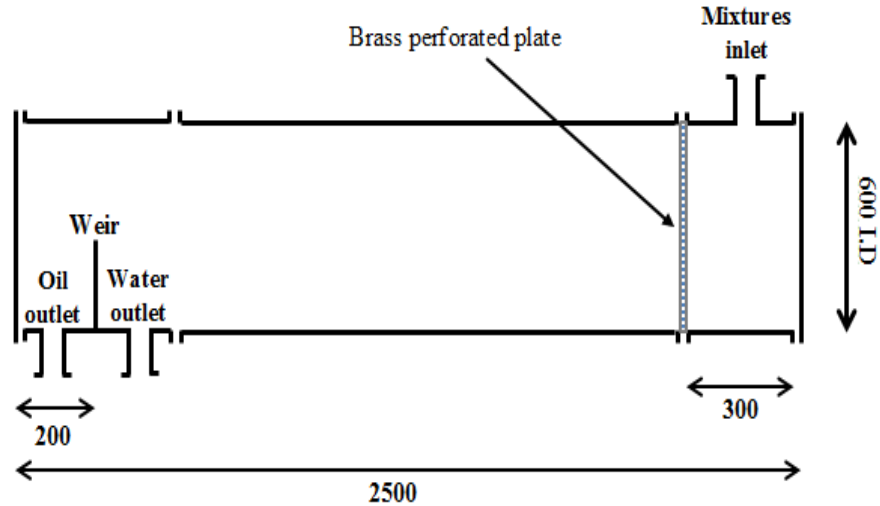


Figure 3.8: Diagram of separator vessel.

The water and silicone oil storage tanks can store 400 litres of water and silicone oil respectively. From the storage tanks, the liquids were fed to the flow facility by means of centrifugal pumps.

3.4 Metering and Control system

The main components of the metering and control system were pumps switch, rotameters, and adjustable butterfly valves. All of these components were manually operated as shown in Figure 3.9.

The liquids flow rates are relatively large, and consequently the velocities are rather high. In order to maintain a continuous fluid feed to the test section, it was decided to use series of storage tank for each liquid. Each series of storage tank can store approximately 400 litres of water and silicone oil respectively. The centrifugal pumps were connected to the tanks with 28mm copper tubing. Butterfly valves then are adjusted in order to get desire liquid flow. Since the pumps had a flow large capacity compared to the flow rates used during the experiments, the loops were also

provided with bypasses to the storage tanks. Butterfly valves were used to regulate the bypass flow. The two liquids (water and silicone oil) were supplied separately from then storage tanks by their own pump. The liquids were measured by variable area meters. Before they were combined at the inlet of the test section, a speciality designed static mixer was used to pre-mix the phases. The pipe was connected to the test section inlet by means of flexible hose and the mixture then flowed into the test section. On leaving the test section, the phases were separated in a horizontal gravitational separator. The outlet of the test section was connected to the separator by a flexible hose. Finally the oil and water returned to respective storage tanks.



Figure 3.9: Components of the control system.

In order to establish stable flow rate, before commencing any measurement, the system were allowed to run 5 times resident time of the acquired flow rate. The level of liquids in the storage tank was checked regularly before starting any experiment. It is important to know how much liquid is left in the tanks so that the operator can plan his experiment. The full operating procedures, including the emergency shut-down measures for the liquid-liquid flow rig are described in Appendix 3A.

3.5 Properties of fluids

Both accuracy and safety are the main important criteria in determining the selection of the physical properties of the fluids used in this study. After reviewing the liquids used by previous workers and balancing involved risks in using particular liquids and flow pattern information that could be obtained from the test fluids, silicone oil and deionised water were chosen for the present experiment. The values of the physical properties of the liquids are given in Table 3.1.

Table 3.1 Physical properties of fluids at 25°C

	Deionised water	Silicone oil, 5cSt
Density ρ (kg/m ³)	997	900
Viscosity η (kg/m.s or Pa s)	0.0010	0.0052
Refractive index	-	1.52045
Permittivity ϵ / m^-	710×10^{-12}	23×10^{-12}
Relative permittivity	79	2.7

3.6 Experimental approaches

In providing a reliable and good data on liquid-liquid two-phase flows through a sudden expansion mounted horizontally and slight inclined, a very thorough consideration has been given on the experimental approach of the study. The assessment of the factors affecting the evolution of phase layers downstream of the singularity was undertaken. The drop size distributions downstream of the expansion are more of a concern in this study due to the purpose of stratification of the dispersed flow by using expansion is considered.

There are two categories of factors affecting the evolution of drop size distribution through a sudden expansion, these which are linked to the rig configuration and others which are limited to the operational conditions.

Factors that are related to the rig configuration could be divided into three areas, which are the pipe orientation, the expansion ratio (the ratio of downstream to upstream pipe cross-sectional area) and the pipe lengths of both the upstream and downstream sections. Studies of the drop size distribution in horizontal pipes have been published by many researchers (Sleicher 1962; Ward and Knudsen, 1967; Collins and Knudsen, 1970; Swartz and Kessler, 1970; Kubie and Gardner, 1977; Karabelas, 1978; Simmons *et al.*, 1998; Angeli and Hewitt, 2000a; Angeli, 2001; Lovick and Angeli, 2004b). Almost all of these were for horizontal pipe. Only Lum *et al.* (2002; 2004; 2006) has reported the effect of upward or downward pipe inclination. Today, there has not many reports on the literature about the drop size distribution evolution through a sudden expansion for liquid-liquid flow and it is still left unsolved.

As for the operational conditions criteria, two factors have been identified. These are input oil fraction and mixture velocity for a given working system. In order to explore the transition of drop size distribution from the dispersed to the segregated flow through the expansion, the experiments were designed to distribute the dispersed regimes in the inlet of test section and expected stratified flow or stratified flow with mixing at the interface after expansion.

The mixture orifice velocity (U_{smo}) is a mixture velocity in the small diameter pipe (38 mm) after the perforated orifice. The downstream velocity is a mixture velocity based on the cross-sectional area of the larger diameter pipe (68 mm). The angle of inclination is the angle between the flow direction and the horizontal. A positive angle is an upward inclination and a negative angle a downward inclination. The range of the inclinations that are worth studying has been determined from calculations of the fully developed stratified flow using the model Taitel and Dukler (1976). The same prediction model was applied in Yang (2003) and Hasan (2006), and it gave a prediction of the position of the aqueous/ oil interface and has been shown to give an accurate prediction for horizontal flows. The result showed the effect of the angle of inclination which had a significant change over $\pm 2^\circ$ from horizontal and become quite small beyond $\pm 6^\circ$ (Taitel and Dukler, 1976).

A multi-hole orifice plate was used in order to produce the dispersed flow in the upstream pipe. The results of El-Hamouz *et al.* (1995) were used to estimate the drops expected. Their results showed that drop sizes increased by 20% when measured at 7 pipe diameters downstream and 40% at 38 pipe diameters downstream of a needle valve. The current study of sudden expansion was 7 pipe diameters downstream of a multi-hole perforated plate; therefore, it was expected that the drop sizes arriving at the sudden expansion would be those created by the perforated plate.

The choice of input oil fraction had been considered in a work by Shi *et al.* (2001) who studied the distribution of phases and velocity profile at the end of a 100 mm internal diameter pipe, 18 m long. They found that separation of oil/water flow was only possible for mixture velocities below 0.75 m/s and for input oil fraction between

20 to 80%. Furthermore, an input oil fraction of 60 to 70% was considered as water dispersed in an oil regime and below 50% was described as oil dispersed in a water regime. According to the flow pattern maps of Trallero *et al.* (1997), stratified flow occurs at velocities in which the order of magnitude is higher than those at the upper limit laminar flow. The limit of stratified flow was then considered as mixture velocity wherein this velocity is 0.2 m/s, and x1.5 and x2 higher. Their results had a good agreement with Shi *et al.* (2001). Based on these facts, the downstream mixture velocities chosen were 0.20 m/s, 0.30 m/s and 0.35 m/s which are x1, x1.5 and x1.75 higher.

In order to understand drop size evolution downstream of a sudden expansion, three positions of drop size measurement in a pipe cross-section were selected and images of phase distributions from WMS measurements were captured at number of downstream location. Details were discussed in subsection 4.2 and 6.2 (Experimental design) of chapters 4 and 6. A similar position of drop size measurement was also used by Simmons (1998) in dispersed flow and his results indicated that there was little effect in the size measured at these positions. Another reason for choosing these measurement positions relates to the interface profiles observed by Yang *et al.* (2003) in which they suggested making investigations between 2 and 35 pipe diameter downstream of the expansion, particularly at the interface between the mixed region and the oil or water region.

3.7 Instrumentation

The main instruments used in this study are rotameters, a differential pressure flow meter, laser backscatter and WMS. An overview of the concepts and operating principles of these are discussed in the following sections.

3.7.1 Rotameters

A rotameter is a device that measures the flow rate of liquid or gas in a closed tube. It belongs to a class of meters called variable area meters, which measure flow rate by allowing the cross-sectional area the fluid travels through to vary, causing some measurable effect. In this experiment, the flow rates of silicone oil and water were measured by individual rotameters. The calibrations of the rotameters were conducted by noting the fluid volume collected in the measuring tank in the flow rig over a time period for each fluid separately. Results of the calibration are as shown in Figure 3.10.

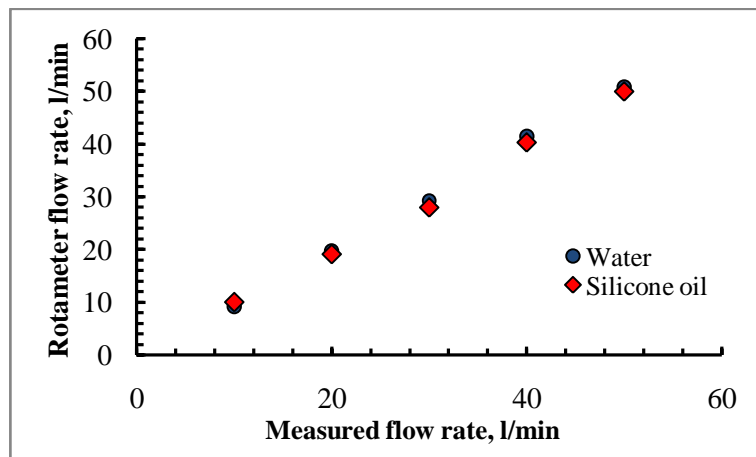


Figure 3.10: The calibration of water and silicone oil flowrates.

3.7.2 Differential pressure flow meter measurements

Differential pressure devices employ the Bernoulli equation to describe the relationship between the pressure difference and velocity of a flow. Many types of differential pressure flow meters are used in the industry. The differential pressure meter is used most extensively due to its simple installation, ease of use, instantaneous reading and reliable accuracy.

In this experiment, the flow rates of silicone oil and water mixtures were measured by D_p flow meters. The flow meters were placed at upstream of the inlet of the test section across the multi-hole orifice plate and on the test section itself as shown in Figure 3.11. The pressure drop across the plate was measured by electronic pressure transducers which were calibrated to convert the voltage generated directly into a pressure drop in mbar and displayed by digital meters.

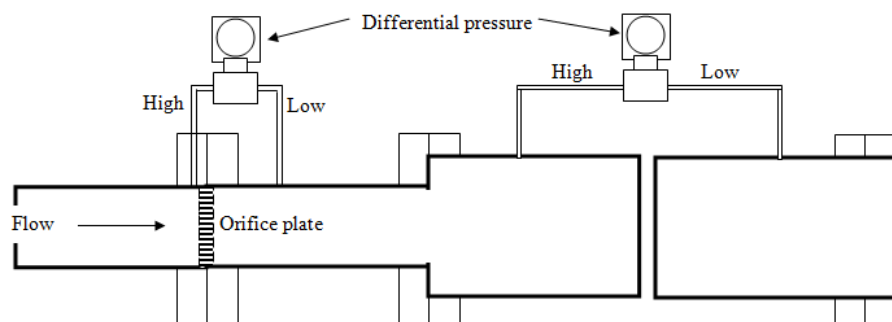


Figure 3.11: Schematic of differential pressure (D_p) flow meters engaged on the flow facility.

For studies on mixture flow rates there was a requirement to have a measure of the mixtures flow rates of the two immiscible liquids. In order to determine this information, the calibrations of differential pressure (D_p) flow meter were performed. These calibrations can be conducted by noting the fluids volume collected in the

measuring tank (separator vessel) in the flow rig over a time period and measuring the pressure difference across the orifice plate. Typical calibration of Dp cell shown in Figure 3.12 proved that flow rates of the rotameters are consistent for all of the mixture velocities.

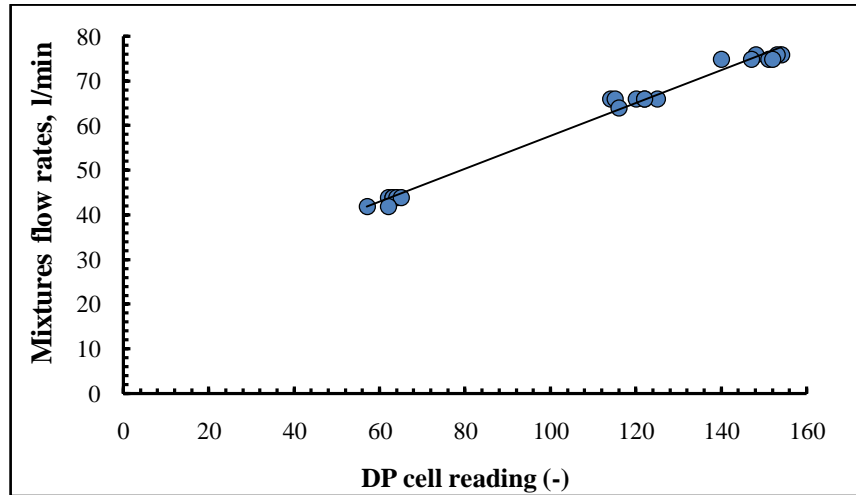


Figure 3.12: Calibration of mixtures flow rates with differential pressure flow meter.

3.7.3 Laser backscatter equipment

An in-situ focused beam reflectance measurement (FBRM), which utilises the laser backscatter techniques, was employed in this work. It is a commercial instrument; FBRM M500P manufactured by Mettler Toledo Inc. (former known as Lasentec Corp.) The Lasentec instrument composed of three major parts: a metal probe (the laser) which can be inserted directly into the process stream, the electronic field unit (EFU) that interprets signal for analysis and a computer for data acquisition as schematically shown in Figure 3.13.

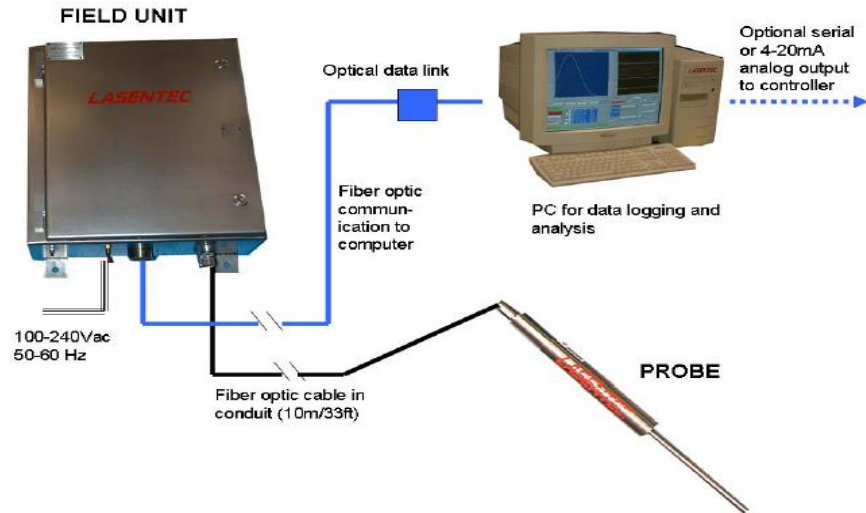


Figure 3.13: Typical diagram of laser backscatter system (Mettler Toledo)

3.7.3.1 Principle of Lasentec FBRM M500P

Figure 3.14 shows the simplified diagram of Focused Beam Reflectance Measurement (FBRM) operation. The external dimensions of the probe were a 24.8 mm diameter and a 318 mm length of stainless steel casing. Inside the metal probe, a solid-state laser emitting at 780 nm wavelength with 0.6 mW of maximum power. This gave it a Class 1 classification. A laser beam is generated in the EFU and sent to the probe via a fibre optic system. The laser beam travels through the probe and exits through the circular, sapphire window at the end the probe. It operates by scanning a high-intensity and sharply focused laser beam over the subject particle. It is focussed just in front of the sapphire window to a small beam spot. The light intensity at the focal point exceeds $2 \times 10^{10} \text{ Wm}^{-2}$. It then traces the probe circumference at a high speed (usually between 2 – 6 m/s) and measures the time duration back-scattered pulse of light. This means that particles can flow through the focal point at speeds of up to 2 m/s. When a particle starts to move past the window, a disruption in the focused ray of light is detected. As the particle moves through the laser beam, the resulting backscattered light is gathered and converted to an electronic signal by the

EFU using a photo-detector which converts the light energy into an electric signal. Right after the opposite edge of the particle is reached, the backscatter of light ceases. A unique discrimination circuit is used to isolate the time period of the backscatter from one edge of an individual particle to its opposite edge. The period over which the backscatter signal was recorded is then multiplied by the scan speed. The result is then converted as distance, hence giving the chord length (Lasentec, 2007). The duration and frequency of signals are indications of particle chord length and counts, respectively. The chord length is defined as “a straight line between any two points on the edge of a particle or particle structure” (Lasentec, 2007).

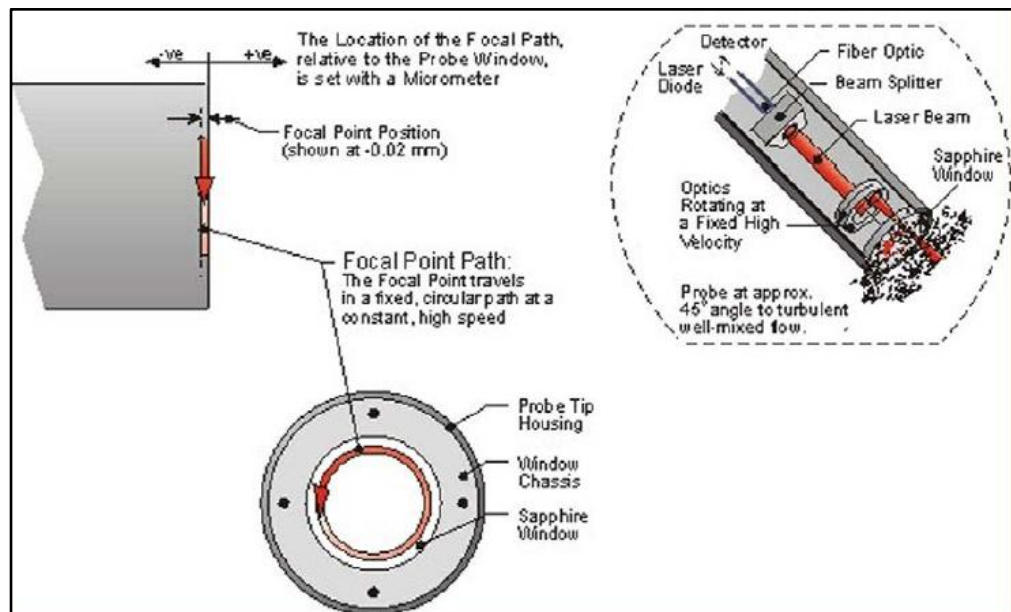


Figure 3.14: Focused Beam Reflectance Measurement, FBRM (Lasentec, 2007)

3.7.3.2 Verification of Lasentec FBRM M500P

As this study was confined to non-aggregated systems, only the F (fine) electronics data were presented. The focal point at the time of purchase was set to few microns (external face of the window) as calibrated by the manufacturer (Lasentec). As the instrument was last used 2 years ago, it needs to be re-calibrated to maintain the integrity of the FBRM. The focal point position of the FBRM device was re-

calibrated according to the *Windows Reference Procedure*. Consequently, the signal of the device was validated with the PVC standard following the *PVC Reference Procedure*.

PVC reference procedure is a means of verifying proper calibration of Lasentec FBRM instrumentation. It is recommended that the procedure be performed regularly. Lasentec recommends that the PVC reference sample included with shipment of the FBRM M500P be analyzed at regular intervals (i.e., monthly, quarterly, etc) as deemed appropriate by the user. The PVC reference procedure should be repeated every time routine maintenance is completed, prior to installing new software, or if the Lasentec probe is transported or dropped.

The configuration and set-up of the FBRM instrument was made in the same manner it was when the initial reference sample output was recorded. FBRM probes were simultaneously trial with Bimodal PVC reference material. Suspensions of known beads (PVC reference samples) were stirred with special impeller at 400 rpm and presented to the FBRM probe. Generally the Particle Size Distribution of the PVC has a peak at around 100 micron and another close to 10 micron. The tip of the probe was positioned at 25 mm above the impeller to ensure optimal sample presentation. According to the manual, 30 second period of stirring was recommended and sufficient to disperse the beads.

The set up for the FBRM instrument during the PVC reference procedure is shown in Figure 3.15. The PVC reference procedure also requires measurement configurations in the Lasentec CI software to be set first and then a reference sample measurement

is taken. Results from the PVC reference experiments were compared to the initial reference sample data file as provided by with the FBRM instrument for this particular FBRM M500P to confirm the instrument repeatability. The FBRM reproduces the 100 micron peak relatively well but the peak at 10 micron (general ideal condition) is slightly shifted to 4 micron. Nevertheless, it was very good and in excellent agreement with the initial calibrated reference sample data file, PVC reference curve provided by the manufacturer for this particular Lasentec as shown in Figure 3.16. The PVC reference procedure (repeatability measurement) was observed at the different dates taken for the same parameters setting.

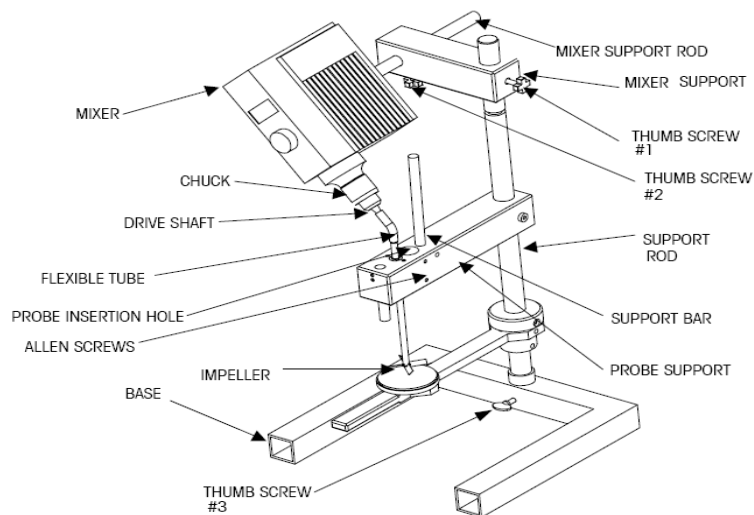


Figure 3.15: PVC Reference procedure set up (Lasentec, 2007)

Correct usage of the PVC reference sample assures instrument repeatability. The percentage different of the median and mean statistic must be within the specified limits, $\pm 2\%$ and $\pm 3\%$ respectively.

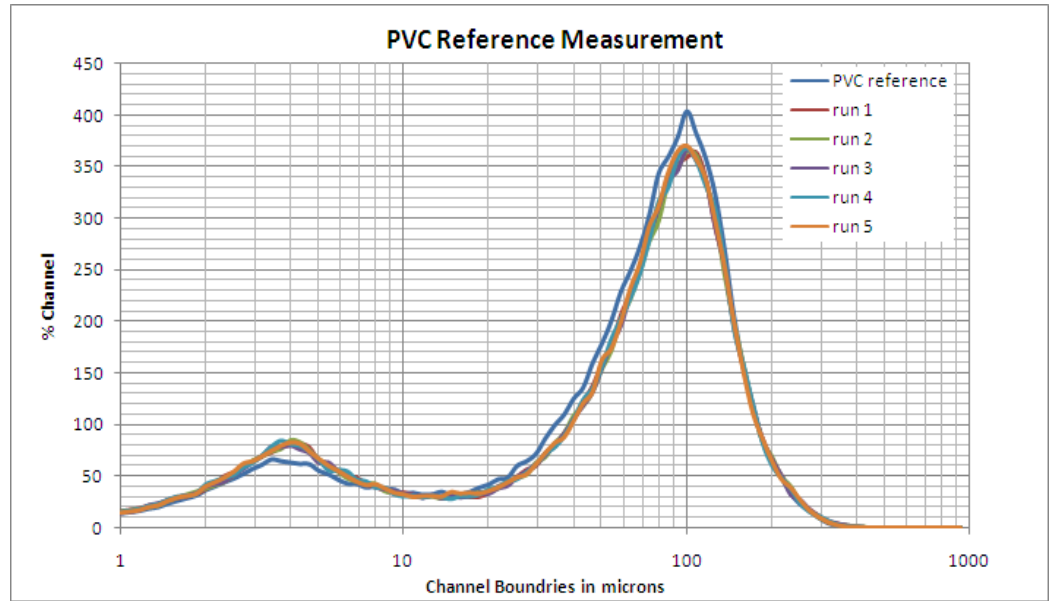
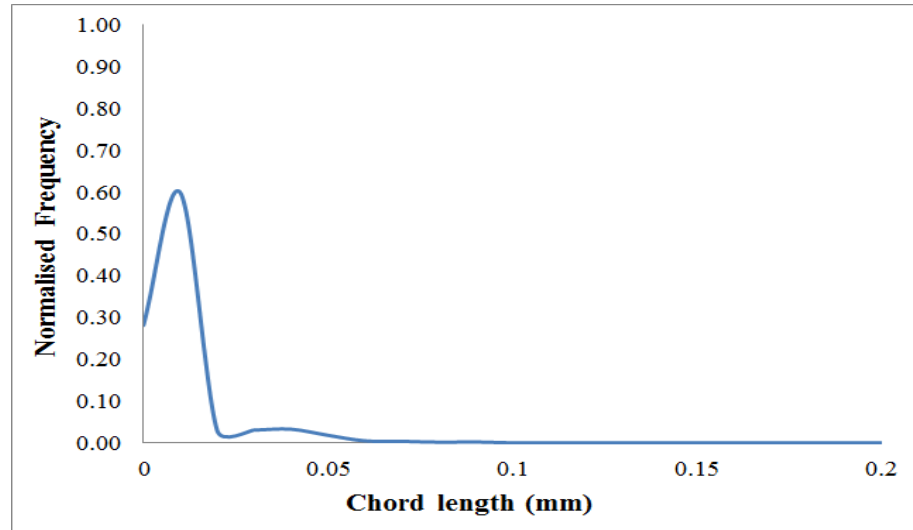


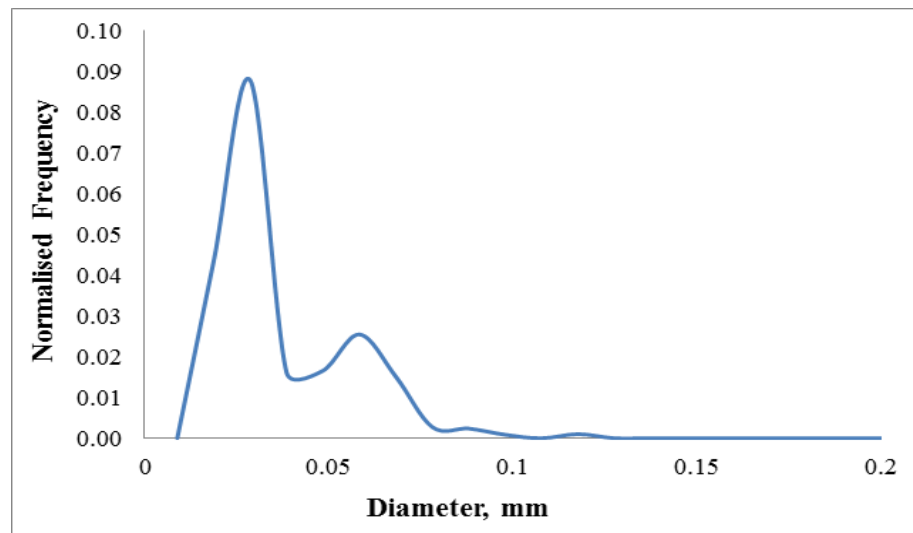
Figure 3.16: PVC reference calibration

3.7.3.3 Measurement of Drop Size

Measurements of drop size were made using Lasentec equipment (FBRM M500P) at the central axis of the test section and also 17 mm above and below at locations downstream pipe diameters from the sudden expansion. A continuous measurement was logged by a dedicated PC. The proprietary software was used to produce distributions of droplet chord. Subsequently, as reviewed in Chapter 2 there are a number of methods available to transform measured chord length distributions into drop diameter distributions. The PAM (version 2) of Langston *et al.*, (2001) was used to transform a measured chord length distribution (CLD) to a drop diameter distribution (DDD). Example of the CLD and DDD graphs as in Figure 3.17. Once the data has been converted to diameter distribution, normal equation (Eq. 2.2) was used to get Sauter mean diameter (SMD). In the material presented then, discussion will done using SMD.



(a)



(b)

Figure 3.17: Example of the (a) CLD and (b) DDD graph.

3.7.4 Capacitance wire mesh sensor (CapWMS)

The development of reliable hydrodynamic models for two-phase flows depends on the availability of accurate data of the phase distribution throughout the cross-section of the channel through which it flows. In gas–liquid systems, the distribution of the volumetric gas fraction has to be measured. Meanwhile in liquid-liquid system, the spatial distribution of the fraction of one of the liquids has to be measured. For this purpose, the spatial resolution must be in the range of the dimensions of the phases to

be detected. Further, the measuring volume must be well defined. Ideally, the extension of a tomographic sensor in the direction perpendicular to the measuring plane should be in the range of the spatial resolution. Last but not least, the measuring time for one complete image must be very short, in order to make it possible to measure instantaneous phase distributions.

Today gamma ray and X-ray computerized tomography were the widely used non-intrusive methods. The spatial resolution achieved is in the range of millimetres. The γ -ray tomograph developed by Kumar *et al.*(1995) and applied to a 260 mm diameter bubble column provides a resolution of 5 mm. A good example of X-ray tomography is given by Schmitz *et al.*(1997), who used a 360 kV X-ray source and 15 detectors to achieve a resolution of 0.4 mm. In both cases, the projections needed for the image reconstruction were produced by rotating either the sourcedetector assembly or the object. The scanning time is in the range of several minutes and it is not possible to measure instantaneous phase distributions.

An attempt to increase time resolution was carried out by Frøystein (1997), who uses a non-rotating configuration with 5 sources and 5 arrays with 17 individual detectors each. In this way, 5 projections are recorded simultaneously. The main factor limiting the resolution of such a configuration is the low number of projections available for the image reconstruction. This problem was solved by Hori *et al.* (1997) by applying 66 X-ray tubes, the electron beam of which is controlled by grids. The projections are produced in a successive order by generating short X-ray flashes. The entire measuring procedure for one frame takes 0.5 ms, i.e. all X-ray tubes flash within this period. The detector array consists of 584 CdTe crystals. Consequently,

66 independent projections are recorded within the measuring period of 0.5 ms. After the image reconstruction, this results in 2000 frames per second with a resolution of about 2 mm. These are by far the best results published up to now.

The main disadvantage of high-speed X-ray tomography is its high costs and also the requirement for shielding. Unfortunately, the much less expensive methods of electrical impedance tomography are not able to provide a comparable spatial resolution for some of the principal reasons. This motivated Prasser *et al.*(1998) to start the development of the electrode-mesh tomograph. The goal was to achieve a similar high-speed visualisation of transient gas fraction distributions in pipelines with a comparatively cheap device. The principle is based on the measurement of the local instantaneous conductivity of the two-phase mixture. The time resolution is 1024 frames per second. The developed signal acquisition circuitry guarantees the suppression of crosstalk between selected and non-selected electrodes. In this way the highest possible spatial resolution is achieved, which is given by the pitch of the electrodes. The sensor is available in two designs: (1) wire-mesh sensor for lab applications and (2) sensor with enforced electrode rods for high mechanical loads. The electrode rods of the second design are manufactured with a lentil shaped cross-section in order to reduce pressure drop over the sensor.

Local time varying void fractions were obtained by using the WMS (conductivity) measurement transducer. It is suitable for studies of transient two-phase flows, as well as for the instrumentation of industrial plants. In those cases, when an intrusive sensor is acceptable, the electrode-mesh sensor is an economic alternative to expensive X-ray or γ -ray tomographs. The design of this sensor formed the basis for

permittivity (capacitance) wire mesh sensor recently developed by Da Silva *et al.* (2007).

3.7.4.1 Design of capacitance wire mesh sensor (CapWMS)

The CapWMS consists of two parts, the acquisition sensor and the wires of the acquisition sensor (the mesh). The acquisition sensor that sits inside the pipe is connected with an electrical leads to an electronics box that collect and stores as raw data. An acrylic frame supports the sensor and allows fixation into the flow pipe section. Figure 3.18 shows an electrical schematic of the CapWMS. The design of the acquisition sensor for the capacitance WMS shown in Figure 3.19, consists of two parallel wire grids positioned orthogonally but offset by a small distance in the axial direction. One grid works as a transmitter while the other as a receiver.

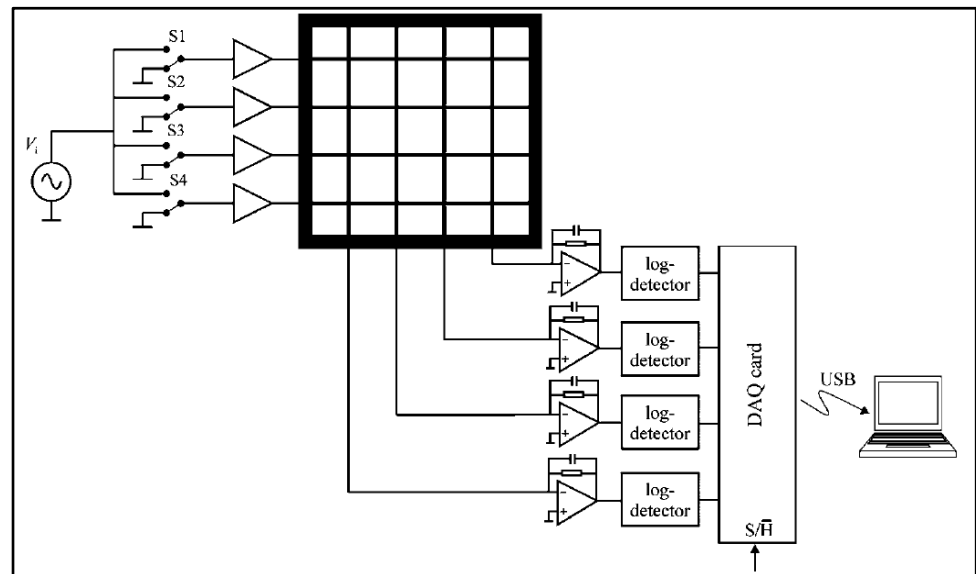


Figure 3.18: Electrical schematic of capacitance WMS (Da Silva *et al.*, 2007)

In the present study, a 24 x 24 wire configuration sensor was used that based on capacitance (permittivity) measurements. The sensor comprises two planes of 24 uncoated stainless steel wires of 0.12 mm diameter, 2.83 mm wire separation within each plane, and 1.35 mm axial plane distance. The pressure drop across the sensor is

small (approximately 3%), because the wires are evenly distributed over the circular pipe cross-section and are widely spread and only occupy 2-3% of the pipe cross-section. Therefore, they will not obstruct or stop the flow. Since the square sensor is installed in a circular pipe, only 440 of the total 576 wire crossing points are within the radius of the pipe. The spatial resolution of the images generated by the sensor is 2.83 mm, which corresponds to the wire separation within a single plane. Though the instrument can sample the entire cross-section at up to 5 kHz, data was acquired at a frequency of 1 kHz as this gave sufficient temporal resolution. Trials showed that a 10 second sampling period gave sufficient data for temporal resolution.

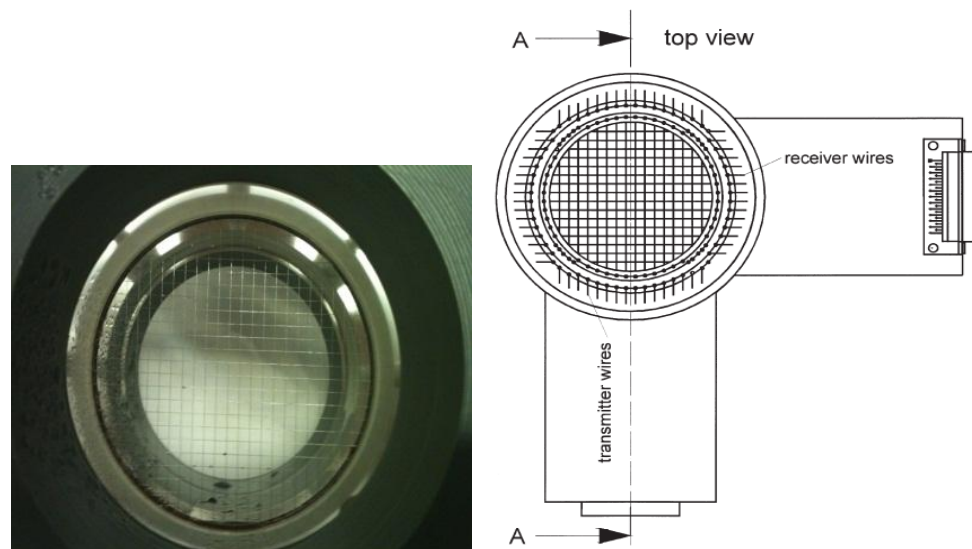


Figure 3.19: Capacitance wire mesh sensor 24 x 24 (Left) Sketch of wire mesh sensor (Right)

3.7.4.2 Principle of capacitance wire mesh sensor (CapWMS)

The principle of the sensor is based on two planes of wires, where one grid works as a transmitter while the other as a receiver. By activating each wire successively, the current at each crossing point is detected. During the measuring cycle, the transmitter wires are activated in a successive order while all other wires are kept at the ground potential. For each time frame, a transmitter wire is activated and all the receiver

wires are sampled in parallel (Da Silva *et al*, 2007a-c). Each crossing point of the transmitter and receiver electrodes is scanned individually, generating a matrix in the x-y plane depending on the size of the sensor. The local instantaneous void fractions are calculated from the measured capacitance between crossing points, a series of 2 dimensional data sets can be obtained. By reconstructing these sets in time sequence, a high speed visualization may be achieved.

3.7.4.3 Calibration and validation of CapWMS

As mentioned earlier in this chapter, this present work is the first attempt to adapt the usage of CapWMS to study two immiscible liquid flowing through pipe expansion in horizontal and inclined horizontal. Therefore, all the necessary precaution needs to be taken in account. Routine calibrations of the system is requires and it is conducted twice daily i.e. in the morning (before start any experimental measurement) and in the evening (after finishing the experimental measurement). In this work, routine calibration of the CapWMS was made on bench due to the difficulty in getting the test section fully occupied by the liquid. Especially, calibration for silicone oil which need to be done without any residual of air or water in the test section. The CapWMS sensor was submerged in one of the liquids i.e. water or silicone oil in a piece of the test section. The liquid was left for appropriate period to settle down before starting to take calibration measurement. A 30-second period of measurement was found to be sufficient for the calibration for each liquid. After each calibration runs, the CapWMS was rinsed with deionised water a few times, generally to ensures the meshes is kept clean before commence calibrations of the other liquid. However, fine droplet/droplets are sometimes remained to adhere to the wires. These droplets will influenced and affect the CapWMS calibration. Wire mesh cleaning was therefore

performed very thoroughly each time before starting any calibration. The images produced during the static calibration of the CapWMS shown in Figure 3.20, with high confidence level in the output of CapWMS instrument used.

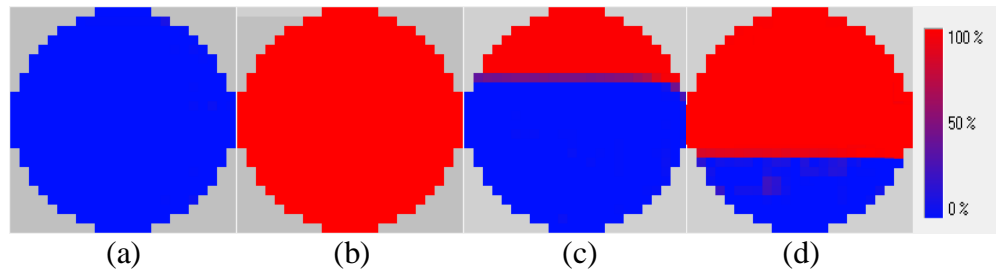


Figure 3.20: Tomographic images of water-oil in horizontal pipe. (a) water only, (b) silicone oil only and (c) oil volume fraction 0.4 (d) oil volume fraction 0.6.

3.7.4.4 Determination of Oil Volume Fraction

The relative volume occupied by oil in the two-phase flow is defined as *oil volume fraction* and it is also known as hold-up. Currently, there are several techniques for imaging the phase distribution in a pipe cross-section, as reviewed in Chapter 2. Wire Mesh Sensor is chosen among them because it is a fast method for imaging the dynamic of the processes.

CHAPTER 4

WIRE MESH SENSOR AND ANALYSIS

When two immiscible liquids flow together through a pipe, then they can distribute themselves in a variety of flow configurations. Therefore, prediction of oil-water flow characteristics such as spatial distribution and interface shapes are of significant importance.

The possibilities of using of Wire Mesh Sensor as a tool to imaging the spatial distribution across the pipe cross-section in liquid-liquid two-phase flows have been reviewed extensively in the previous chapters. Thus in that chapters, the fundamental concept of wire mesh sensor is briefly described. This included the design of sensor and calibration of sensor system for oil-water system.

A new 24 x 24 capacitance sensor has been developed. With this, cross section oil-water distribution images of the spatial distribution and interfaces curve were obtained at the various flow conditions for horizontal and small inclination angles. In addition, this is the simplest and fastest procedure capable of real-time operation in dynamic two-phase flows.

The prescription of the free interface configuration in gas-liquid and liquid-liquid systems is of importance in a variety of equipment and processes. Of particular importance is the interface curvature in two-phase flow systems. In stratified flow pattern, particularly when the viscosity ratio is high, the interface curvature and its influence on wetted areas may be of crucial effect on the flow pressure drop; for example, the performance of crude-oil/water transportation lines (Russell & Charles 1959; Charles 1960; Charles & Redberger 1962).

So far, stratified two-phase flow studies have assumed plane interface between the phases, which may be reasonable in gas-liquid (air-water) systems (Gemmell & Epstein, 1962; Wallis, 1969; Taitel & Dukler, 1976; Brauner & Moalem Maron, 1989; Hall & Hewitt, 1993). Previous studies, focusing on liquid-liquid two-phase systems, point out the need to account for phases wet ability properties and of the interface curvature in solving for the two-phase pressure-drop, in-situ holdup and the stability of the free interface (Russell *et al.*, 1959; Bentwich, 1964, 1976; Yu & Sparrow, 1969; Hasson *et al.*, 1970; Brauner & Moalem Maron, 1992(a), 1992(b); Barajas & Panton, 1993).

It is therefore, the objective of the present study to provide a predictive tool for determining the spatial distribution and characteristic interface curvature in two phase liquid-liquid systems. The prescription of the interface configuration is a basic input which is needed to further the modelling of two-phase flow problems in a variety of two-fluid systems (Brauner, 1996)

4.1 Wire Mesh Sensor Results

In several areas of liquid-liquid flow there are conflicts between the results obtained by some researchers. Most of these conflicts originate from the limitations in equipment and instrumentation. These limitations prevented the study of various phenomena deeper and the establishment of consensus on the subject. In response to reasons above and also the need for better understanding in liquid-liquid flow, ideas to study on application of tomography to internally diagnose the mixing and phase distributions within process units was developed. Tomographic techniques generally produce cross-sectional or 'slice images' illustrating the spatial variation in a one or more physical parameter based on sets of boundary measurements. Currently, there are several techniques for imaging the phase distribution in a pipe cross-section, as reviewed in Chapter 2. Wire mesh sensor is chosen among them because it is a fast method for imaging the process dynamics. Furthermore, WMS system has not been used for liquid-liquid two-phase flow. In other word, this is the first attempt to adapt the usage of WMS in such flow system. The purposes of this study are to explore and examine the ability of capacitance wire mesh sensor in imaging stratifying oil-water flow and each liquid in a background of the other at steady state.

4.2 Experimental Design

In order to explore the spatial distribution, variation of interfacial shape and waves evolution of a dispersed to segregated flow through sudden expansion, the experiments are designed to distribute the inlets conditions in dispersed regimes as many flow pattern encountered as possible within the rig and possible operational limits as shown in Figure 4.1. Three flows encountered for the inlets flows are Dw/o & Do/w, o/w and Do/w & w. All downstream flows in the expansion are designed to

distribute in the ST and ST&MI regimes. For a given condition set, the flow pattern evolution from a dispersed to segregated flow through the sudden expansion is along its oil volume fraction line as shown in Figure 4.2. It starts from superficial mixture orifice velocity (U_{smo}) and ends at a corresponding superficial downstream mixture velocity (U_{sme}) in the test section (expansion).

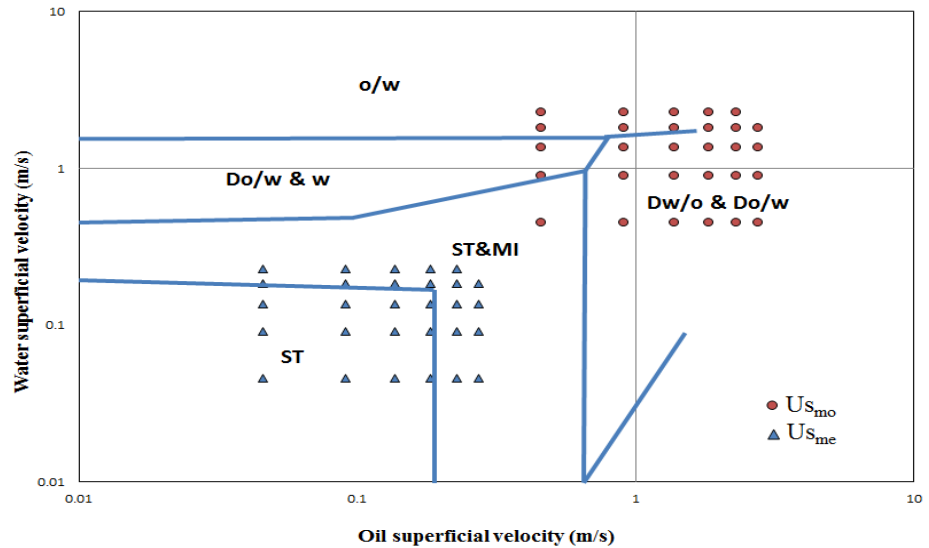


Figure 4.1: Mixture velocities after orifice (U_{smo}) and mixture velocities downstream (U_{sme}) of flow pattern encountered within the rig and possible operational limits plotted on flow pattern map of Trallero *et al.* (1997).

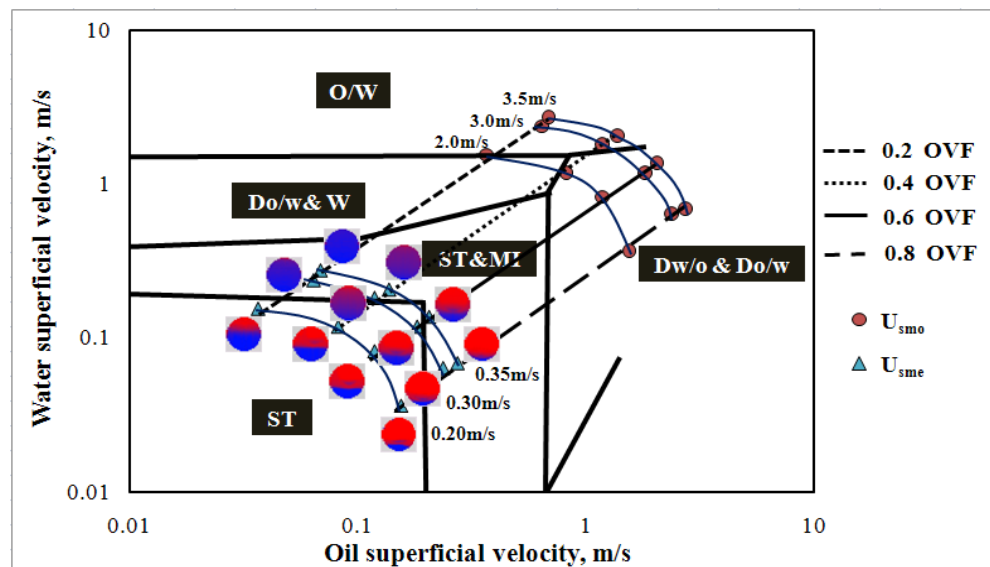


Figure 4.2: U_{smo} and U_{sme} of flow pattern transition through the system and WMS images plotted on horizontal liquid-liquid flow pattern map of Trallero *et al.* (1997).

All the experiments were carried out using CapWMS. Such experiments using CapWMS were the first time to be carried out in the oil-water flow system. Measurements were performed at three distances downstream of the expansion of 10D (near), 20D (middle) and 34D (far), where D is the internal diameter of the pipe (68 mm). Experiments were conducted for input oil fractions ranging from 0.2 to 0.8 OVF, orifice open area 32%, downstream expansion mixture velocities (U_{sme}) of 0.20, 0.30, & 0.35 m/s with a horizontal pipe or inclined at angles of +6, +3, -3 & -6 degrees. The CapWMS calibration method is applied in all experiments. The summary of the experimental conditions is given in Table 4.1.

A continuous measurement was then logged by a computer and allowed the proprietary software to produce volume fraction as shown in Figure 4.3. The data collection was carried out using a PC associated with data acquisition system and WMS equipment wherein the CapWMS was employed at locations along the test section (expansion pipe). This PC was utilised as a tool for data collecting and storage only. The raw data then analysed using copyrighted software supplied by the manufacturer to produce images of spatial volume fraction results. These data then was used for further data processing.

Table 4.1 Summary of Experimental conditions.

Input oil fraction (%)	Mixture orifice velocity, U_{smo} (m/s)	Downstream velocity, U_{sme} (m/s)	Angle of inclination	Orifice open area
20	2.00	0.20	+6°	32%
40	3.00	0.30	+3°	
60			0°	
80	3.50	0.35	-3°	
			-6°	

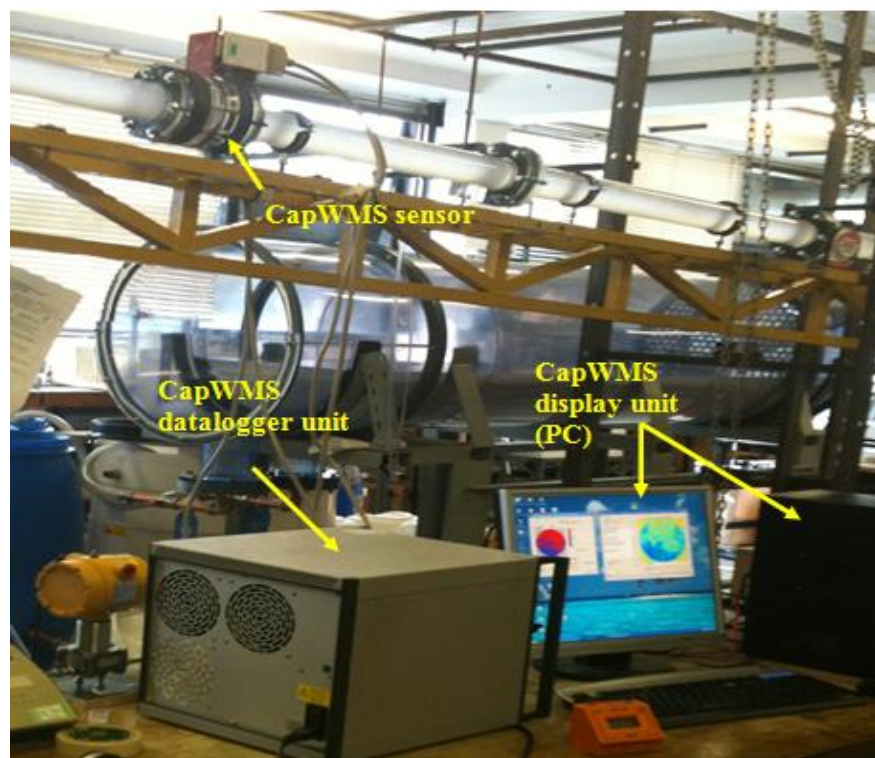


Figure 4.3: The capacitance wire mesh sensor (CapWMS) system on experimental rig.

4.3 Experiment results and discussion

According to the flow pattern map of Trallero *et al* (1997), all the downstream flow patterns in the expansion in the present study are in the segregated flow regimes, if they were fully developed horizontal flows. However, in real situation there are other factors assisting the flow segregation as discussed in details in Chapter 3. Input oil volume fraction (OVF) and the downstream superficial mixture velocity (U_{sme}) are among the factors that affect the phase layer evolution. In this section the flow development along expansion pipe and interface shapes of the singularity are to be recognised by data and images obtained from the CapWMS. Furthermore, the effect of the mixture velocity, oil volume fraction and distance from expansion are explored for the different pipe orientations. As well as explaining the relationship between the data and images captured with phase volume fraction distributions of oil-water flow established by previous researchers.

Many analysis of stratified flow assume that the interface between the phases is flat (Agrawal *et al*, 1973; Taitel and Dukler, 1976 and Hall, 1992). However actual interface may not be flat; there are, of course, interfacial waves in many cases, but even in time averaged sense, the interface may be curved. Interface curvature introduced by interfacial tension may occur in all two phase flow but it is likely to be most severe in case of liquid-liquid flow.

In this chapter, discussions were made based on the first interpretation of the CapWMS results to demonstrate the advantages of Wire Mesh Sensor, i.e., good in-line visualization capabilities due to its high resolution, providing reliable information across the full cross section of a pipe.

4.3.1 WMS results for horizontal pipe expansion

Figures 4.4 and 4.5 show the phase volume fraction in horizontally pipe flow at $10D$ and $34D$ measurement distance from expansion respectively, for downstream mixture velocity, 0.2 m/s . Figure 4.4 shows that at a downstream mixture velocity of 0.2 m/s , in water continuous flow at $10D$ distance from expansion the flow is semi-dispersed. However for $0.6 - 0.8$ oil input volume fraction, the separation layer started to evolved to a stratified with mixed layer at interface (ST&MI). Therefore, for a downstream mixture velocity of 0.20 m/s , a shorter pipe distance is sufficient for a flow to be developed to stratified mixed with layer at the interface (ST&MI).

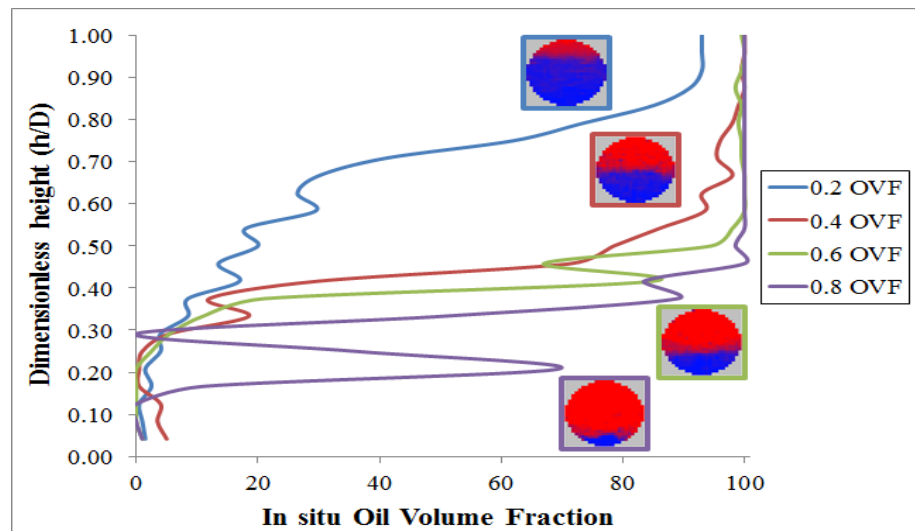


Figure 4.4: Oil volume fraction and phase distributions in a pipe cross section for distance from expansion $10D$, mixture velocity 0.20 m/s and horizontal flow, at different input oil fractions

Interestingly as demonstrated in Figure 4.5, for a downstream mixture velocity of 0.2 m/s at $34D$ distance from expansion, the layers of oil and water could be seen more clearly. At all input volume fraction at this flow conditions, the flow evolves to either stratified mixed with layer at the interface (ST&MI) or fully developed stratified (ST) regime.

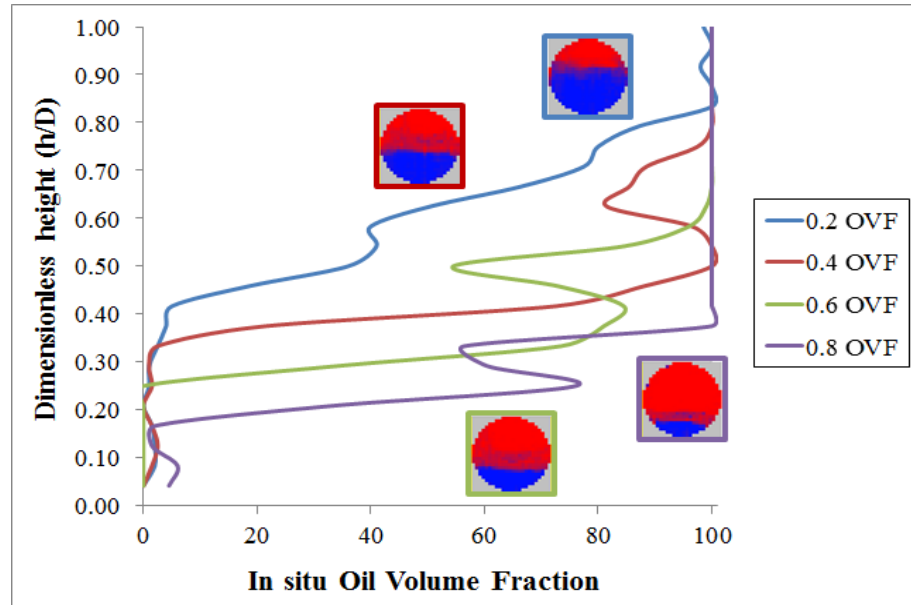


Figure 4.5: Oil volume fraction and phase distribution in a pipe cross section for distance from expansion $34D$, mixture velocity 0.20 m/s and horizontal flow, at different input oil fractions.

In order to associate the effect of downstream mixture velocity to the phase volume fraction along the expansion for horizontally pipe orientations flow, results from the CapWMS were presented as Figures 4.6 -4.7. As Figure 4.6 shows the liquids are homogeneous flow for a higher downstream mixture velocity, U_{sme} 0.30 and 0.35 m/s. At this point, the dispersed flows are well mixed, so that the oil and water velocities are similar. This confirms the results of Charles *et al* 1961; Martinez *et al.* (1988) and Soleimani *et al.* (1999a) who studied hold-up at the higher mixture velocity. However, for the downstream mixture velocity, U_{sme} 0.20 m/s, at $10D$ from expansion, it can be seen that segregation started to take place. The same phenomenon was also observed for 0.4 OVF as presented in Figure 4.7. Therefore, for water continuous flow, only at low downstream mixture velocity, the phase distribution is affected. It could be conclude that by increasing the downstream mixture velocity, the segregation process is diminished.

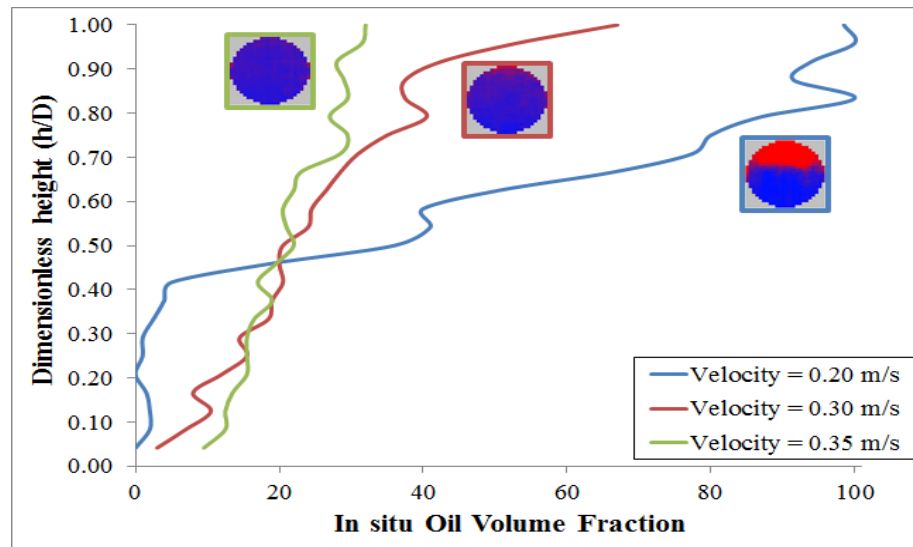


Figure 4.6: Oil volume fraction in a pipe cross section for distance from expansion $34D$, input oil fraction 0.2 and horizontal flow, at different mixture velocities.

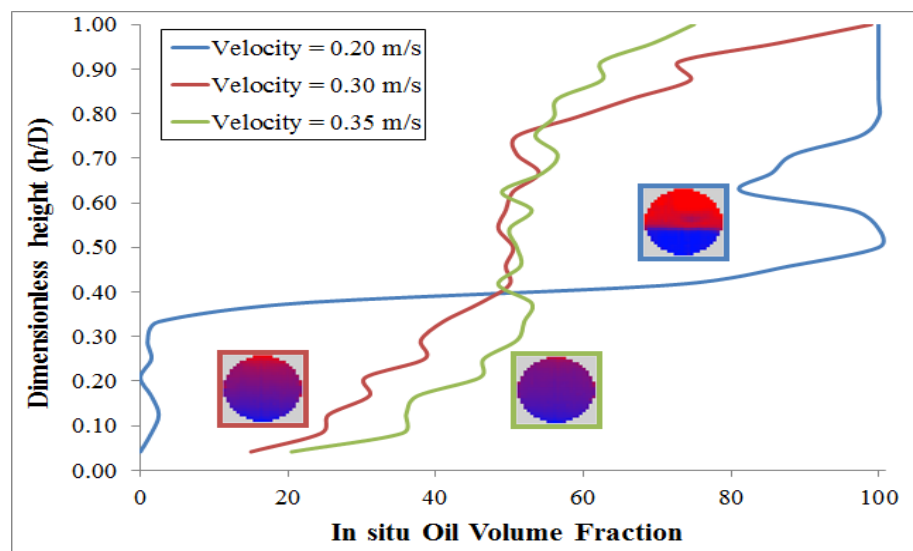


Figure 4.7: Oil volume fraction in a pipe cross section for distance from expansion $34D$, input oil fraction 0.4 and horizontal flow, at different mixture velocities.

As exemplified in Figures 4.8 and 4.9, at higher input oil volume fraction, downstream mixture velocity has minimal effect on the phase separation. Segregation of phases occurs at all U_{sme} . At higher downstream mixture velocities, U_{sme} 0.30 and 0.35 m/s, the flow is stratified with mixed layer at the interface. As for U_{sme} 0.20 m/s, stratified flow had been achieved.

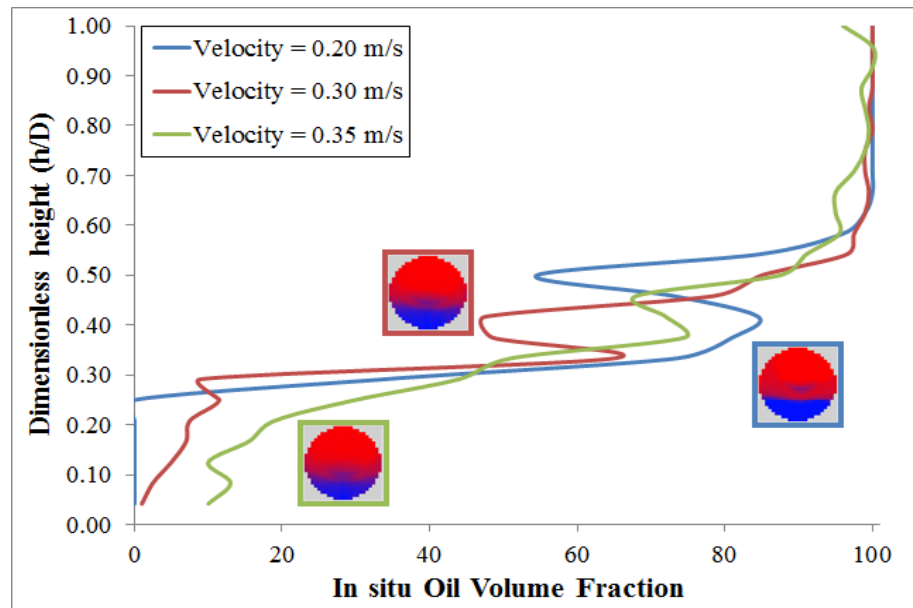


Figure 4.8: Oil volume fraction in a pipe cross section for distance from expansion $34D$, input oil fraction 0.6 and horizontal flow, at different mixture velocities.

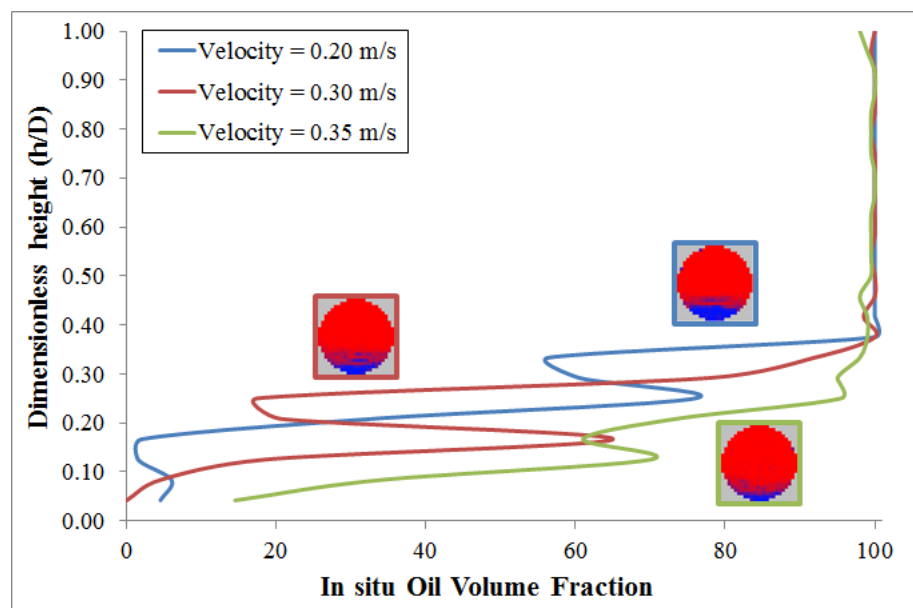


Figure 4.9: Oil volume fraction in a pipe cross section for distance from expansion $34D$, input oil fraction 0.8 and horizontal flow, at different mixture velocities.

The growth of oil layer at the top of the pipe cross section is constant as it moves toward the $34D$ (far position) as shown in Figure 4.10. At $34D$ distance from the expansion, the two liquids were clearly separated.

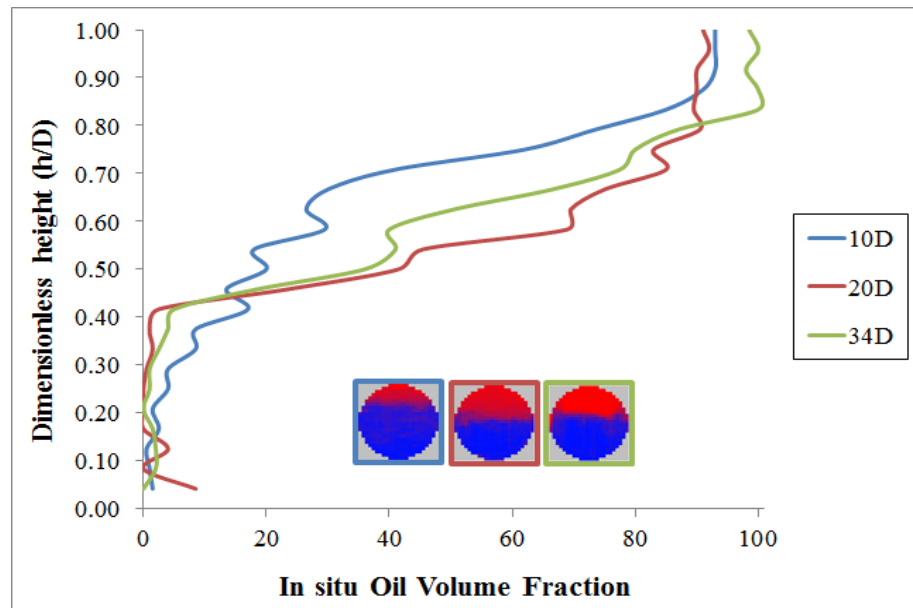


Figure 4.10: Oil volume fraction in a pipe cross section for mixture velocity 0.20 m/s, input oil fraction 0.2 and horizontal flow, at different distances from expansion.

With further analysis, the WMS images can be used to identify the development of the stratified (ST) or stratified mixed with layer at the interface (ST&MI) flow at the far position as resulted from dispersed flow at upstream expansion.

4.3.1.1 Interface Shapes and Waves – Horizontal pipe orientation

The interface shape for the stratified oil-water flow in horizontal pipeline can be classified into three types: namely plane horizontal interface, concave interface and convex interface as proposed by Brauner *et al.* (1996). Similar interface shapes were also reported using a high frequency probe and a gamma densitometer system (Soleimani *et al.*, 1999a; Angeli and Hewitt, 2000b; Lovick and Angeli, 2004; Lum *et al.*, 2006).

Figures 4.11 - 4.13 show the interface shapes of the flow downstream of the expansion at mixture velocity 0.20 m/s for different input oil fractions. It can be seen that at the nearest axial position (10D) from the expansion, the water interface (blue)

shapes are convex for water and oil continuous flow regime. However as for the oil interface (red) shapes, further increase the input oil fraction within the water continuous flow regime, the interface shape developed to concave shape. Whilst, for oil continuous flow regime, the oil interface shapes converted to convex with the increases of input oil fraction. With, 0.6 OVF is the transition from concave to convex oil interface as shown in Figure 4.11.

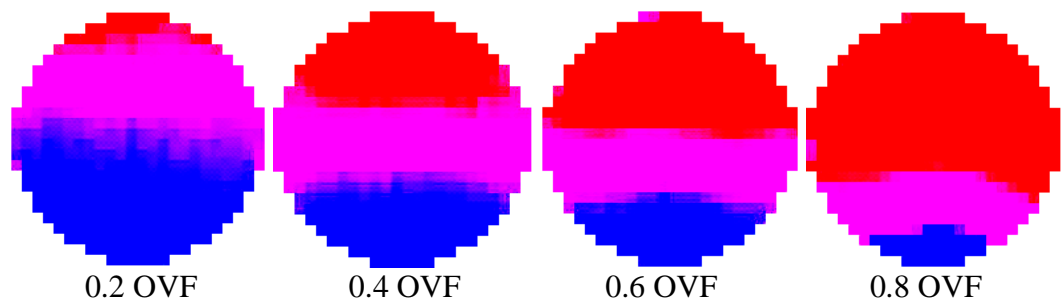


Figure 4.11: Interface shape for distance from expansion $10D$, mixture velocity 0.2 m/s and horizontal flow, at different input oil fractions.

Further downstream the expansion, at $20D$, due to segregation processes starting to take place, the interface shape changes as illustrated in Figure 4.12. Convex oil interface could be seen at the lower input oil fraction (0.2 OVF). Interestingly, concave oil interface were observed for the other input oil fractions at these position. Therefore, the present result is in agreement with Hasan (2006) and also confirms the results of Valle and Kvandal (1995), Soleimani et al. (1999a), Angeli and Hewitt (2000) and Lovick and Angeli (2004a). As for the water interface; for water continuous flow regime, the interfaces are convex, while for oil continuous flow nearly flat interfaces were observed.

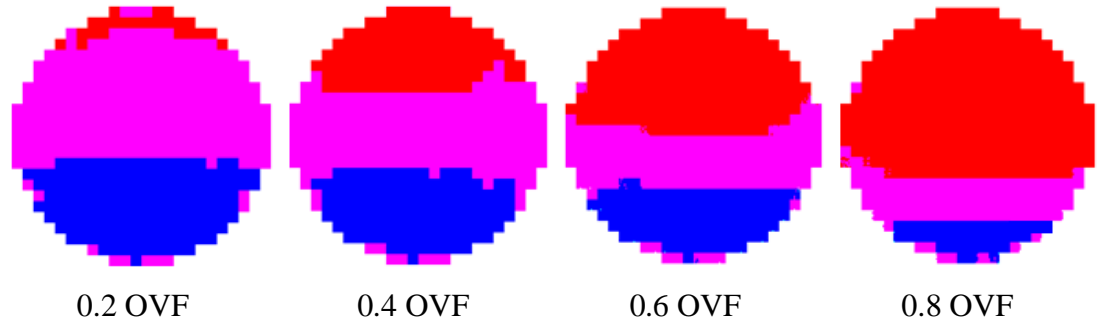


Figure 4.12: Interface shape for distance from expansion $20D$, mixture velocity 0.2 m/s and horizontal flow, at different input oil fractions.

Figure 4.13 shows the interface shapes at the farthest downstream of the expansion ($34D$), at 0.2 OVF, convex water interface could be seen. For the others input oil fraction, flat water interface shapes were detected. However, in oil continuous flow regime, the oil interfaces were flat shapes. In contrary, the oil interface shape for water continuous flow regime, particularly at 0.2 input volumes fraction is concave interface. Interestingly, the interface is convex for 0.4 input oil volume fractions, while it was initially concave in shape for the near ($10D$) and middle ($20D$) axial position of the expansion. It was observed this phenomenon is due to the influences of large oil drops layer flowing in the core of the pipe.

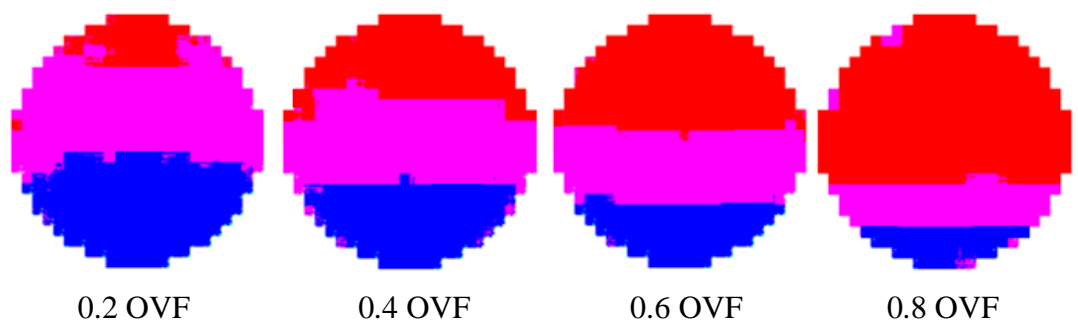


Figure 4.13: Interface shape for distance from expansion $34D$, mixture velocity 0.2 m/s and horizontal flow, at different input oil fractions.

As for the horizontal pipe orientation, there were no waves observed for all the flow conditions whether at the near or far axial position downstream of the expansion. In water continuous flow, the flow is dispersed flow. Increases the input oil fractions,

the dispersed flow at the near position developed to segregated flow. In general, $10D$ downstream the expansion, higher input oil volume fraction produces larger water drops dispersed in the mixed layer near to the water layer as shown in Figure 4.14.

At 0.2 input oil volume fractions, the flow was ST&MI flow whilst at an OVF of 0.4; large oil droplets were observed flowing in between the water mist and the water layer. Interestingly, at the far position, in oil continuous flow, 4 layers were observed i.e., oil- mixed layer-oil-water as shown in Figures 4.15. This probably occurring because the drops are coalescing due to the high concentration of drop at that zone, near to the interface. Also due to the velocity gradient which is affecting their ability to coalesce with the mass body of water. Furthermore, increase in oil fraction, the water mist layer becomes nearer to the water layer.

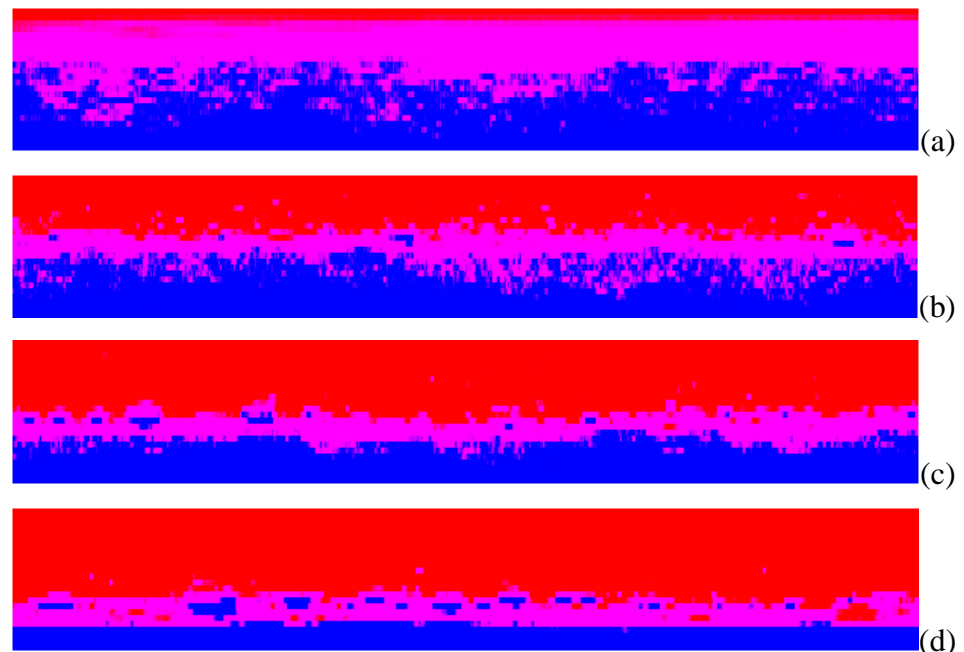


Figure 4.14: Spatial distribution for distance from expansion $10D$, mixture velocity 0.2 m/s and horizontal flow: (a) 0.2 OVF (b) 0.4 OVF (c) 0.6 OVF (d) 0.8 OVF.

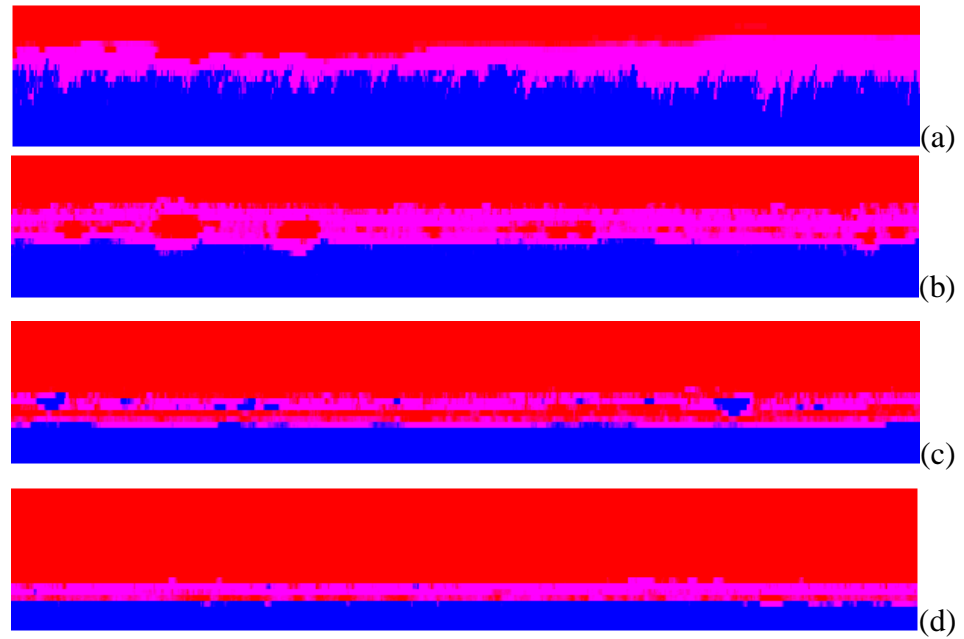


Figure 4.15: Spatial distribution for distance from expansion $34D$, mixture velocity 0.2 m/s and horizontal flow:(a) 0.2 OVF (b) 0.4 OVF (c) 0.6 OVF (d) 0.8 OVF .

4.3.2 WMS results for an upward inclined pipe expansion

The interface level decreased fairly as the input oil volume fraction increases when the orientation of the pipe is set to be upward inclination (Taitel and Dukler, 1976). Figures 4.16 demonstrated the spatial distribution in the pipe cross section at $34D$ distance from expansion, downstream mixture velocity, $U_{\text{sme}} 0.20 \text{ m/s}$ for $+6^\circ$ inclination from horizontal. It can be seen that these WMS images of phase volume fraction is in agreement with the prediction of the model of Taitel and Dukler (1976). Further, in present work, the input oil volume fraction was found to have minimal effect on the phase distributions at the near position but very strong influence at the far position for upwardly flow.

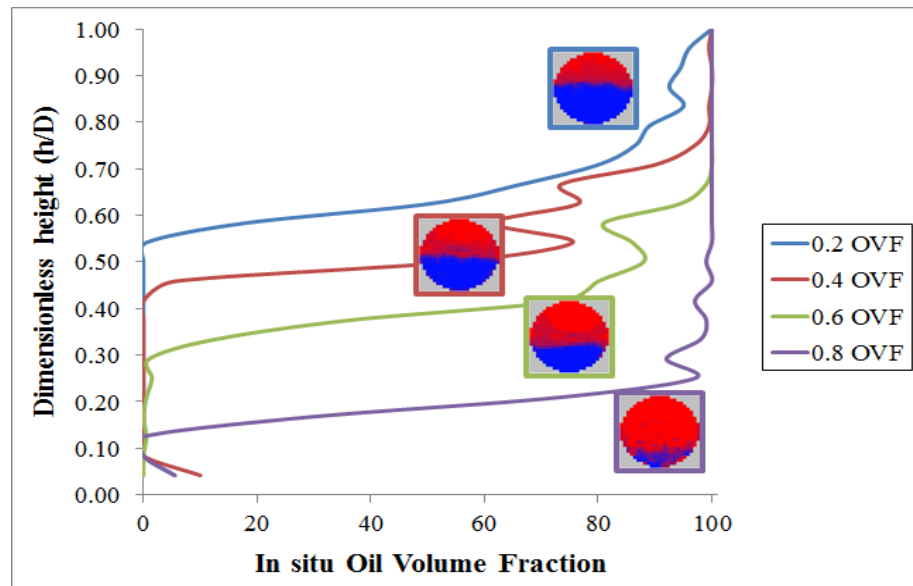


Figure 4.16: Oil volume fraction in a pipe cross section for distance from expansion $34D$, mixture velocity 0.2 m/s and $+6$ degree flow, at different input oil fractions.

The influences of downstream mixture velocities on the in-situ oil volume fraction downstream of the expansion for upward flow are presented in Figures 4.17 and 4.18. In water continuous flow, increases of the downstream mixture velocity, the oil phase layer that can be seen at lower U_{sme} gradually diminished. The transition of the flow is as shown in Figure 4.17. At higher U_{sme} , a fully dispersed flow was recorded.

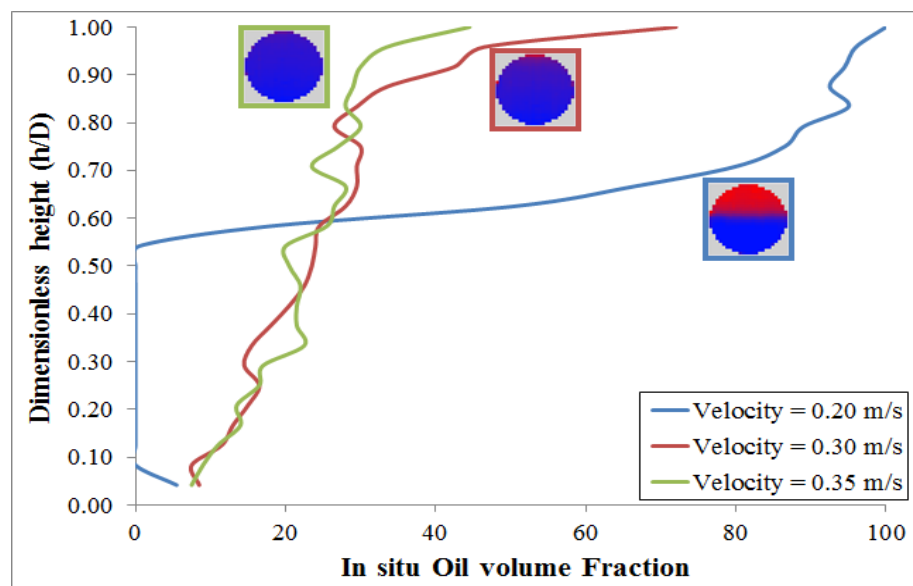


Figure 4.17: Oil volume fraction in a pipe cross section for distance from expansion $34D$, input oil fraction 0.2 and $+6$ degree flow, at different mixture velocities.

In contrary, oil continuous flow, the effect of the downstream mixture velocity on the in-situ volume fraction at 34D distance from expansion is different. Figure 4.18 demonstrate that for all downstream mixture velocity, segregation occurs.

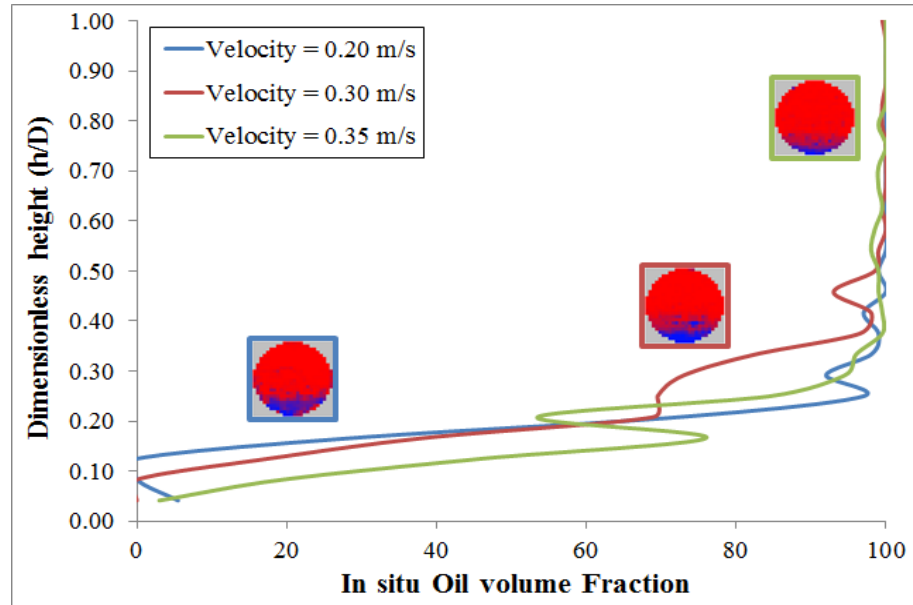


Figure 4.18: Oil volume fraction in a pipe cross section for distance from expansion 34D, input oil fraction 0.8 and +6 degree flow, at different mixture velocities.

The development of water layer is constant further downstream the expansion. Rapid change to the water level occurs beyond 10D downstream expansion as shown in Figure 4.19. Interestingly, the height of the water layer is higher (Figure 4.19) compared to the water layer of horizontal pipe orientation (Figure 4.10). Generally, it indicates that within +6° upward inclination angles, the lighter phase layer at the pipe top flows faster than the heavier phase layer that flowing at the bottom of the pipe. This is in agreement with the prediction of interfacial level with the model of Taitel and Dukler (1976) by Yang (2003). Further, in present work, the input oil volume fraction was found to have minimal effect on the phase distributions at the near position (10D) but very strong influence at the far position for upwardly flow.

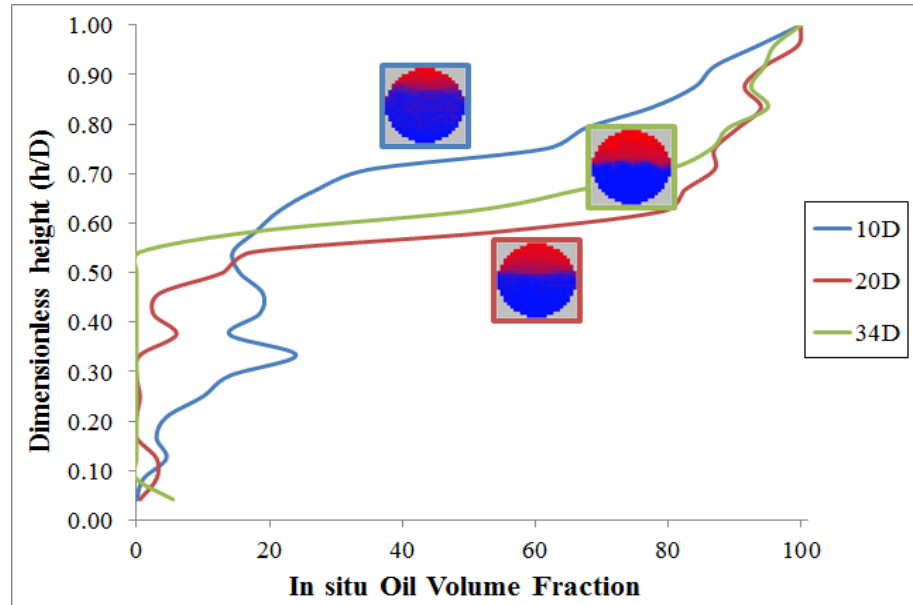


Figure 4.19: Oil volume fraction and phase distribution in a pipe cross section for mixture velocity 0.20 m/s, input oil fraction 0.2 and +6 degree flow, at different distances from expansion.

Conversely, flow pattern observed in +6° upward inclined pipe flows for high input oil volume fraction (0.8) at 0.20 m/s downstream mixture velocity (Figure 4.20), was stratified flow (ST). Nonetheless, for all the high downstream mixture velocity, 0.35 m/s at both +6° and +3° upward inclination, there are no clear oil and water interfaces occurring within the test section distance.

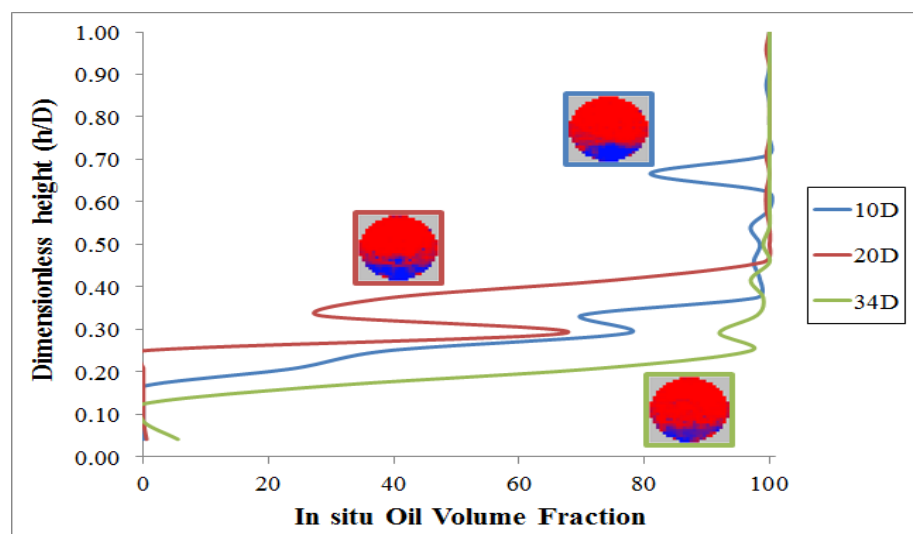


Figure 4.20: Oil volume fraction and phase distribution in a pipe cross section for mixture velocity 0.20 m/s, input oil fraction 0.8 and +6 degree flow, at different distances from expansion.

4.3.2.1 Interface Shapes and Waves – Upward pipe orientation

Figures 4.21 - 4.23 show the interface shapes of the flow downstream of the expansion at mixture velocity 0.20 m/s for different input oil fractions at upward pipe orientation. It can be seen that at the nearest axial position (10D) from the expansion, the water interface shapes for flow that have large ratio differences of the continuous and dispersed phase, are not clear. Meanwhile convex water interface were observed for 0.4 and 0.6 OVF. As for the oil interface, concave shapes developed as the input oil volume fraction increased as shown in Figure 4.21.

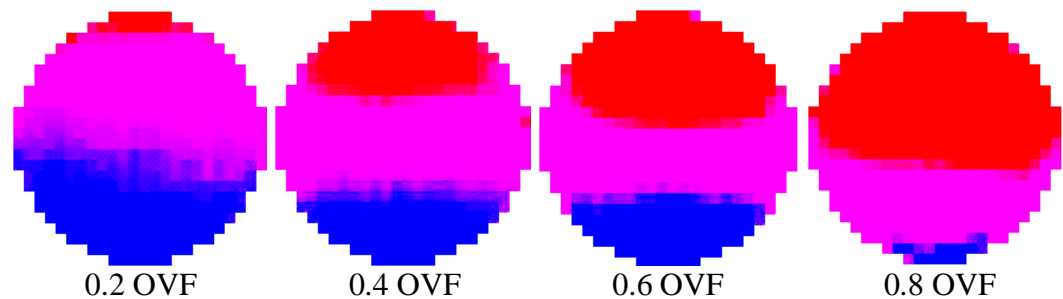


Figure 4.21: Interface shape for distance from expansion 10D, mixture velocity 0.2 m/s and $+6^\circ$ upward flow, at different input oil fractions.

As seen in Figure 4.22, concave oil interface remains seen at 20D downstream of the expansion for 0.4 and 0.6 OVF. Meanwhile, the oil interface starting to develop to convex interface at this distance from expansion. Interestingly, plane horizontal water interface were observed for the 0.2 input oil fractions at these position. As for the other OVF, water interfaces are convex, except for 0.8 OVF, no clear interface shapes were observed.

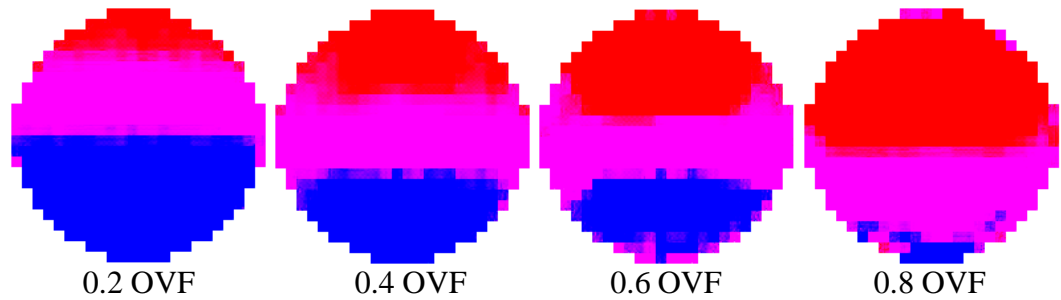


Figure 4.22: Interface shape for distance from expansion $20D$, mixture velocity 0.2 m/s and $+6^\circ$ upward flow, at different input oil fractions.

Figure 4.23 shows the interface shapes at the farthest downstream the expansion. The oil interface shapes are similar to Figure 4.22. The water interfaces were flat shapes for all input fraction except at 0.8 , where the interface shape is not clear due to the thin water layer.

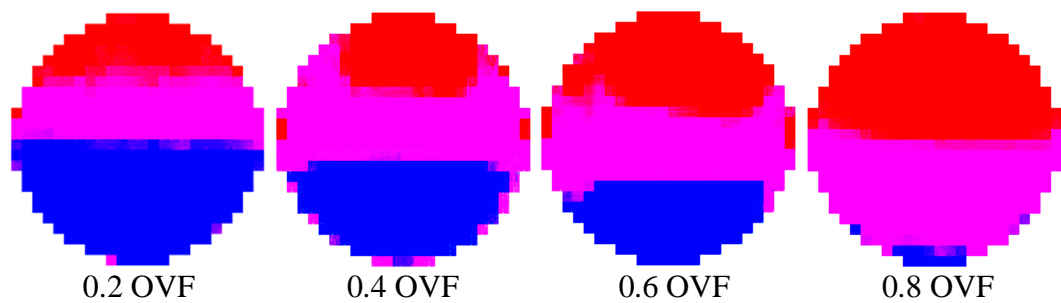


Figure 4.23: Interface shape for distance from expansion $34D$, mixture velocity 0.2 m/s and $+6^\circ$ upward flow, at different input oil fractions.

As for the upward inclined pipe orientation, due to the breakdown process of the dispersion, waves were observed at the interface between water and the mixed layer. The initial occurrences of waves were observed to be at the near axial position ($10D$) at all input oil volume fraction except at 0.2 OVF (Figure 4.24). However the breakdown process is more severe at 0.8 OVF. The amplitude of the waves is: $\sim 0.29D$ for 0.8 OVF; $\sim 0.22D$ for 0.6 OVF and $\sim 0.26D$ for 0.4 OVF. The higher the input oil volume fraction within its flow regime (oil continuous or water continuous), the larger the waves become. Subsequently, at the outlet end ($34D$), waves were only

observed at the highest input oil volume fraction (0.8) as in Figure 4.25 with amplitude of $\sim 0.37D$.

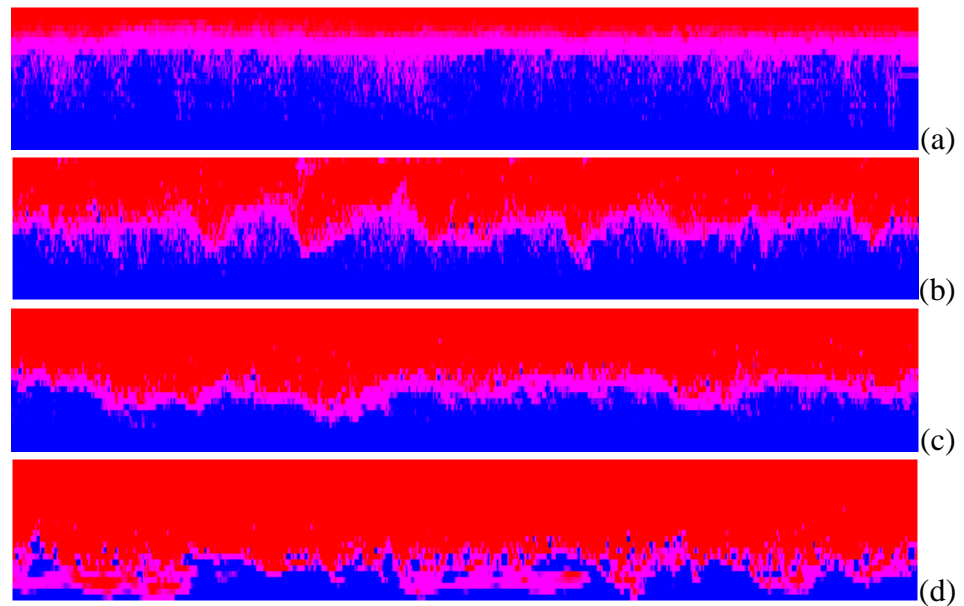


Figure 4.24: Spatial distribution for distance from expansion $10D$, mixture velocity 0.2 m/s and $+6^\circ$ upward flow: (a) 0.2 OVF (b) 0.4 OVF (c) 0.6 OVF (d) 0.8 OVF .

Similarly to what has been observed at horizontal pipe orientation, 4 layers phase also could be seen flowing in the upward flow for 0.4 and 0.6 OVF at this farthest axial position.

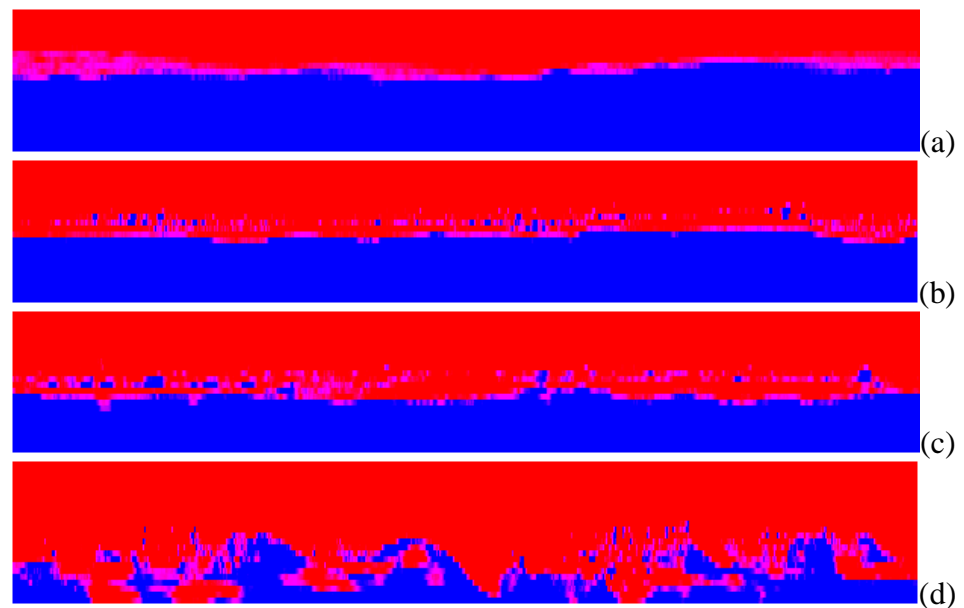


Figure 4.25: Spatial distribution for distance from expansion $34D$, mixture velocity 0.2 m/s and $+6^\circ$ upward flow, (a) 0.2 OVF (b) 0.4 OVF (c) 0.6 OVF (d) 0.8 OVF .

4.3.3 WMS results for a downward inclined pipe expansion

In this section, oil distributions in two-phase oil-water flow were measured for downward flow at the same experiments conditions as stated for upward flow.

Figures 4.26 demonstrated the spatial distribution in the pipe cross section at $34D$ distance from expansion, downstream mixture velocity, U_{sme} 0.20 m/s for downward inclined pipe orientation. It can be seen that these WMS images of phase volume fraction is in agreement with the prediction of the model of Taitel and Dukler (1976). Even though for 0.4 and 0.6 OVF, the interface level of water are about the same height. Interestingly, the thicknesses of water layer were found to be lower in downward flow compared to the other pipe orientations (horizontal and upward). This indicates water phase flows much faster than the oil phase. Thus, slower flows of an oil phase, the growth of the oil layer occurs much faster than the fast moving water.

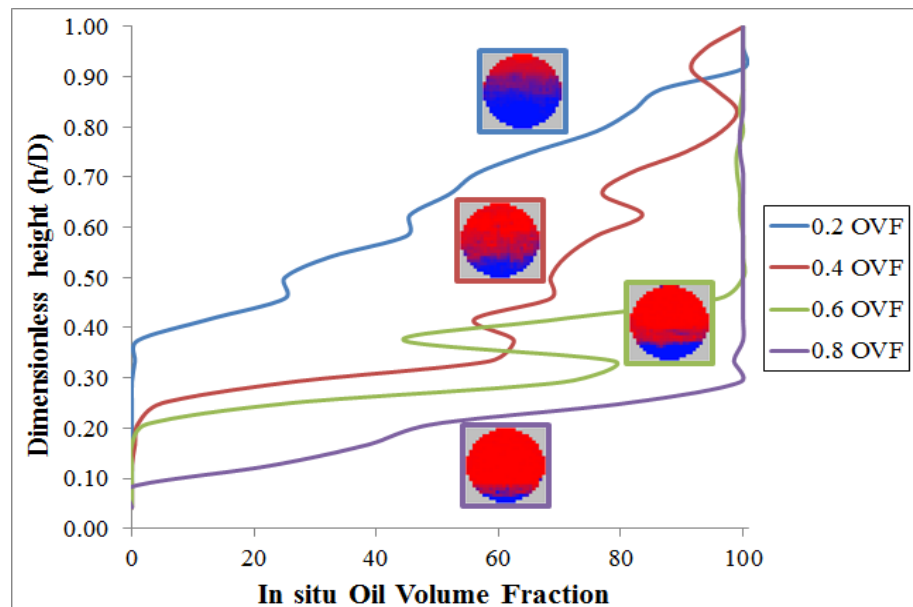


Figure 4.26: Oil volume fraction in a pipe cross section for distance from expansion $34D$, mixture velocity 0.2 m/s and -6 degree flow, at different input oil fractions.

As the inclination angle were decreased, at -3° downward flow, elevation of water layer at all OVF increases as demonstrated in Figure 4.27. However it is minimal as compared to the growth of the oil layer which accumulates rapidly at the pipe top due to the aforesaid reasons as in -6° flow conditions.

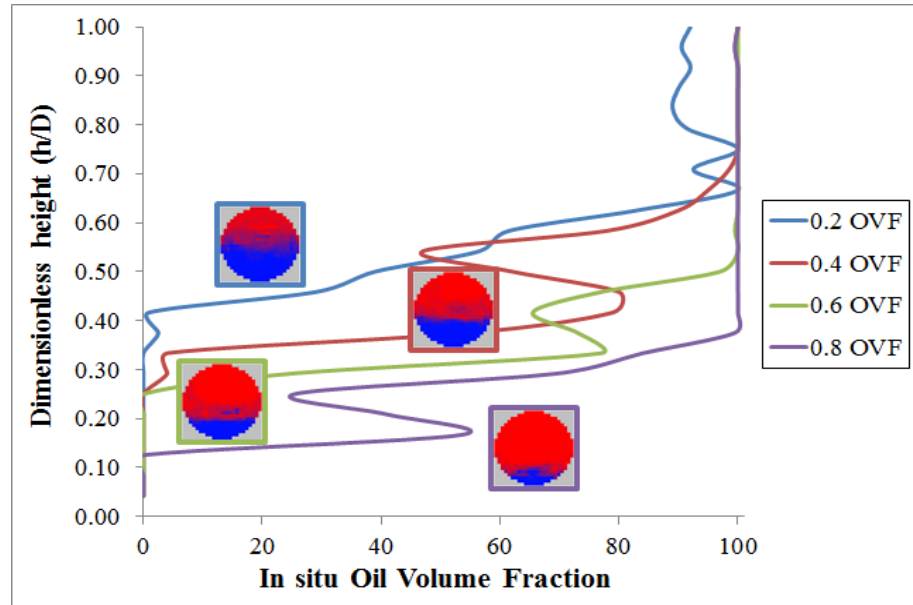


Figure 4.27: Oil volume fraction in a pipe cross section for distance from expansion $34D$, mixture velocity 0.20 m/s and -3 degree flow, at different input oil fractions.

Figure 4.28 shows the influences of downstream mixture velocities on the in-situ oil volume fraction in water continuous flow downstream of the expansion for downward flow. At lower U_{sme} , the mixtures flow was segregated, and at the farthest position downstream, clear oil layer at the pipe top and water at pipe bottom can be seen. The oil layer at the pipe top diminished as the mixture velocity increases due to this high mixture velocity and to the fast flow of the heavier layer, i.e., mixed layer in this case. Affecting the coalescence and settling process of oil droplets, hence no clear oil layer occurs within the test distance.

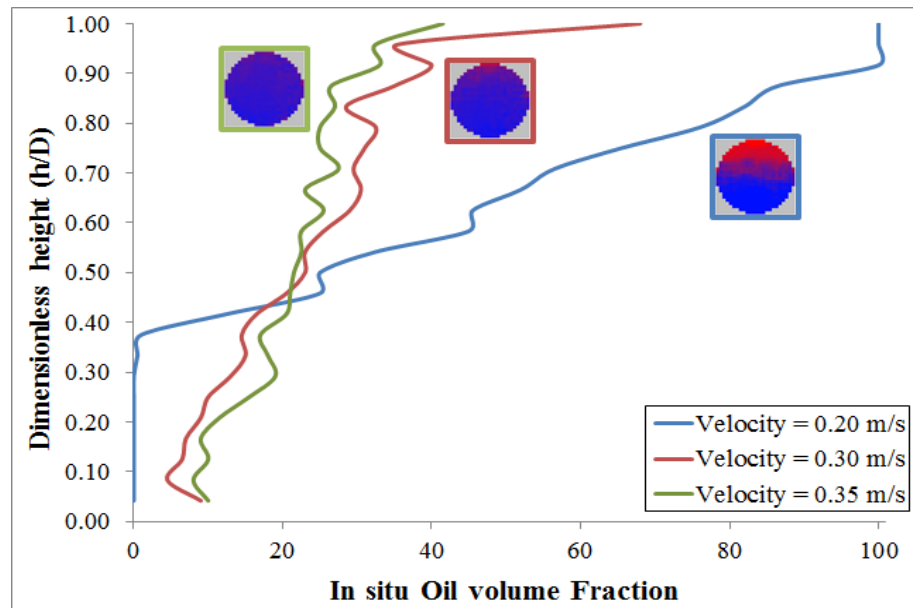


Figure 4.28: Oil volume fraction in a pipe cross section for distance from expansion $34D$, input oil fraction 0.2 and -6 degree flow, at different mixture velocities.

The effect of the downstream mixture velocity at $34D$ distance from expansion was further investigate, this time for an oil continuous flow as shown in Figure 4.29. Similarly, water layer could be observed flowing at the pipe bottom for low downstream mixture velocity. Yet, the layer is a thinner water layer. Increasing the downstream mixture velocity, the segregation process was delayed due to slower coalescence rate of the droplets in this higher turbulence intensity dispersion. Therefore, within the test distance, at the highest U_{sme} , water droplets were still dispersed. Hence, the thin water layers disappear.

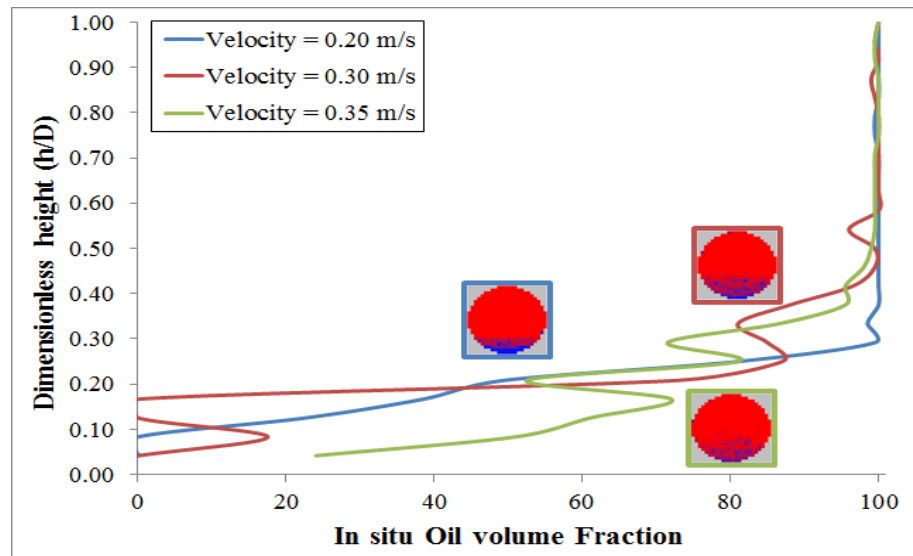


Figure 4.29: Oil volume fraction in a pipe cross section for distance from expansion $34D$, input oil fraction 0.8 and -6 degree flow, at different mixture velocities.

Influences of the distances from expansion on the volume fraction distribution for downward flow, results from the capacitance WMS were presented as Figures 4.30 and 4.31. In both water and oil continuous flow the development of water and oil layer is stable further downstream the expansion. Segregation has started occurring at $10D$ downstream the expansion. Therefore, in downward inclined flows, effect of distance from expansion on the oil volume fraction is minimal.

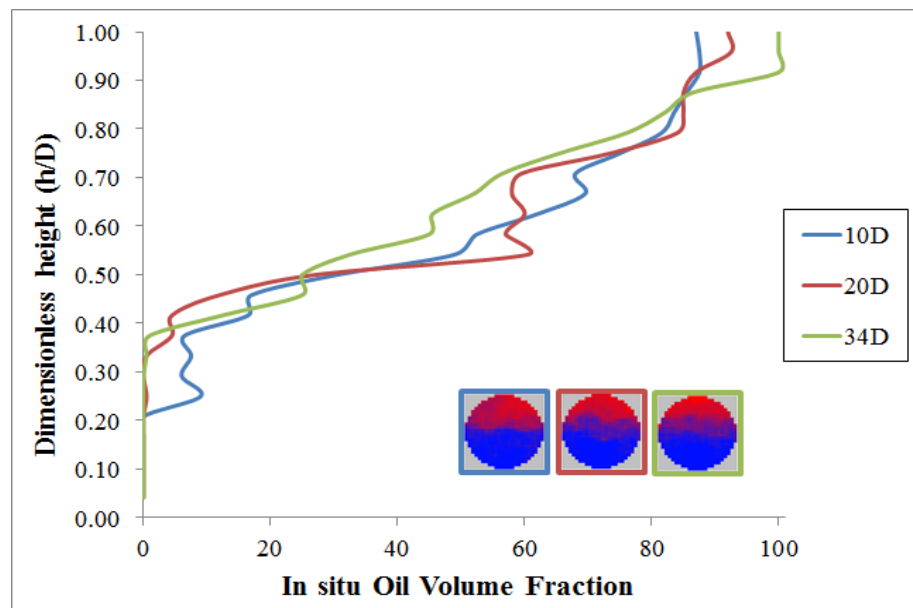


Figure 4.30: Oil volume fraction in a pipe cross section for mixture velocity 0.20 m/s, input oil fraction 0.2 and -6 degree flow, at different distances from expansion.

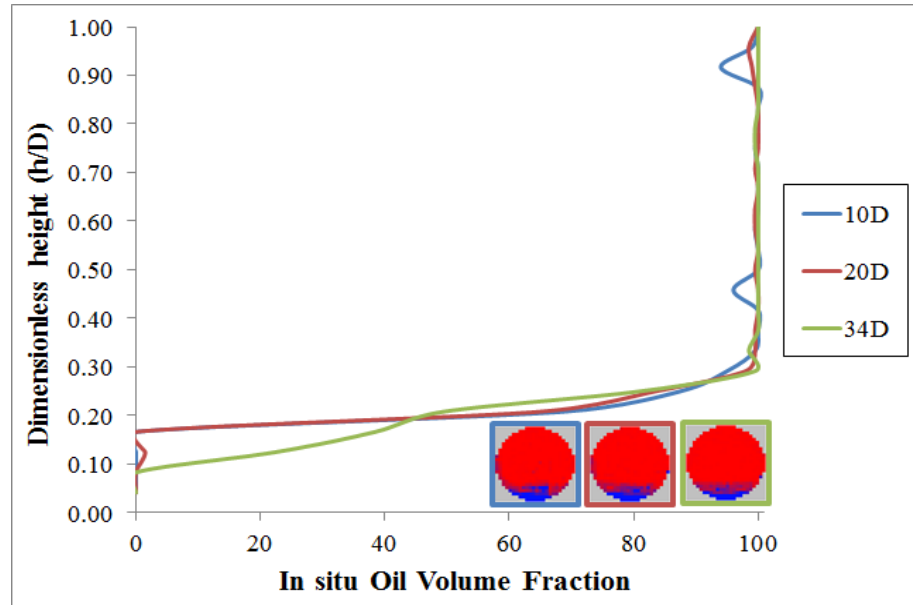


Figure 4.31: Oil volume fraction in a pipe cross section for mixture velocity 0.20 m/s, input oil fraction 0.8 and -6° flow, at different distances from expansion.

4.3.3.1 Interface Shapes and Waves –Downward pipe orientation

Figures 4.32 - 4.34 show the interface shapes of the flow downstream of the expansion at mixture velocity 0.20 m/s for different input oil fractions in a downward pipe orientation. At the near position, the water interface shapes are convex in both oil and water continuous flow regime as shown in Figure 4.32. However for mixture with lower ratio differences of the dispersed and continuous phase, i.e., 0.4 and 0.6 OVF, concave oil interfaces could be seen. In contrary, at 0.8 OVF, nearly horizontal shapes of oil interface appear at these near position whilst no clear interface layer could be seen at 0.2 OVF.

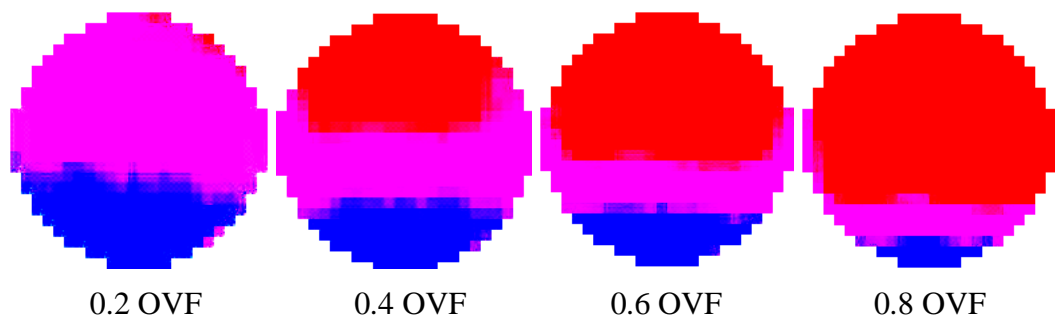


Figure 4.32: Interface shape for distance from expansion $10D$, mixture velocity 0.2 m/s and -6° downward flow, at different input oil fractions.

At the middle position of the test distance, 20D, similar oil interface shapes as at 10D occurs for 0.4, 0.6 and 0.8 OVF. This concave interface shape was also observed by Hasan (2006). Meanwhile, at lowest input oil volume fraction (0.2), due to segregation processes starting to take place, the oil interface shape evolves to convex shapes as illustrated in Figure 4.33. Interestingly, convex water interface seen earlier at 10D evolves to plane horizontal interfaces at these axial positions for all input oil volume fraction.

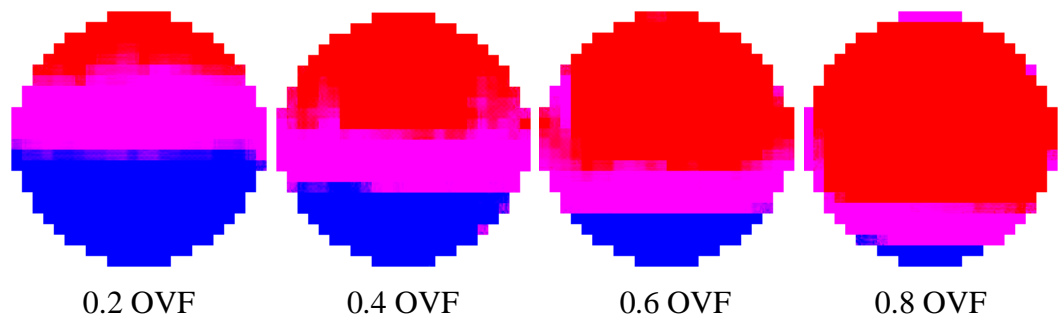


Figure 4.33: Interface shape for distance from expansion 20D, mixture velocity 0.2 m/s and -6° downward flow, at different input oil fractions.

Figure 4.34 show the interface shapes at 34D downstream the pipe expansion. At this position, segregation is clearly observed as the layer of oil and water are well distinguished. Besides, the water interface shape is plane horizontal at this position except at 0.8 OVF which is concave, due to the thin layer of water being pushed to the wall by the oil. Whilst, the oil interface shapes remains convex for 0.2 OVF and concave for 0.4 and 0.6 OVF. The oil interface evolves to plane horizontal for 0.8 input oil volume fraction.

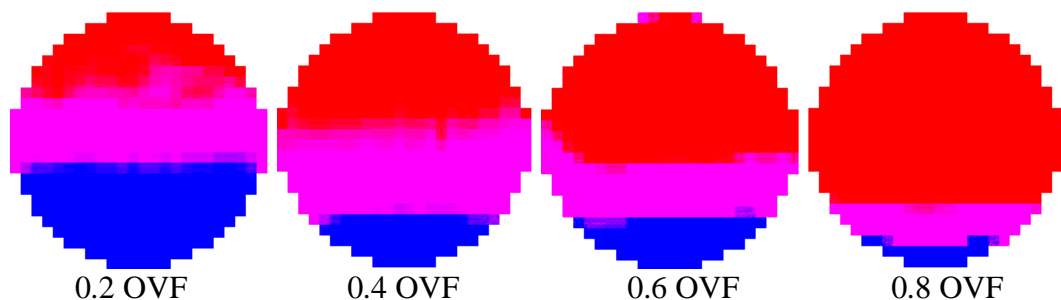


Figure 4.34: Interface shape for distance from expansion 34D, mixture velocity 0.2 m/s and -6° downward flow, at different input oil fractions.

As for the downward pipe orientation, there were no waves observed for all the flow conditions whether at the near or far axial position downstream of the expansion. In water continuous flow regime, the flow is ST&MI flow at 0.2 and 0.4 OVF. However, at 0.4 OVF, the mixed layer is more chaotic. Increases the input oil fractions to oil continuous flow regime, the ST&MI flow was observed as shown in Figure 4.35.

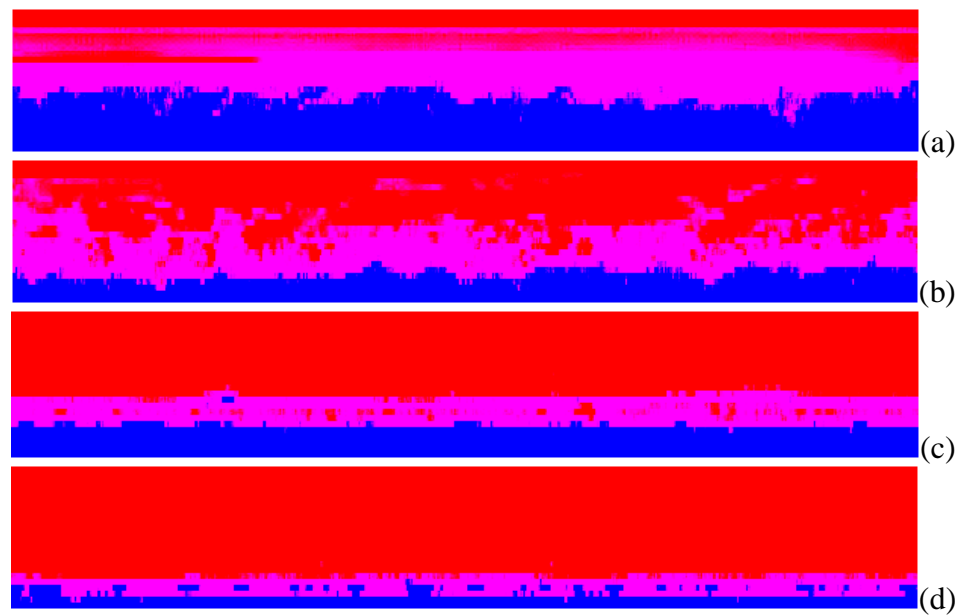


Figure 4.35: Spatial distribution for distance from expansion $34D$, mixture velocity 0.2 m/s and -6° downward flow:(a) 0.2 OVF (b) 0.4 OVF (c) 0.6 OVF (d) 0.8 OVF

4.3.4 Comparison between different angles of inclination

Figure 4.36 shows that the effect of the angle of the pipe inclination on the evolution of volume fraction layer at $10D$, downstream mixture velocity of 0.20 m/s for 0.2 input oil fraction. The stratified with mixed layer at the interface (ST&MI) flow pattern is developing at all of the pipe orientation. Interestingly, it could be observed that the thickness of water layer increases as the inclined angle increases during the volume fraction layer evolution downstream of the singularity. This phenomenon was also observed by Yang (2003). However, as it moves toward the far end of the test section, at $34D$ downstream the expansion, the flow pattern evolve to stratified

flow (ST) for horizontal and upward inclination pipe orientation. Whilst for downward pipe orientation, the flow pattern remains to be stratified with mixed layer at the interface (ST&MI) as shown in Figure 4.37. Furthermore, due to the low downstream mixture velocity, stratification of water has occurred at this axial position downstream the expansion (34D). As a result, the thickness of the water layer at this position is the same, even though the angle of the inclination was increases.

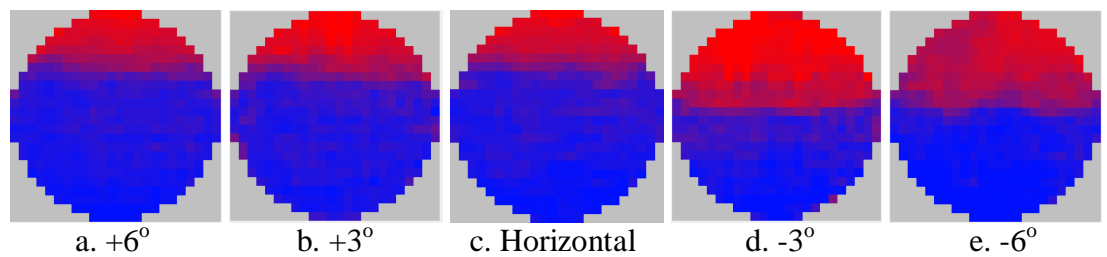


Figure 4.36: Phase distribution in a pipe cross-section for distance from expansion 10D, mixture velocity 0.20 m/s, input oil fraction 0.2 at different angles of inclination.

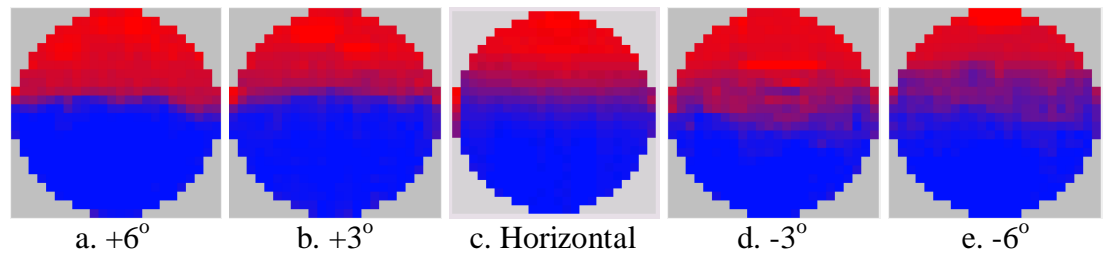


Figure 4.37 Phase distribution in a pipe cross-section for distance from expansion 34D, mixture velocity 0.20 m/s, input oil fraction 0.2 at different angles of inclination.

As for higher input oil volume fraction (0.8), Figure 4.38 shows the effect of the angle of the pipe inclination on the evolution of volume fraction layer at 10D, downstream mixture velocity of 0.20 m/s. In general, the same phenomenon as for lower input oil volume fraction occurred. For all angle of the pipe orientation, the dispersed flow evolved to stratify with mixed layer at the interface (ST&MI) flow. The thickness of water layer also increases as the inclined angle increases during the

volume fraction layer evolution downstream of the singularity as were also reported by Yang (2003). As for the volume fraction distribution at 34D downstream the expansion, the flow pattern evolve to stratified flow (ST) for horizontal and downward inclination pipe orientation. Whilst for upward pipe orientation, the flow pattern remains to be stratified with mixed layer at the interface (ST&MI) as shown in Figure 4.39. This occurrence is contrary to what happen in the lower input oil volume fraction system. The chaotic interface according to Yang (2003) is due to when the angle of inclination increase, the amplitude of the waves increases. Nonetheless, at the downward inclined angles, these waves dissipate quickly with very thin water layer. Hence, by visual observation (naked eyes) and data from WMS (Figure 4.1), segregated flow could be observed at these conditions as demonstrated in Figure 4.39 (d&e).

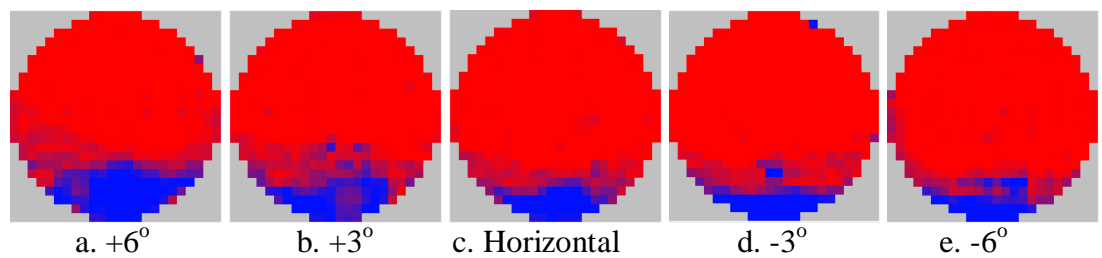


Figure 4.38: Phase distribution in a pipe cross-section for distance from expansion 10D, mixture velocity 0.20 m/s, input oil fraction 0.8 at different angles of inclination.

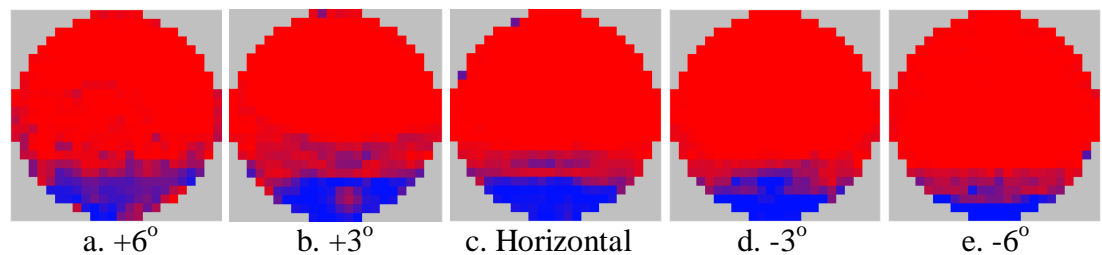


Figure 4.39: Phase distribution in a pipe cross-section for distance from expansion 34D, mixture velocity 0.20 m/s, input oil fraction 0.8 at different angles of inclination.

Results of the interface shapes for the stratified oil-water flow of Hasan (2006) at 24D were compared with present data at 20D. Hasan (2006) observed a concave interface shape at this position for horizontal and downward pipe orientation as shown in Figure 4.40 and 4.41. Interestingly, in the present work this was confirmed (refer to Figure 4.12 and 4.33), the same interface shapes was also identified. Even though the spatial accuracy of the WMS better than the spatial accuracy of ECT. The fact that both techniques giving the same trend, basically give confirmation of the results presented above.

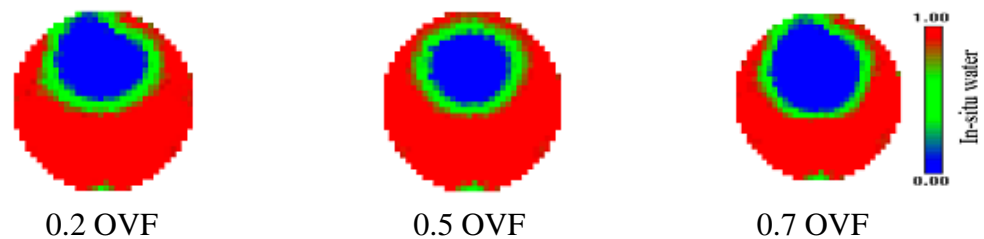


Figure 4.40: Phase distribution in a pipe cross-section for distance from expansion 24D, mixture velocity 0.2 m/s and horizontal flow, at different input oil fractions (Hasan, 2006).

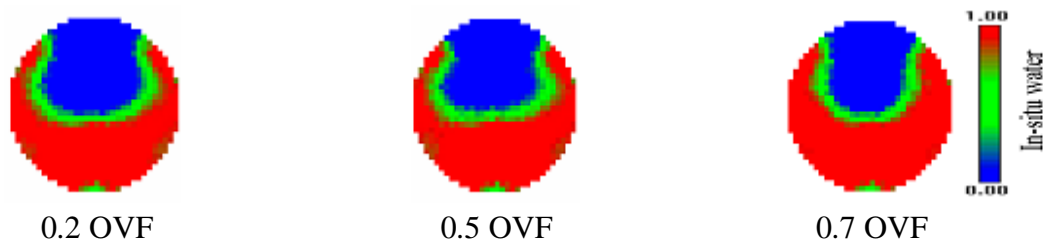


Figure 4.41: Phase distribution in a pipe cross-section for distance from expansion 24D, mixture velocity 0.2 m/s and -4 degree flow, at different input oil fractions (Hasan, 2006).

Furthermore, WMS image of the spatial distribution time average were shown in Figure 4.42 to visualize the phenomenon of waves in the pipe expansion to show the effect of pipe inclination. It was observed that with decrease in the inclined angle, the waves gradually dissipate. The highest waves amplitude for $+6^\circ$ orientation is $\sim 0.29D$ whereas for $+3^\circ$ the waves amplitude is $\sim 0.23D$. Furthermore, it is noticeable

that the occurrence of the waves varies, with the larger the upward angle, the higher the frequency of the waves.

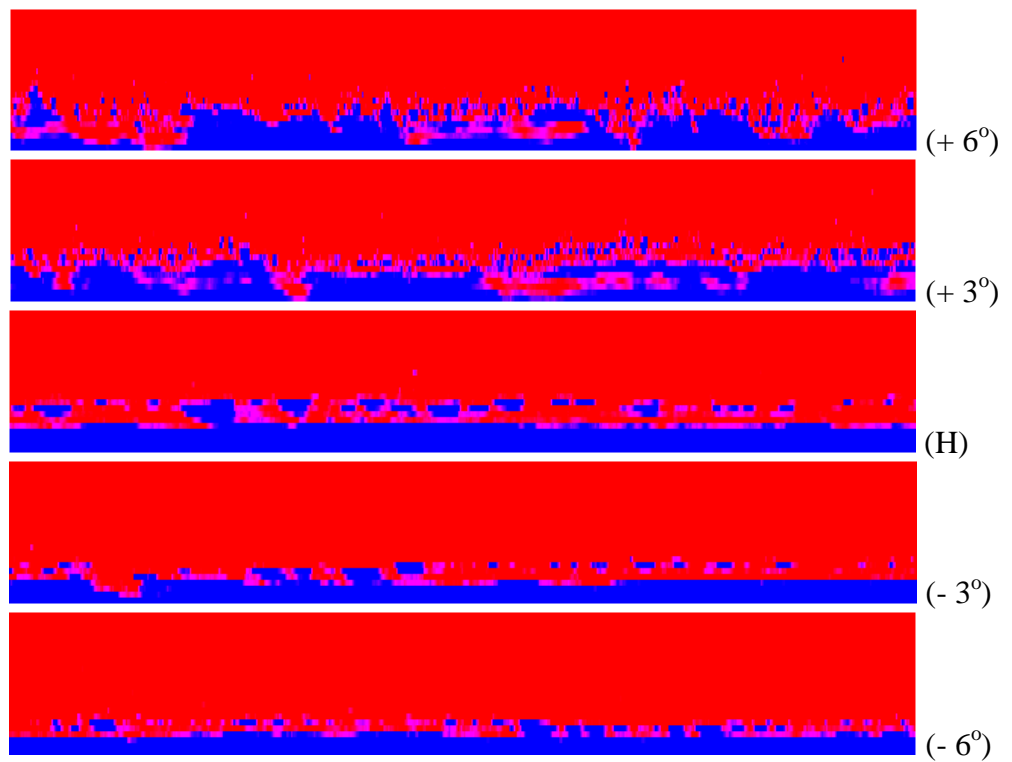


Figure 4.42: Spatial distribution for distance from expansion $10D$, mixture velocity 0.2 m/s and 0.8 input oil volume fractions at different angles of inclination.

CHAPTER 5

EVOLUTION OF INTERFACE

Separation of two immiscible liquids is important in the petroleum and chemical industries. As many liquid-liquid systems travel as one phase dispersed in another. To achieve separation these dispersion have to be converted into stratified flow. In the previous chapter, application of the latest tomography techniques; capacitance wire mesh sensor (CapWMS), tomography techniques to internally diagnose the mixing and phase distributions within process units was implemented of the test section. The purposes of this study are to explore the factors (rig configuration and operational conditions) affecting the evolution of phase layers downstream of the pipe expansion.

In designing such simple phase separator, as high a velocity as possible is sought so as to minimize the size of equipment. Extensive studies have been reported on the liquid-liquid two-phase flow in pipes (Valle, 1998; Azzopardi, 2001; Brauner, 2002). When the flow is stratified, the position of the interface can be reasonably predicted using the model of Taitel and Dukler (1976), originally developed for gas-liquid flow. Kurban *et al.* (1995) and Simmons *et al.* (1998) have shown the method to be accurate for the horizontal flows. The effect of upward pipe inclination on flow pattern in liquid-liquid flows has been the subject of study by Vedapuri *et al.* (1997

and 1999), Lum *et al.* (2002), Alkaya (2000) and Kurban (1997). However little data has been reported in the literature for the flow pattern maps in downwardly inclined pipes. Meanwhile there is no report in the literature about the flow pattern evolution through a sudden expansion for liquid-liquid two-phase flows. Therefore, the aim of this study is to provide data on liquid-liquid two-phase flows through sudden expansion for the horizontal and inclined horizontal flows. This chapter reports an experimental investigation which has been undertaken to explore the factors affecting the evolution of phase layers downstream of the expansion.

5.1 Flow pattern evolution.

Flow pattern evolution through a sudden pipe expansion for liquid-liquid two phase flow has been studied by Yang (2003) and Hasan (2006). In general, dispersed flow is characterized by the flow where one phase is dispersed in the other continuous phase. The dispersed phase is often present in the form of small droplets that are non-uniformly scattered within the continuous phase in two immiscible liquids. On the other hand, segregated flow is defined as the flow pattern where there is continuity of both phases (liquids) in the axial direction. The two liquids flow tends to stratify when flowing together in a pipe due to their different densities. There are two flow regimes which can be identified as segregated flow pattern, i.e., stratified flow (ST) and stratified with mixed layer at the interface (ST&MI). For the ST flow, there are only two layers in the pipe: oil layer at the pipe top and water layer at the pipe bottom. Whereas ST&MI flow, there are three layers in the pipe: oil layer at the pipe top, water layer at the pipe bottom and mixed layer between them.

In order to explore the flow pattern evolution from the dispersed to segregated flow through the sudden expansion as subjected to operating conditions and pipe configurations, an experimental investigation has been commenced.

5.2 Experimental Design

The experiments have been carried out on the liquid-liquid flow facility as described in detail in Chapter 3. The experimental set up using capacitance wire mesh sensor (CapWMS) was installed in order to explore the flow pattern evolution from the dispersed to segregated flow through the sudden expansion. A range of operating conditions (mixture velocities, input oil volume fraction) and pipe configuration (horizontal and small inclination from horizontal) were employed, as described in Chapter 4. A capacitance wire mesh sensor (CapWMS) was used. Details of the experimental design are as in Chapter 4. Here, the data obtained from the CapWMS were analysed further.

5.3 Experiment results and discussion

Yang *et al.* (2003) had performed visual observations of flow patterns downstream of a sudden expansion and reported three distinct layers: an oil layer at the pipe top; a water layer at the pipe bottom and a mixed layer between them (Figure 5.1). Fully stratified flow was hardly ever achieved. Visual assessment and analysis of the cross section of the WMS image (WMS_p), together with the water (W_{wms}) and oil (O_{wms}) interface level obtained from WMS measurement were performed in the present experiment. The findings are in agreement with Yang *et al.* (2003). Furthermore, this was confirmed by the observation of Vedapuri (1999) as shown in Figure 5.2 who studied long pipes.

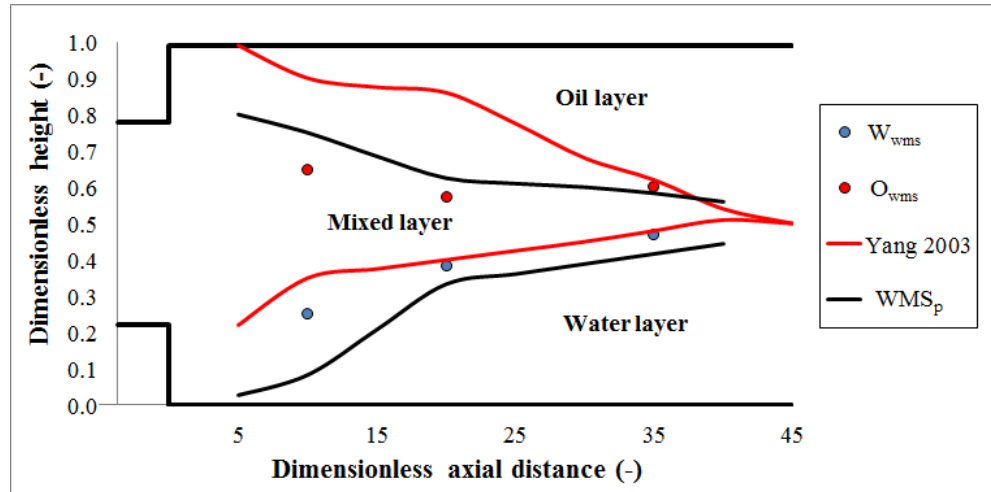


Figure 5.1: Phase layer evolution downstream of the pipe expansion at U_{sme} 0.20 m/s, oil volume fraction 0.5 for horizontal pipe orientation plotted with Yang (2003).

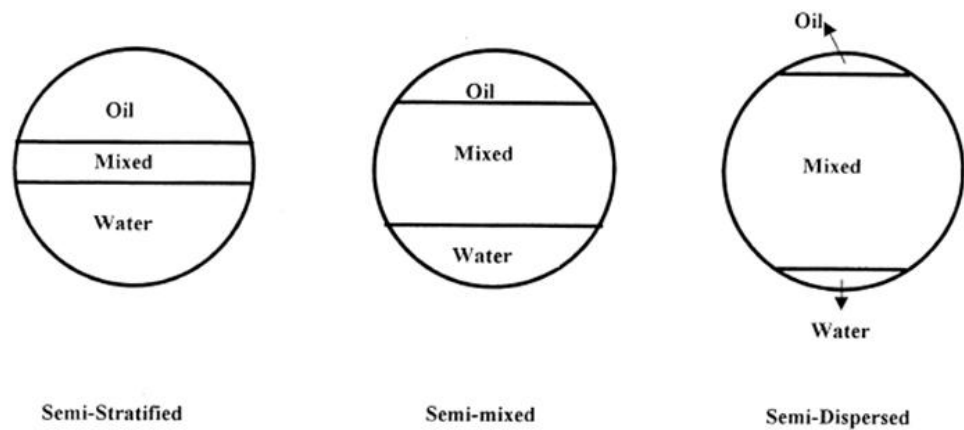


Figure 5.2: Analysis of the cross section for the three flow pattern observed by Vedapuri (1999).

5.3.1 Flow pattern evolution in horizontal pipe expansion

As observed by Yang (2003), for flow conditions; horizontally pipe orientation, downstream velocity 0.2 m/s and 0.5 input oil fraction, the phase layer evolution downstream of the singularity was shown earlier in Figure 5.1. Yang (2003) established that both the top oil layer and the bottom water layer increase their thicknesses along the pipe length whilst the mixed layer diminished. This supported the flow pattern maps of Trallero *et al.* (1997); the flow pattern is converting from o/w or Dw/o& Do/w to the ST regime.

The physical properties of the phases, the flow pattern and drop sizes present in the inlet of the pipe are parameters which are likely to affect the separation. It is therefore of interest to examine the effect of input oil volume fraction, the mixture velocity and the distance from expansion, for horizontally piping orientations. In this chapter, the purpose of these studies is to investigate the effects of the experimental conditions on the phase volume fraction distribution and the flow development in horizontal pipe.

Figure 5.3 shows the effect of the input oil volume fraction on the phase layer evolution downstream of the horizontally pipe expansion at a downstream mixture velocity (U_{sme}) 0.20 m/s. The phase layer evolution could be clearly distinguished with oil flowing on the pipe top and water on the pipe bottom while mixed layer were in flowing in between them. For all input oil volume fractions employed, the flows were not fully developed to ST regime within the length of the test pipe. The nearest approach was oil volume fraction of 0.2 and 0.8.

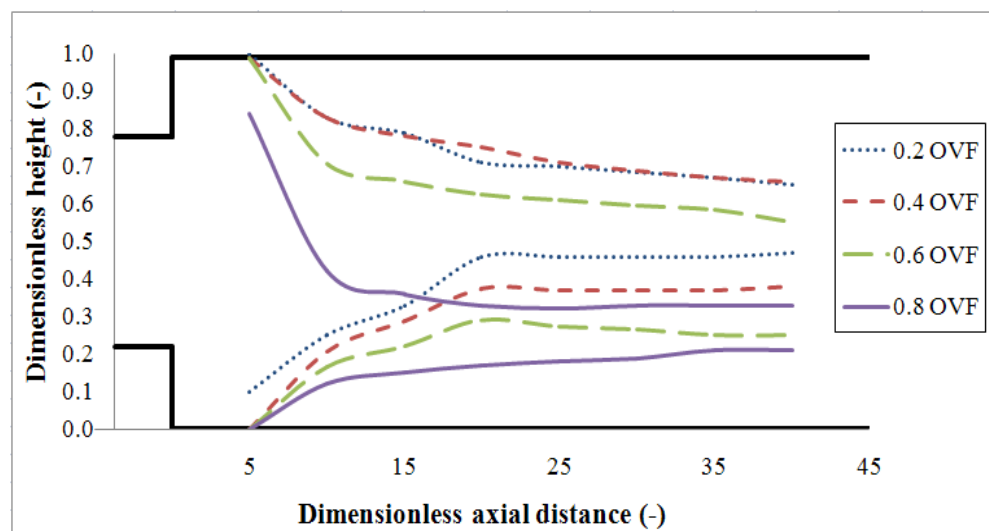


Figure 5.3: Effect of the oil volume fraction on the phase layer evolution downstream of the horizontally pipe expansion at U_{sme} 0.20 m/s

Figure 5.4 presented the same experimental observation of phase layer evolution at downstream mixture velocity of 0.30 m/s. If a higher downstream mixture velocity i.e. > 0.20 m/s is considered, the approach to stratification is much poor. Indeed for an OVF of 0.2, the oil layer was infinitesimal, insignificant layer of the oil only occur after 20D downstream the expansion, whilst no clear water layer occurs within the test section. This phenomenon was also observed by Yang (2003). At an OVF of 0.4, water layer and oil layer started to appear, however the layers are slim. Conversely, for higher input oil volume fraction, clear water layer could be observed especially for 0.6 OVF, beyond 5 downstream pipe diameter of the expansion. The oil layer were also clearly evolves within the test section, with thick oil layer were observed occurring at 10D downstream the expansion both for 0.6 and 0.8 input oil volume fraction. Interestingly, the oil layers at these high OVF, the thickness of the oil layer still increasing, indicating that phase layer evolution were still developing.

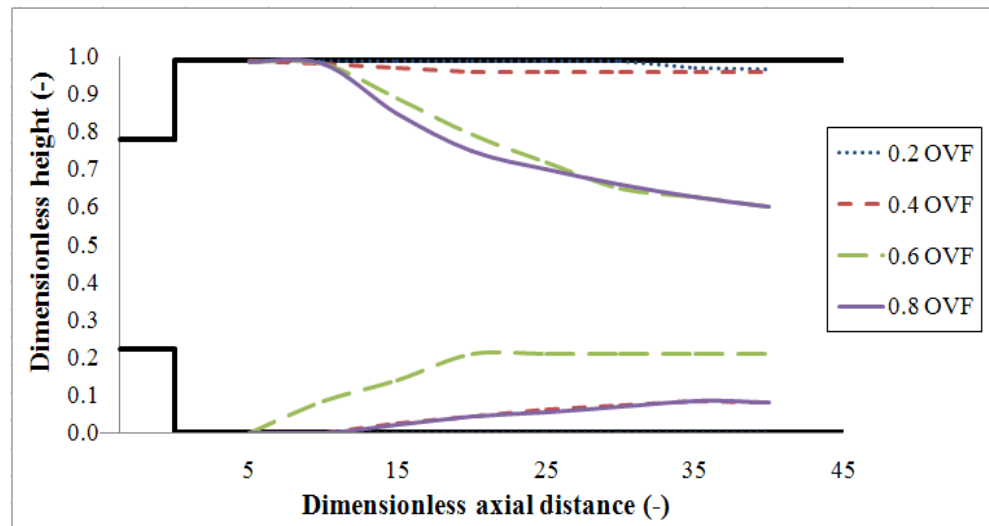


Figure 5.4: Effect of the oil volume fraction on the phase layer evolution downstream of the horizontally pipe expansion at U_{sme} 0.30 m/s

Figure 5.5 demonstrated the phase layer evolution at even higher downstream mixture velocity, 0.35 m/s. The same phenomenon was attained as for the phase

layer evolution at 0.30 m/s; apart from the thickness of the phase's layer decreased and the oil layer for 0.2 OVF and water layer for 0.4 OVF were not visible.

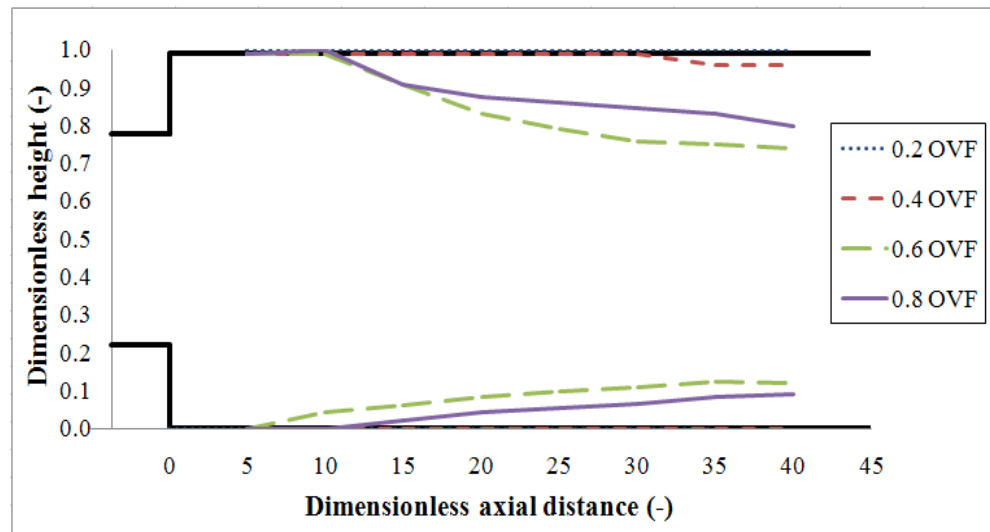


Figure 5.5: Effect of the oil volume fraction on the phase layer evolution downstream of the horizontally pipe expansion at U_{sme} 0.35 m/s

5.3.2 Flow pattern evolution in an upward inclined pipe expansion

Most of the flow pattern studies of the two immiscible liquid in pipelines concentrated at horizontal or vertical pipe orientation only. Therefore, fairly substantial data are available for these conditions. However, for flows at small inclination angles, it is still lots to explore. Up to date, there are only a few researches on flows pattern for small upward inclinations from horizontal reported in journals etc. As predicted by the model of Taitel and Dukler (1976) as show in Figure 5.6, pipe inclination will affect the interface level between the two phases for the ST regime flow pattern. Generally, it indicates that within $+6^\circ$ upward inclination angles, the lighter phase layer at the pipe top flows faster than the heavier phase layer that flowing at the bottom of the pipe. However, there are others factors that also affect these evolution processes. Therefore, in this section, phase layer in two-phase oil-water flow were measured for an upwardly flow inclined which were at the same

experiments conditions used in horizontal flow. Analysis of results and discussion are presented below.

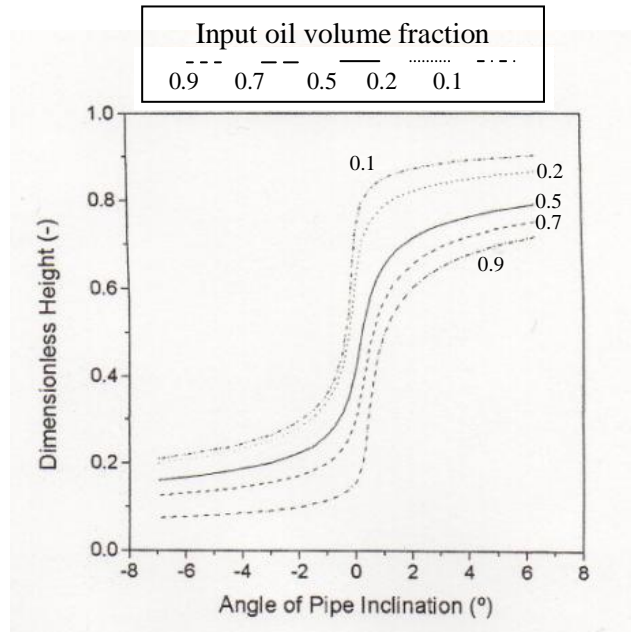


Figure 5.6: Prediction of interfacial level for stratified flow with the model of Taitel and Dukler, 1976 by Yang (2003)

Figure 5.7 shows the trend of the interface between the water layer and oil layer at a lower downstream velocity of 0.20 m/s for $+3^\circ$ upward inclined pipe orientation. It can be seen that within the test distance, the data from this present work as shown in Figure 5.7 are in agreement with Taitel and Dukler (1976) predictions. Phase layer of oil and water layer of those flow conditions could be distinct clearly; the oil layer was visibly flow at the pipe top and the water layer at the pipe bottom. Nevertheless, the flow could not develop to ST regime within the test distance. Instead, the mixed layer thicknesses growth to thicker layer compared to the horizontal counterpart.

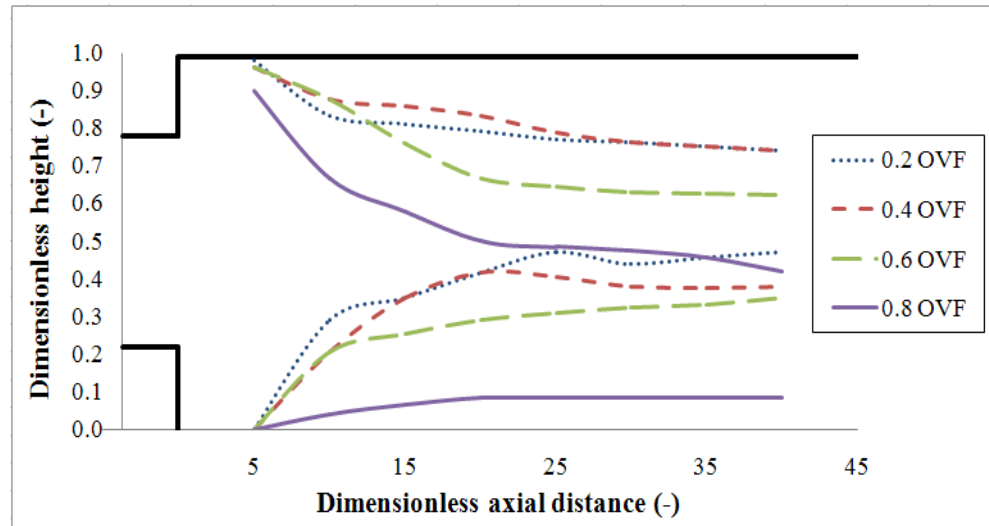


Figure 5.7: Effect of the oil volume fraction on the phase layer evolution downstream of the $+3^\circ$ upward inclined pipe expansion at $U_{sme} 0.20$ m/s

Figure 5.8 shows the trend of the interface between the water layer and oil layer at a lower downstream velocity of 0.20 m/s for $+6^\circ$ upward inclined pipe orientation. Again, Taitel and Dukler (1976) predictions was seen come to an agreement with the data presented. All oil volume fractions disclose a clear interfacial layer of oil flowing at the pipe top and water at the pipe bottom while mixed layer flowing in between them. With, 0.2 and 0.8 OVF showed noticeably exhibit a clear distinguished interfacial phase layers of oil flowing at the pipe top and water at the pipe bottom while mixed layer flowing in between them. While, 0.4 and 0.6 OVF, the water layer of those two could not be distinct clearly (both have same interface height), whereas the oil layer was visibly flow at the pipe top. Even Yang (2003) did not report such occurrences of an oil layer. This might be due to the observation of the phase layer evolution were made by naked eyes, while in the present work much advances techniques (CapWMS) was used.

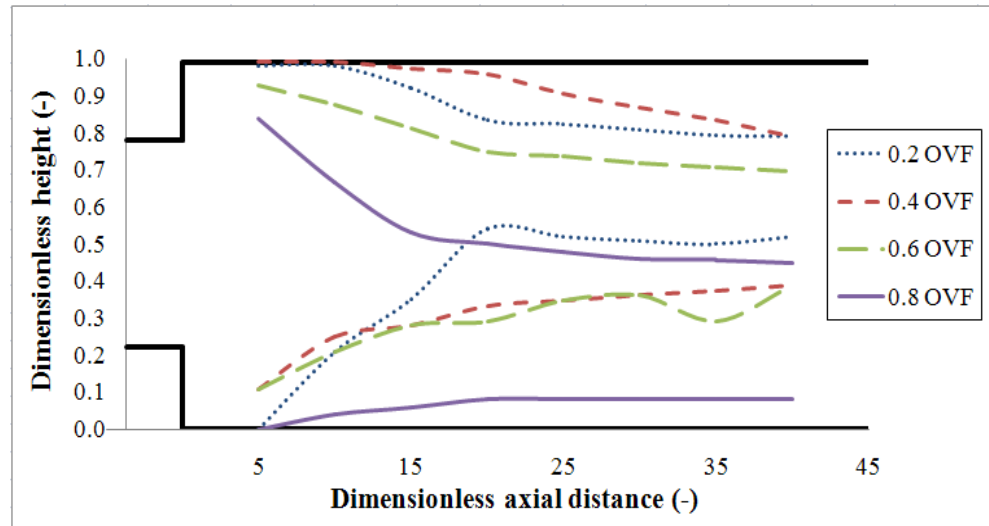


Figure 5.8: Effect of the oil volume fraction on the phase layer evolution downstream of the $+6^\circ$ upward inclined pipe expansion at U_{sme} 0.20 m/s

However for the higher downstream mixture velocity, the phase layer evolution at $+3^\circ$ and $+6^\circ$ angle of inclination are respectively shown in Figure 5.9 and 5.10. For oil dispersed flow at both upward inclination angles, there is no water and oil layer measure by the wire mesh sensor. Even though, a very thin oil layer appeared for 0.4 OVF system for $+3^\circ$ upward inclination, the layer seems to be insignificant (Figure 5.9). It implies that the flow is still fully mixed for 0.2 and 0.4 OVF within the test section.

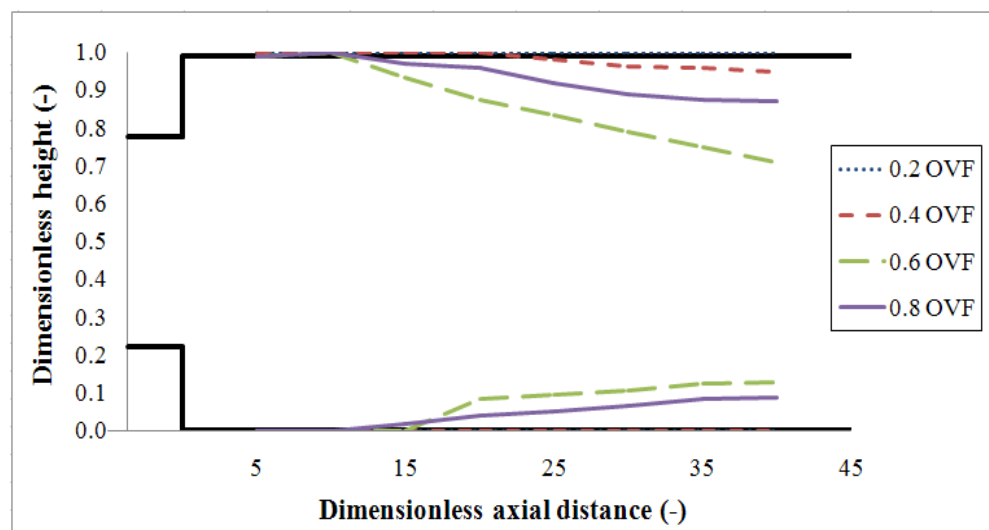


Figure 5.9: Effect of the oil volume fraction on the phase layer evolution downstream of the $+3^\circ$ upward inclined pipe expansion at U_{sme} 0.35 m/s

Interestingly, at higher OVF, i.e., 0.6 and 0.8 input oil volume fraction, layer of water could be seen as shown in both Figure 5.9 and 5.10, even though the layer is considered as a thin water layer. Conversely, a clear oil layer could be seen occurring at such OVF. However, these layer thickness decreases with the increase of angle inclination.

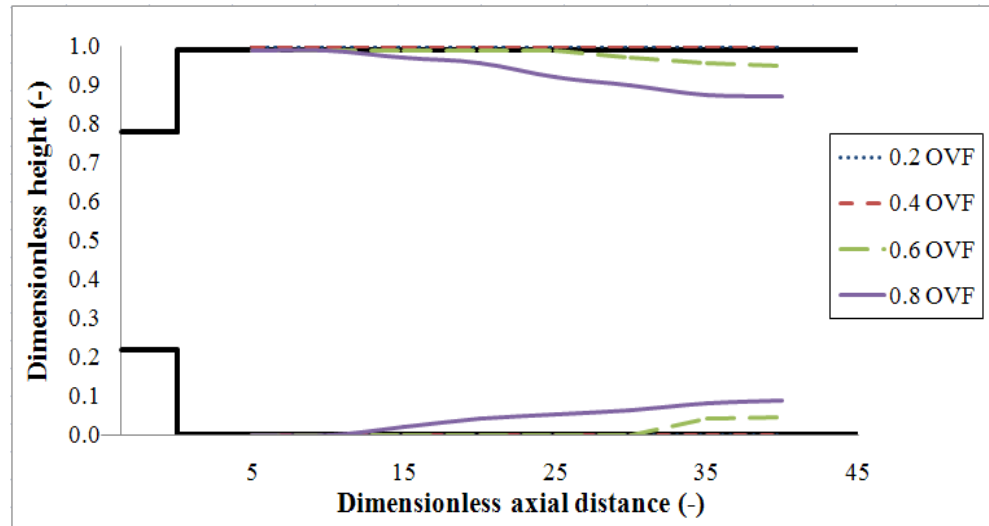


Figure 5.10: Effect of the oil volume fraction on the phase layer evolution downstream of the $+6^\circ$ upward inclined pipe expansion at U_{sme} 0.35 m/s

5.3.3 Flow pattern evolution in downward inclined pipe expansion

In this section the oil measured distributions for downward flow at the same experiments conditions as for upward flow are considered.

In downward inclined pipe orientation, the heavier phase layer moves faster and the lighter phase move more slowly. Figure 5.11 and 5.12 show the effect of the input oil volume fraction on the phase evolution downstream of the pipe expansion at a downstream velocity of 0.20 m/s for a downward inclination. At the same pipe distance, as the input oil volume fraction decreases, the thickness of the water layer increases. Accordingly, the heavier phase, i.e., water and the mixed layer flowing faster than the oil phase. Due to the fast flowing water layer, the evolutions of the

water layer were constrained. Hence, the layer was found to be slightly thinner. Contrariwise, the oil layer moves slightly slower, therefore evolution of the oil layer occurs with thicker layer. Nevertheless, phase layer of oil and water layer of those flow conditions could still be distinct clearly; the oil layer was visibly flow at the pipe top and the water layer at the pipe bottom.

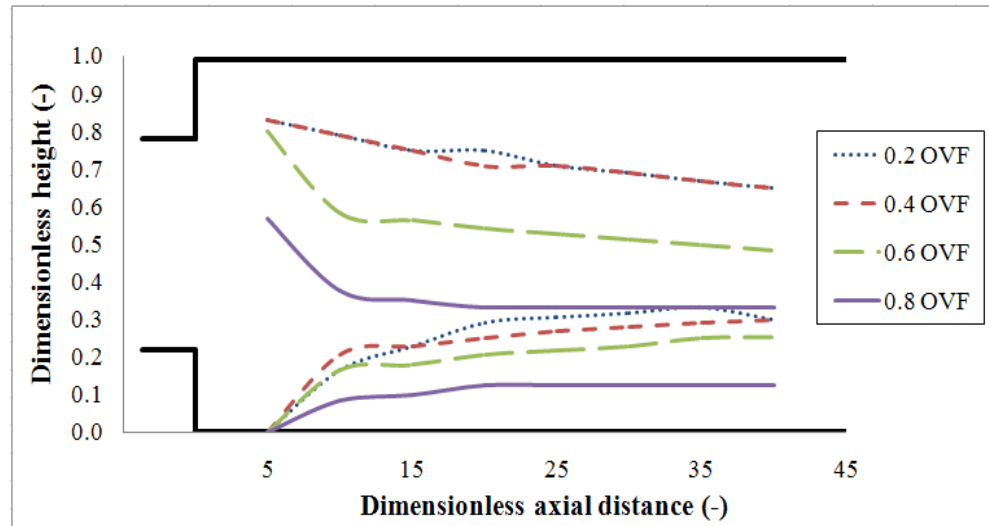


Figure 5.11: Effect of the oil volume fraction on the phase layer evolution downstream of the -3° downward inclined pipe expansion at U_{sme} 0.20 m/s

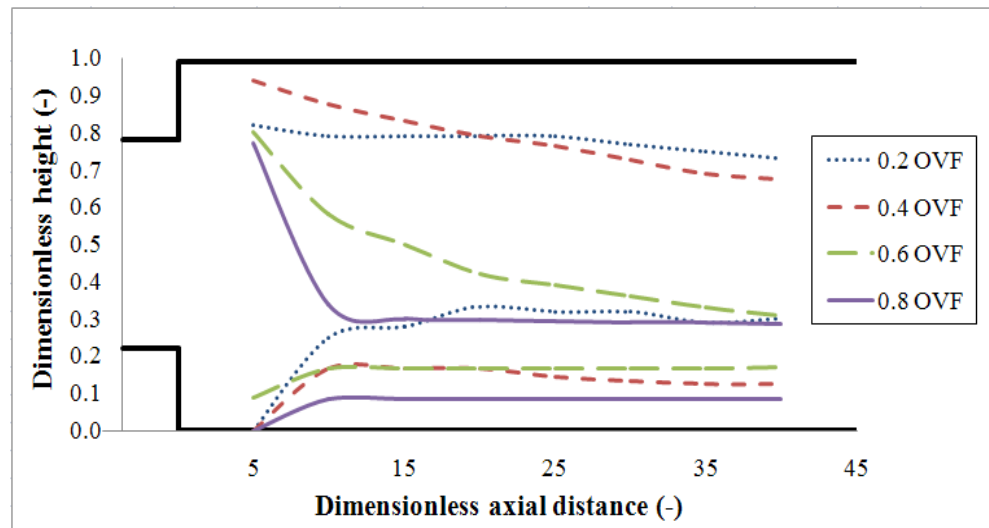


Figure 5.12: Effect of the oil volume fraction on the phase layer evolution downstream of the -6° downward inclined pipe expansion at U_{sme} 0.20 m/s

At higher downstream mixture velocity, the phase layer evolution at -3° and -6° angle of inclination are respectively shown in Figure 5.13 and 5.14. As revealed earlier, for

oil dispersed flow at upward inclination angles, there is no clear water and oil were observed. Accordingly, such phenomena only occur at 0.20 input oil volume fractions for downward pipe orientation. This indicates that the flow is still fully mixed for 0.2 OVF within the test section. Increase the input oil volume fraction within the Do/w regime, i.e., 0.4 OVF; thin oil layer was detected on the top of the pipe expansion whilst water layer were only observed for larger inclination angle ($+6^\circ$). Further increase the input oil volume fractions to 0.6 and 0.8, the oil are now becomes the continuous phase. At these input oil volume fractions, layer of oil were clearly emerge. Besides, the water layer was also visibly distinguished at 0.6 OVF for both inclinations. Interestingly, there is no water layer occurred at 0.8 OVF at -6° downward inclined pipe orientation due to the fast flowing heavier (water) phase. Actually, even if the water layer could occur, it may turn into mixed layer due to this high velocity.

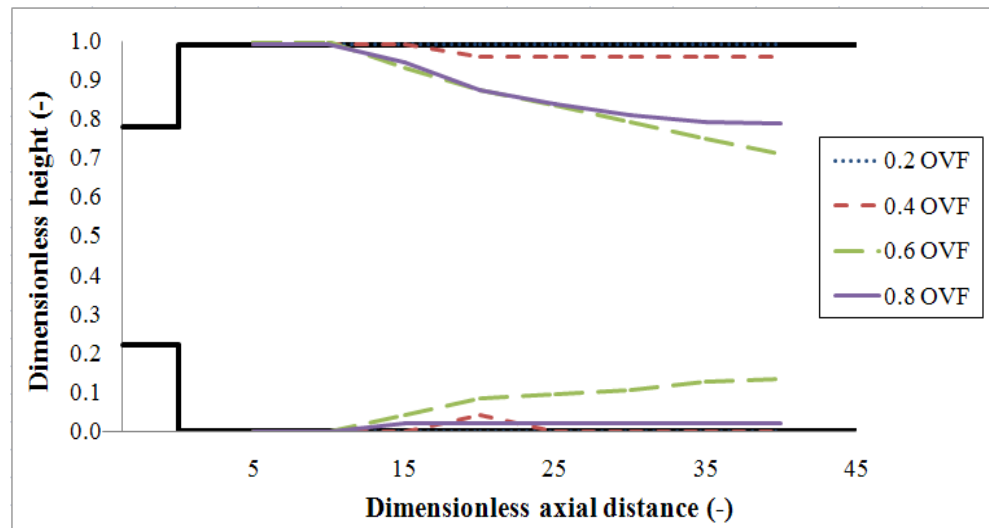


Figure 5.13: Effect of the oil volume fraction on the phase layer evolution downstream of the -3° downward inclined pipe expansion at U_{sme} 0.35 m/s

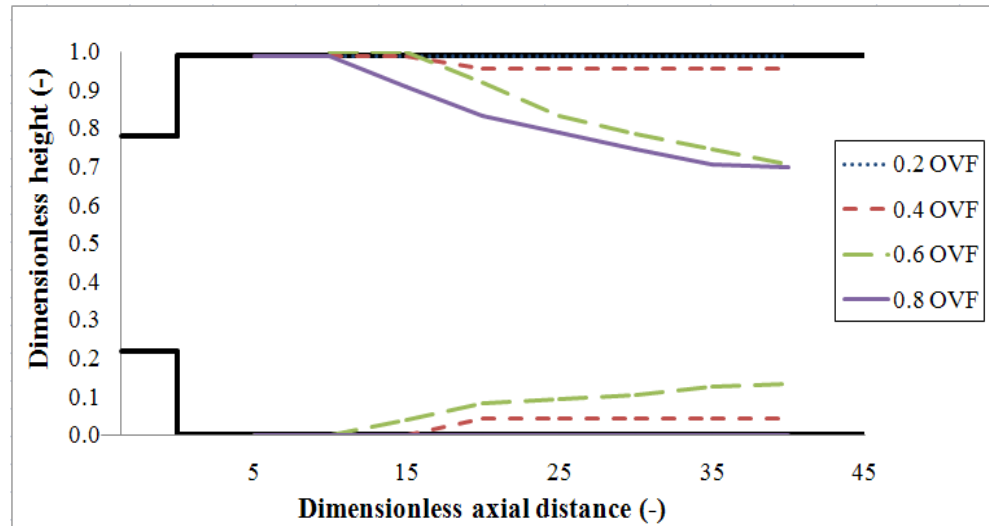


Figure 5.14: Effect of the oil volume fraction on the phase layer evolution downstream of the -6° downward inclined pipe expansion at U_{sme} 0.35 m/s

5.4 Comparison between different angles of inclination

In this section, the influences of the pipe inclination on the phase layer evolution for different angles of inclination at downstream of sudden expansion at U_{sme} 0.20 and 0.30 m/s respectively are shown in Figure 5.15 - 5.17. Analysis of results and discussion are presented below.

Figure 5.15 shows the effect of pipe inclination angles on the phase layer evolution of a water continuous flow system (0.2 OVF) at downstream mixture velocity of 0.20 m/s. At lower downstream mixture velocity, i.e., 0.20 m/s, the dispersed flow produced by the multi-hole orifice evolved to semi-stratified flow at the upward and horizontal inclinations. Nonetheless, the mixed layer thickness varies; with the mixed layer thickness of the horizontal pipe orientation is the smallest. While, at downward inclinations, the mixed layer thickness was wider, hence dispersed flow only evolve to semi-mixed flow pattern for these conditions. Furthermore, the thickness of the water layer increases as the inclined angle increases during the phase layer evolution downstream of the singularity.

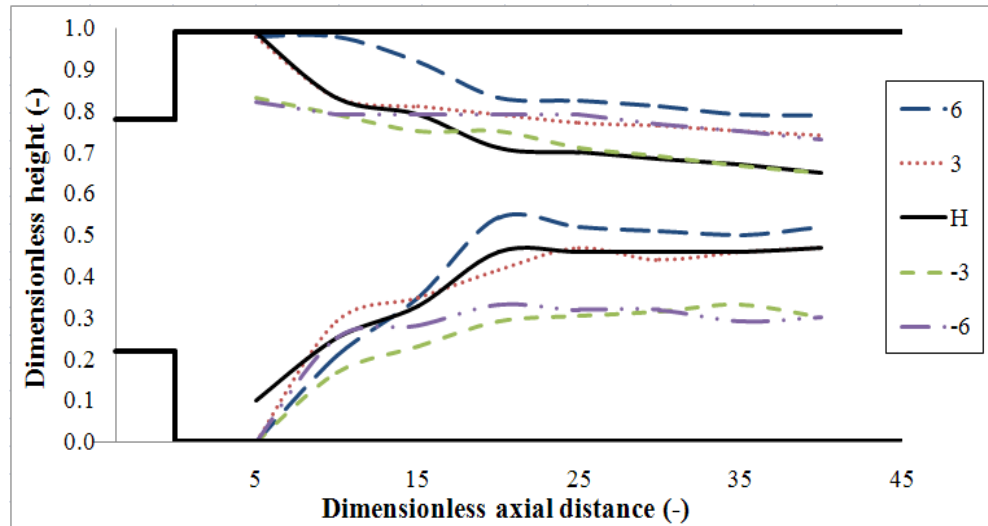


Figure 5.15: Effect of the angles inclination on the phase layer evolution downstream of the pipe expansion for 0.2 OVF at downstream mixture velocity, $U_{sme} = 0.20$ m/s.

In the water continuous flow, when the downstream mixture velocity is increased to 0.30 m/s, there was no separation visible irrespective of orientation of the pipe. As for higher input oil volume fraction i.e., 0.8 OVF, Figure 5.16 and 5.17 show the effect of pipe inclination angles on the phase layer evolution of an oil continuous flow system downstream mixture velocity of 0.20 and 0.30 m/s respectively. In general, the patterns of phase layer evolution of water continuous flow are the same as for oil continuous flow system. As seen in Figure 5.16, the different is the interfacial level of the phase layer, due to the input oil volume fraction. Besides, at lower downstream mixture velocity, i.e., 0.20 m/s, the dispersed flow evolved to semi-stratified flow at all of pipe inclinations. The semi-stratified flow pattern initially occurs at 10D downstream the expansion, earlier than that of phase layer evolution downstream of the pipe expansion for 0.2 OVF at the same U_{sme} (0.20 m/s). Moreover, the mixed layer thickness varies; with the mixed layer thickness of the horizontal pipe orientation is the slimmest. Interestingly, during the phase layer evolution downstream of the singularity, the thickness of the water layer increases as the inclined angle increases as were also reported by Yang (2003).

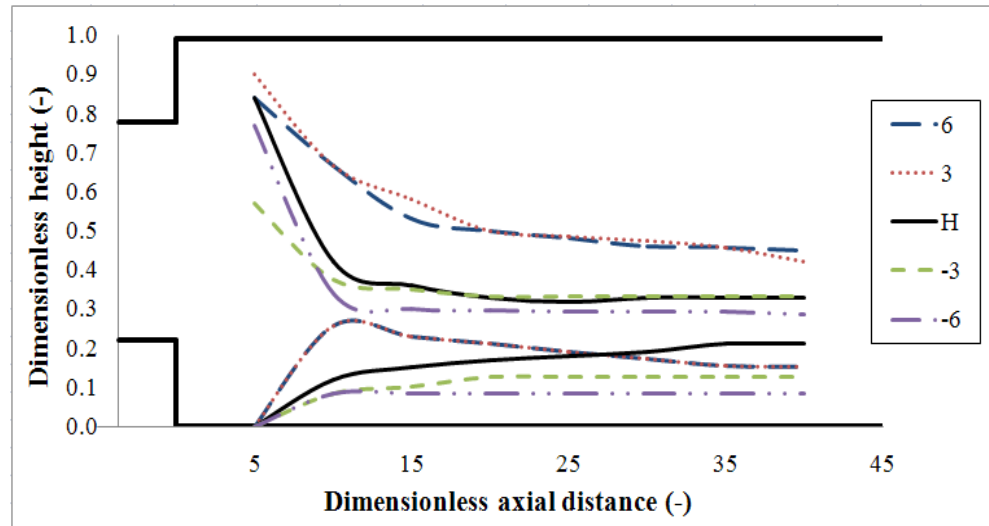


Figure 5.16: Effect of the angles inclination on the phase layer evolution downstream of the pipe expansion for 0.8 OVF at downstream mixture velocity, $U_{sme} = 0.20$ m/s.

Effect of angle inclinations for the same input oil volume fraction at downstream mixture velocity to 0.30 m/s, least variations of the phase layer evolution could be seen as shown in Figure 5.17. There are insignificant changes of the evolution of the water phase. All of the water layers are small and their thicknesses are about the same height. Contrariwise, the oil layer could be clearly seen in the oil continuous flow, which was not observed at water continuous flow. With -6° downward pipe orientation giving the thickest oil layer. Remarkably, towards the end of the test distance, the height of the oil layer was about the same for all angle inclinations. Therefore, it can be conclude that angle of inclinations has minimal effect on the phase layer evolution of oil continuous flow at higher downstream mixture velocity.

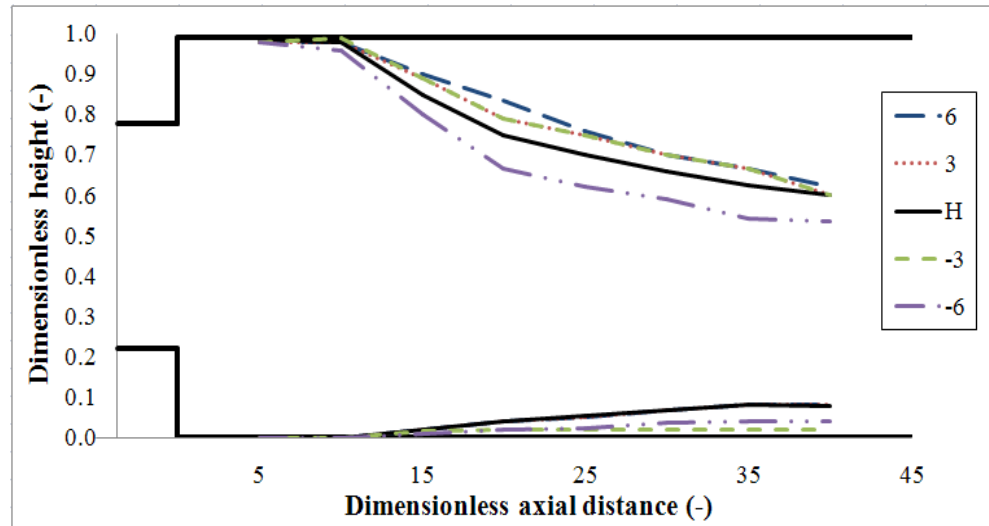


Figure 5.17: Effect of the angles inclination on the phase layer evolution downstream of the pipe expansion for 0.8 OVF at downstream mixture velocity, $U_{sme} = 0.30$ m/s.

In addition, it can be seen that at slower downstream mixture velocity, the thickness of the water layer generally increases as the incline angle increases. However, the thickness of the kerosene layer is not always decreasing with the inclined angle. The thickness of the mixed layer is thinnest at the horizontal orientation. Both upward and downward inclinations tend to increase the mixed layer. It can be concluded that the dispersed flows can be converted to the segregated flows by an expansion with short pipe length, especially at the horizontal flow.

CHAPTER 6

DROP SIZES DOWNSTREAM OF PIPE EXPANSION

In most of industrial processes, knowledge of the nature of multiphase flow is important. For example, in chemical, petrochemical and food industries, liquid-liquid dispersions appear in processes such as emulsification and two-phase reactions. Therefore, knowledge of drop formation and the nature of dispersions mechanisms involve in their formation, as well as the size distribution of any particles or liquids droplets existent are important. This information is important for analysing the hydrodynamic and transport phenomena in the flow of liquid-liquid dispersions and also a valuable design parameter in order to design efficient and cost effective equipment. Hence, information of the drop size and drop size distribution over the cross section of the pipe downstream of an expansion is presented in this chapter.

6.1 Drop size distribution

Knowledge and evidence of the drop size distribution is necessary when subsequent separation of two phases of liquids is considered. Most of the experimental works on drop break-up and coalescence has mainly been conducted in stirred tanks. As a result, several models for the relationships between drop size, physical properties and operating conditions have been proposed for predicting the maximum drop diameter and minimum drop diameter during turbulent dispersion flow that can then be correlated with drop break-up and drop coalescence. Conversely, due to the nature of

the experiments involved, in-situ and on-line (during pipe flow) drop size distributions data conducted in pipelines are very much inadequate compared to the ones conducted in stirred vessels or tanks.

Number of studies that address the drop size distribution in pipe flow of two immiscible fluids is few. Evolution of drops emerging from homogenise system into a pipe flow merely exist. The inclination of the piping can also have a significant effect on drop size distribution. Up to date, there have only been a small number of studies on the effect of expansions and inclinations on the drop size distribution of oil-water dispersions. Even though, the effect of inclination on momentum transport is readily estimated but the effect of pipe expansion with a small inclination is again unknown. In other words, these sections of research area are remains unstudied.

Pipe expansion and inclination have been considered as the imposition on the flow of an external field that affects momentum. Total pressure gradient for two-phase flow has three components; frictional, acceleration and gravitational pressure gradients. For horizontal oil-water flow, acceleration and gravitational components can be neglected. For steady flows in inclined pipe the acceleration component can still be neglected but the gravitational component becomes very significant. An expansion provides an unfavourable pressure gradient in multiphase flow, whereas inclination is a skewing of the buoyant body force to the stream wise pressure gradient. Therefore, particular attention in this research has been applied to the drop size measurements of two immiscible liquids downstream of an expansion in a pipe with small inclination angles. The size of the dispersed phase is important when interfacial mass and/or heat transfer are involved and will affect phase separation at the end of the process.

6.2 Experimental Design

Here, an experimental study of drops downstream of a pipe expansion using a laser backscatter technique is presented. Measurements were taken downstream of the expansion both for horizontal and small positive or negative inclinations for a range of flow rates.

Measurements of drop size were made using Lasentec equipment (FBRM M500P) at the central axis of the pipe and also 17 mm either side (top or bottom) of the central axis of the test section. The probe positions in a pipe cross-section were then labelled as Top, Middle and Bottom. As for the axial positions, the terms used are defined as *near*, for the distance from expansion of $10D$; *middle*, for the distance from expansion of $20D$; and *far*, for the distance from expansion of $34D$, where D is the internal diameter of the pipe (68 mm) as shown in Figure 6.1.

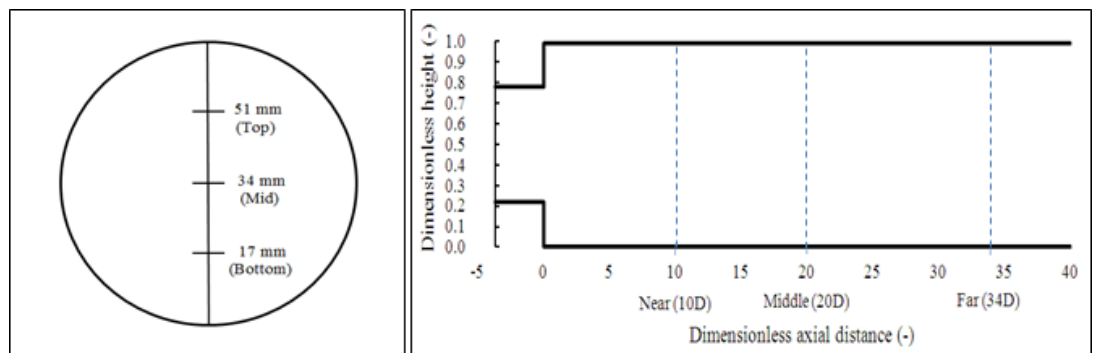


Figure 6.1: Locations of probe positions downstream of the expansion and in a pipe cross-section with height from the bottom of the pipe.

In order to explore the flow pattern from the dispersed to the segregated flow through the expansion, the experiments are designed to distribute the inlet conditions in dispersed regimes (Dw/o & Do/w , o/w and $Do/w\&w$), and downstream mixtures velocities (0.20, 0.30 and 0.35 m/s) in the expansion are in the segregated flow (ST and ST&MI). Furthermore, the experiments were executed for input oil volume

fractions ranging from 0.2 - 0.8 for horizontal and inclined pipe orientations of -6, -3, +3, +6 degrees. The positive and negative degrees indicated upward flow and downward flow from horizontal, respectively.

By means of the FBRM M500P, a continuous measurement was then logged by a computer and allowed the copyrighted software to produce distributions of droplet chord as reviewed in Chapter 2. Diagram of the Lasentec FBRM M500P settings are as shown in Figure 3.13.

The FBRM control software allows the acquired chord length data to be discretised into a series of user-defined intervals that is 100 linear-channels over the range of 1 to 1,000 microns. Six consecutive measurements were averaged to produce each distribution, which one measurement duration was ten seconds. Furthermore, measurements were made after 5 residence times of the system. Both, measurement duration and 5 times residence time were to ensure the flow is in stable state and sufficiently robust sample numbers for all condition that being investigated. In this measurement campaign, FBRM software had been used to record the data before it was transferred to Excel data format. These chord data were then converted to diameter distribution using PAM2 and used for further statistical data processing.

6.3 Results and discussions

Previous researchers have made several important investigations of the simultaneous flow of two immiscible liquids through sudden expansion in a pipe. Thus from their preliminary investigations they have established three flow patterns which involved in the flow of two immiscible liquids through sudden pipe expansion. These patterns were *dispersed flow*, which appeared at the near position, followed by *stratified flow with mixing at the interface* (ST&MI) at the middle position and *stratified flow* (ST) at the far position (Yang *et al.*, 2003). According to Yang *et al.* (2003), there are clearly three regions of phase profile downstream of a pipe expansion. The regions were classified as; oil region, at the top of the pipe cross section; mixed region, in between lighter and heavier phase and; water region, at the bottom of the pipe cross section (Yang *et al.*, 2003). Yang *et al.* also reported that the mixed region was dominating at the near position and diminished downstream in the pipe length whilst the top oil region and bottom water region increased their layer until they achieved fully stratified flow. In terms of the microscopic level, the mixed region is actually occupied by different sizes of drops. These sizes, in principle, are then determined by a balance between the overall rates of drop break-up and coalescence.

As mentioned earlier, phase profiles development downstream of a pipe expansion was recorded by Yang *et al.* (2003). Later on, based on the profiles of Yang's, Hasan (2006) performed experiments on the drops size distribution (chord length). A laser backscatter technique was employed to measure the drop size distributions downstream of the expansion. The Probability Apportioning Method (version 2) of Langston *et al.* (2001) was used to transform a measured chord length distribution into a drop size distribution. However, according to Hasan (2006) the results of the

transformation of chord lengths were shown unsatisfactorily. On the other hand, in this present work the computational coding for the PAM2 has been updated and upgraded as shown in Appendix 2B. This allowed the measured chord length distribution to be transformed into a drop size distribution successfully. Since PAM2 (newer version) methods were found to successfully convert a chord length distribution to a drop diameter distribution, the latter were then analysed further to obtain Sauter mean diameter (SMD). This SMD of the drop diameter distribution were then used in the results, discussion and comparisons between different conditions.

6.3.1 SMD of drop size distribution in mixed and interface layer

With the intention of exploring the flow pattern evolution from the dispersed to the segregated flow, factors affecting the flow pattern evolution through the sudden expansion as mentioned earlier (Chapter 3) were studied. The flow patterns downstream of the system are more concerned in this study due to the purpose of stratification of the dispersed flow by using the expansion.

For the better understanding of the stratifications of the dispersed flow based on the phase profile observations of Yang *et al.* (2003), the location at 34D was selected as the main position to be measured. According to the flow pattern map of Trallero *et al.* (1997), for the downstream mixture velocity of 0.20 m/s, its predicted flow pattern might develop to the stratified flow (ST) or stratified mixed with layer at the interface (ST&MI). Hence, SMD of drops diameter for several axial measurement point (10D, 20D and 34D) from expansion within the test section at downstream mixture velocity, $U_{sme} = 0.20$ m/s and 0.8 input oil fraction at various probe positions

of the pipe cross section were measured and are presented as in Figure 6.2. The probe positions were employed at 17, 34 and 51 mm from the bottom of the pipe cross-section as illustrated in Figure 6.2. In this case, oil is considered as the continuous phase while water is the dispersed phase. It can be seen that the SMD was the largest for the probe positioned at the bottom (17 mm) of the pipe cross section throughout the test section. The reason was that the probe position was at the mixed region but very close to the silicone oil region where droplets of water dispersed in the mixed layer and continuous oil flow. At this position, the result shows that the drops were coalescing together to form large drops, especially at position nearest to the interface layer. In that region, the coalescence rate starts to dominate over the breakage rate as described theoretically by Shinnar (1961) and Sprow (1967). In contrast, that phenomenon does not occur for the probe positioned at the middle (34 mm) and top (51 mm), where the SMD were small, less than 100 μm . This could be because of the probe was positioned at considerable distance away from the interface layer. Lovick and Angeli (2004b) also found a similar trend of chord lengths frequency to the present results of this experiment when their probe was positioned far-off the interface.

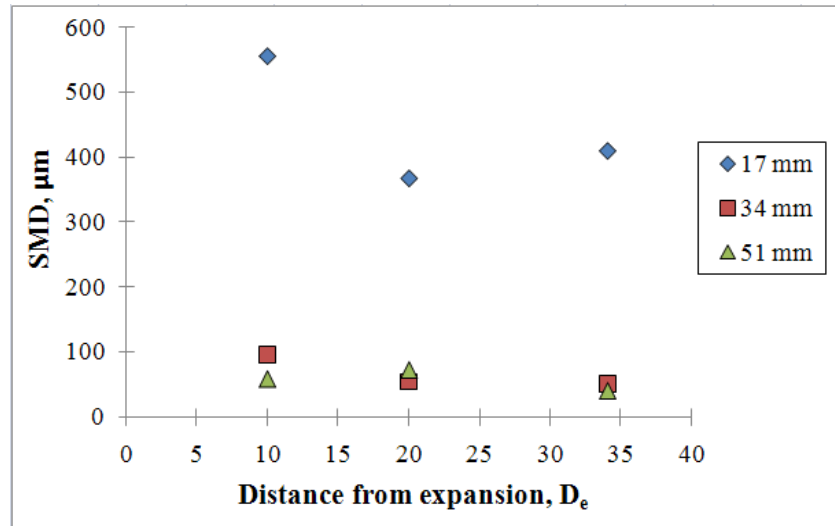


Figure 6.2: D_{32} of water droplets for downstream mixture velocity, $U_{sme} = 0.20$ m/s, within test distance in horizontally pipe orientation at oil volume fraction system, $OVF = 0.8$, at different probe position.

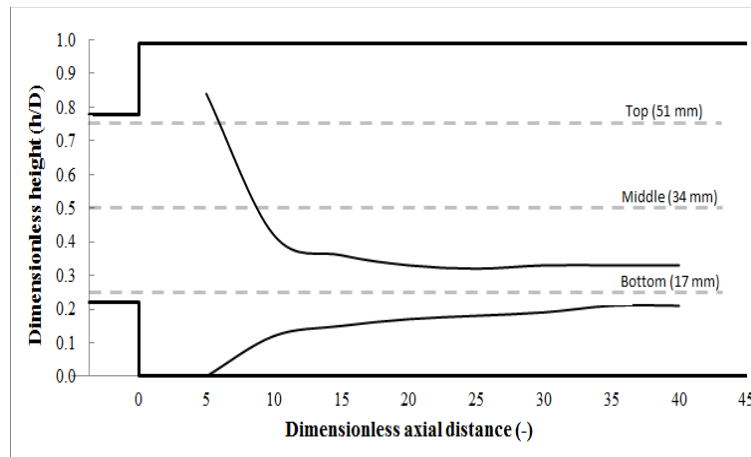


Figure 6.3: Interface mapping along the axial length of the pipe. The lower line indicates the interface between water and the mixture whilst the upper line shows the interface between oil and the mixture at downstream of the horizontal pipe expansion at $U_{sme} 0.20$ m/s, $OVF = 0.8$.

6.3.2 SMD of drop diameter distribution in horizontal expansion.

Superficial mixtures velocities at orifice (U_{smo}) and superficial mixtures velocities downstream the expansion (U_{sme}), were plotted on the flow pattern maps of Trallero *et al* (1997) as shown in Figure 6.4. According to this flow pattern maps, all the downstream flow patterns in the expansion in the present study, theoretically should be in the segregated flow regimes if they were fully horizontal flows.

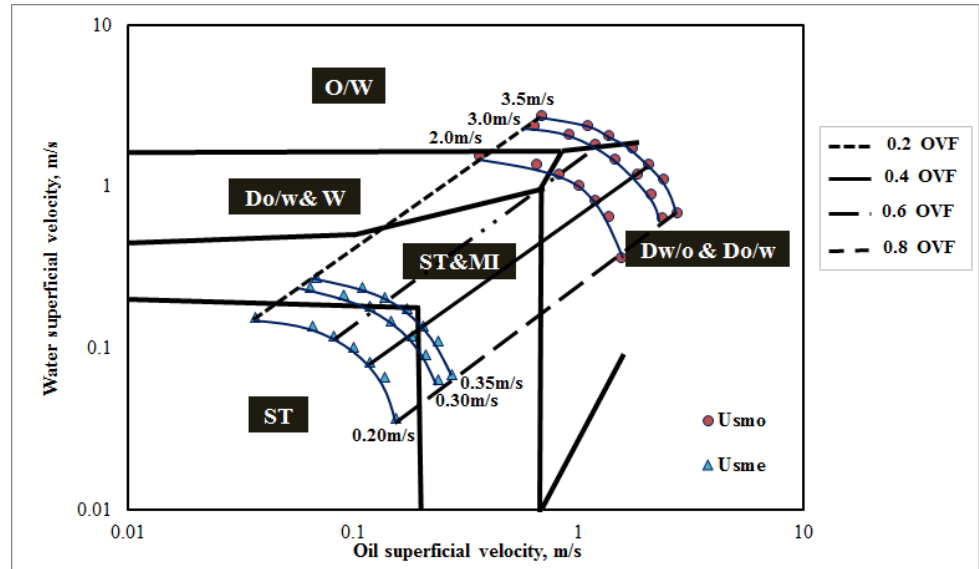


Figure 6.4: Orifice and downstream mixture velocities of flow pattern transition through the sudden expansion plotted on the flow pattern maps of Trallero *et al.* (1997).

It is therefore of interest to examine the effect of input oil volume fraction, the mixture velocity and the distance from expansion, for horizontally piping orientations. Hence, one of the main parts of these studies is to investigate and relate the effects of the experimental conditions and axial tabular positions with the drop size distribution and the flow development in horizontal pipe.

6.3.2.1 SMD of drops distribution - Effect of the oil volume fraction

Generally the flow patterns seem to be rapidly stratifying for low downstream mixture velocities (U_{sme}). Trallero (1997), affirmed the phenomenon and produce a well-known flow pattern maps that been used by many of liquid-liquid multiphase researchers (Figure 6.4).

SMD of drop diameter distributions for downstream mixture velocity, U_{sme} 0.20 m/s, at several axial positions after expansion within test distance in horizontally pipe orientation for probe position 17, 34 and 51 mm from bottom at different oil volume

fraction are displayed in Figure 6.5, 6.6 and 6.7 respectively. Blue marker represents the water droplets and red marker is for oil droplets unless otherwise stated. It can be noticed in Figure 6.5, at 0.8 OVF, the mean drops diameter are the biggest, followed by mean drops diameter for 0.6 OVF, 0.4 OVF and finally 0.2 OVF, in descending sequent (big to small SMD) for 10D and 20D distance after expansion. This is due to the probe position was engaged at 17 mm from bottom of the pipe, at the mixed region of 0.8 OVF. However, at 34D after the expansion, for 0.4 and 0.6 OVF, SMD for the latter is smaller. This would suggest that the phase inversion point occur at this OVF (0.4 - 0.6 OVF). This finding of phase inversion point was also observed by Yang (2006).

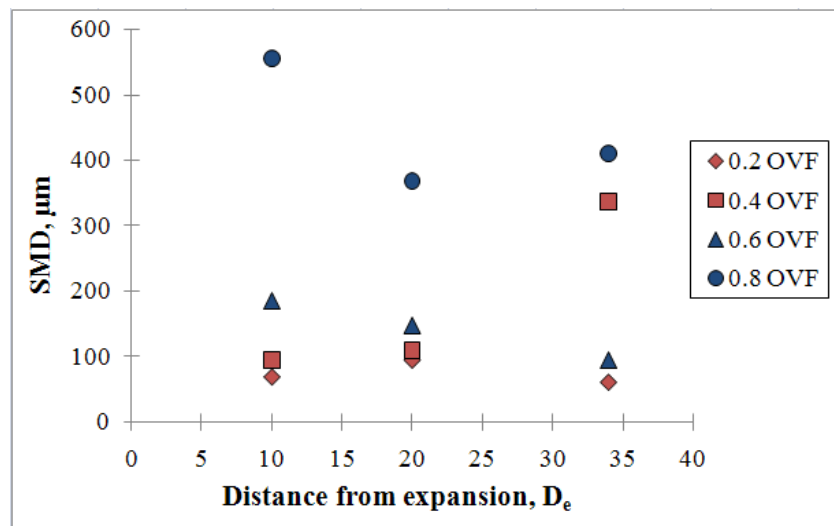


Figure 6.5: Sauter mean diameter for downstream mixture velocity, U_{sme} 0.20 m/s, within test distance in horizontally pipe orientation, probe position 17 mm from bottom at different oil volume fraction, OVF.

Figure 6.6 shows the influence of oil volume fraction on the SMD of drop diameter for downstream mixture velocity, U_{sme} 0.20 m/s, at several axial positions in horizontally pipe orientation for *centre* probe position (34 mm) at different oil volume fraction, OVF. Obviously, it could be seen that the SMD for 0.8 OVF is no longer the biggest drops to be detected at this particular vertical position (centre of

the pipe). Now, the largest drops were detected at the centre of the pipe cross section, where the interfaces of system with 0.4 and 0.6 OVF were the closest to the probe positioned. These findings confirmed the assumption made earlier, near to the interfaces of the two phases, droplets were larger. Furthermore, at 20D, for oil as a continuous phase and water is the dispersed phase (0.6 OVF), SMD of the drops decreased. It was suspected that at this position, initial water drops present at 10D has coalesced here (20D). As for axial position 34D, further coalescence of the remaining water drops that were in the oil regime occurs, due to the narrowing of the mixed layer and level of the oil interface is nearer to the probe position. Therefore more drops are being formed from the liquid-liquid interface and more drops are experiencing coalescence forming large drops. This finding confirmed and in agreement with Hasan (2006), which stated at furthest axial position, drops formed at the liquids interface, coalesced.

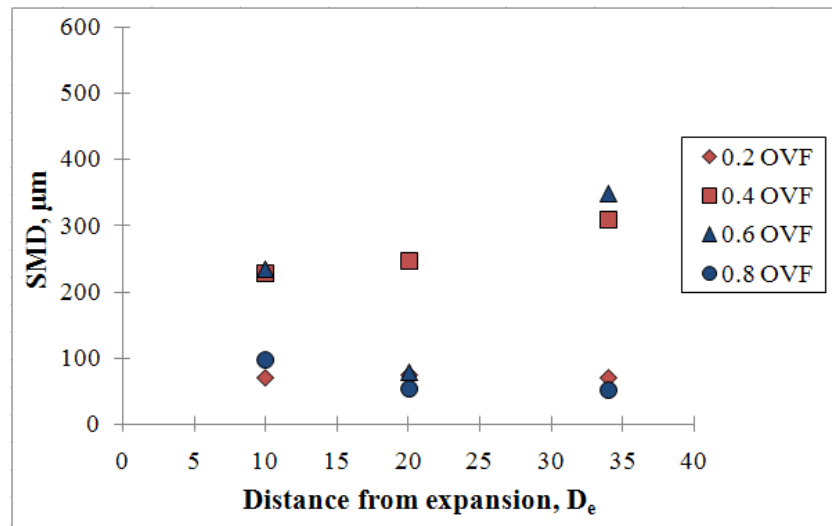


Figure 6.6: Sauter mean diameter for downstream mixture velocity, $U_{\text{smc}} 0.20$ m/s, within test distance in horizontally pipe orientation, probe position 34 mm from bottom at different oil volume fraction, OVF.

Further move the probe location (top) away from the interface position, the influence of oil volume fraction on the SMD of drop diameter for downstream mixture

velocity, U_{sme} 0.20 m/s, at several axial positions after expansion in horizontally pipe orientation is shown in Figure 6.7. Clearly shown in Figure 6.7, for the entire oil volume fraction range, SMD of drops distribution for either oil or water drops were small. Consequently, these indicate that drops distribution (SMD) have been influenced by positions of the phase layer rather than input oil fractions.

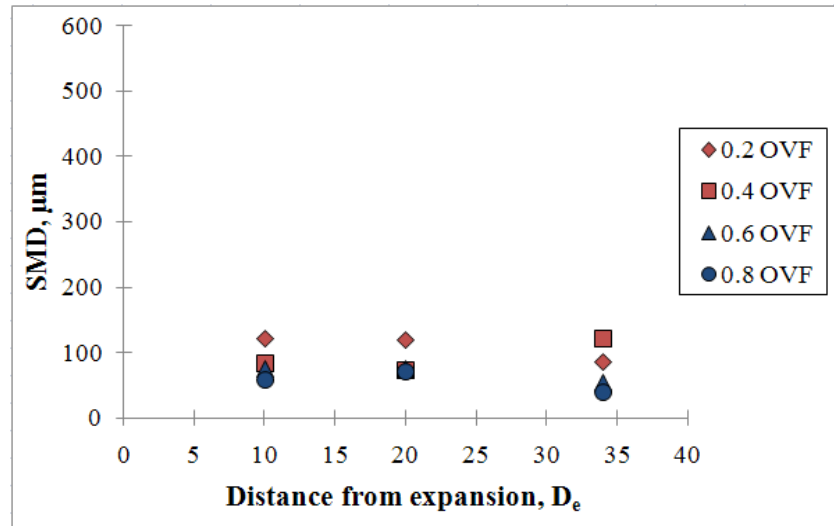


Figure 6.7: Sauter mean diameter for downstream mixture velocity, U_{sme} 0.20 m/s, within test distance in horizontally pipe orientation, probe position 51 mm from bottom at different oil volume fraction, OVF.

6.3.2.2 SMD of drops distribution - Effect of mixture velocity

Figure 6.8 shows the SMD for 0.2 oil volume fraction system, within the test section in horizontally pipe orientation at probe position 51 mm from bottom for different downstream mixture velocity. It is clearly shown that for all downstream mixture velocities and at near, middle and far axial position within the test section of the expansion the droplet sizes are small, ranging from 70 – 120 μm . However, for the lowest downstream mixtures velocity, 0.20 m/s, SMD is slightly larger compared to the SMDs of the other U_{sme} . This phenomenon is suspected due to the low mixture velocity; therefore drops acceleration is low at the near entry region of the pipe. Hence drop coalesced and larger drops were detected at distance $10D$. Whereas at

higher U_{sme} , deformation and breakup due to the rapid acceleration of drops, bursting from the multi-hole orifice resulting smaller drops. This singularity was also observed in Hasan (2006) which proclaimed D_{32} was found to decrease slightly with increasing mixture velocity.

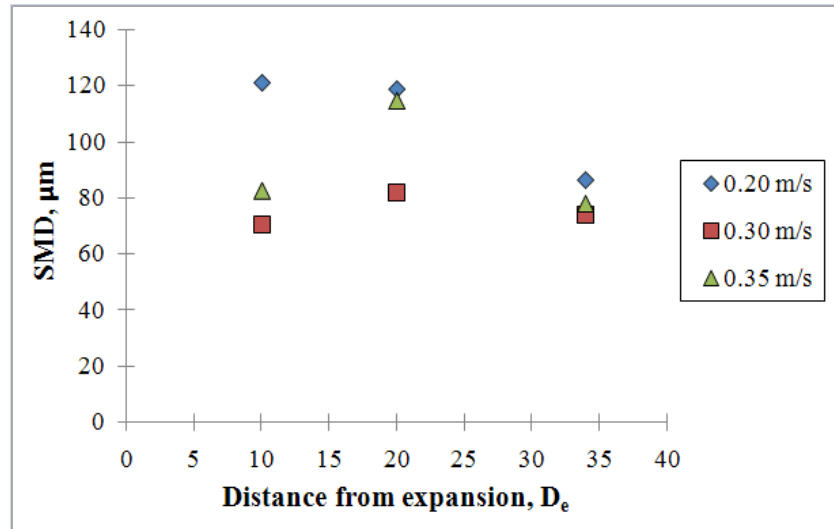


Figure 6.8: D_{32} of oil droplets for 0.2 oil volume fraction system, within test distance in horizontally pipe orientation, probe position 51 mm from bottom at different downstream mixture velocity, U_{sme} .

The same phenomena could be seen in the 0.4 oil volume fraction system at 10D and 20D for all the downstream mixture velocities as shown in Figure 6.9. In contrary for the same system at 34D and $U_{sme} = 0.20$ m/s, slightly bigger droplets were detected by the laser. At this position and downstream mixture velocity, the drops collisions happened more frequent due to the narrowing of the mixed region. Furthermore, collisions time was longer due to the low U_{sme} , providing sufficient time for the drops to coalesce. Therefore droplets started to coalesce more and formed bigger drops. As for higher mixture velocities, droplet size decreased and is in agreement with the model of Sleicher (1962), which proposed at high velocities, droplet size decreased.

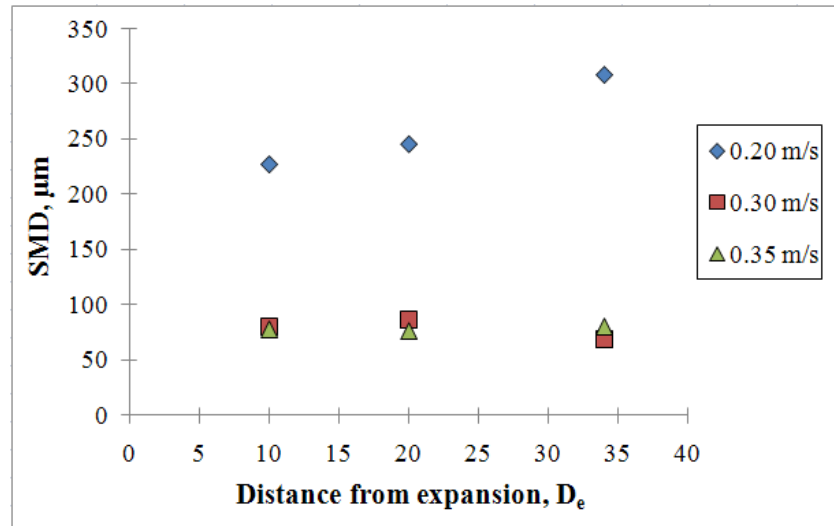


Figure 6.9: D_{32} of oil droplets for 0.4 oil volume fraction system, within test distance in horizontally pipe orientation, probe position 34 mm from bottom at different downstream mixture velocity, U_{sme} .

Further increased the oil volume fraction to 0.6, the dispersed phase is now water and the oil become continuous phase. Figure 6.10 illustrated the SMD for 0.6 oil volume fraction system for various U_{sme} . As demonstrated in that figure, at 10D downstream the expansion at U_{sme} 0.30 and 0.35 m/s, the drop size was medium size drops. Nevertheless, at U_{sme} 0.20 m/s for the same position downstream the expansion (10D) the drop size was slightly larger. While at 20D downstream the pipe expansion, water droplet become smaller for U_{sme} 0.20 and 0.30 m/s. This was not observed for system of 0.4 OVF earlier. In contrary, at U_{sme} 0.35 m/s, the drop sizes remain the same throughout the whole test section. Further downstream the test section, SMD for U_{sme} 0.20 m/s increased from 70 μm at 20D to about 350 μm at 34D. This is due to coalescence of the dispersed water drop from the oil layer with the drops in the mixed layer due to the narrowing of the mixed region. Stratification is predicted to start beyond this position; if longer test section were to be used probably this could be confirmed.

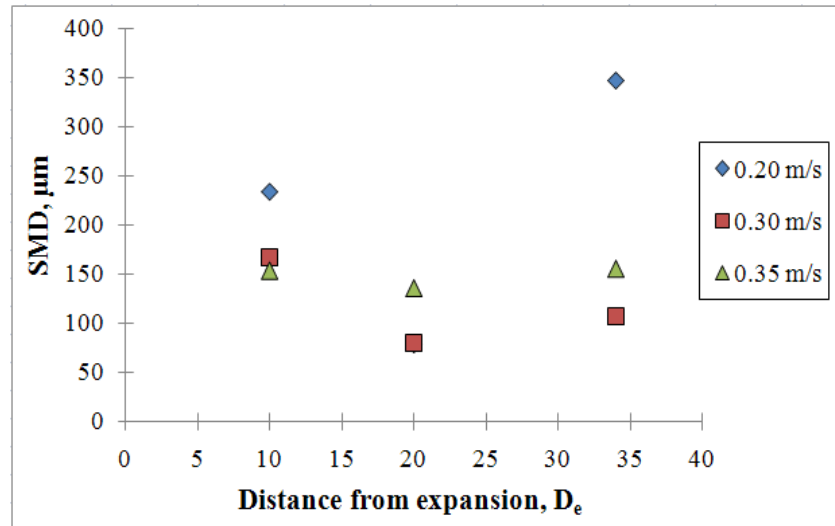


Figure 6.10: D_{32} of water droplets for 0.6 oil volume fraction system, within test distance in horizontally pipe orientation, probe position 34 mm from bottom at different downstream mixture velocity, U_{sme} .

As oil volume fraction was increased further to 0.8, the effect of mixture velocities downstream of pipe expansion on the drops size is presented in Figure 6.11. In general, the drops size detected by the laser for this particular setting; probe position at 17 mm, were bigger. This is due to the probe was near to the interface of the two liquids layer.

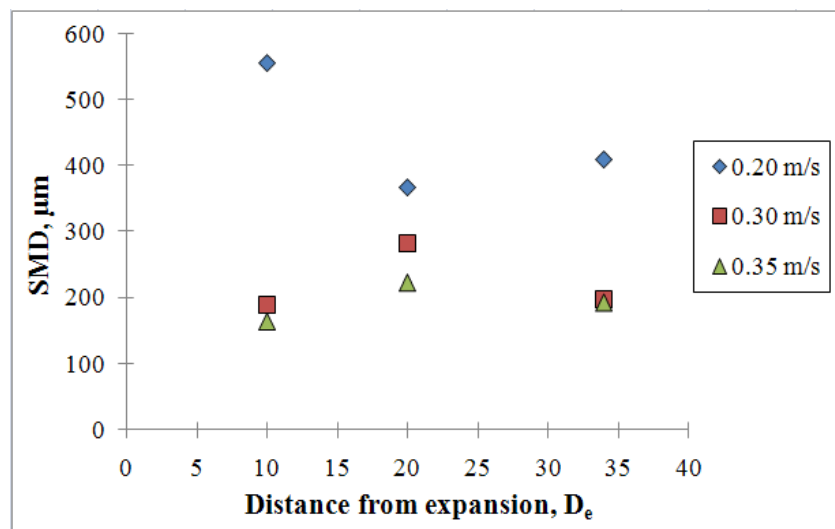


Figure 6.11: D_{32} of water droplets for 0.8 oil volume fraction system, within test distance in horizontally pipe orientation, probe position 17 mm from bottom at different downstream mixture velocity, U_{sme} .

Downstream of the pipe expansion 10D, the biggest water drops were detected by the laser for U_{sme} 0.20 m/s. For this flow conditions, the interface is a bit chaotic and produced bigger droplets near to the interface of these two liquids. Furthermore, the probe was slightly above this interface, in the mixed layer where these big droplets occurred. However as for higher downstream mixture velocities, coalescence did not happened due to time of collision is not enough for the droplets to coalesce. Therefore, droplets with medium size were obtained at these velocities. As for 20D downstream the pipe expansion, size of the water droplets at U_{sme} 0.20 m/s decreased, owing to the stratification process that started to happen which make the interface less disturbed. Hence, the bigger water droplets start to merge with the water layer and left only medium droplet that burst into the mixed layer and detected by the laser. Promoting higher downstream mixture velocity to 0.30 or 0.35 m/s, resulted contrary finding with U_{sme} 0.20 m/s. Instead of decreasing in size, it increased to some extent. The drop size increased as the chaotic interface of the system created by higher mixture velocities causing bigger droplet to be produced then burst into the mixed layer and be detected by the laser. Even though Sleicher (1962) mentioned about decrease in size at high velocities, Howarth (1964) did also mentioned about an increase in velocity causes an increase in coalescence frequency. It is suspected that at 0.30 m/s of these particular conditions and axial position, the velocity of the mixture is optimal for collision of the droplets to happen. Hence increases the coalescence frequency and produced larger droplet. As for axial position 34D downstream the pipe expansion, at U_{sme} 0.20 m/s, the drop size is about the same as at 20D. For higher U_{sme} i.e. 0.30 m/s, the drops size decreased back to medium droplet size as at 10D, because the larger droplet has coalesce at 20D, and

this left only the medium size of water droplets bursting into the mixed layer and detected by the laser.

6.3.2.3 SMD of drops distribution - Probe position

Figure 6.12 shows the progress of drops vertically throughout the test section of 0.2 oil volume fraction system at downstream mixture velocity, $U_{sme} = 0.20$ m/s for horizontal pipe orientation. For 0.2 OVF systems, flowing at lowest U_{sme} , 0.20 m/s, the flow pattern is expected to be dispersed at the near axial position (10D) and stratified flow towards the far end of the expansion (34D). It was also noticed that larger drops is to be exist nearer to the interface (~ 51 m). In general, it could be noticed that the SMD of the drop distribution shown in Figure 6.12 agreed with this assumption. Larger drops were detected at the top of the pipe (near to the interface).

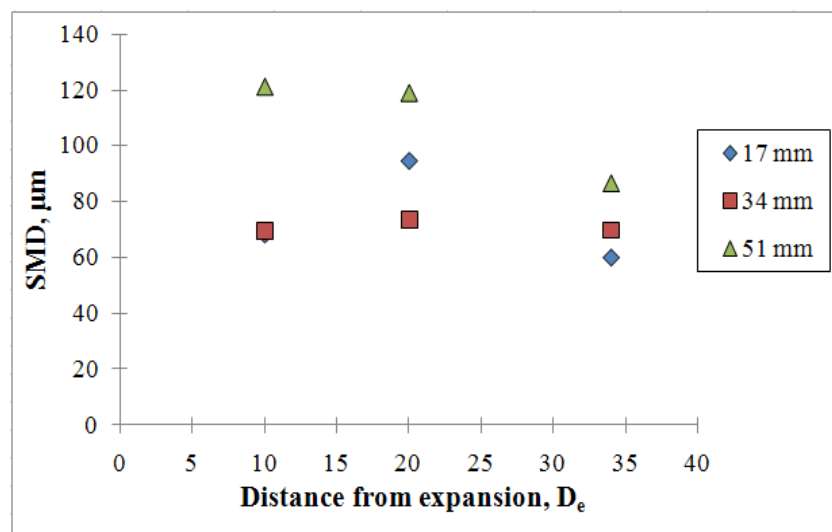


Figure 6.12: D_{32} of oil droplets for downstream mixture velocity, $U_{sme} = 0.20$ m/s, within test distance in horizontally pipe orientation at oil volume fraction system, OVF = 0.2, at different probe position.

Figure 6.13 also illustrate the drop progress vertically throughout the test section with the same flows conditions as Figure 6.12, apart from the oil volume fraction was increased to 0.4. It also shows the same findings as 0.2 oil volume fraction,

larger drops exist near to the interface. In Figure 6.13, the largest drops detected at the middle of the pipe (34 mm from pipe bottom) in agreement with the assumption made earlier. Nevertheless, at the far end (34D) of the expansion, stratification of droplets started to happen. It could be noticed when large droplet also detected at the pipe bottom (17 mm from bottom). Whereas, at the axial position 10D downstream of the pipe expansion, drops size are smaller, due to the dispersion flow at this points. This phenomenon shows that the finer drops (away from interface) begin to coalesce when its flow further downstream the pipe and produce larger drops headed for the interface. Furthermore, as the distance from expansion moved to 34D, the mixed layer has now becoming narrow to the centre (interface) and more drops begin to coalesce to form large drop.

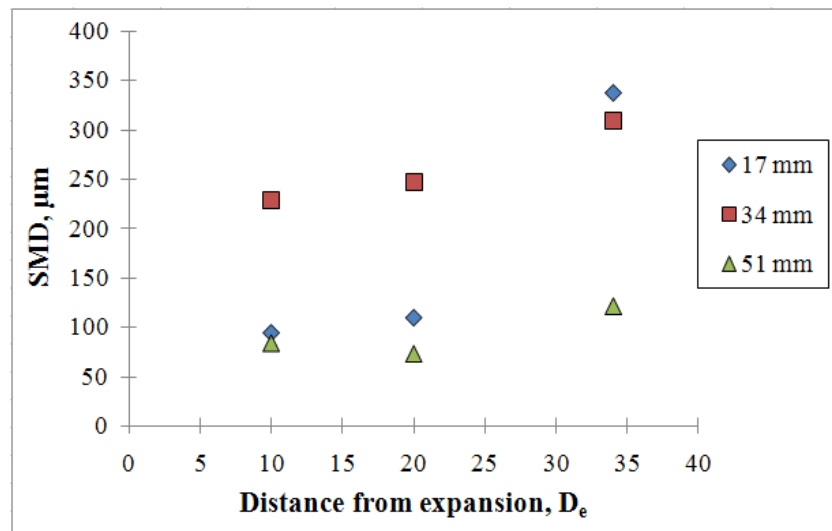


Figure 6.13: D_{32} of oil droplets for downstream mixture velocity, $U_{\text{sme}} = 0.20$ m/s, within test distance in horizontally pipe orientation at oil volume fraction system, $\text{OVF} = 0.4$, at different probe position.

However, this phenomenon can be more clearly observed at the 34D distance from expansion as presented in Figure 6.14. The drops have larger sizes at the centre than at the top and bottom of the pipe cross-section. Larger SMD at the bottom position as can be seen in Figure 6.13 diminishes which mean that the settling process is starting

in here. Consequently, the positions of probe in a pipe cross-section played an important role in determining the drops size especially at the settling region.

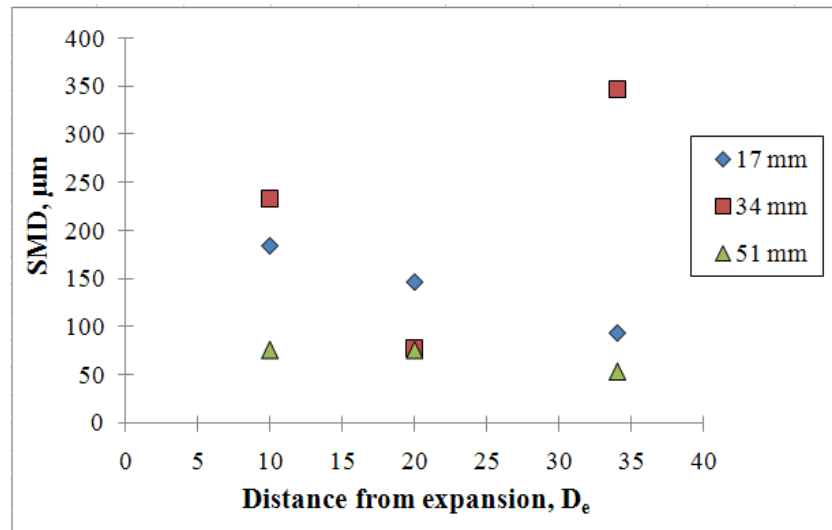


Figure 6.14: D_{32} of water droplets for downstream mixture velocity, $U_{sme} = 0.20$ m/s, within test distance in horizontally pipe orientation at oil volume fraction system, $OVF = 0.6$, at different probe position.

Further increased the oil volume fraction to 0.8, where now water is the dispersed phase and oil is continuous phase. It also agrees with the statement, concentration of larger droplet is at near to the interface as presented in Figure 6.15. Existence of larger droplet could be seen at bottom of the pipe (17 mm).

Nevertheless, due to limitation of the Lasentec, the dispersed phase droplets were expected to affect the reflection of the laser beam to some extent. In particular a combination of the difference in refractive index and the proportion of light that is diffusely reflected (as opposed to specular reflection) from the droplet surface. Typically when silicone oil is the dispersed phase, the amount of FBRM laser light being reflected is a bit lower than if water is the dispersed phase - because of the optical properties. This makes it a bit easier for the FBRM detector to "see" the water droplets compared to the silicone. Now, the optics and electronics of FBRM are

designed in such a way that some degree of variability in the amount of reflected light should not affect the size of the chord length being measured. However in the older models of FBRM such as FBRM M500P that degree of variability is quite modest - thus it is quite likely droplets detected will yield slightly smaller chord lengths in the system of oil dispersed compared to water dispersed.

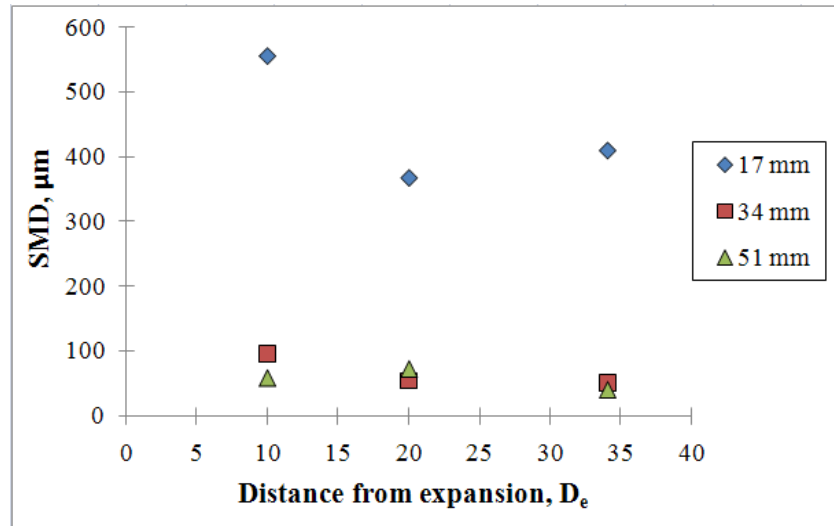


Figure 6.15: D_{32} of water droplets for downstream mixture velocity, $U_{sme} = 0.20$ m/s, within test distance in horizontally pipe orientation at oil volume fraction system, $OVF = 0.8$, at different probe position.

6.3.2.4 Development of drops size - Cross-sectional of horizontally pipe expansion

SMD for drops distribution of two immiscible liquids flowing at various downstream mixture velocities after pipe expansion in horizontal with effect of vertically cross section of the pipe will be presented in this sub-section. Measurement of the drops distribution were made at 3 vertically position from pipe bottom, namely bottom (17 mm), middle (34 mm) and top (51 mm).

In the two-phase flow pattern there is a mixed layer of oil/water flow along the larger pipe downstream of the expansion. However, in this case, the centre of mixed region

is considered as the centre of the interface (Z), while the distances above and below from the centre of interface are measured and identified as a function of distance from centre of the interface, $|Z|$. Figure 6.16 below demonstrated the mean drops diameter of oil-water two phase flow in a horizontally pipe orientation, 10D downstream the expansion for mixture velocity 0.20 m/s, as a function of distance from centre of the interface, $|Z|$. Overall it is clearly shown that larger drops were dispersed nearer to the interface. Nevertheless, there are also smaller drops near to the interface, due to the dispersion of droplets in the entry region of the pipe (adjacent to sudden expansion).

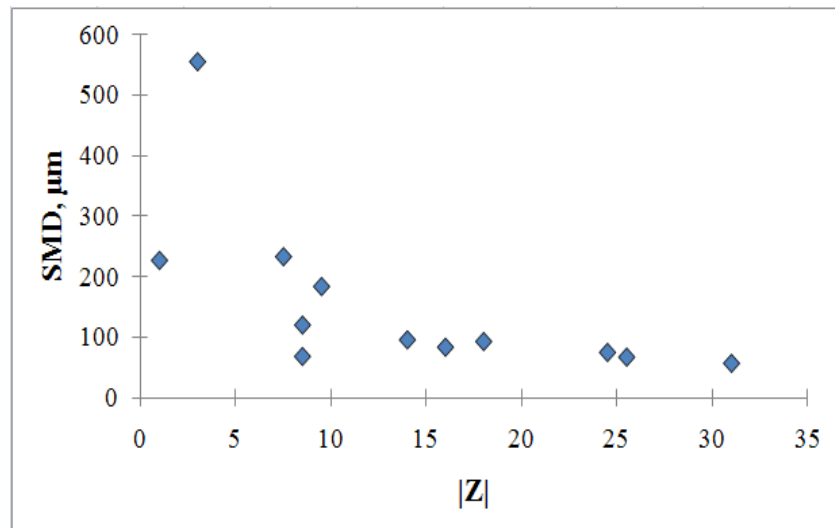


Figure 6.16: Sauter mean diameter as a function of the distance from $|Z|$ at U_{sme} 0.20 m/s of horizontal pipe orientation flow, 10D downstream the expansion.

Figure 6.17 revealed the mean drops diameter of oil-water two phase flow in a horizontally pipe orientation, 34D downstream the expansion for mixture velocity 0.20 m/s, as a function of distance from centre of the interface, $|Z|$. Clearly shown drops were large nearer to the interface. Thus, from the present data, it is established that drops size decreased when the distance from the interface increased (further away).

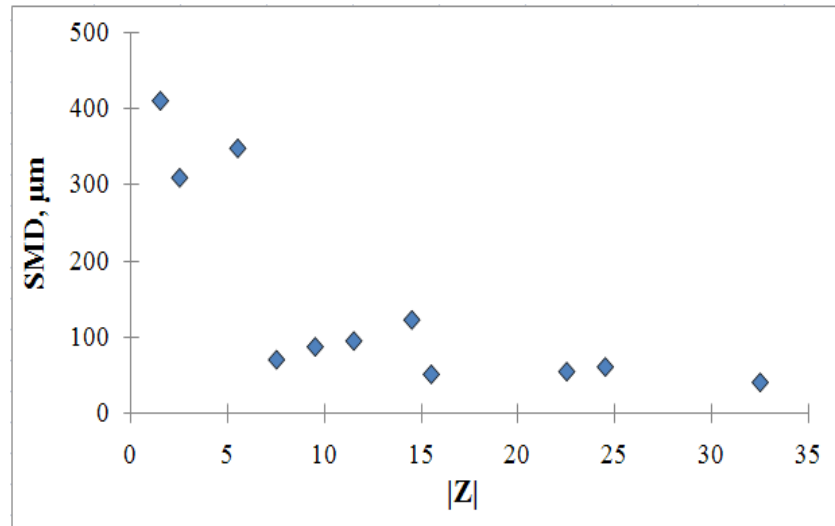


Figure 6.17: Sauter mean diameter as a function of the distance from $|Z|$ at U_{sme} 0.20 m/s of horizontal pipe orientation flow, 34D downstream the expansion.

As a result, the succeeding outcomes can be summarised for SMD of drop diameter distribution in horizontal expansion:

1. Drops distributions (SMD) have been influenced by positions of the phase layer (interfaces) rather than input oil fractions.
2. Phase inversion occurs at the range of input oil volume fraction 0.4 - 0.6.
3. Higher mixture velocities (0.30 & 0.35 m/s) have directly impact on D_{32} along the test section (pipe expansion).
4. D_{32} are strongly influenced by the probe positions. It was noticed and proven that larger drops are to be existing nearer to the interface.

6.3.3 SMD of drop diameter distribution in an upward inclined expansion

A significant body of work on studies of the two immiscible liquid in pipelines at horizontal or vertical pipe orientation has been published. However, for flows of two immiscible liquids in pipelines at small inclination angles, little attempt has been made to provide sufficient drop size data of such configurations.

Dispersion of one phase in the other can occur at the interface in stratified flow and is a common phenomenon in several flow patterns. When the flow pattern of two immiscible liquids is in a dispersed flow, the drop size and drop size distribution will become an important characteristic of the flow. Up to date, there are only a few researches on flows pattern for small upward inclinations from horizontal reported in journals etc.

As predicted by the model of Taitel and Dukler (1976), pipe inclination will affect the interface level between the two phases for the ST regime flow pattern. Generally, it indicates that the lighter phase layer at the pipe top flows faster than the heavier phase layer that flowing at the bottom of the pipe for upward pipe orientations. However, there are others factors that also affect these evolution processes. Therefore, in this section, SMD of drop diameter distribution in two-phase oil-water flow were measured for an upwardly flow inclined which were at the same experiments conditions used in horizontal flow. The angles of an upward inclination flow are +3 and +6 degrees respectively. Analysis of results and discussion are presented below.

6.3.3.1 SMD of drops distribution - Effect of input oil volume fraction

In order to investigate the relation of upward pipe orientation and drop diameter distributions with effect of oil volume fraction (OVF), a few experimental conditions and setting were set up. Result of the experiments were presented and discussed in the following sub-paragraph.

SMD of drop diameter distributions for downstream mixture velocity, $U_{\text{smc}} 0.20$ m/s, at several axial position after expansion in upward pipe orientation ($+6^\circ$) for probe position 17, 34 and 51 mm from bottom at different oil volume fraction are displayed in Figure 6.18 - 6.20 respectively. In general, SMD of the drop diameter distributions for 0.8 OVF was found to be larger than 0.2 OVF systems for the same probe position (17 and 34 mm from pipe bottom) except for top position (51 mm). In Figure 6.18, at 0.2 OVF, throughout the test section the oil droplets are very fine droplets which concentrating at bottom of the pipe throughout the test section. In contrary, at 0.8 OVF, due to the probe position engaged at 17 mm from bottom of the pipe, at the mixed region of 0.8 OVF, larger droplets were detected. The highest SMD of the distribution for this system is about $350\mu\text{m}$ at 10D downstream from expansion. Towards the end (downstream) of the pipe expansion, SMD of drop diameter distribution become smaller, at 20D SMD is about $290\mu\text{m}$ and at 34D is $240\mu\text{m}$. The reason being is that, the flow entered the pipe expansion as dispersed flow and coalescence has already happen by the time the drops reached 10D. Moreover, beyond 10D the process of stratification is starting to begin. Therefore at 10D for probe position 17 mm from bottom, larger droplets were detected by the laser. Whereas at 20D and 34D downstream of the expansion, the flow near the interface becoming less wavy and stratified, respectively. Hence, fewer bigger water droplets were detected in the mixed layer. In other words, settling has happened. Therefore, smaller droplets compared to droplets produced at 10D were detected by the laser at 20D and 34D.

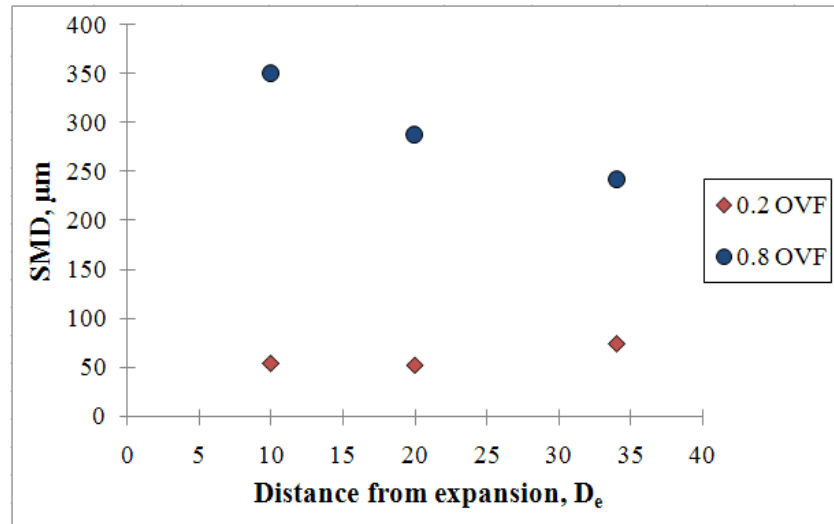


Figure 6.18: Sauter mean diameter for downstream mixture velocity, U_{sme} 0.20 m/s, within test distance in upward 6° pipe orientation, probe position 17 mm from bottom at different oil volume fraction, OVF.

Figure 6.19 shows the influence of oil volume fraction on the SMD of drop diameter for downstream mixture velocity, U_{sme} 0.20 m/s, at several axial positions after expansion in $+6^\circ$ upward pipe orientation for probe position 34 mm from bottom at different oil volume fraction, OVF. Throughout the test section there are only small sizes of oil droplet detected at middle of the pipe cross section for 0.2 OVF systems. Interestingly, at 10D from expansion the SMD of the distribution is as small as SMD for 0.2 OVF. It is suspected that at 34 mm vertically from pipe bottom, for 10D axial distance downstream from expansion, the position of the laser probe are in the dispersed flow with the probe position located in the mid position for both systems (0.2 and 0.8 OVF). Hence, smaller SMD of water drops was observed at this location. Conversely, for 0.8 OVF at probe position 34 mm from bottom of the pipe, medium/ large water droplets were detected at 20D and 34D downstream expansion. Nevertheless, the SMD of the drops diameter distribution were comparatively slightly smaller than SMD at probe position 17 mm from pipe bottom of the same flow condition, about 180 and 240 μ m at 20D and 34D downstream of the pipe

expansion respectively. At 20D position, coalescence of smaller droplets started to materialize. Further coalescence of the drops take place at the farthest position within the test section (34D). Therefore size of drops increased towards the end of the pipe expansion as can be seen in Figure 6.19.

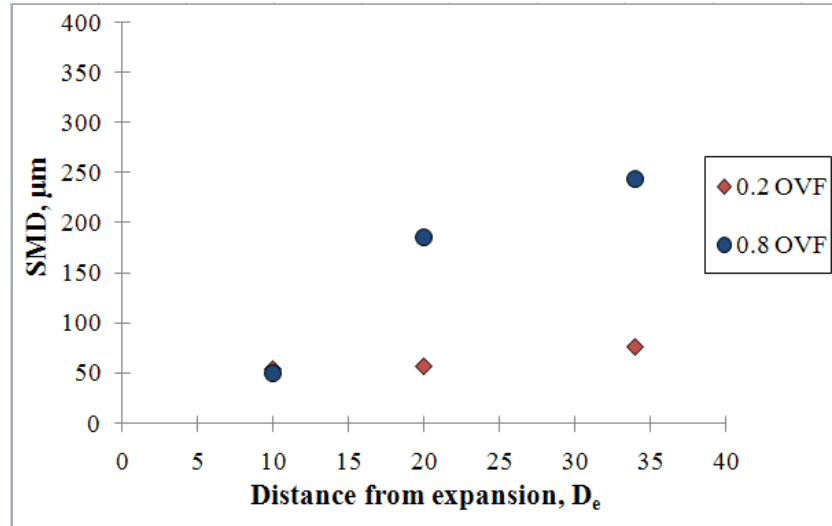


Figure 6.19: Sauter mean diameter for downstream mixture velocity, U_{sme} 0.20 m/s, within test distance in upward 6° pipe orientation, probe position 34 mm from bottom at different oil volume fraction, OVF.

Figure 6.20 demonstrated the effect of oil volume fraction on SMD for drop diameter distributions at top (51 mm from pipe bottom) of the pipe expansion for $+6^\circ$ pipe orientation at U_{sme} 0.20 m/s. It is clearly seen that SMD of the distributions were small for both volume fraction. The water droplets in the 0.8 OVF systems, throughout the test section are very fine droplets. This is due to the interface of the two fluids are relatively far down from the detection point. Hence, only small droplets were burst to the top of the pipe and be detected by the laser. Contrariwise, for 0.2 OVF system, the oil drops detected at 10D were slightly bigger compared to oil drops detected at other vertically position (17 and 34 mm) at the same distance downstream of the expansion. Further downstream of the expansion, at 20D, SMD of the oil drop distributions are the biggest. It is assumed that at 20D, coalescence of the

oil drops occurred, larger droplets were formed. As the drops travelled further downstream, it merges with the bulk of the oil layer before $34D$, encouraging stratification. Henceforth, SMD decreased due to the merging of the larger droplets and left only the smaller drops to be detected by the laser.

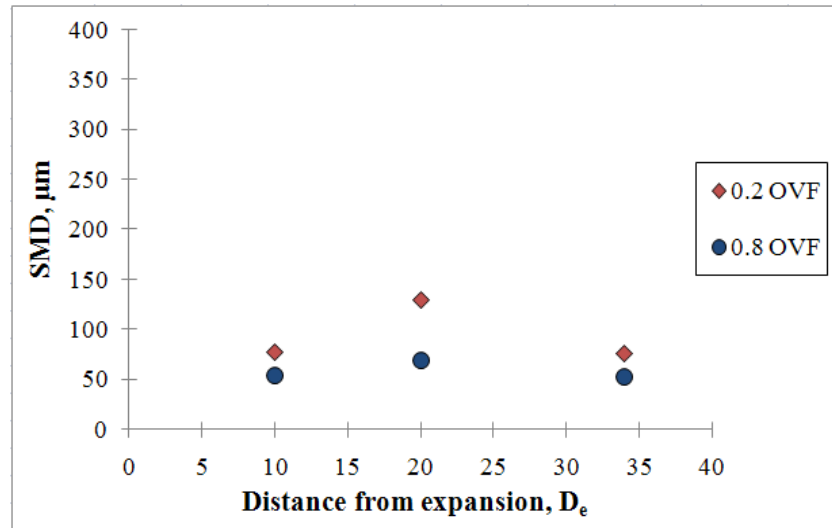


Figure 6.20: Sauter mean diameter for downstream mixture velocity, $U_{\text{sme}} 0.20$ m/s, within test distance in upward 6° pipe orientation, probe position 51 mm from bottom at different oil volume fraction, OVF.

6.3.3.2 SMD of drops distribution - Effect of mixture velocity

Figure 6.21 represent the SMD of water droplets in upward $+6^\circ$ pipe orientation with effect of downstream mixture velocity. The probe position is positioned close to the interface of the liquids i.e. 17 mm from pipe bottom. It can be seen, at $10D$ axial position downstream of the expansion for $U_{\text{sme}} 0.20$ m/s, larger water droplets were detected. The highest SMD of the distribution for this system is approximately $350 \mu\text{m}$ at $10D$ downstream from expansion. SMD of the drops decreased as the mixtures flows towards to the end of the pipe expansion (further downstream). Furthermore, as the U_{sme} increased to 0.30 and 0.35 m/s correspondingly, flows in the system becoming more dispersed. As Sleicher (1962) proposed in his model, increased in mixture velocity causes decreases in droplets size. Interestingly, in present research,

the findings are in good agreement with the model of Sleicher (1962); the higher the U_{sme} , the smaller the droplets sizes. In general, the same phenomenon was also observed for horizontally pipe orientation. However, SMD of the drops distribution for horizontally pipe configuration was larger compared to upward 6° , for all of the axial position downstream the expansion as shown later on in Figure 6.53.

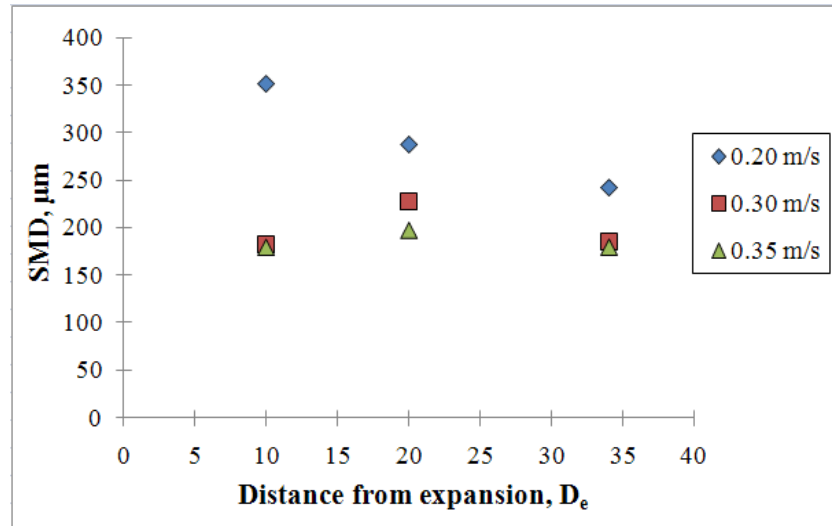


Figure 6.21: D_{32} of water droplets for 0.8 oil volume fraction system, within test distance in upward 6° pipe orientation, probe position 17 mm from bottom at different downstream mixture velocity, U_{sme} .

As the probe position moved up to the centre cross section of the pipe expansion, the effect of U_{sme} on the SMD of the drops distribution is shown in Figure 6.22. At the near (10D) measurement position, at U_{sme} 0.20 m/s, the drops started small (fine droplets) as the probe was in the mixed layer but closer to the continuous phase (oil layer) and away from the interface. However, at the same axial position, for U_{sme} 0.30 and 0.35 m/s, medium size droplets were detected at 34 mm from pipe bottom. The same SMD was also observed at 10D for measurement position 17 mm of the pipe cross section (Figure 6.21). This indicates that in oil continuous flow, higher U_{sme} causes the water droplets to be dispersed at the near position (10D) for U_{sme} 0.30 m/s and throughout the entire pipe expansion section for U_{sme} 0.35 m/s. Further

downstream of the expansion (20D) at U_{sme} 0.20 m/s, water droplets start to gained size through coalescences of the smaller droplets. Hence, at the far position, 34D, the drops distribution giving the largest SMD of all axial position as presented in Figure 6.22.

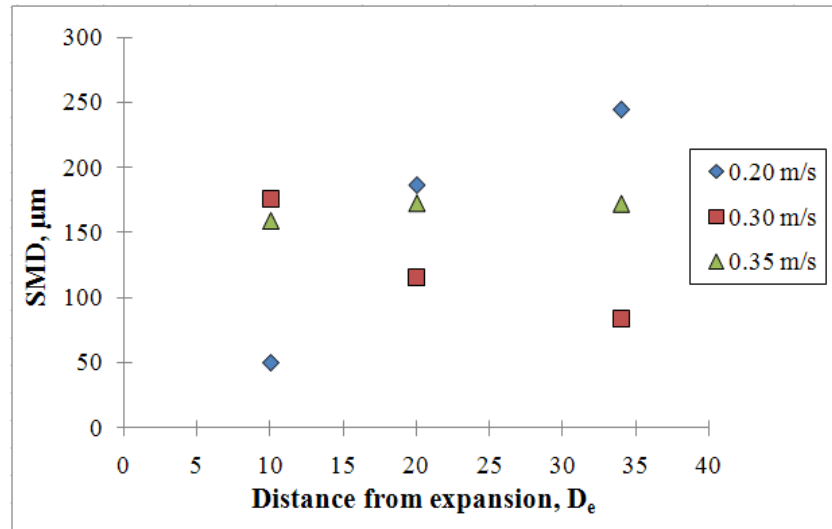


Figure 6.22: D_{32} of water droplets for 0.8 oil volume fraction system, within test distance in upward 6° pipe orientation, probe position 34 mm from bottom at different downstream mixture velocity, U_{sme} .

Interestingly, at U_{sme} 0.30 m/s, SMD of the drops distribution decreased gradually as the measurement position moved axially toward downstream from the expansion. This was found to be opposing to SMD for U_{sme} 0.20 m/s for the same experimental conditions. Reason being is that at centre cross section of the expansion, at 0.30 m/s, water droplets started to coalesce in between 10D and 20D downstream of the expansion. Consequently, leaving the medium size droplet flowing in the detection region and be detected by the FBRM. Further coalescence of the medium size droplets continue to take place at 34D, leaving only the smaller droplet flows in the region of detection point (probe position). Nevertheless, at the highest U_{sme} , 0.35 m/s, the SMD of the drops distribution remains the same (size) at all point of the pipe

cross section throughout the test section (pipe expansion), indicated that water droplets were fully dispersed along the expansion.

Figure 6.23 denoted the SMD of water droplets in upward $+3^\circ$ pipe orientation with effect of downstream mixture velocity, U_{sme} . Oil volume fraction for the system is 0.8 with the probe positioned 17 mm from the pipe bottom. As the probe was close to the interface, the drops were found to be as large as for the other pipe orientations i.e. horizontal and $+6^\circ$ upward inclination, for U_{sme} 0.20 m/s. Furthermore, at higher U_{sme} , the drops size decreased, with $U_{sme} = 0.35$ m/s giving the smallest SMD of drop distribution. Interestingly, for such flow system (oil continuous flow), the drops size were about the same size throughout the test section. Additionally, the drops size were nearly the same for all pipe orientation; horizontal, $+6^\circ$ and $+3^\circ$. This points out that the drops sizes were measured in the mixed layer of the flow system.

Figure 6.24 shows the influence of downstream mixture velocity (U_{sme}) on drop size distribution for oil continuous flow system (0.8 OVF) at several axial position downstream expansion and probe position at centre of the pipe cross section (34 mm) in $+3^\circ$ upward pipe orientation. The highest SMD of the drops distribution were found to be at the near (10D) position of detection for U_{sme} 0.20 m/s. For the same mixture velocity, it can be seen that SMD of the drops decreased as the mixtures flows towards to the end of the pipe expansion (further downstream).

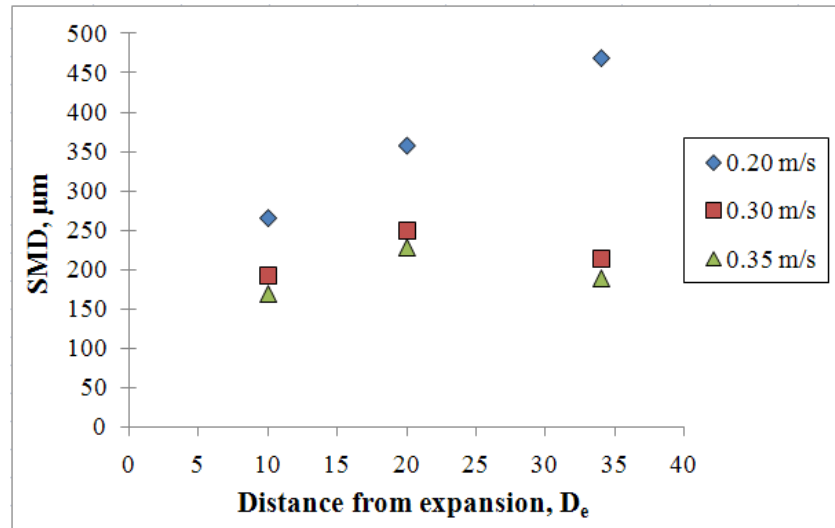


Figure 6.23: D_{32} of water droplets for 0.8 oil volume fraction system, within test distance in upward 3° pipe orientation, probe position 17 mm from bottom at different downstream mixture velocity, U_{sme} .

It is observed that at $34D$ downstream of the expansion, the flow was ST&MI and the probe was in the oil layer. Hence, only smaller droplets or less large water droplets were detected by the probe at this position as presented in Figure 6.24.

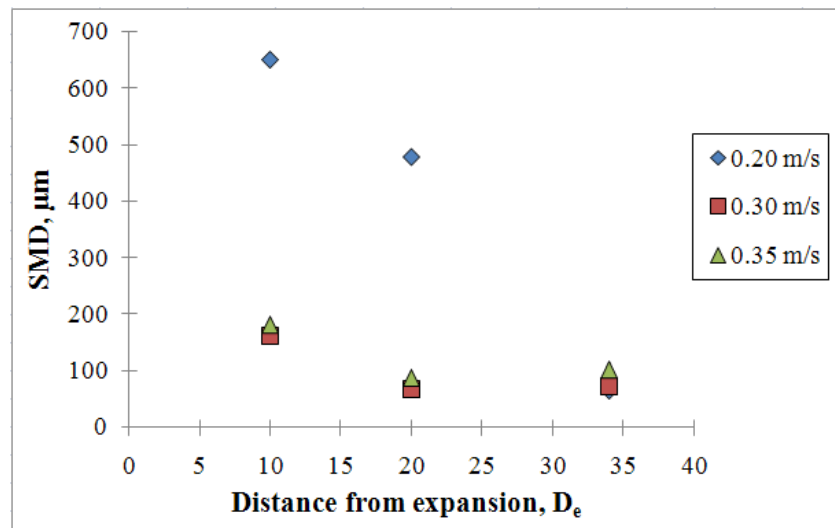


Figure 6.24: D_{32} of water droplets for 0.8 oil volume fraction system, within test distance in upward 3° pipe orientation, probe position 34 mm from bottom at different downstream mixture velocity, U_{sme} .

Increased the U_{sme} to 0.30 and 0.35 m/s correspondingly, flows in the system becoming more dispersed, particularly at the near ($10D$) position downstream the

expansion. Therefore, water layer become fully dispersed and water droplets were detected at all point in the cross section of the pipe at this position. Most importantly this findings are in good agreement with what Sleicher (1962) proposed in his model, increased in mixture velocity causes decreases in droplets size.

6.3.3.3 SMD of drops distribution - Probe position

Figures 6.25 - 6.27 show results of SMD for drops distribution at various probe positions in a pipe cross-section, downstream of the +6° upward inclination expansion. The evolution of drops size distribution for 0.2 OVF in +6° upward pipe orientation at U_{sme} 0.20 m/s is shown in Figure 6.25. The results show that when the probe was positioned at the top (51 mm) of the pipe cross section, the mean diameter of the droplets are larger than the other two, bottom (17 mm) and middle (34 mm) position. The same phenomenon occurs at 20D from expansion; however the SMD of the drop distribution increased further to nearly twice as at 10D. This indicates that the dispersed finer drops has started to coalesced, hence bigger droplets were detected by the probe at this location (top of the pipe cross section). As the droplets travelled further downstream the expansion, at 34D after expansion, the flow pattern was observed to be as semi-stratified with the centre of the interface is at about 0.65 of the expansion height. Therefore, the probe was neither in oil layer nor water layer, detecting only smaller droplets, producing smaller SMD as shown in Figure 6.25.

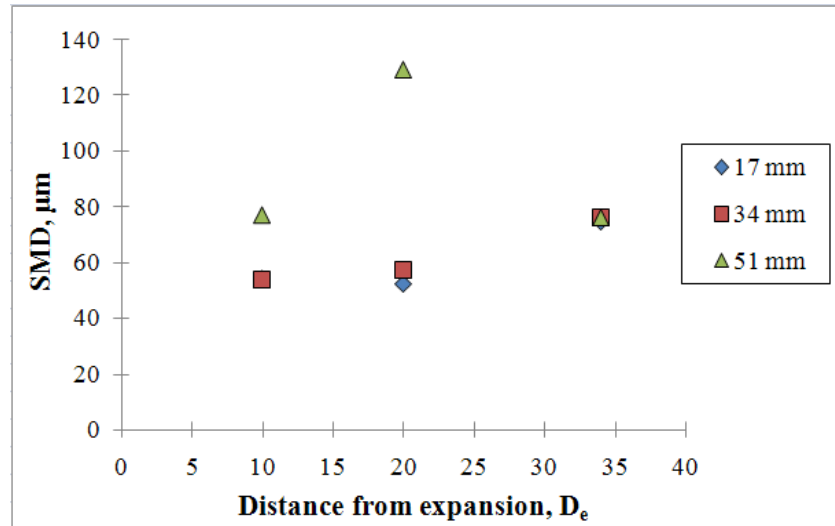


Figure 6.25: D_{32} of oil droplets for downstream mixture velocity, $U_{\text{sme}} = 0.20$ m/s, within test distance in upward 6° pipe orientation at oil volume fraction system, $\text{OVF} = 0.2$, at different probe position.

Figure 4.26 illustrated the evolution of drops size distribution for 0.8 OVF in $+6^\circ$ upward pipe orientation at $U_{\text{sme}} 0.20$ m/s. At distance 10D downstream expansion when the probe was positioned at the bottom (17 mm) of the pipe cross section, the mean diameter of the droplets are larger than the other two, middle (34 mm) and top (51 mm) position. This is due to the probe was positioned near the interface and larger droplets is to be exist near the interface. Further downstream the expansion, at 20D, the same singularity occurs; the droplets were larger at the bottom of the pipe, medium size at the centre (34 mm) of the expansion cross section and smallest at top of the expansion. For bottom and centre probe position, the probe was in the mixed layer and oil layer, respectively. However it can be noticed that at 20D, the SMD of the drop distribution at centre of the cross section has increased. This indicates that the dispersed finer drops (at 10D) have started to coalesced, hence an increase of drops sizes were detected by the probe at this location (34 mm). As further downstream the expansion, at 34D after expansion, both positions (bottom and centre) showed the drops have the same size which indicated that these drops are in

the mixed layer. Therefore, the height of the mixed layer has increased toward the downstream of the expansion.

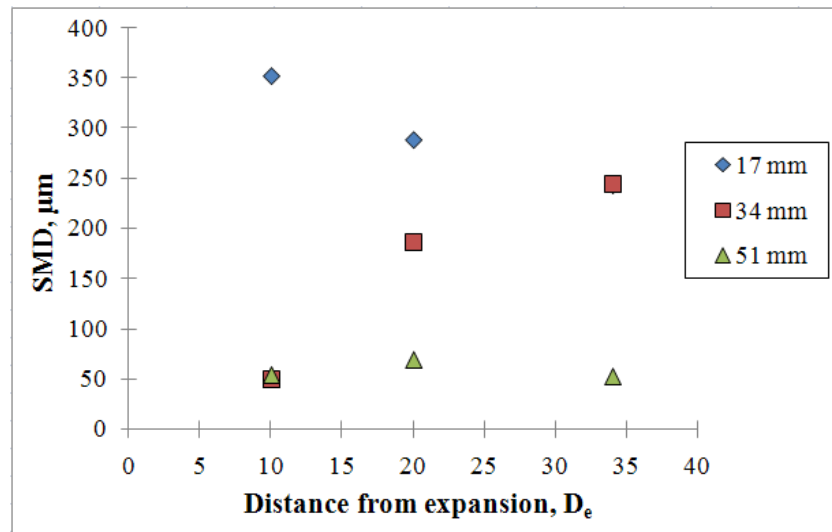


Figure 6.26: D_{32} of water droplets for downstream mixture velocity, $U_{\text{sme}} = 0.20$ m/s, within test distance in upward 6° pipe orientation at oil volume fraction system, $\text{OVF} = 0.8$, at different probe position.

Figures 6.27 show the results of SMD for drops distribution in a pipe cross-section, downstream of the $+6^\circ$ upward inclination expansion for higher U_{sme} (0.35 m/s). As the oil volume fraction is 0.8, the continuous flow is oil and dispersed flow is water. The results show that at 10D downstream the expansion, the mean diameter of the water droplets is the same at any point in the pipe cross-sectional area. This indicates that at 10D the two liquids are nearly homogeneous flow. At this point, the dispersed flows are well mixed, so that the oil and water velocities are similar. The same mean diameters were also detected, further downstream at 20D and 34D of the expansion for bottom and centre of the expansion cross section. In contrary, mean diameter at the pipe top (51 mm from bottom) decreased, due to the droplet (at 10D) has settle due to gravity forces. However as for bottom and centre of the pipe cross section, the mixed layer hardly decays. Owing to higher U_{sme} , the turbulence intensity also increase, hence coalescence of the droplets in the dispersion were delayed.

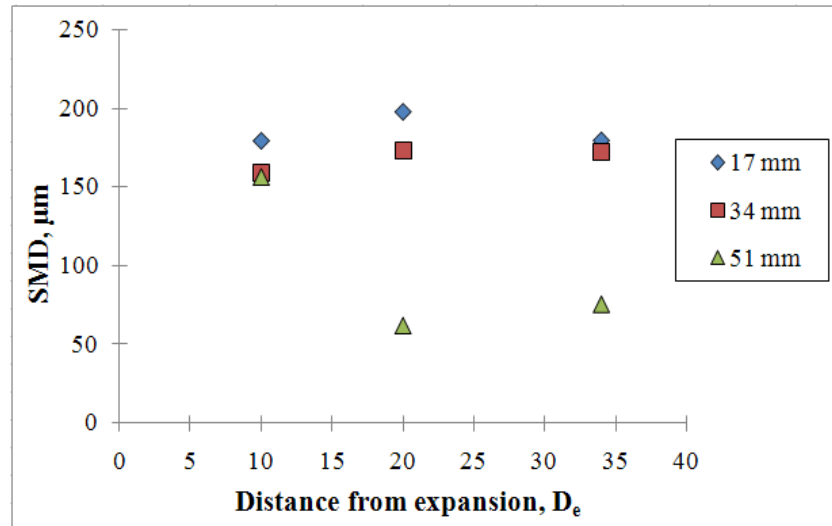


Figure 6.27: D_{32} of water droplets for downstream mixture velocity, $U_{sme} = 0.35$ m/s, within test distance in upward 6° pipe orientation at oil volume fraction system, $OVF = 0.8$, at different probe position.

In the studies of the development of drops size in the entire pipe cross-sectional area downstream of an expansion, measurement of drops size distribution were made at the same conditions as in the previous measurement except that now the inclined angle are $+3^\circ$ upward. Figure 6.28 - 6.29 show results of SMD for drops distribution at various probe positions in a pipe cross-section, downstream of the $+3^\circ$ upward inclination expansion. The evolution of drops size distribution for 0.8 OVF in $+3^\circ$ upward pipe orientation at U_{sme} 0.20 m/s is shown in Figure 6.28. The results demonstrate that at 10D, largest droplets were detected when the probe was positioned at centre (34 mm) of the pipe cross section followed by medium size at pipe bottom and the smallest at 51 mm (pipe top). The reason is because at this position the mixed layer was slightly below to centre of the pipe cross section, even though the oil volume fraction is 0.8. As observed by Hasan (2006), drops size tend to increase above and below the centre of the mixed layer. At the middle of the pipe expansion (axially), the mixed layer become narrow and the level of the water/mixed layer interface increased. This indicates that coalescence and settling at the centre

and bottom of the expansion has started. Therefore, at 20D downstream expansion water droplets detected at centre of the pipe cross section decreased and at 17 mm from pipe bottom increased. Drops size at the pipe top remains the same (~ 60 micron), as at this position the probe are in the oil layer and further away from the water/mixed layer interface. Therefore, less water droplets or only smaller droplets were detected by the probe at this location. Meanwhile, as the droplets travelled further downstream the expansion, at 34D after expansion, the mixed layer become narrower and water/mixed layer interface are semi-stratified. As can be seen in Figure 6.30, mean diameter of the drops distribution at 34 mm has decreased. Indicating that stratification nearly completed with the interface is at about 0.3 of the expansion height.

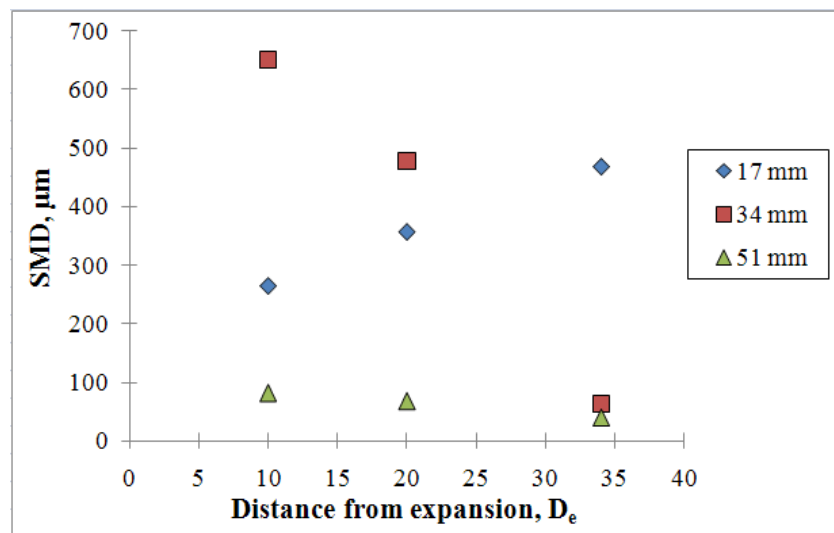


Figure 6.28: D_{32} of water droplets for downstream mixture velocity, $U_{\text{sme}} = 0.20$ m/s, within test distance in upward 3° pipe orientation at oil volume fraction system, $\text{OVF} = 0.8$, at different probe position.

Figures 6.29 show the results of SMD for drops distribution in a pipe cross-section, downstream of the $+3^\circ$ upward inclination expansion for higher U_{sme} (0.35 m/s). As the oil volume fraction is 0.8, the continuous flow is oil and dispersed flow is water. The results show that at 10D downstream the expansion, the mean diameter of the

water droplets is the same at any point in the pipe cross-sectional area. This indicates that at 10D the two liquids are nearly homogeneous flow. At this point, the dispersed flows are well mixed, so that the oil and water velocities are similar. In contrary, at 20D, mean diameter for middle (34 mm) and top (51 mm) decreased steeply and remain about the same size throughout the test section (34D). Furthermore, mean diameter at the pipe bottom (17 mm from bottom) slightly increase, perhaps due to collisions frequency increased. However, there are no further coalescence happened at 34D, as for higher U_{sme} , collision time is not sufficient enough for drop-drop coalescence to materialise. Owing to higher U_{sme} , the turbulence intensity also increase, hence coalescence of the droplets in the dispersion were delayed. Hence, the mixed layer hardly decays within the test section.

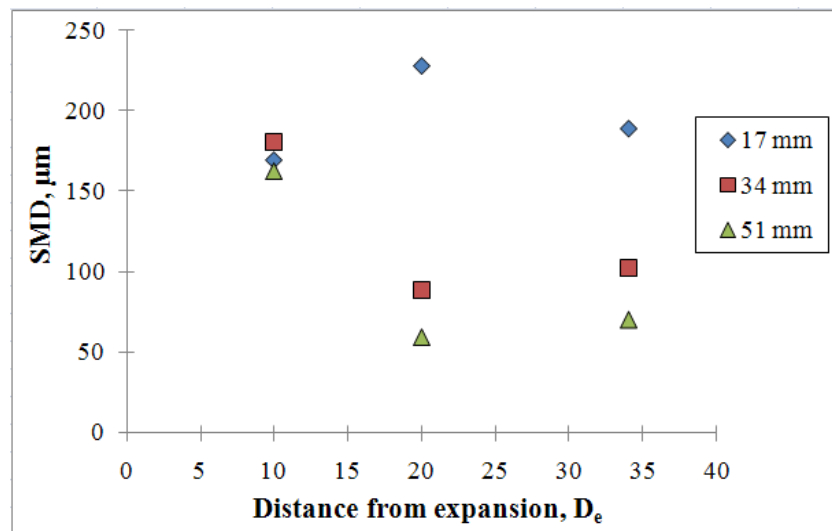


Figure 6.29: D_{32} of water droplets for downstream mixture velocity, $U_{sme} = 0.35$ m/s, within test distance in upward 3° pipe orientation at oil volume fraction system, $OVF = 0.8$, at different probe position.

6.3.3.4 Development of drops size - Cross-sectional of the upward pipe expansion

As mentioned earlier in this chapter, in order to studies the development of drops size in the entire pipe cross-sectional area downstream of an expansion, measurement of drops size distribution were made at several position of the pipe expansion for

various downstream mixture velocities. In this sub-section though, the test section were set to be upward inclination.

Figure 6.30 below demonstrated the mean drops diameter of oil-water two phase flow in $+6^\circ$ upward pipe orientation, 10D downstream the expansion for mixture velocity 0.20 m/s, as a function of distance from the interface, $|Z|$. Clearly shown drops were large nearer to the interface at axial position 10D downstream the expansion.

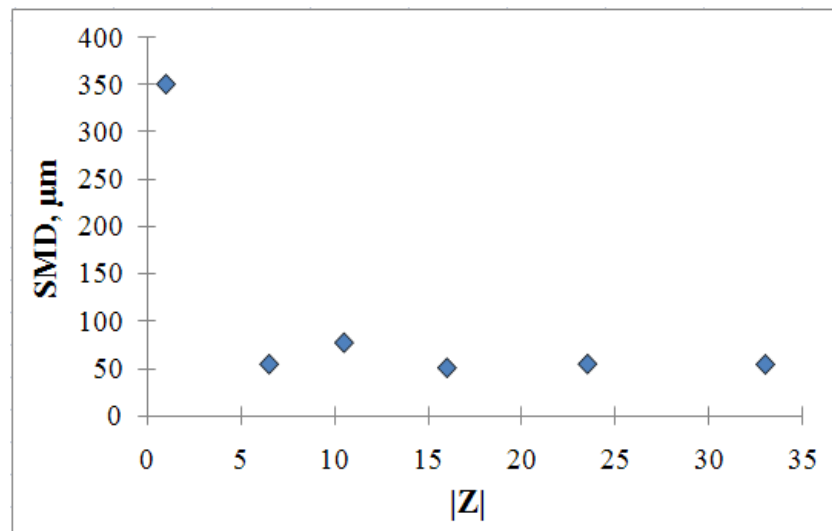


Figure 6.30: Sauter means diameter as a function of the distance from $|Z|$ at U_{sme} 0.20 m/s of $+6^\circ$ upward inclined pipe orientation flow, 10D downstream the expansion.

However, for the mean drops diameter as a function of distance from the interface, $|Z|$ at U_{sme} 0.20 m/s of $+6^\circ$ upward inclined pipe orientation at 34D from expansion as shown in Figure 4.31, different phenomena arises. The assumption made for horizontal flow is no longer valid for $+6^\circ$ upward inclined flow. This is in line for the force equilibrium conditions were modifies when the pipe orientation was changed from horizontal to $+6^\circ$ upward inclined. The flow gravity force is now divided into two components, normal and parallel to the pipe axis. The normal gravity component enhances the segregation of the fluids, similar to the horizontal case. However the

parallel component act in the opposite mean direction, therefore the water flow is retarded (waves) and accumulates in the upward flow. As a result larger droplets could be seen at distance away from the interface and vice versa as illustrated in Figure 6.31

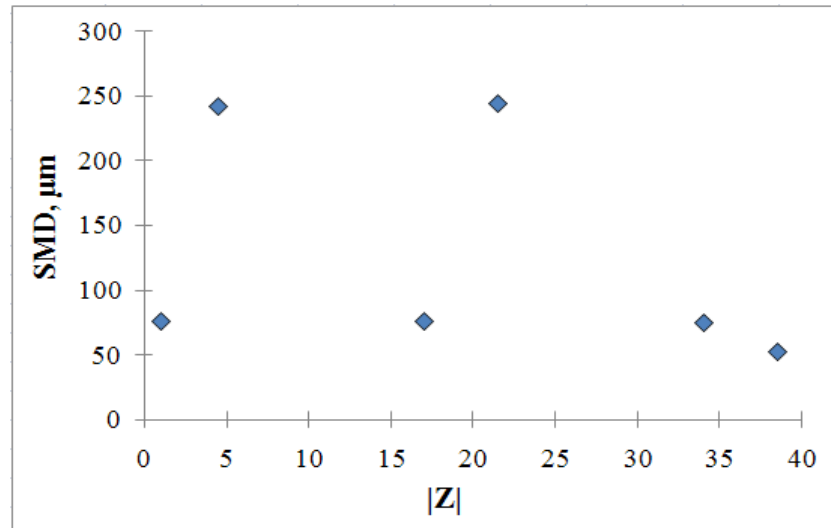


Figure 6.31: Sauter means diameter as a function of the distance from $|Z|$ at $U_{\text{sme}} 0.20$ m/s of $+6^\circ$ upward inclined pipe orientation flow, 34D downstream the expansion.

Figure 6.32 below demonstrated the mean drops diameter of oil-water two phase flow in $+3^\circ$ upward pipe orientation, 10D downstream the expansion for mixture velocity 0.20 m/s, as a function of distance from the interface, $|Z|$. Overall it is clearly shown that larger drops were dispersed nearer to the interface. Nevertheless, there are also smaller drops near to the interface, due to the dispersion of droplets in the entry region of the pipe (adjacent to sudden expansion).

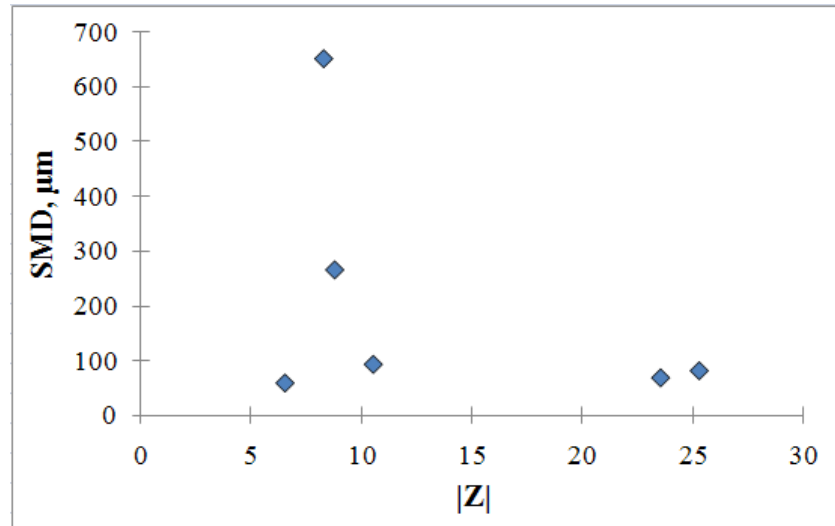


Figure 6.32: Sauter mean diameter as a function of the distance from the interface, $|Z|$ at $U_{\text{sme}} 0.20$ m/s of $+3^\circ$ upward inclined pipe orientation flow, 10D downstream the expansion.

The same occurrences for the mean drops diameter of oil-water two phase flow in $+3^\circ$ upward pipe orientation (Figure 6.32), at 34D downstream the expansion for mixture velocity 0.20 m/s, as a function of distance from the interface, $|Z|$ as shown in Figure 6.33. It shows that larger drops were dispersed nearer to the interface. Nevertheless, there are also smaller drops near to the interface, due to the dispersion of droplets in the entry region of the pipe (adjacent to sudden expansion). However, at 34D, the large droplets were slightly closer to the interface compared to 10D, indicates that stratification is begin to take place.

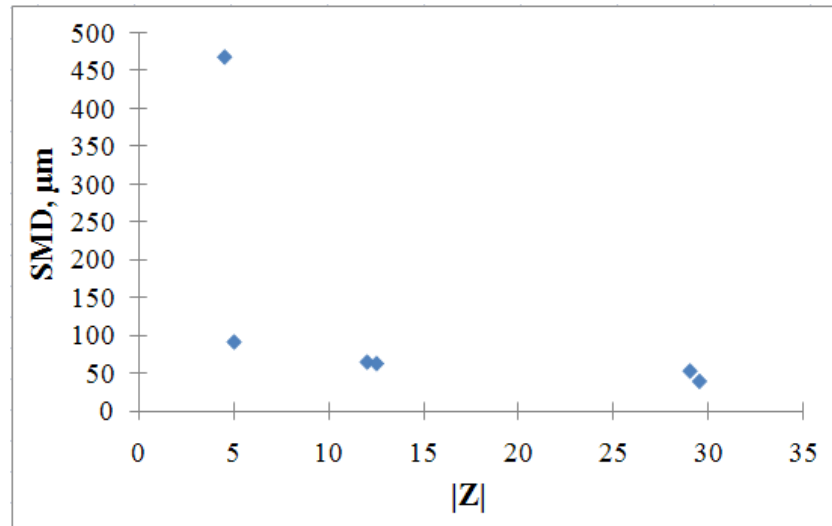


Figure 6.33: Sauter means diameter as a function of the distance from $|Z|$ at $U_{\text{sme}} 0.20$ m/s of $+3^\circ$ upward inclined pipe orientation flow, 34D downstream the expansion.

The following points can be concluded for the D_{32} in the upward inclination:

1. Droplets in oil continuous flow, settle down (stratified) slightly quicker than droplets in water continuous flow.
2. In higher input oil volume fractions, waves could be observed especially at 10D and then become weaker further downstream.
3. Distance from the interface $|Z|$ increase, mean drops diameter decreased only true for upward inclination angle $\leq +3^\circ$.

6.3.4 SMD of drop size distribution in a downward inclined flow

As predicted by the model of Taitel and Dukler (1976), pipe inclination will affect the interface level between the two phases for the ST regime flow pattern. Therefore, in this section, SMD of drop diameter distribution in two-phase oil-water flow were measured for downward flow inclined which were carried out in the same conditions as in the previous section but in the opposite direction. The angles of downward inclination flow are -3 and -6 degrees respectively. The effect of downward

inclination flow on development of drop size distributions is again investigated and demonstrated.

6.3.4.1 SMD of drops distribution - Effect of input oil volume fraction

Earlier in this chapter, the relation of upward pipe (expansion) orientation and drop diameter distributions with effect of oil volume fraction (OVF) has been investigated. In this subsection, the same parameter was also being investigated, however this time the orientation of the pipe expansion was downward angle inclination. Result of the experiments were presented and discussed in the following sub-paragraph.

Figures 6.34- 6.35 represented the results for SMD of drop diameter distributions for downstream mixture velocity, U_{sme} 0.20 m/s, at several axial position after expansion in downward pipe orientation (-6°) for probe position 17 and 34 mm from bottom at different oil volume fraction, OVF. As presented in Figure 6.34, two significant that are clearly showed by the figure; (a) oil droplets started small ($D_{32} = 50 \mu\text{m}$) at 10D and 20D indicating that it is still in dispersed regime, thereafter, the droplets gained size (coalescence) when flowing further downstream to $D_{32} = 300 \mu\text{m}$ at 34D. (b) water droplets started big ($D_{32} = 200 \mu\text{m}$) at 10D, drop size decreased at 20D due to coalescence of the bigger droplet leaving the medium drops ($D_{32} = 116 \mu\text{m}$) dispersed in the detection region and further towards the end of the test section, coalescence and stratification of droplets occurs here at 34D, D_{32} decreased to $80 \mu\text{m}$.

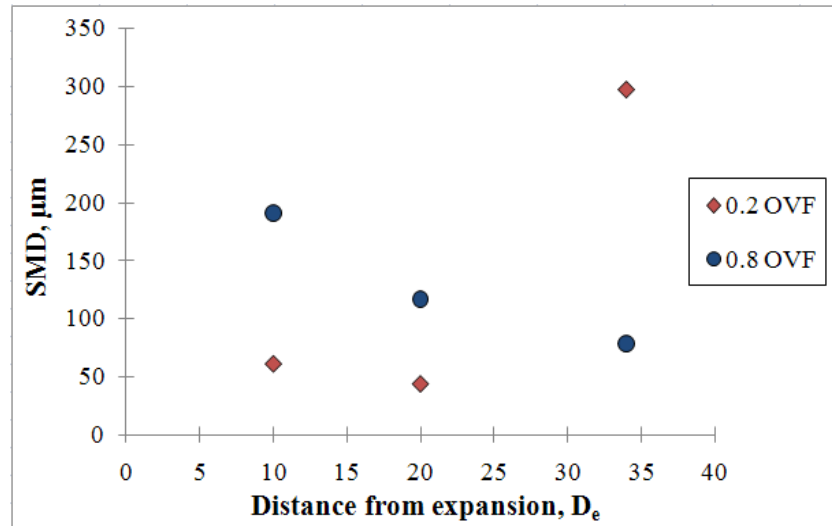


Figure 6.34: Sauter mean diameter for downstream mixture velocity, $U_{\text{sme}} 0.20$ m/s, within test distance in downward 6° pipe orientation, probe position 17 mm from bottom at different oil volume fraction, OVF.

Figure 6.35 demonstrated the results for probe position 34 mm from bottom at different oil volume fraction, throughout the test section the droplets size are considered small whether it is oil or water droplets. Nonetheless, at 10D downstream the expansion, the droplets; oil and water drops were about the same size, and they starts to gain size further downstream, at 20D from expansion, giving slightly larger drops. Again the drops size for both oil and water drops were about the same size (around 110 μm). Further downstream, at 34D, oil drops size decreased to 100 μm , however it is not significant as the different is very little. Contrariwise, the decreased of the SMD of water drop at 34D downstream of the pipe expansion were large, water drops size decreased to 50 μm . The reason being is that, when larger drops produced at 20D travelled further downstream, coalesced. Hence, leaving smaller droplets compared to droplets produced at 20D, dispersed in the mixed layer and detected by the laser at 34D.

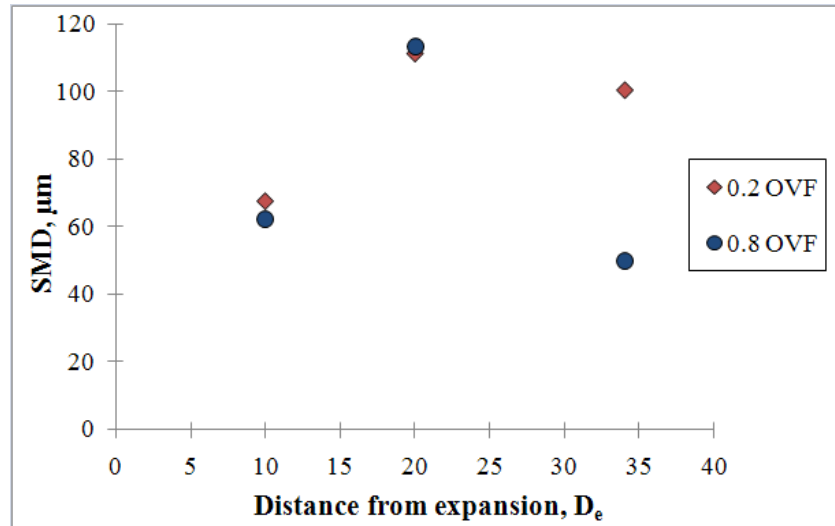


Figure 6.35: Sauter mean diameter for downstream mixture velocity, $U_{\text{sme}} 0.20$ m/s, within test distance in downward 6° pipe orientation, probe position 34 mm from bottom at different oil volume fraction, OVF.

As for -3° downward pipe orientation, Figure 6.36 - 6.37 respectively representing the results for SMD of drop diameter distributions for downstream mixture velocity, $U_{\text{sme}} 0.20$ m/s, at probe position 17 and 34 mm from bottom for different oil volume fraction. Figure 6.36 and 6.38 show the same pattern, especially for water drops of the drops evolution throughout the test section, water droplets started big ($D_{32} = 300 \mu\text{m}$) at 10D, drop size decreased sharply at 20D due to stratification and coalescence of the bigger droplet leaving only the drops of mean size around $70 \mu\text{m}$ dispersed in the detection region. Further towards the end of the test section, at 34D, D_{32} remain the same as at 20D.

Interestingly, the same occurrences as Figure 6.34 and 6.36 could be seen for mean diameter at $U_{\text{sme}} 0.20$ m/s, in downward 3° pipe orientation for probe position 34 mm from bottom as shown in Figure 6.37. However the D_{32} decreased gradually rather than sharply decreased for D_{32} measured at bottom of the pipe cross section (17 mm).

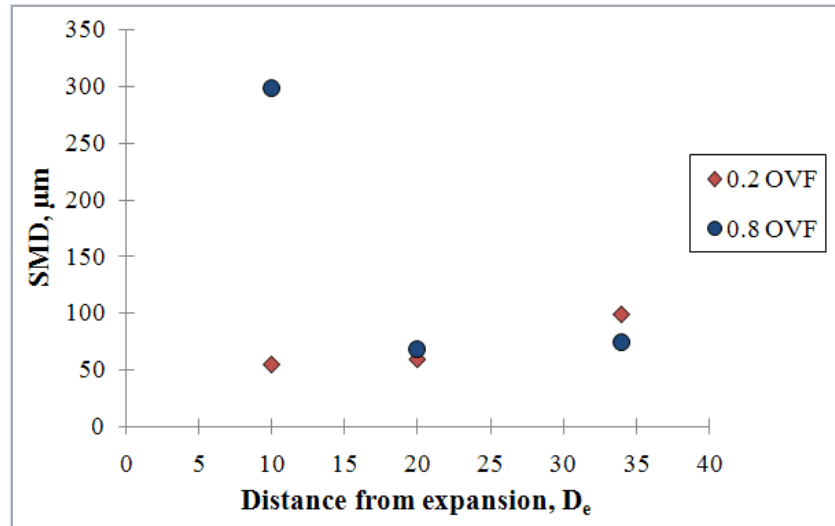


Figure 6.36: Sauter mean diameter for downstream mixture velocity, U_{sme} 0.20 m/s, within test distance in downward 3° pipe orientation, probe position 17 mm from bottom at different oil volume fraction, OVF.

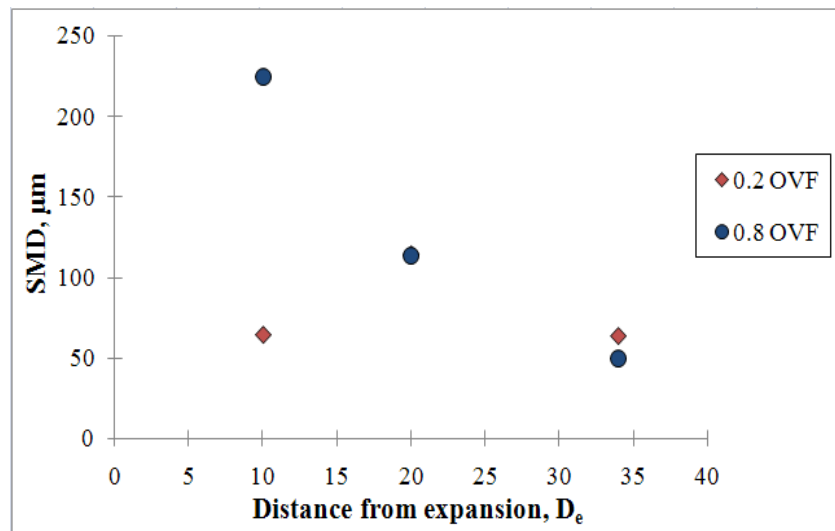


Figure 6.37: Sauter mean diameter for downstream mixture velocity, U_{sme} 0.20 m/s, within test distance in downward 3° pipe orientation, probe position 34 mm from bottom at different oil volume fraction, OVF.

6.3.4.2 SMD of drops distribution - Effect of mixture velocity

The effect of mixture velocity on the drops mean diameter downstream of the expansion at constant input oil volume fraction either 0.2 or 0.8 for a downward inclination flow is shown in Figure 6.38 - 6.43.

Figure 6.38 shows the mean drops diameter at bottom of the pipe cross section for -6° downward pipe inclination at 0.2 input oil volume fraction for various U_{sme} . When an increase in mixture velocity at constant input oil volume fraction while probe was moved along the expansion, for position 10D and 20D the mean drops diameter changes are insignificant. Even though the mixture velocity increases, the mean drops diameter for downward flow, at near and middle positions were not affected. At the far position, however, the D_{32} are influenced by mixture velocity. This suggests that the level of the interface in the downward flow is narrowing with the layer of oil moved further down. Therefore larger drops accumulate at the bottom of the pipe cross section at 34D downstream of the expansion for U_{sme} 0.20 m/s for this input oil volume fraction.

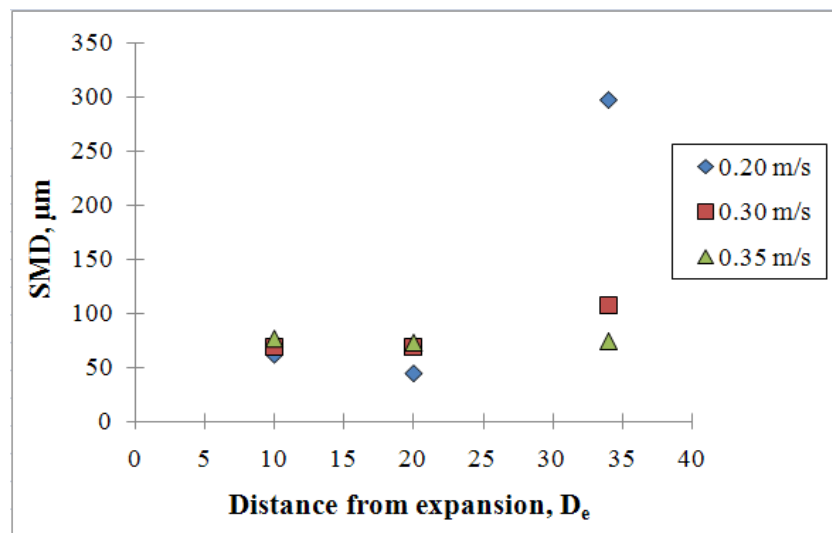


Figure 6.38: D_{32} of oil droplets for 0.2 oil volume fraction system, within test distance in downward 6° pipe orientation, probe position 17 mm from bottom at different downstream mixture velocity, U_{sme} .

Figure 6.39 shows the mean drops diameter at bottom of the pipe cross section for -6° downward pipe inclination at 0.8 input oil volume fraction for various U_{sme} . At 10D the mean drops diameter were about the same for all U_{sme} due to probe in the downward flow is situated in the dispersed region. Further downstream at lower

downstream mixtures velocity, D_{32} measured gradually becomes smaller, owing to the coalescence has occurred, leaving medium drops dispersed in the detection region. Followed by semi-stratification of water droplets at 34D, where only small water drops left in the mixed layer. At 20D downstream the expansion, for 0.30 and 0.35 m/s, seems like coalescence beginning to happen. This could be noticed as the mean drops size start to become slightly larger than that of 10D. Nevertheless, at higher U_{sme} , coalescence was minimal due to the collisions time were not sufficient enough, even though it is expected that more droplets are created as the mixture velocity increases. Interestingly, at 34D, D_{32} turn out to be smaller, in fact smaller than the initial drops size (10D). Beyond this distance from expansion further coalescence of the medium size drops is predicted to take place, if looking and based on the progress of the drops size. However how much further downstream, that is something needs to be determined further by future researcher.

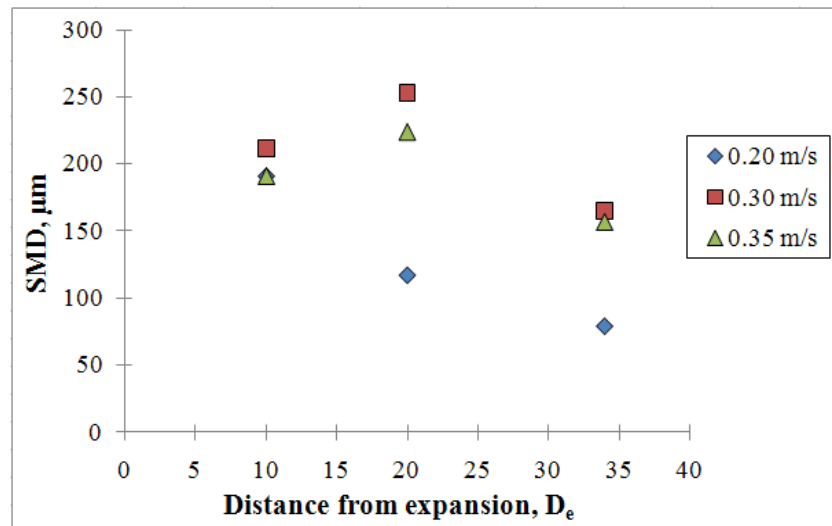


Figure 6.39: D_{32} of water droplets for 0.8 oil volume fraction system, within test distance in downward 6° pipe orientation, probe position 17 mm from bottom at different downstream mixture velocity, U_{sme} .

Figure 6.40 shows the mean drops diameter at the centre of the pipe cross section for the same experimental conditions as demonstrated in Figure 6.39. The mean drops

diameters for higher U_{sme} were about the same as for D_{32} at the bottom of the pipe cross section (Figure 6.41). However at U_{sme} 0.20 m/s due to the low mixture velocity, large drops was not dispersed up to centre of the pipe cross-section. Furthermore, throughout the test section water drops were small at lower mixture velocity as for the aforesaid reason.

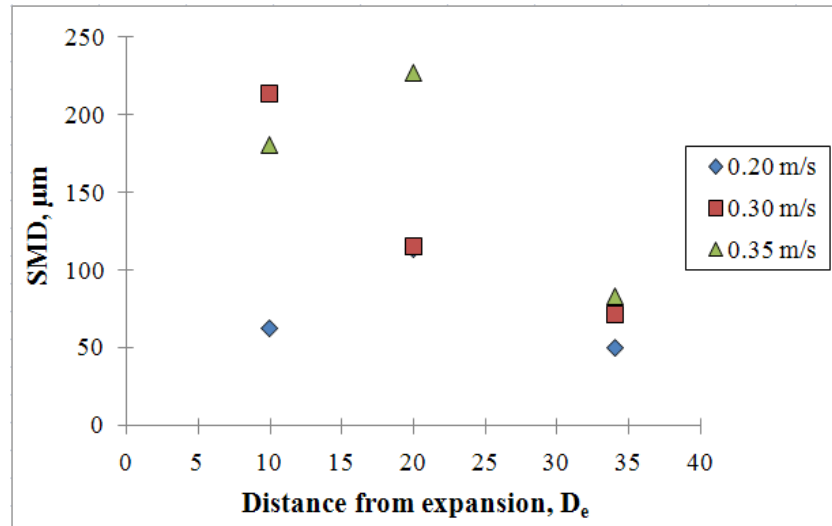


Figure 6.40: D_{32} of water droplets for 0.8 oil volume fraction system, within test distance in downward 6° pipe orientation, probe position 34 mm from bottom at different downstream mixture velocity, U_{sme} .

The most interesting occurrences are that in Figure 6.39, 6.40 and 6.41 showing the same pattern of the Sauter mean diameter progression within the test section. Figure 6.39, D_{32} for 0.20 m/s gradually decrease further away from the expansion. The same pattern of D_{32} gradually decreased for system flowing at 0.30 m/s as shown in Figure 6.40. Finally, the pattern become obvious as D_{32} also decreased for system flowing at 0.35 m/s as illustrated in Figure 6.41. These findings indicate and proved that, at higher mixture velocity, the dispersed drops were scattered all over the pipe cross-section and further distance from the expansion they coalesced, and stratification should materialize if longer test section were to be used. Furthermore, the results

showed that coalescence process initially occur at the bottom of the pipe cross section within the pipe expansion (test section).

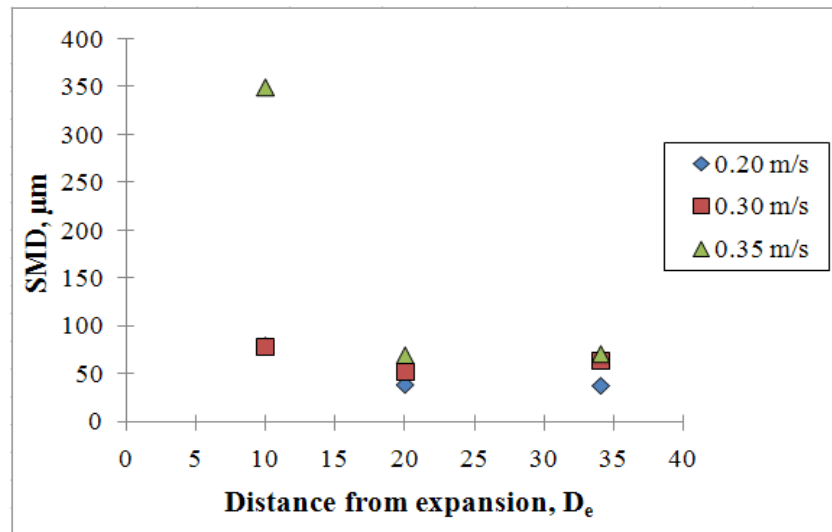


Figure 6.41: D_{32} of water droplets for 0.8 oil volume fraction system, within test distance in downward 6° pipe orientation, probe position 51 mm from bottom at different downstream mixture velocity, U_{smc} .

6.3.4.3 SMD of drops distribution - Probe position

Variations of probe positions in a pipe cross-section downstream of the -6° downward expansion are presented in Figure 6.42 and 6.45. The results generally show that when the probe is positioned at the bottom of the pipe cross-section, the mean drops diameters are strongly affected whereas when the probe is positioned at the centre and top of the pipe, D_{32} are less influenced either in oil or water continuous downwardly flow.

As for water continuous flow of the -6° downward orientation, this phenomenon suggesting that the drops at the bottom position are experiencing a more rapid coalescence process to form larger drops compared to those at the top position, in particular at the furthest distance from the expansion (Figure 6.42).

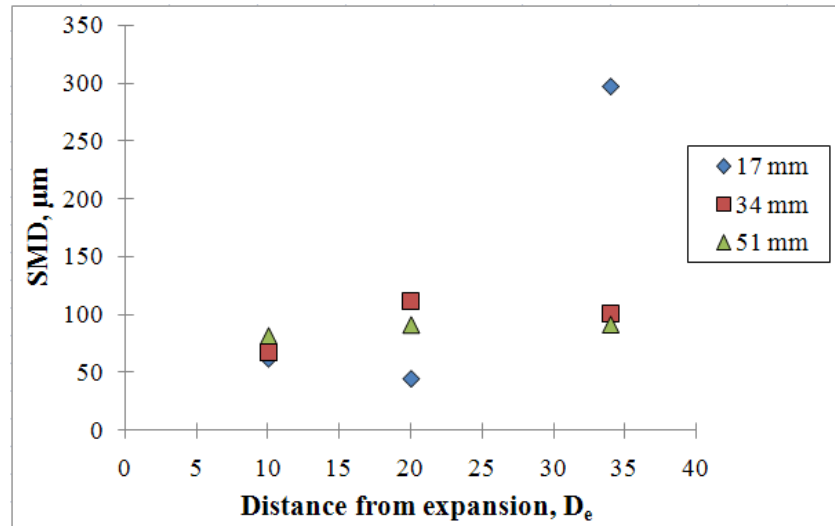


Figure 6.42: D_{32} of oil droplets for downstream mixture velocity, $U_{sme} = 0.20$ m/s, within test distance in downward 6° pipe orientation at oil volume fraction system, $OVF = 0.2$, at different probe position.

Inversely, for oil continuous downwardly flow of the same pipe orientation, drops at the bottom position are experiencing a steadily stratification process, initially started at bottom position at $10D$ downstream pipe expansion. Hence, beyond this distance ($10D$), smaller droplets were measured, producing smaller D_{32} as shown in Figure 6.43.

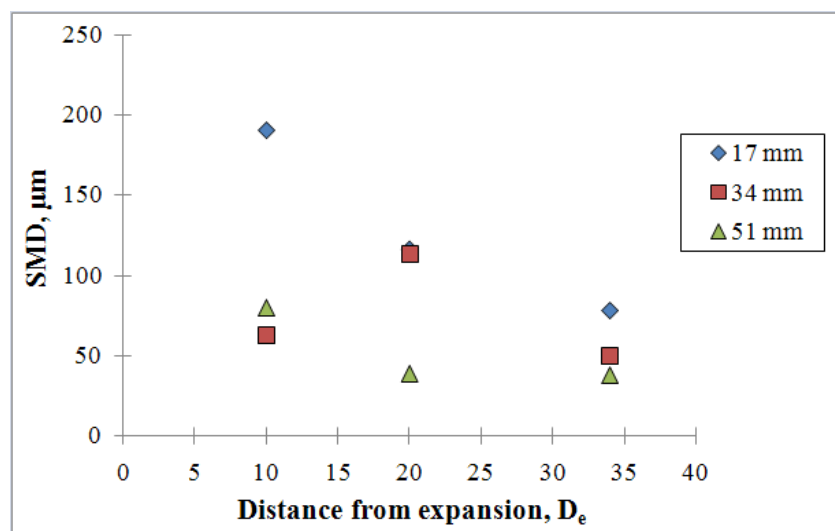


Figure 6.43: D_{32} of water droplets for downstream mixture velocity, $U_{sme} = 0.20$ m/s, within test distance in downward 6° pipe orientation at oil volume fraction system, $OVF = 0.8$, at different probe position.

Furthermore, variations of probe positions in a pipe cross-section for the same pipe orientations and input oil volume fractions with higher downstream mixture velocity (0.35 m/s) are presented in Figure 6.44 and 6.45.

Figure 6.45 shows D_{32} at various probe position for water continuous flow of the -6° downward orientation at U_{sme} 0.35 m/s. The drops at all vertically position in the pipe cross section are experiencing hasty break up process due to high mixture velocity, therefore, the drops are small at all positions all the way through the test section.

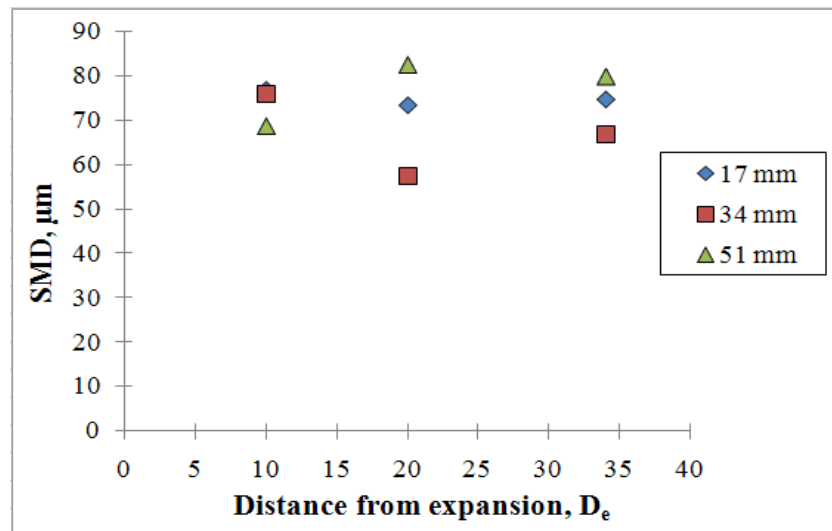


Figure 6.44: D_{32} of oil droplets for downstream mixture velocity, $U_{sme} = 0.35$ m/s, within test distance in downward 6° pipe orientation at oil volume fraction system, $OVF = 0.2$, at different probe position.

Even though at higher mixture velocity for water continuous flow, the D_{32} are uniformly in size, it is not the case in oil continuous flow. At higher U_{sme} for oil continuous downwardly flow of the same pipe orientation; drops at the top position are experiencing a rapid coalescence process at $10D$ downstream pipe expansion. Yet due to gravity forces, these large drops migrate to the centre of the pipe cross section, hence D_{32} at 34 mm (centre) engendering medium size of D_{32} as demonstrated in Figure 6.45. Moreover, D_{32} for higher mixture velocity were found to be slightly

bigger than of for 0.20 m/s at all vertically position along the test section. This is expected to be the influences of collisions frequency and time as alleged by Howarth (1964).

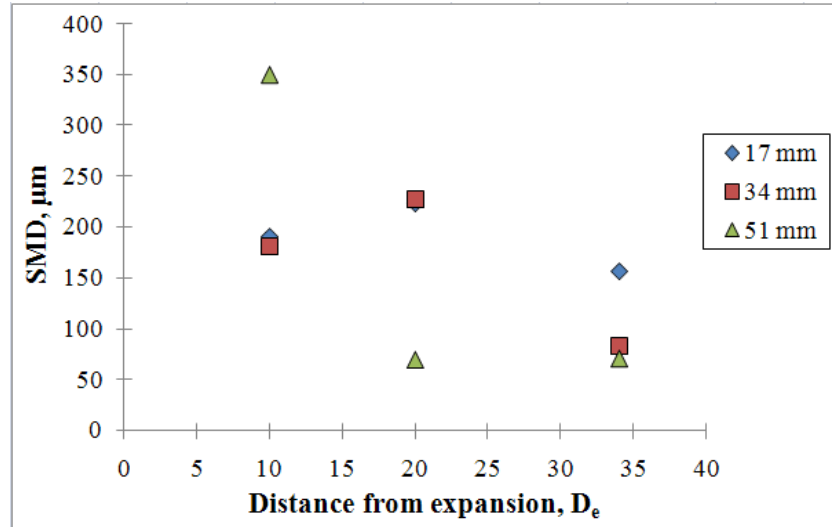


Figure 6.45: D_{32} of water droplets for downstream mixture velocity, $U_{sme} = 0.35$ m/s, within test distance in downward 6° pipe orientation at oil volume fraction system, $OVF = 0.8$, at different probe position.

Subsequently when the inclination angle were reduced to -3° downward orientation, for water continuous flow as presented in Figure 6.46, the same phenomenon as Figure 6.43 occurs. However for -3° downwardly flow, due to slower in-situ water velocity compared to -6° , at 10D downstream of the expansion, D_{32} were found to be larger at probe position centre of the pipe cross section which was not observed in -6° downwardly flow. Suggesting that the drops at the centre position too are experiencing coalescence process to form larger drops owing to slower in-situ water velocity which allowed sufficient time for oil drops to coalesce.

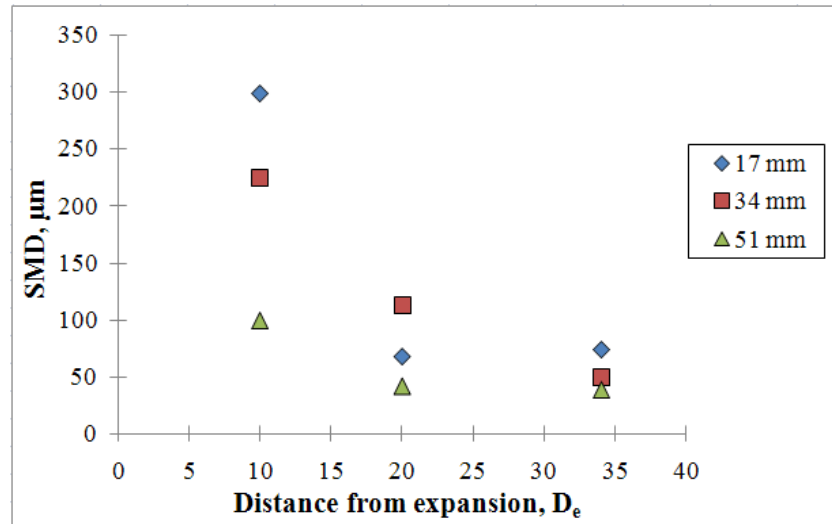


Figure 6.46: D_{32} of water droplets for downstream mixture velocity, $U_{sme} = 0.20$ m/s, within test distance in downward 3° pipe orientation at oil volume fraction system, $OVF = 0.8$, at different probe position.

Figure 6.47 shows D_{32} at various probe position for water continuous flow of the -3° downward orientation at $U_{sme} 0.35$ m/s. The mean drops pattern was found to be about the same as for -6° downward flow, except that at position $10D$ of -3° pipe orientation, the mean drops size is smaller. This is due to the turbulent forces at a lower in-situ water velocity may not be large enough to overcome the frictional drags on the drops. Hence, larger drops were less dispersed to the top of the pipe cross section, thus producing smaller value of D_{32} at this position.

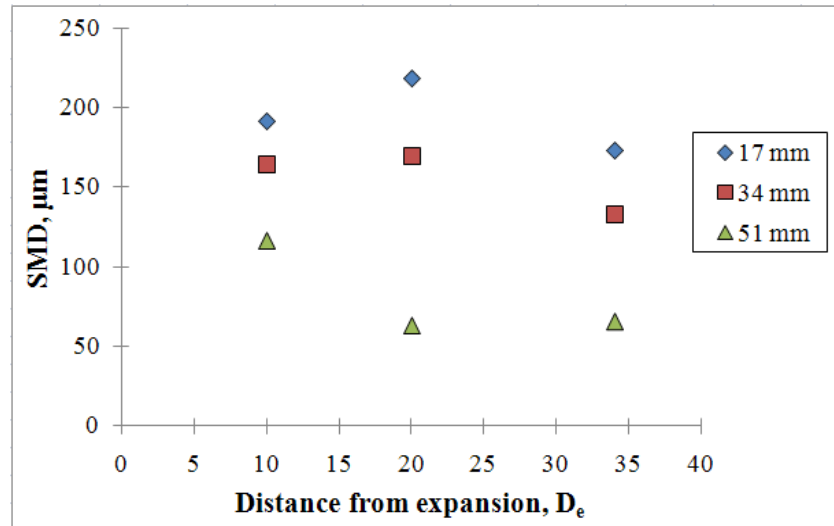


Figure 6.47: D_{32} of water droplets for downstream mixture velocity, $U_{\text{smc}} = 0.35$ m/s, within test distance in downward 3° pipe orientation at oil volume fraction system, $\text{OVF} = 0.8$, at different probe position.

6.3.4.4 Development of drops size - Cross-sectional of downward pipe expansion

Figure 6.48 below demonstrated the mean drops diameter of oil-water two phase flow in -6° downward pipe orientation, $10D$ downstream the expansion for mixture velocity 0.20 m/s, as a function of distance from the interface, $|Z|$. Remarkably, the pattern of droplets dispersion is similar to the droplets dispersion at the other pipe orientations (Figure 6.16, 6.30 and 6.32); larger drops were dispersed closer to the interface. However, the largest mean drops diameter for this condition (-3° downward) were slightly smaller compared to the D_{32} at the other orientations.

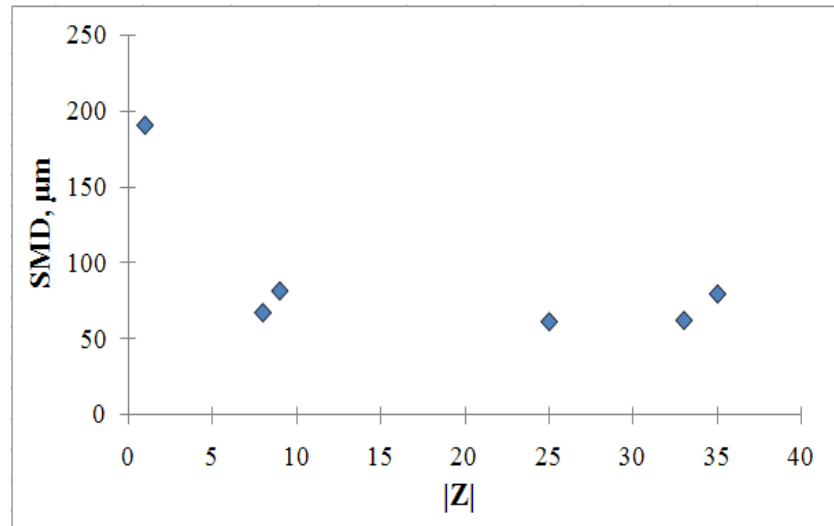


Figure 6.48: Sauter mean diameter as a function of the distance from $|Z|$ at $U_{\text{sme}} 0.20$ m/s of -6° downward inclined pipe orientation flow, 10D downstream the expansion.

However, for the mean drops diameter as a function of distance from the interface, $|Z|$ at $U_{\text{sme}} 0.20$ m/s of -6° downward inclined pipe orientation at 34D from expansion as shown in Figure 6.49, once again different singularities could be observed. Large mean drops diameter was found to be further away from the interface, the same occurrences was also observed for $+6^\circ$ upward pipe orientation (Figure 6.31). Nonetheless, larger mean drops diameter were only observed further from the interface for -6° downward inclined pipe orientation at this axial position. This was suspected due to the fast flowing water phase (heavier layer) in the downward pipe orientation causing droplets to disperse into the mixed layer, away from the interface.

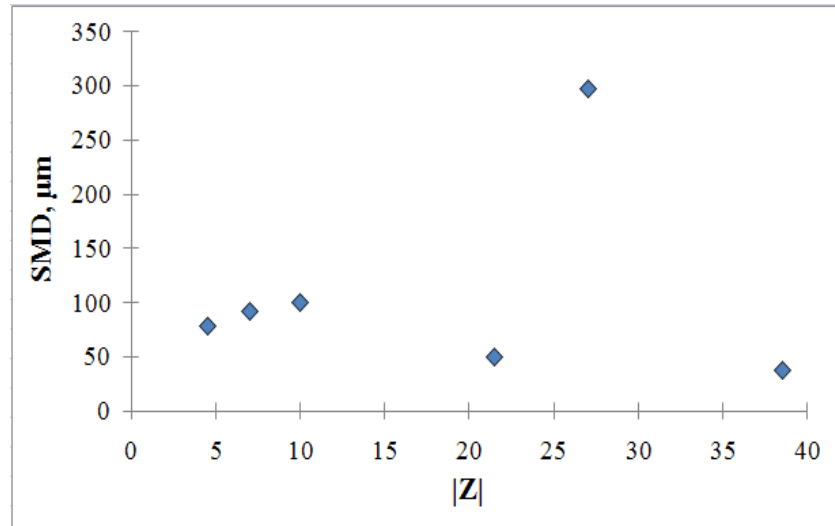


Figure 6.49: Sauter mean diameter as a function of the distance from $|Z|$ at $U_{\text{sme}} 0.20$ m/s of -6° downward inclined pipe orientation flow, $34D$ downstream the expansion.

For the mean drops diameter downstream of the expansion at a downward pipe orientation, the following points can be drawn:

1. The variation of input oil volume fractions caused dissimilarity of droplet size evolution downstream of the expansion. In water continuous flow, drops coalesced and evolved as they moved further from the expansion but still stratification of droplets were not materialise within the tests section. In contrary with oil continuous flow, stratification of droplets started beyond $10D$.
2. The higher the mixtures velocity, the more the large drops scattered (dispersed) occupying the pipe cross section at near position.
3. Most of the bigger droplets were found at the bottom of the pipe cross-section; the far location ($34D$) for water continuous flow, and at the near location ($10D$) for oil continuous flow while smaller droplets appeared at the top in all locations downstream of the expansion for low mixture velocity ($U_{\text{sme}} = 0.20$ m/s).

6.3.5 Comparison between different angles of inclination

The effect of angles of inclination for 0.20 and 0.35 m/s with 0.2 input oil volume fractions downstream of the expansion is shown in Figure 6.50, 6.51 and 6.52. Results of the drop size measurements of water continuous flow in a sudden expansion at $U_{sme} 0.20$ m/s downward inclination flow show only minimal effect of the inclination angle. The noticeable effect of the inclination angle of this flow conditions are at axial position 34D for -6° downward inclination flow, where large droplet were detected as shown in Figure 6.50.

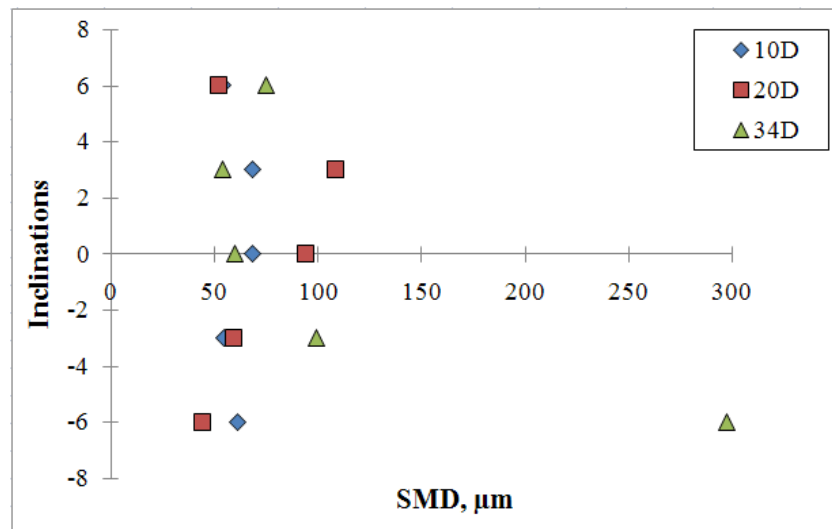


Figure 6.50: D_{32} of oil droplets for downstream mixture velocity, $U_{sme} = 0.20$ m/s, oil volume fraction system, $OVF = 0.2$, at 17 mm probe position from bottom, along test section distance for different pipe orientation.

Furthermore, the angle of inclination has negligible effect on drop size distributions when the downstream mixture velocity is increased to 0.35 m/s (Figure 6.51 and 6.52). In this condition, the mixed layer would be responsible for the droplet size for horizontal and both inclination of pipe orientation, whether it is upward or downward. It should be noted that the mixed layer almost entirely dominated in a pipe cross-section even with the probe positioned at the top (Figure 6.52), and this is clearly supported by the results of Hasan (2006) and Yang *et al.* (2003).

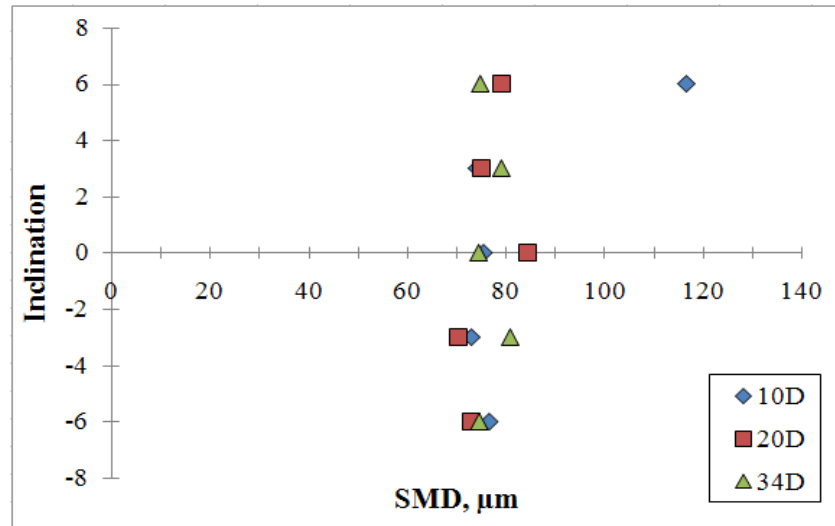


Figure 6.51: D_{32} of oil droplets for downstream mixture velocity, $U_{sme} = 0.35$ m/s, oil volume fraction system, $OVF = 0.2$, at 17 mm probe position from bottom, along test section distance for different pipe orientation.

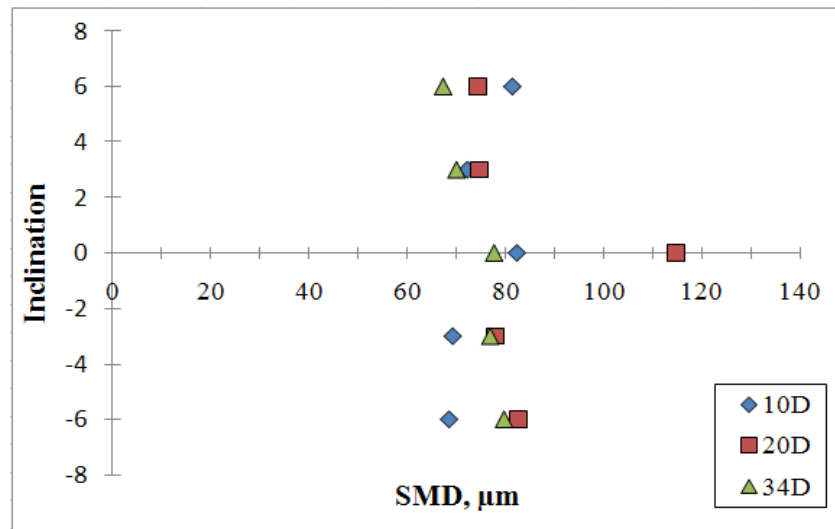


Figure 6.52: D_{32} of oil droplets for downstream mixture velocity, $U_{sme} = 0.35$ m/s, oil volume fraction system, $OVF = 0.2$, at 51 mm probe position from bottom, along test section distance for different pipe orientation.

Increased the oil volume fraction to 0.8 and now the oil is the continuous phase, the results of the drop size measurements in a sudden expansion at $U_{sme} 0.20$ m/s show strong effect caused by the inclination of the pipe expansion. In $+3^\circ$ upward inclination, drop size started small at the near position (10D); with the distance further away from the expansion, the drops coalesced and gained size. However stratification of droplets does not occurs within the test section. Whereas, for

downward flow, droplets detected were small, indicated that stratification of droplets has occurred beyond 10D for downward pipe orientation as shown in Figure 6.53.

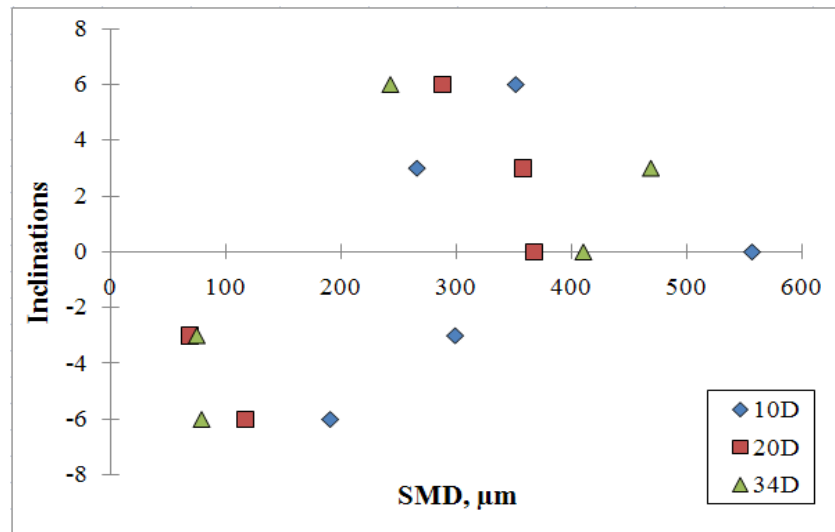


Figure 6.53: D_{32} of water droplets for downstream mixture velocity, $U_{sme} = 0.20$ m/s, oil volume fraction system, $OVF = 0.8$, at 17 mm probe position from bottom, along test section distance for different pipe orientation.

As the downstream mixture velocity is increased to 0.35 m/s, the angle of inclination has insignificant effect on drop size distributions. This was demonstrated in the Figure 6.54. Similar to the phenomena in water continuous flow (0.2 OVF), the mixed layer would be responsible for the droplet size for horizontal and both inclination of pipe orientation, whether it is upward or downward. The mixed layer dominated almost entirely in the pipe cross-section.

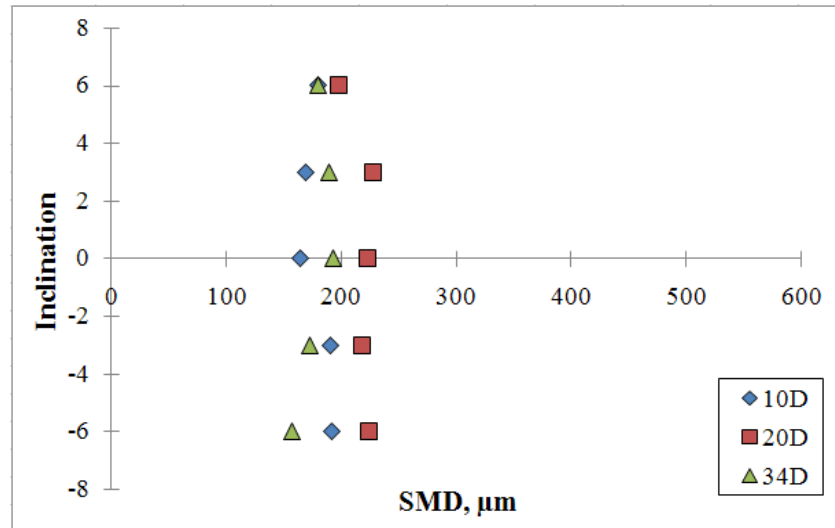


Figure 6.54: D_{32} of water droplets for downstream mixture velocity, $U_{sme} = 0.35$ m/s, oil volume fraction system, $OVF = 0.8$, at 17 mm probe position from bottom, along test section distance for different pipe orientation.

CHAPTER 7

PRELIMINARY INVESTIGATION ON INFLUENCE OF SURFACE TENSION ON DROP SIZE

Many researchers have reported experimental works on measurement of average droplet size used light transmittance techniques or chemical methods. Size distributions were also studied by measurements with photography, encapsulation, sedimentation and electro-resistivity measurements. Concurrently, droplet mixing measurements were made by various indirect methods such as following a chemical reaction or dispersion of a non-transferring dye in the dispersed phase. A number of investigators reported experimental data on interfacial areas (Mok and Treybal, 1971; Schindler and R. E., 1968; Weinstein and Treybal, 1973) and drop distributions (Bouyatiotis and Thornton, 1967) in flow systems.

In certain industrial flows or experimental facility, the presence or usage of surfactants is reported. In the process industry, surfactants are added to process liquids to prevent unwanted deposits by keeping them finely dispersed. These agents influence the interfacial tension interaction in liquid-liquid multiphase system. Therefore, as a starting point the droplet generation under controlled conditions and the impact of surfactants are investigated.

This chapter presents briefly the apparatus, methodology and results of interfacial tension experiments of two liquids and liquid-liquid mixing in fully baffle mixing vessel. The criteria of experimental design and the principle work of each instrument are explained. The experiment procedures for the measurement of interfacial tension, drop size and drop size distribution performed on the rig are briefly covered.

7.1 Influence of interfacial tension on drop size

Interfacial tension plays a greater role in homogenization. In order to investigate the impact of interfacial tension on breakage and coalescence behaviour, dynamics of droplet clusters needs to be investigated under controlled environment. The experiment on effect of interfacial tension on drop size and drop size distribution in a static flow and dynamic liquid-liquid flow (mixing vessel), two measurement methods were used. In static flow, interfacial tensions were measured by mean of drop weight method and high speed camera. Whereas in mixing vessel, the laser backscattered technique (Lasentec FBRM M500P) was used to determine the drop size and drop size distribution of the system. However, to understand what really happened to the droplet clusters in homogenisation and coalescence process, measurement for a single droplet under controlled environment must first be studied.

7.1.1 Interfacial tension – static flow

One of most frequently used method to measure interfacial tension involves the formation of a drop of one liquid in the bulk of the other. Either the drop is allowed to fall when fully grown (Harkins and Humphery, 1916) or the contours of the partly grown pendent drop are measured (Andreas *et al.*, 1938). In static flow, interfacial tensions were measured by mean of drop weight method and high speed camera. The

criteria of experimental design and the principle work of each instrument are explained.

7.1.1.1 Drop weight method

The drop-weight method is a known method for measuring surface tension and is one of the simplest and reasonably acceptable methods which have been used for interfacial tension. Interfacial tension was measured by mean of drop weight method as proposed in the Practical Physical Chemistry (James, 1967) as shown in Appendix 7A. Interfacial tension measurement of water-kerosene oil with surfactant added was performed. The accuracy of a drop-weight method is improved by increasing the number of drops.

The methods depend on the equilibrium of the two forces; the weight of a drop of liquid (m) just about to fall from a vertical tube with an external radius, r and the force due to the surface or interfacial tension (γ) acting around the periphery of the needle holding the drop. The weight of a drop that falls should be given by:

$$mg = 2\pi.r.\gamma \quad 7.1$$

In actual fact, only a portion of the drop falls; Harkins and Brown proposed that the drop of weight (mg) given by the equation 7.1 be called the 'ideal drop'. The fraction of the ideal drop which falls was determined by these workers in an extensive series of experiments. The form of the maximum stable hanging drop is a function of $r/v^{1/3}$, where r is the outer radius of the tube and v the volume of the drop (determined from the mass of the drop and the density of the liquid). This determines the fraction $f(r/v^{1/3})$ of the drop which falls. The actual weight of the drop which falls is thus:

$$mg = 2.\pi.r.\gamma.f(r/v^{1/3}) \quad 7.2$$

Hence

$$\begin{aligned}\gamma &= (m \cdot g) / \{ 2 \cdot \pi \cdot r \cdot f(r/v^{1/3}) \} \\ &= (F \cdot m \cdot g) / r\end{aligned}\tag{7.3}$$

Thus, to determine the surface tension of a liquid it is only necessary to determine the mass of 1 drop of the liquid, calculate its volume v from a rough density determination, multiply this by $1/r^3$, look up the value of F (Figure 7.1) and finally multiply by mg/r . The density of the liquid is involved only in determining the value of the correction which is not sensitive to density differences.

As for measuring interfacial tension of two immiscible liquids, the mass (m) in the equation 7.3 is replaced by $v(\rho_1 - \rho_2)$, where v is the recorded volume and ρ_1 and ρ_2 the densities of water and kerosene respectively. Thus

$$\sigma = \{F \cdot v \cdot g(\rho_1 - \rho_2)\} / r\tag{7.4}$$

The Antonoff's rule was used to get an approximation values for water – kerosene interfacial tension. Antonoff's rule says that the interfacial tension between two liquids is approximately equal to the difference between the surface tensions of the two liquids:

$$\sigma \approx \gamma_1 - \gamma_2\tag{7.5}$$

The experimental results may then be compared with Antonoff's rule to make sure the result obtained is reasonable and acceptable.

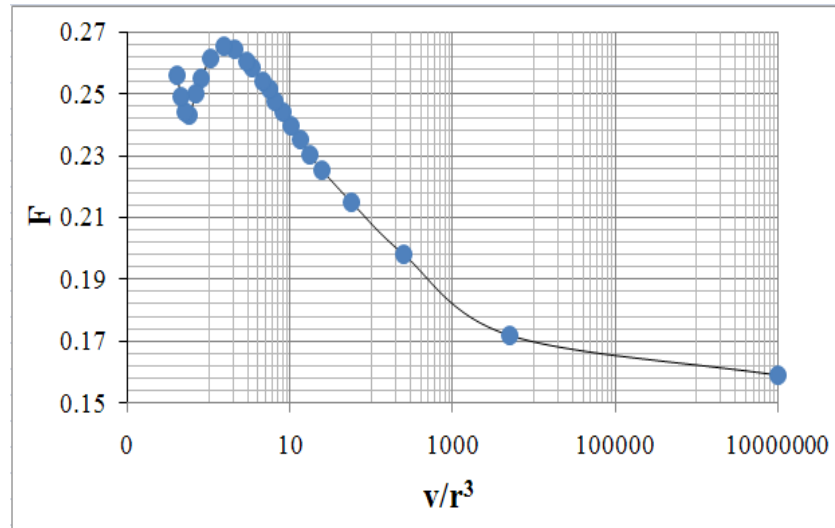


Figure 7.1: Correction factors (F) for the drop weight method (Harkins and Brown, 1919)

7.1.1.2 High speed camera (CCD)

Droplets of water/kerosene were generated using a nozzle fitted in cylindrical Perspex column. Experiments for water droplet in kerosene oil system and droplets of kerosene oil in water system were conducted. In both conditions, a known amount of surfactant has been added to water allowing a decrease in the interfacial tension without modifying the viscosity and the density of the liquid phases. Measurement of single droplet diameter for both conditions were investigated using high speed CCD camera and high speed digital imaging software. A maximum recording time of 7 sec could be stored for each acquisition, which is well above the maximum residence time of the drops inside the measurement zone. The camera shutter exposure time was set to 1/250 s in order to reduce image fuzziness due to drop displacement to acceptable level. The camera is focused on the central plane of the pipe (cylindrical Perspex), allowing a reasonable depth of focus. Repeatability of the measurement was determined.

Droplet images data were taken using the high speed CCD camera for sets of mixtures conditions. Droplet images from the high speed CCD camera were analysed using high speed digital imaging software (PFV Ver. 318). Then digitize using the software to get the diameter of the drops.

7.1.1.3 Interfacial tension results - Static flow results

Drop weight results:

The mean value of interfacial tension obtained from the experiments is 0.0437 N/m. In literature we found the value of 0.0728 N/m for water surface tension and 0.024 N/m for kerosene surface tension. Using these values, the Antonoff's rule predicts that the water-kerosene interfacial tension has to be 0.0488 N/m which is 10.4% greater than measured interfacial tension value. The result of the mean value for the measured interfacial tension is shown in Figure 7.2.

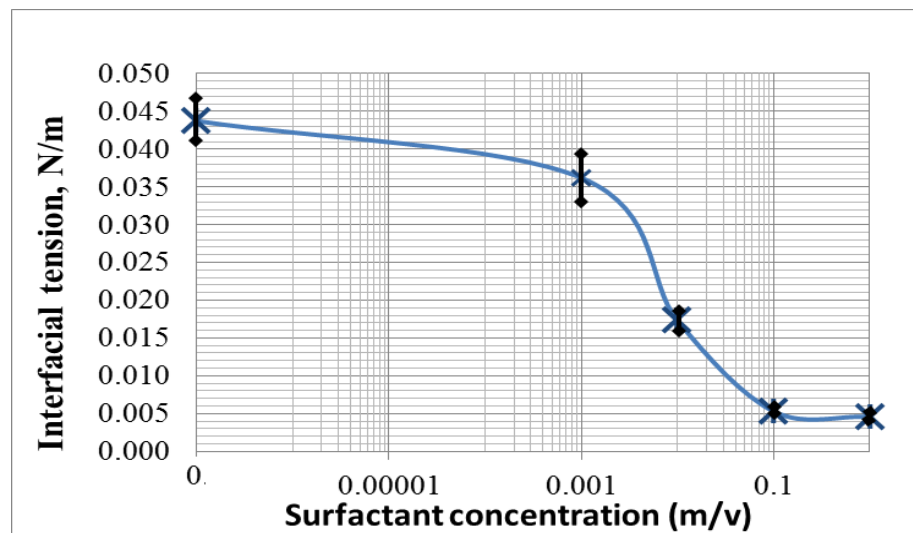


Figure 7.2: Effect of surfactant on interfacial tension.

High speed camera results:

Figure 7.3 shows the IFT for different surfactant CMC obtained from drop weight method. In correspondence to the result shown in Figure 7.3, series of droplet image with effect of the same surfactant CMC concentration used is shown in Figure 7.4. It clearly shows that, for different surfactant concentration, diameter of drops at the same position taken (height) varies.

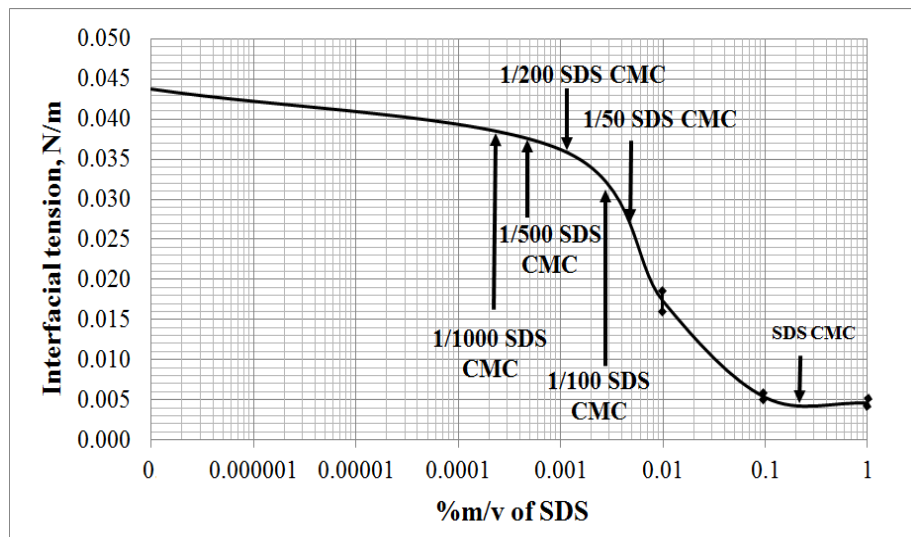


Figure 7.3: Interfacial tension for different surfactant CMC.

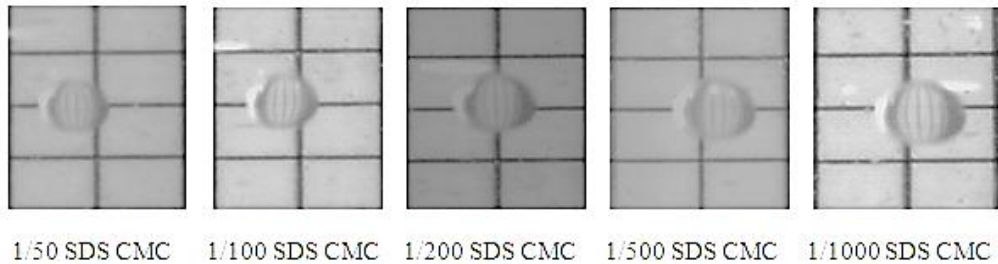


Figure 7.4: Effect of surfactant CMC concentration on droplet size

7.1.2 Interfacial tension – mixing flow

An experimental liquid-liquid dispersions facility has been constructed and measurements of mean drop and drop size distribution using Laser focused beam reflectance measurement technique are reported. Lasentec M500P FBRM manufactured by Mettler-Toledo Ltd has been employed on a vessel 125 mm

diameter. An experimental investigation has been carried out to characterise the influences of impurities on the drop size distributions of liquid–liquid dispersion in a stirred vessel. Water/kerosene oil system in the 125 mm vessel was agitated using 38 mm diameter radial impeller (6 paddles). Each experiment was performed by pouring the kerosene oil and water into the mixing vessel, let it settle and then agitation was commenced. Dispersion was produced in the mixing vessel. Drop size measurements were taken when the process reached steady-state conditions.

7.1.2.1 Experimental conditions

In order to study the effect of the surfactant presence on drop size distributions, series of experiments were performed. At the first series, the drop size distributions were investigated for pure system, IFT 44 mN/m (kerosene/water) at various oil volume fractions (0.8, 0.6, 0.5, 0.4 and 0.15) with different impeller Reynolds number, N_{Re} 10000 and 15000 respectively. At the second series, drop size distributions have been investigated at the same oil volume fractions and impeller Reynolds numbers as the first series. However, this time with addition of surfactant at different concentrations, ranges from 0.005% - 0.5 % SDS_{cmc} . With these additions of surfactant concentrations, interfacial tensions of the system ranges are 37- 6mN/m (kerosene/water).

In all of the experiments, the probe was placed at the liquids interface and the system was then agitated for 5 minutes using radial 6 paddle impeller (RP 6) for N_{Re} 10000 and 15000 respectively before commence measurements. This procedure is performed to make sure that the system break up and coalescence is well balance as

shown in Figure 7.5. All experiments were performed three times to test reproducibility and repeatability of experiments.

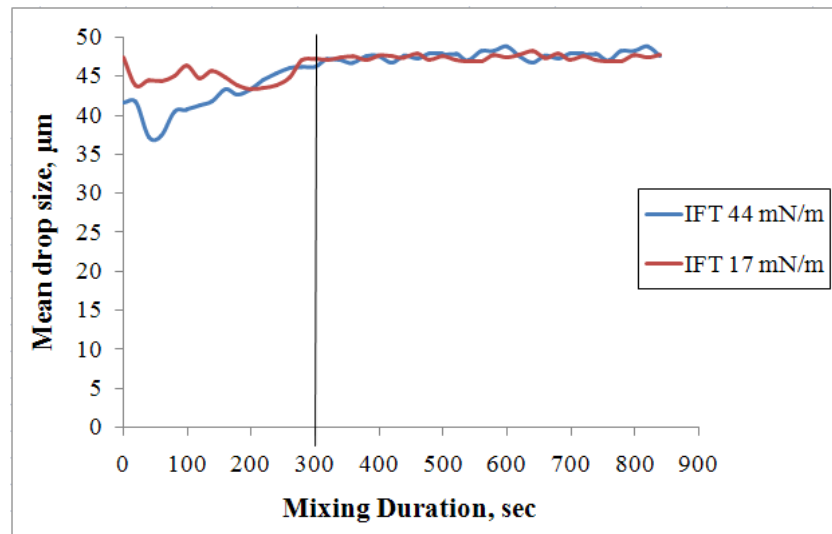


Figure 7.5: The effect of mixing time for 0.5 OVF at $N_{Re}=10000$.

7.1.2.2 Interfacial tension results - Mixing flow results

Effect of surfactant (SDS) concentration on drop size distribution:

Figures 7.6 to 7.10 show the effect of interfacial tension (IFT) on the drop size distribution for oil volume fractions (OVF = 0.8, 0.6, 0.5, 0.4 and 0.15) at Reynolds number (N_{Re}) 10000. Interfacial tension varies from 44mN/m to 6mN/m corresponding to the concentrations used.

Figure 7.6, shows the drop size distribution for 0.8 OVF. Water is dispersed in kerosene (continuous phase). Drop size distribution for the highest IFT (44mN/m) shows the presence of larger water droplets dispersed in kerosene compared to the two systems with IFT 36 and 6mN/m. The same trend has been reported by Khapkay *et al* (2009). They stated that by decreasing the IFT of the system, the drop size will decreased. Hence the frequency of the smaller drops increase. However, it is noticed that for system with IFT 17 mN/m, this is not the case.

Larger water droplets were present in this system. It is suspected that at IFT 17mN/m, due to the impurities (surfactant) affect the water phase, caused reduction of systems IFT i.e. energy per unit surface area. Resulting the droplets to move more freely, hence less restriction for the water droplets to have a collision. Thus increased the probability of having drops-drops coalescence (dominant). Hence, larger drops were formed.

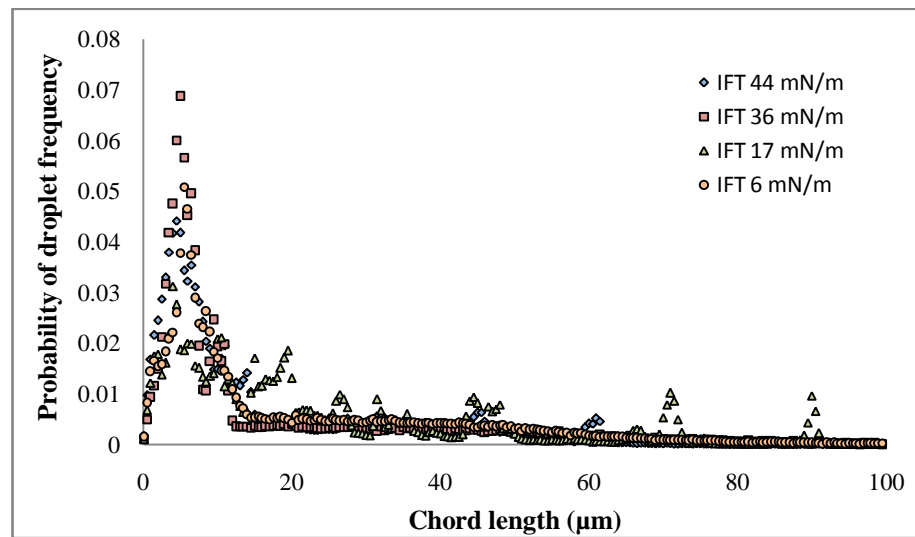


Figure 7.6: The effect of IFT on drop size distribution for 0.8 OVF at $N_{Re}=10000$.

Decreasing oil volume fraction to 0.6 and 0.5, due to the phase inversion, frequency of the water droplets collisions increased and drop-drop breakage is dominant. This is due to at these volume fractions no clear continuous phase can be determined. This ambiguity may lead to a finer mixture of droplets of both phases due to the complex interactions between droplets of the same phase as well as between droplets of the two phases. Hence larger droplets were break to form smaller droplets. This is shown in Figure 7.7 and 7.8.

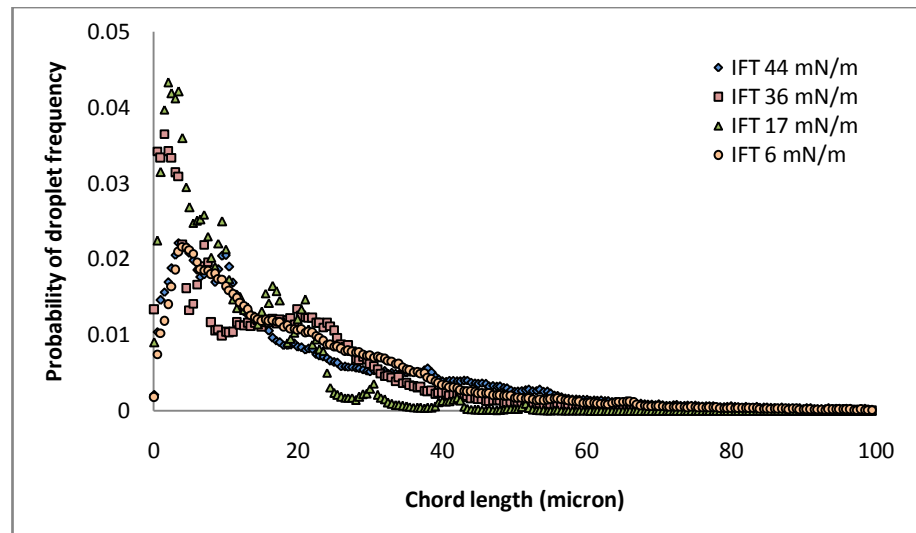


Figure 7.7: The effect of IFT on drop size distribution for 0.6 OVF at $N_{Re}= 10000$.

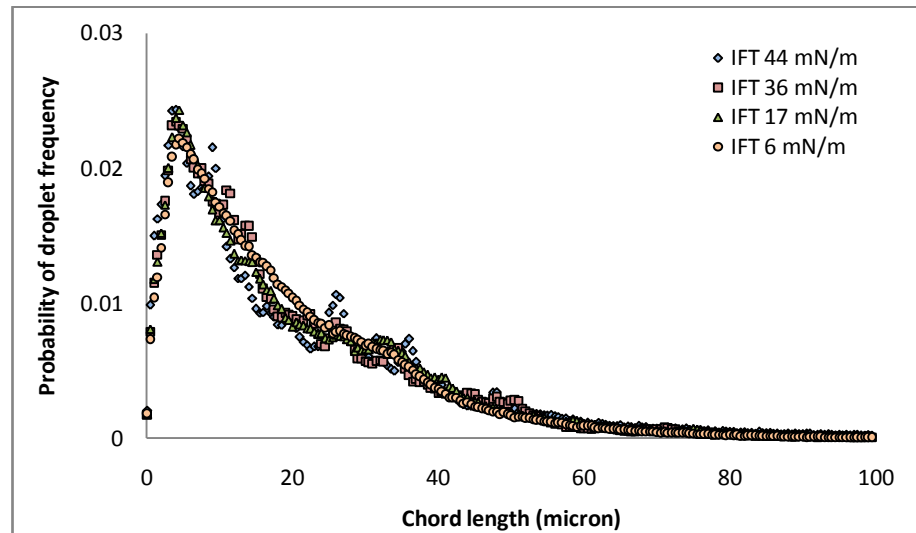


Figure 7.8: The effect of IFT on drop size distribution for 0.5 OVF at $N_{Re}= 10000$.

Whereas, Figure 7.9 and 7.10, kerosene is dispersed phase and water is continuous phase. In Figure 7.9, for IFT 44mN/m shows kerosene droplet dispersed in water is slightly larger compare to the other drop size distribution (IFT 36 and 6mN/m). Generally, with decreasing IFT in two phase systems, it is observed that the drop size decrease. Therefore, the drop size is expected to decrease with decreasing IFT, giving a high frequency of smaller drops.

Conversely, this is not the case when oil volume fraction decrease from $\phi = 0.4$ to 0.15. Larger kerosene droplets were observed for 0.15 OVF at lower IFTs (see Figure 7.10). This is due to collisions of kerosene droplets; drop-drop coalescence is dominant. Due to the impurities (surfactant) affect the water phase, caused reduction of systems IFT.

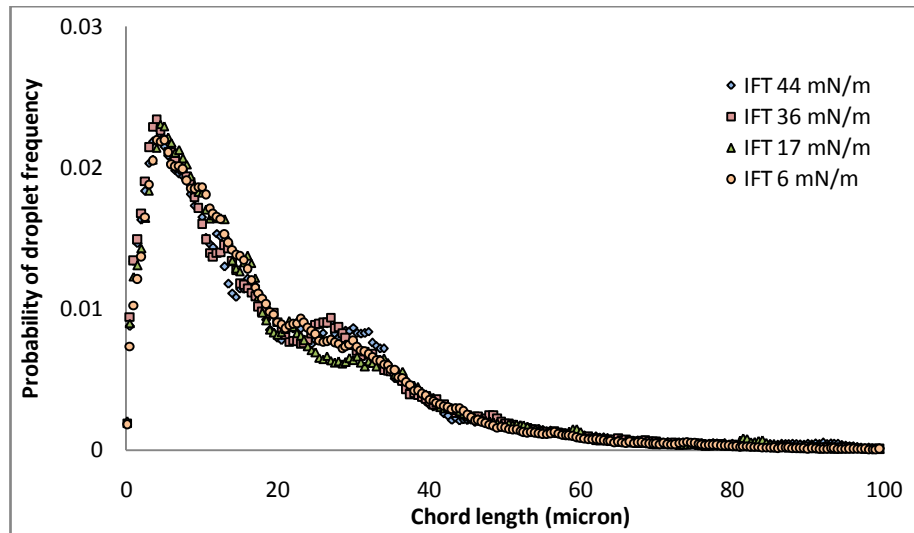


Figure 7.9: The effect of IFT on drop size distribution for 0.4 OVF at $N_{Re} = 10000$.

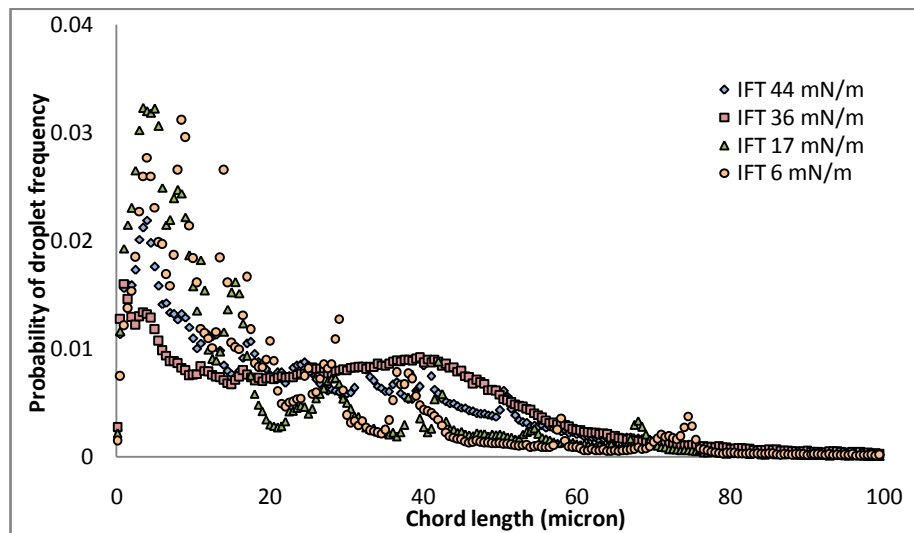


Figure 7.10: The effect of IFT on drop size distribution for 0.15 OVF at $N_{Re} = 10000$.

Effect of the impeller Reynolds number (impeller speed) on drop size distribution:

Drop size distributions were investigated for two different impeller Reynolds numbers ($N_{Re} \sim 10000$ to 15000). Again, the IFT of the water/kerosene system is altered to vary between 6 and 44 mN/m. The impeller transfer mechanical energy required to create droplets. In essence, this means that the impeller “work” on the system to increase the “energy” which goes into the increase in the surface area (the IFT is a measure of energy per unit surface area). Therefore, the impeller speed is inversely proportional to the drop size. The higher the impeller speed, the smaller will be the drop size.

Figure 7.11 displays the effect of the impeller speed on the drop size distribution of water/kerosene system free of surfactants at oil volume fraction, $\phi = 0.8$. The IFT of the system is 44 mN/m. It can be seen that the drop size is larger for the smaller Reynolds number (N_{Re}). This finding is in agreement with the statement stated earlier.

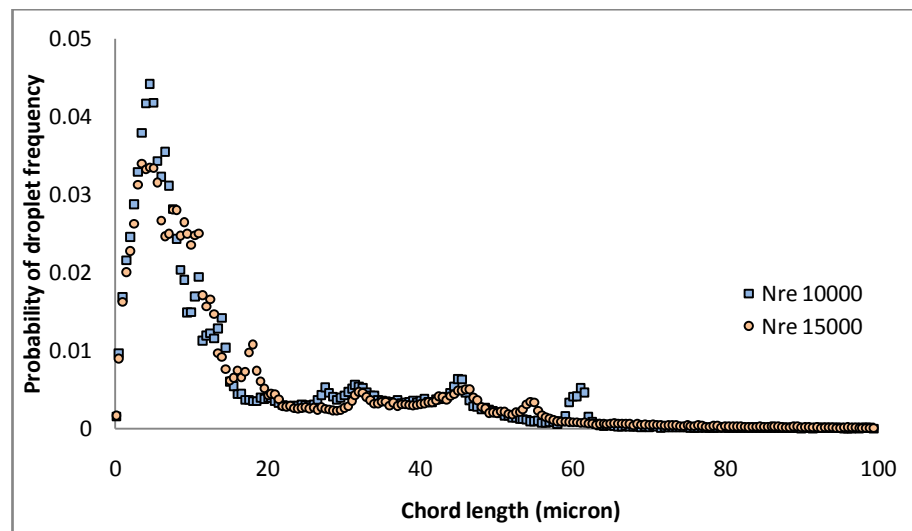


Figure 7.11: The effect of the impeller Reynolds number (impeller speed) on drop size distribution for OVF = 0.8 system with IFT 44 mN/m.

When the IFT is reduced by adding the surfactant to the above system, larger droplets were observed at $N_{Re} = 10000$. This is due to less ‘work’ is needed for the droplets to coalesce. Hence, larger drop sizes were formed as shown in Figure 7.12.

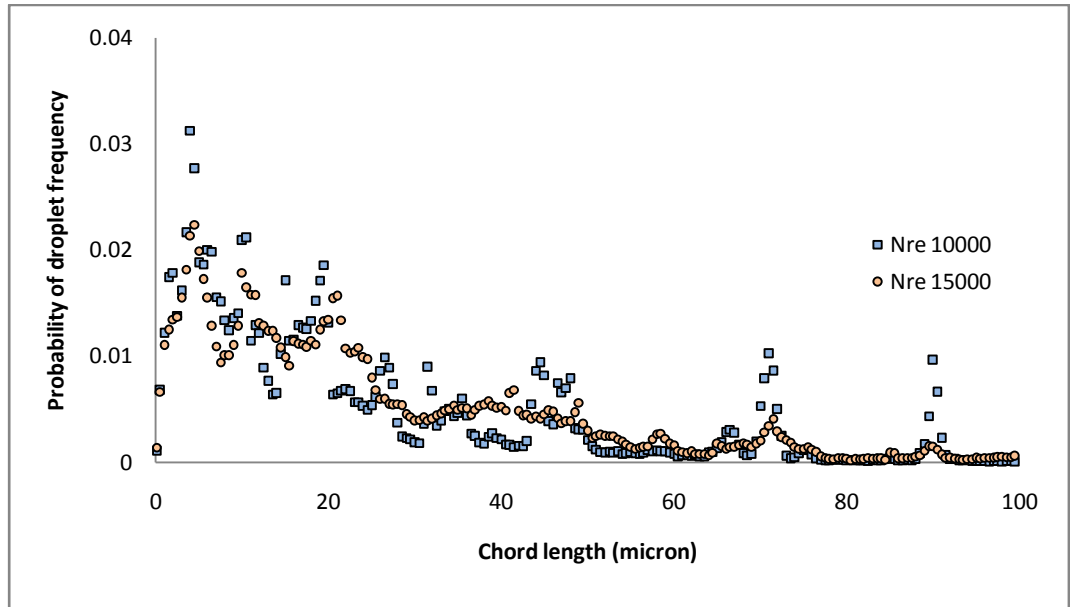


Figure 7.12: The effect of the impeller Reynolds number (impeller speed) on drop size distribution for $\varnothing = 0.8$ systems with IFT 17 mN/m.

Figure 7.13 displays the effect of the impeller speed on the drop size distribution of water/kerosene system at oil volume fraction 0.15, IFT of the system is 44 mN/m. It can be seen that the drop size increased when the system has lower Reynolds number (N_{Re}). This finding is in agreement with the results for the system of oil volume fraction 0.8, showing that an increased in N_{Re} caused a reduction in drops size and vice versa. The same trend was also observed in the water/kerosene system with added surfactant for the same 0.15 oil volume fraction, IFT of the system is 17 mN/m. However, in the latter system condition (added surfactant), decrease of N_{Re} caused an increase of droplets coalescence. Due to lowering the IFT, the resistance of the drops (dispersed phase) and continuous phase were decreased. Hence, larger drop sizes were formed ($\sim 70\mu\text{m}$) as shown in Figure 7.14 compared to system with IFT 44 mN/m (Figure 7.13).

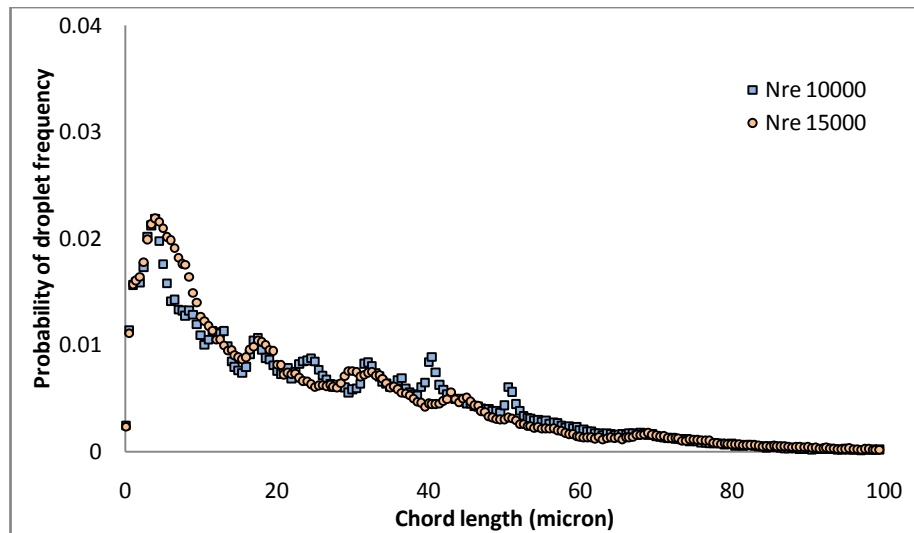


Figure 7.13: The effect of the impeller Reynolds number (impeller speed) on drop size distribution for 0.15 OVF systems with IFT 44 mN/m.

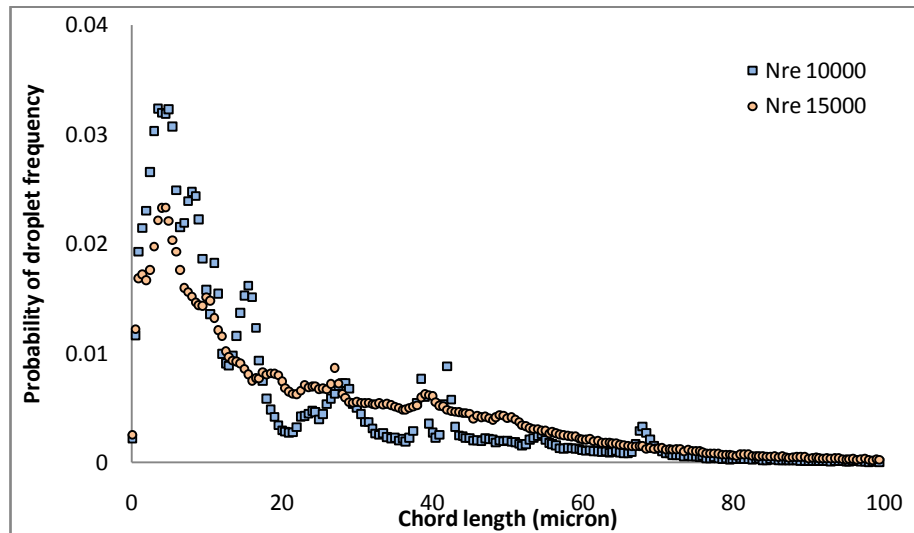


Figure 7.14: The effect of the impeller Reynolds number (impeller speed) on drop size distribution for 15 OVF systems with IFT 17 mN/m.

However, further decreased the IFT to 6mN/m, impeller speed seems to not have significant influence on the drop size distribution for 0.8 oil volume fraction system (as shown in Figure 7.15). On the contrary, for 0.15 OVF system with IFT 6 mN/m, by lowering the impeller Reynolds number, larger drops is detected in the system (Figure 7.16).

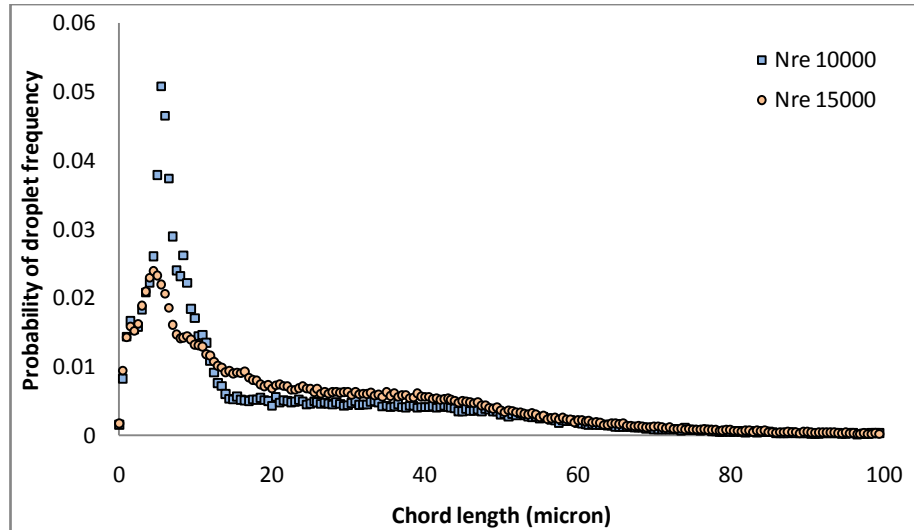


Figure 7.15: The effect of the impeller Reynolds number (impeller speed) on drop size distribution for 0.8 OVF systems with IFT 6 mN/m.

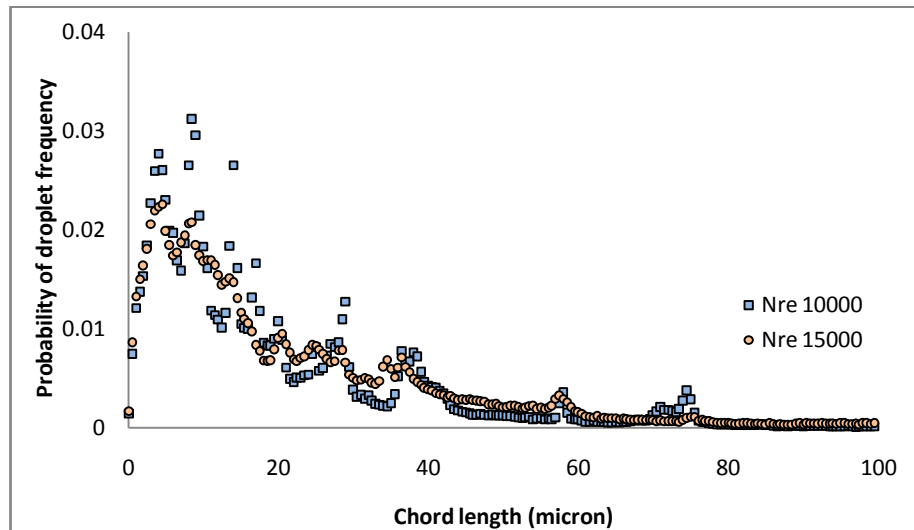


Figure 7.16: The effect of the impeller Reynolds number (impeller speed) on drop size distribution for 0.15 OVF systems with IFT 6 mN/m.

It can be concluded that the presence of SDS and N_{Re} (impeller speed) had a strong effect on the interfacial tension and the drop size distribution, especially at low concentrations of SDS. For the systems containing surfactant, around and above the surfactant CMC region ($SDS, \text{mmol/dm}^3 \geq 8.2$) drop size did not depend on the surfactant concentration. The drops did not coalesce at high surfactant concentration and the interfacial tension exhibited a slight variation (Figure 7.3).

For the system below of surfactant CMC region (SDS, $\text{mmol/dm}^3 \leq 8.2$), drop size depend strongly on the surfactant concentration. In this region, drop size steeply reduced with the increased of surfactant concentration.

CHAPTER 8

CONCLUSIONS AND RECOMMENDATIONS

Primary separators perform a vital role in providing the initial separation of hydrocarbon production (upstream industry) that consist water, gas, hydrocarbon liquids and solids (sands), obtained from oil wells. The solid and water loading add to the production cost as they needed to be pump and separated. If removed at an early stage, the pumping cost and further downstream cost can be deducted. For this purpose, separation of solids and water from the crude coming out from the well is an important step in oil and gas industry. Conventionally, a separator such as a vessel or cyclone is employed to accomplish this task. However, the production rates demands large vessels that lead to high capital cost. At the same time, safety measures are extremely restrictive, particularly on offshore platforms. Therefore, there has been a considerable industrial motivation to remove this economic and safety problem by reducing size and improved the efficiency of the process vessels or by introducing alternative method (expansion pipe) for efficient separation of the phases. Compared to conventional separators, a pipe expansion can be considered to be a continuous, compact, economical and safer phase separator (Yang, 2003).

This demand on continuous separation methods was at the core of the work carried out in this research project. Quantitative and qualitative studies of separation of one liquid phase from another after an expansion in pipe diameter have been carried out.

The findings were presented in detail in preceding chapters of this thesis and also summaries of the investigations main findings are presented. The main conclusions are presented below and followed by some future works related and recommended to the present study.

8.1 Contributions to knowledge

The present work is the first that explored the application of capacitance wire mesh sensor (CapWMS) in liquid-liquid flow system to define stratification of liquid-liquid two phase flow through sudden pipe expansion. The results show that it can be used to achieve information here to deem not possible. This has lead to the reconstruction of cross-sectional plots which provide information on the phase distribution at any given point in the pipe. Therefore, a significant amount of data has been collected and analysed in attempt to understand the two-phase flow behaviour downstream of the expansion.

8.2 Evolution of Interface

New experimental data of spatial distributions have been generated for a two-phase oil-water flow. The capacitance wire mesh sensor used in this study proves to be an appropriate tool for an on-line visualisation of spatial distribution in a pipe cross-section. The data gathered using the WMS show instantaneous information about the interface shapes, waves and phase layer evolution of oil-water flow. The WMS images demonstrated that the spatial distributions are strongly dependent on the mixture velocity, input oil fraction and inclination angles for the far position.

In the present study, the location of the two interfaces that form between the separated phases and the oil-water mixture were obtained. In water continuous flow, convex and concave of oil-mixed layer interfaces were observed for all pipe orientation. However, in oil continuous flows, concave interfaces of the oil-mixed later were observed only at upward and downward flow at the far position, except for high input oil fractions where horizontal plane interface were detected. Meanwhile, plane horizontal interfaces were identified for horizontal pipe orientation.

Subsequently, for water-mixed layer interfaces in water continuous flow, convex and horizontal interfaces were observed for upward and horizontal pipe orientation whilst only convex interfaces at downward orientation. In oil continuous flows, convex interfaces of the water-mixed layer were observed only at upward flow at low input oil volume fraction within the oil continuous flow regime (0.4 OVF). Meanwhile, plane horizontal interfaces were identified for horizontal and downward pipe orientation.

There are no waves at the interface between the water and the mixed layers for oil continuous flow at downward flow as they are dissipated due to the thinner water layer. As for upward inclined orientation, waves were observed at near axial position (10D) for all input oil volume fractions except for 0.2 OVF. The amplitude of the waves is: $\sim 0.29D$ for 0.8 OVF; $\sim 0.22D$ for 0.6 OVF and $\sim 0.26D$ for 0.4 OVF. The larger the upward inclined angle, the shorter the distance downstream of the expansion at which the waves occur. Furthermore, the higher the input oil volume fraction within it flow regime (oil continuous or water continuous), the larger the

waves become. Subsequently, at the outlet end (34D), waves were only observed at the highest input oil volume fraction (0.8) with wave's amplitude of $\sim 0.37D$.

8.3 Flow patterns

Liquid-liquid two phase flows through a sudden expansion evolve from a dispersed flow to a segregated flow. The flow patterns were observed along the test section. The flow pattern for $U_{\text{smc}} \leq 0.20$ m/s is semi-stratified flow. By increasing the mixture velocity, the flow pattern change to semi-mixed flow with wider mixture layer between the two separated phases. Further increase of the mixture velocity changes the flow pattern into a dispersed flow especially for water continuous flows.

Generally, the flow patterns presented in this work are similar to that given by Vedapuri (1999). The difference is that the 4 layers observed in the present work which has not been reported in the previous studied. At a fixed inlet mixture velocity within the ST&MI regime, increase of the input oil volume fraction, the 4 layers thickness decreased. Layers of oil/water mist/oil/water were observed at high input oil volume fraction for horizontal and downward pipe orientation.

Horizontal orientation is the best pipe position for a dispersed flow to evolve quickly to a segregated flow through the expansion within a relatively short test distance. However, for upward and downward inclinations the mixed layer tends to increase and slow down the evolution process.

8.4 Drop size distributions

Drop size distributions in liquid-liquid system as a subjected to operating conditions (mixture velocities and input oil volume fractions) and pipe configurations (inclination angles) were obtained using a laser backscatter technique. Positioning of the probe at various axial locations of the test section and at various depths in the pipe has provided excellent drop size distributions without causing appreciable flow disturbance. These results are unique and comprehensive as they are not only represent the evolution of drop size distribution along the pipe expansion but also show the evolution of drops size distributions from the top to the bottom of the pipe cross-section. This technique measured the chord length distributions rather than drop diameter distributions. The chord length data was then converted to diameter distribution using a statistical technique reviewed in the literature. The drop diameter distributions obtained were then characterised by use of the Sauter Mean Diameter (SMD) and used in the discussion of the experimental data.

The evolution of drops size distributions at various depths of the pipe cross-section was measured. It was discovered that the drops were large nearer the interface at the near position (10D) for all pipe orientations and throughout the test section for horizontal flow. Thus, from the present data, it is concluded that drop size decreased when the distance from the interface increased (further away) for these pipe configurations. Contrarily, at the furthest position from the expansion for upward and downward inclined pipe orientation, larger droplets could also be seen at distance away from the interface and vice versa.

Furthermore, the experimental results show that large drops were primarily found to be at the bottom of the pipe cross-section for high input oil volume fraction at low mixture velocity. This indicates that the mechanisms of coalescence occurred faster at the bottom than the other locations in a pipe cross-section. For a better separation design, the coalescence process should occur at the bottom within the length of the pipe. However, at higher mixture velocity the mixed layer would be responsible for the smaller droplet size for horizontal and both inclination of pipe orientation, whether it is upward or downward. The mixed layer dominated almost entirely in the pipe cross-section.

The experiment results show a significant influence of both operating conditions and inclination angles on the drop size distributions. The results presented in this study can be used to optimise the separation processes involving liquid-liquid two-phase flow.

Consequently, the understanding of characterisation of liquid-liquid flow through expansion is important for a successful development of the separator performances. Within the present work, knowledge of the stratifying of two immiscible liquids has been extended in several areas. Special consideration was given to the operational flow conditions and geometry of the pipe with the aim of enhancing the phase separation qualities of the phases. The evolution of drop size distribution axially and vertically of the pipe expansion were prudently observed. Hence, the experiments reported in this work certainly represent the most comprehensive study of the drop size distributions of the expansion.

8.5 Recommendations for future work

In this work, the use of the wire mesh sensor on liquid-liquid system has been explored. It has been shown that it can be used to collect substantial amounts of novel and useful information in the present study. Even though the method is intrusive, the information it gives is valuable. Without such a technique, mapping the phase evolution across the cross-sectional area would be a difficult task to achieve. Furthermore, this technique captured the waves at the interface. The formation and subsequent evolution of interfacial waves in stratified system is an important phenomenon that needs further attention.

The system used has not addressed the presence of any surface active materials. The presence of such substances has a bigger influence on coalescence. Even though a little attempt has been made here, this has to be investigated in greater detail in order to have a better understanding that requires for the design of inline phase separators.

Even though the industry does not encourage the installation of internal structures such as honeycomb packing or plates could improve the phase separation. The influence of such modification could be attempted a modest effort to investigate the separation efficiencies. Detail investigation should include installing such internals after an expansion and monitoring the effect of the drop size distribution at downstream of the expansion.

In the present work, only semi-stratified was achieved within the test section due to the length of the expansion part is not is enough for the fully stratification process to

happens. Therefore, it is suggested to use longer test section together with the aforesaid internal structures to accomplished fully stratified (ST) flow.

Though numerous attempts have been made to predict the stratifying water-oil flow downstream of the expansion, there are still some issues that need further investigation. In order to better understanding these issues, i.e., the phase evolution of two phase liquid-liquid flows, more thorough full parameter space has to be investigated. There may be regions where the flow becomes unstable hindering the separation process. Even though it has not been observed in this work, the formation of interfacial tension waves has been observed.

Pressure drop measurements along the axial distance should be carried out to complement the present data. These would be of interest for the phase separation predictions and in determining the nature of the pressure reversal phenomena occurred during the experimentation.

Although an adequate effort has been taken to quantify the wave's amplitude that occurs at the interface between the water and mixed layer, further experimental study using WMS is recommended to be undertaken to produce and establish more concrete argument on the occurrences and properties of these waves.

Though the existing database has been expanded by considering industrially relevant fluids, consideration should also be paid to investigate the effect of fluid properties (viscosity, density and interfacial tension) and temperature on the phase separation downstream of the expansion. For instance, altering the interfacial tension of the

liquids by addition of surfactant to the liquid-liquid dispersed flow to investigate the effect of coalescence and break up on pressure drop and its influence on the stratification downstream of an expansion. Such information would be useful in order to build on the preliminary investigation work completed and extend the work presented in Chapter 7 onto pipe flow.

The current technique for converting chord length distribution to diameter distribution was found to be successful in the present work. In some cases it still need to be improved further to make sure the results obtained is beyond reasonable doubt. This could be achieved by improving the PAM2 by validating its data with other instrumentation data.

The evolution of the mixed layer downstream of the expansion, presents the macro-scale of the interaction of drops in dispersion. Therefore, to rectify this shortcoming, micro-scale information, i.e., drop size distribution profiles along the expansion and across the pipe cross section were attained from the Lasentec FBRM. However, it would be of great advantage if the size distribution data was also obtained from the WMS. It is therefore encouraging if the instruments could have directly or indirectly validated each other by producing drop size distribution results. Nevertheless, further improvisation of WMS, especially on the spatial resolution is needed. As up to date, the WMS manufacturers is in the final stage of the development of drop size distribution software, and soon the software will be launch and available to be applied in the future research. Furthermore, drops size could also be measured with more sophisticated instrumentation which is now available at the University of Nottingham, such as Super High Speed Camera and Boroscopic camera.

Last but not least, it would be a useful aid to the understanding of flow development if more drop size distribution profiles along the expansion and across the pipe cross section at different distances from the expansion, and for different expansion ratios could be established. Furthermore, a systematic study of flow development in different diameter pipes would add greatly to the current knowledge.

BIBLIOGRAPHY

Allen, T., (1990), "Particle Size Measurement 4th Edition", Chapman and Hall, London.

Alkaya, B., (2000), "Oil-water flow pattern and pressure gradients in slightly inclined pipes", *M.S Thesis*, The University of Tulsa.

Andreas, J.M., Hauser, E.A. and Tucker, W.B., (1938), "Boundary tension by pendant drops", *The Journal of Physical Chemistry*, Vol. 42, pp. 1001-1019.

Angeli, P., (2001), "Droplet size in two-phase liquid dispersed pipeline flows", *Chemical Engineering Technology*, Vol. 24, pp. 431-434.

Angeli, P. and Hewitt, G. F., (1998), "Pressure gradient in horizontal liquid-liquid flows", *International Journal of Multiphase flow*, Vol. 24, pp. 1183-1203.

Angeli, P. and Hewitt, G. F., (2000a), "Drop size distributions in horizontal oil-water dispersed flows", *Chemical Engineering Science*, Vol. 55, pp. 3133-3143.

Angeli, P. and Hewitt, G. F., (2000b), "Flow structure in horizontal oil-water flow", *International Journal of Multiphase Flow*, Vol. 26, pp. 1117-1140.

Angeli, P., Lovick, J., and Lum, J. Y.-L., (2002), "Investigations on the three-layer pattern during liquid-liquid flows", *40th European Two-Phase Flow Group Meeting*, Stockholm.

Arirachakaran, S., Oglesby, K. D., Malinovsky, M. S., Shoham, O., and Brill, J. P., (1989), "An analysis of oil-water flow phenomena in horizontal pipes", *SPE Professional product operating symposium, SPE paper 18836*, Oklahoma, US.

Baker, G., (2003), "Separation and control of gas-liquid flows at T-junction", *Ph.D. Thesis*, The University of Nottingham, United Kingdom.

Barrett, P. and Glennon, B., (1999), "In-line FBRM monitoring of particle size in dilute agitated suspensions", *Part. Part. Syst. Charact.*, Vol. 16, pp. 207-211.

- Beretta, A., Ferrari, P., Galbiati, L. and Andreini, P.A., (1997), "Horizontal oil-water flow in small diameter tubes: Flow patterns", *Int. Comm. Heat Mass Transfer*, Vol. 24, No. 2, pp. 223-229.
- Beck, M. S., Green, R. G., and Thorn, R., (1987), "Non-intrusive measurement of solids mass flow in pneumatic conveying", *J. Phys. E: Sci. Instrum.*, Vol. 20, pp. 835-840.
- Beggs, H. D. and Brill, J. P., (1973), "A study of two-phase flow in inclined pipes", *Journal of Petroleum Technology*, Vol. 25, pp. 607-617.
- Bolton, G. T., Korchinsky, W. J., and Waterfall, R. C., (1998), "Calibration of capacitance tomography system for liquid-liquid dispersions", *Measurement Science Technology*, Vol. 9, pp. 1797-1800.
- Bolton, G. T., Bolton, G. T., Korchinsky, W. J. and Waterfall, R. C. (1999), "Imaging Immiscible Liquid-Liquid Systems By Capacitance Tomography", *Trans IChemE 77A*, pp. 699-707.
- Bouyatiotis, B.S. and Thornton, J.D., (1967), "Liquid-liquid extraction studies in stirred tanks, Part 1, Droplet Size and Hold-up", *Inst. Chem. Engrs. (London) Symp. Ser.*, Vol. 26, pp. 43.
- Brauner, N., Rovinsky, J. and MoalemMaron, D., (1996), "Determination of the interface curvature in stratified two-phase systems by energy considerations", *International Journal of Multiphase Flow*, Vol. 22, No. 6, pp. 1167-1185.
- Brauner, N. and MoalemMaron, D., (1998), "The effect of surface forces on flow pattern and flow characteristics in two-phase system", *International Symposium on Liquid-liquid Transport Phenomena, International Centre for Heat and Mass Transfer, Antalya, Turkey*.
- Brauner, N., (1998b), "Liquid-liquid two phase flow", *Heat exchanger design update*, Vol. 5, pp. 1-40.
- Brauner, N., (2001), "The prediction of dispersed flows boundaries in liquid-liquid and gas-liquid system", *International Journal of Multiphase Flow*, Vol. 27, pp. 885-910.

Brauner, N., (2002), "Liquid-liquid two-phase flow systems", Modelling and control of two-phase phenomena, Udine.

Brauner, N. and MoalemMaron, D., (1992a), "Flow pattern transitions in two-phase liquid-liquid flow in horizontal tubes", *International Journal of Multiphase Flow*, Vol. 18, No. 1, pp. 123-140.

Brauner, N. and MoalemMaron, D., (1992b), "Stability analysis of stratified liquid-liquid flow", *International Journal of Multiphase Flow*, Vol. 18, No. 1, pp. 103-121.

Brauner, N. and MoalemMaron, D., (1989), "Two phase liquid-liquid stratified flow", *PhysicoChemical Hydrodynamics*, Vol. 11, No. 4, pp. 487-506.

Brauner, N. and Ullmann, A., (2002), "Modelling of phase inversion phenomenon in two-phase pipe flows", *International Journal of Multiphase Flow*, Vol. 28, pp. 117-1204.

Charles, M.E., Govier, G.W. and Hodgson, G.W., (1961), "The horizontal pipe flow of equal density oil-water mixtures", *Can. J. Chem. Eng.*, Vol. 39, pp. 27-36.

Clark, N. N., Liu, W., and Turton, R., (1996), "Data interpretation techniques for inferring bubble size distribution from probe signals in fluidized systems", *Powder Technology*, Vol. 88, No. 2, pp. 179-188.

Clark, N. N. and Turton, R., (1988), "Chord length distributions related to bubble size distributions in multiphase flows", *International Journal of Multiphase Flow*, Vol. 14, No. 4, pp. 413-424.

Clay, P. H., (1940), "The mechanism of emulsion formation in turbulent flow", *Proceedings*, Akademie van Wetenschappen, (Amsterdam), Vol. 43, pp. 852-965.

Collins, S. B. and Knudsen, J. G., (1970), "Drop size distributions produced by turbulent pipe flow of immiscible liquids", *AIChE Journal*, Vol. 16, No. 6, pp. 1072-1080.

Coulaloglou, C.A. and Tavlarides, L.L., (1977), "Description of interaction processes in agitated liquid-liquid dispersions", *Chemical Engineering Science*, Vol. 32, pp. 1289-1297.

Cox, A. L., (1985), "A study of horizontal and downhill two-phase oil-water flow", *M.S. Thesis*, The University of Texas, US.

- Cullen, L., (1990), "The public inquiry into the Piper Alpha disaster", London: His Majesty's Stationery Office (HMSO).
- CVCP, (1992), "Safety in Universities: Notes of Guidance part 2:1 Laser", Committee of Vice Chancellors and Principals (CVCP), U.K.
- Da Silva M.J., Schleicher E. and Hampel U., (2007a), "Capacitance wire-mesh sensor for fast measurement of phase fraction distributions", *Meas. Sci. Technol.*, Vol. 18, pp. 2245–2251.
- Da Silva M.J., Schleicher E. and Hampel U., (2007b), "Capacitance wire-mesh tomography for multiphase flow applications", *5th World Congress on Industrial Process Tomography.*, Norway, pp. 624–629.
- Da Silva M.J., Schleicher E. and Hampel U., (2007c), "Novel wire mesh sensor for the investigation of non-conducting fluids", *6th International Conference on Multiphase flow, ICMF 2007, S7_Thu_B_51*.
- Desnoyer, C., Masbernat, O. and Gourdon, C., (2002), "Experimental study of drop size distributions at high phase ratio in liquid-liquid dispersions", *Chemical Engineering Science*, Vol 58, pp. 1353-1363.
- Dong, F., Liu, X., Deng, X., Xu, L.J. and Xu, L.A., (2001), "Identification of two-phase flow regimes in horizontal, inclined and vertical pipes", *Measurement Science Technology*, Vol. 12, pp. 1069-1075.
- Dyakowski, T., (1996), "Process tomography applied to multi-phase flow measurement", *Measurement Science Technology*, Vol. 7, pp. 343-353.
- Dyakowski, T., Edwards, R. B., Xie, C. G., and Williams, R. A., (1997), "Application of capacitance tomography to gas-solid flows", *Chemical Engineering Science*, Vol. 52, No. 13, pp. 2099-2110.
- Dyakowski, T., Jeanmeure, L.F.C. and Jaworski, A.J., (2000), "Applications of electrical tomography for gas-solids and liquid-solids flows - a review", *Powder Technology*, Vol. 112, No.3, pp. 174-192.
- El-Hamouz, A. M., Stewart, A. C., and Davies, G. A., (1995), "A study of kerosene-water dispersion in shear flow through pipes and fittings", *Proc. of the 1st Int. Symp. on Two-Phase Modelling and Experimentation*, Rome, Italy.

El-Hamouz, A. M. and Stewart A. C., (1996), "On-line drop size distribution measurement of oil-water dispersion using a Par-Tec M300 laser back-scatter instrument", *SPE International*, SPE 36672, pp. 1-14.

Elseth, G., Kvandal, H. K. and Melaaen, M. C., (2000), "Measurement of velocity and phase fraction in stratified oil-water flow", *International Symposium on Multiphase Flow and Transport Phenomena*, Antalya, Turkey, pp. 206-210.

Fairuzov, Y.V., Arenas-Medina, P., Verdejo-Fierro, J. and Gonzales-Islas, R., (2000), "Flow pattern transitions in horizontal pipeline carrying oil-water mixtures: Full-scale experiments", *J. Energy Resources Technology*, Vol. 122, pp. 169-176.

Flores, J. G., Chen, X. T., Sarica, C. and Brill, J. P., (1997), "Characterization of oil-water flow pattern in vertical and deviated wells", *SPE Annual Technical Conference and Exhibition*, San Antonio, Texas, SPE paper 38810, pp. 1-10.

Frøystein T., (1997), "Flow imaging by gamma-ray tomography: data processing and reconstruction techniques", *In Proceedings of Frontiers in Industrial Process Tomography II*, Delft, pp. 185–187.

Gao, H., Gu, H.-Y. and Guo, L.-J., (2003), "Numerical study of stratified oil-water two-phase turbulent flow in a horizontal tube", *Int. J. Heat and Mass Transfer*, Vol. 46, pp. 749-754.

Gomez, S., Ono, M., Gamio, C., and Fraguera, A., (2003), "Reconstruction of capacitance tomography images of simulated two-phase flow regimes", *Applied Numerical Mathematics*, Vol. 46, pp. 197-208.

Govier, G. W., Sullivan, G. A., and Wood, R. K., (1961), "The upward vertical flow of oil-water mixtures", *Canadian Journal of Chemical Engineering*, Vol. 39, pp. 27-36.

Guzhov, A., Grishin, A.D., Medredev, V.F. and Medredeva, O.P., (1973), "Emulsion formation during the flow of two immiscible liquids", *Neft.Khoz.*, No. 8, pp. 58-61 (in Russian).

Han, J. H. and Kim S. D., (1993), "Bubble chord length distribution in three-phase fluidized beds", *Chemical Engineering Science*, Vol. 48, No. 6, pp. 1033-1039.

Hanzevack, E.L. and Demetriou, G.D., (1989), "Effect of velocity and pipeline configuration on dispersion in turbulent hydrocarbon-water flow using laser image processing", *International Journal of Multiphase Flow*, Vol. 15, pp. 985-996.

Hapanowicz, J. and Troniewski L., (2002), "Two-phase flow of liquid-liquid mixture in the range of the water droplet pattern", *Chemical engineering and processing*, Vol. 41, pp. 165-172.

Harkins, W.D. and Humphery, E.C., (1916), "Apparatus for the determination of the surface tension at the interface between two liquids (Surface tension II)", *Journal of the American Chemical Society*, Vol. 38, pp. 236-241.

Harkins, W.D. and Brown, F.E., (1919), "The determination of surface tension (free surface energy), and the weights of falling drops: The surface tension of water and benzene by capillary height method", *Journal of the American Chemical Society*, Vol. 41, pp. 499-524.

Hasan, N.M., (2006), "Stratifying liquid-liquid flows", *Ph.D. Thesis*, University of Nottingham, United Kingdom.

Hasson, D., Mann, U. and Nir, A., (1970), "Annular flow of two immiscible liquids I - Mechanisms", *The Canadian Journal of Chemical Engineering*, Vol. 48, pp. 514-520.

Herringe, R.A. and Davis M. R., (1976), "Structural development of gas - liquid mixture flow", *Journal of Fluid Mechanics*, Vol. 73, No. 1, pp. 97-123.

Hinze, J.O., (1955), "Fundamentals of the hydrodynamic mechanism of splitting dispersion processes", *AIChE Journal*, Vol. 1, pp. 289-295.

Hobbel, E.F., Davies, R., Rennie, F. W., Allen, T., Butler, L. E., Waters, E. R., Smith, J. T., and Sylvester, R. W., (1991), "Modern Methods of On-line Size Analysis for Particulate Process Streams", *Part. Part. Syst. Charact.*, Vol. 8, pp. 29-34.

Hori K., Fujimoto T., Kawanishi K. and Nishikawa H., (1997), "Advanced high speed X-ray CT scanner for measurement and visualisation of multi-phase flow", In: *OECD/CSNI Specialist Meeting on Advanced Instrumentation and Measurement Techniques*, Santa Barbara, USA.

Howarth, W.J., (1964), "Coalescence of drops in a turbulent flow field", *Chemical Engineering Science*, Vol. 19, pp. 33-38.

Huang, S.M., Plaskowski, A.B., Xie, C.G. and Beck, M.S., (1989), "Tomography imaging of two-component flow using capacitance sensors", *J. Phys. E: Science Instrum.*, Vol. 22, pp. 173-177.

Hughmark, G.A., (1971), "Drop break-up in turbulent pipe flow", *AIChE Journal*, Vol. 17, No. 4, p. 1000.

Hwang, C. J. and Pal, R., (1998), "Performance characteristics of pipe bends as metering devices for oil/water mixtures", *Chemical Engineer Communications*, Vol. 169, pp. 185-195.

Isaksen, O., (1996), "A review of reconstruction techniques for capacitance tomography", *Measurement Science Technology*, Vol. 7, pp. 325-337.

Ishii, M and Zuber, N., (1979), "Drag coefficient and relative velocity in bubbly, droplet or particulate flows", *AIChE Journal*, Vol. 25, pp. 843-855.

Issa, R.I., (1988), "Prediction of turbulent, stratified, two-phase flow in inclined pipes and channels", *International Journal of Multiphase Flow*, Vol. 14, pp. 141-154.

James, A.M., (1967), "Practical physical chemistry", *J&A Churchill Ltd*, London

James, P. W., Azzopardi, B. J., Graham, D. I., and Sudlow, C. A., (2000), "The effect of a bend on droplet size distribution in two-phase flow", *7th International Conference on Multiphase Flow in Industrial Plants*, Bologna, Italy, 19-23 September, pp. 211-222.

Jaworski, A.J. and Bolton, G.T., (2000), "The design of an electrical capacitance tomography sensors for use with media of high dielectric permittivity", *Measurement Science Technology*, Vol. 11, pp. 743-757.

Jaworski, A.J. and Dyakowski, T., (2001), "Application of electrical capacitance tomography for measurement of gas-solid flow characteristics in a pneumatic conveying system", *Measurement Science and Technology*, Vol. 12, pp. 1109-1119.

Jeanmeure, L. F. C., Dyakowski, T., Zimmermen, W. B. J., and Clark, W., (2002), "Direct flow pattern identification using electrical capacitance tomography", *Experimental Thermal and Fluid Science*, Vol. 26, pp. 763-773.

Jayawardena, S.S., Alkaya, B., Redus, C.L. and Brill, J.P., (2000), "A new model for dispersed multi-layer oil-water flow", *Proceedings of BHR 2000 Multiphase Technology*, Banff, Canada, pp.77-89.

Johansen, G. A., Froystein, T., Hjertaker, B. T., and Olsen, O., (1996), "A dual sensor flow imaging tomographic system", *Measurement Science and Technology*, Vol. 7, pp. 297-307.

Karabelas, A. J., (1978), "Droplet size spectra generated in turbulent pipe flow of dilute liquid-liquid dispersions", *AIChE Journal*, Vol. 24, No. 2, pp. 170-180.

Karabelas, A. J., (1996), "Droplet size spectral generated in turbulent pipe flow of dilute liquid-liquid dispersion", *AIChE Journal*, Vol. 24, pp. 170-180.

Khapkay, A., Abolghasemi, H. and Khorsidi, A.S., (2009), "The effect of a surfactant on mean drop size in mixer-settler extractor", *Chemical Engineering and Processing*", Vol. 48, pp. 1105-1111.

Kolmogorov, A.N., (1949), "On the breaking of drops in turbulent flow", *DokladyakadNauk (USSR)*, Vol. 66, pp. 825-828.

Kostoglou, M. and Karabelas A. J., (2001), "A contribution towards predicting the evaluation of droplet size distribution in flowing dilute liquid/liquid dispersions", *Chemical Engineering Science*, Vol. 56, pp. 4283-4292.

Kostoglou, M. Dovas S. and Karabelas A. J., (1997), "On the steady state size distribution of dispersions in breakage processes", *Chemical Engineering Science*, Vol. 52, No. 8, pp. 1285-1299.

Kostoglou, M and Karabelas, A. J., (1998), "On the attainment of steady state in turbulent pipe flow of dilute dispersions", *Chem. Eng. Sci.*, Vol. 53, No. 3, pp. 505-513.

Krepper, E., Lucas, D. and Prasser, H-M., (2005), "On the modeling of bubbly flow in vertical pipes", *Nuclear Engineering and Design*, Vol. 235, pp. 597-611.

Kubie, J. and Gardner, G. C., (1977), "Drop sizes and drop dispersion in straight horizontal tubes and in helical coils", *Chemical Engineering Science*, Vol. 32, No. 2, pp. 195-202.

Kumar, S., Kumar, R. and Gandhi, K.S., (1993), "A new model for coalescence efficiency of drops in stirred dispersions", *Chemical Engineering Science*, Vol. 48, No. 11, pp. 2025-2038.

Kumar SB., Moslemian D. and Dudukovic' M., (1995), "A g-ray tomographic scanner for imaging voidage distribution in two-phase flow systems", *Flow Meas. Instrum.* Vol. 6, No. 1, pp. 61-73.

Kurban, A. P. A., Angeli, P. A., Mendes-Tatsis, M. A., and Hewitt, G. F., (1995), "Stratified and dispersed oil-water flows in horizontal pipes", *Proceedings of the 7th International Conference on Multiphase Flow Production*, Cannes, France, pp. 277-291.

Kurban, A. P. A., (1997), "Stratified liquid-liquid flow", *Ph.D. Thesis*, Imperial College of Science, Technology and Medicine, The University of London.

Langston, P. A., Burbidge, T. F., Jones, T. F., and Simmons, M. J. H., (2001), "Particle and droplet size analysis from chord measurement using Bayes' theorem", *Powder Technology*, Vol. 116, pp. 33-42.

Langston, P. A. and Jones, T. F., (2001), "Non-spherical 2-Dimensional particle size analysis from chord measurements using Bayes' theorem", *Part. Part. Syst. Charact.*, Vol. 18, pp. 12-21.

Lasentec, (2007), "Lasentec M-Series hardware manual", Mettler-Toledo, Rev 1.

Launder, B. E., Reece, G. J. and Rodi, W., (1975), "Progress in the developments of a Reynolds-stress turbulence closure", *J. Fluid Mechanics*, Vol. 68, pp. 537-566.

Launder, B. E. and Spalding, D. B., (1974), "The numerical computation of turbulent flows", *Comp. Meth. Appl. Mech. Eng.*, Vol. 3, pp. 269-289.

Levick, V. G., (1962), "Physicochemical hydrodynamics", Prentice Hall, Englewood Clifls, New York, USA.

Li, D., (1994), "Coalescence between two small bubbles or drops", *Journal of Colloid and Interface Science*, Vol. 163, pp. 108-119.

Li, D., (1996a), "Coalescence between small bubbles: Effects of bulk and surface diffusion", *Chemical Engineering Science*, Vol. 51, No. 14, pp. 3623-3630.

Li, D., (1996b), "Coalescence between small bubbles: Effects of surface tension gradient and surface viscosities", *Journal of Colloid and Interface Science*, Vol. 181, pp. 34-44.

Lim, K.S. and Agarwal, P.K., (1990), "Conversion of pierced lengths measured at a probe to bubble size measures: an assessment of the geometrical probability approach and bubble shape models", *Powder Technology*, Vol. 63, pp. 205-219.

Liu, S. and Li, D., (1999), "Drop coalescence in turbulent dispersions", *Chemical Engineering Science*, Vol. 54, pp. 5667-5675.

Liu, S., (2005), "Novel separator for liquid-liquid flow", *M.Sc. Thesis*, The University of Nottingham, UK.

Liu, W. and Clark, N. N., (1995), "Relationships between distributions of chord lengths and distributions of bubble sizes including theory statistical parameters", *International Journal of Multiphase Flow*, Vol. 21, No. 6, pp. 1073-1089.

Liu, W., Clark, N. N., and Karamavruc, A. I., (1996), "General method for the transformation of chord-length data to a local bubble-size distribution", *AIChE Journal*, Vol. 42, No. 10, pp. 2713-2719.

Liu, W., Clark, N. N., and Karamavruc, A. I., (1998), "Relationship Between Bubble Size Distribution and Chord Length Distribution in Heterogeneously Bubbling System", *Chemical Engineering Science*, Vol. 53, No. 3, pp. 1267-1276.

Lucas, D., Krepper, E. and Prasser, H.-M., (2005), "Development of co-current air-water flow in a vertical pipe", *International Journal of Multiphase Flow*, Vol. 31, pp. 1304-1328.

Lum, J. Y.-L., Lovick, J., and Angeli, P., (2002), "Two-phase flows in inclined pipelines", *3rd North American Conference on Multiphase Technology*, 6-7 June, Banff, Canada, pp.219-231.

Lum, J. Y.-L., Lovick, J., and Angeli, P., (2004), "Low inclination oil-water flows", *The Canadian Journal of Chemical Engineering*, Vol. 82, pp. 303-315.

Lum, J. Y.-L., Al-Wahaibi, T., and Angeli, P., (2006), "Upward and downward inclination oil-water flows", *International Journal of Multiphase Flow*, Vol. 32, pp. 413-435.

Luo, S. M. and Svendsen, H., (1996), "Theoretical model for drop and bubble breakup in turbulent dispersion", *AIChE Journal*, Vol. 42, pp. 1225-1233.

Lovick, J. and Angeli, P., (2001), "Impedance probe for phase distribution measurements and flow pattern identification in oil-water flows", *In: Proceedings of 5th International Conference on Experimental Heat Transfer, Fluid Mechanics and Thermodynamics*, Thessaloniki, Greece.

Lovick, J. and Angeli, P., (2003), "Drop size during dual continuous, oil-water flows", *41st European Two-phase Flow Group Meeting*, Trondheim, Norway, 12-13 May.

Lovick, J. and Angeli, P., (2004a), "Experimental studies on the dual continuous flow pattern in oil-water flows", *International Journal of Multiphase Flow*, Vol. 30, No. 2, pp. 139-157.

Lovick, J. and Angeli, P., (2004b), "Droplet size and velocity profiles in liquid-liquid horizontal flows", *Chemical Engineering Science*, Vol. 59, pp. 3015-3115.

McQuillan, K.W. and Whalley, P.B., (1985), "Flow patterns in vertical two-phase flow", *International Journal of Multiphase Flow*, Vol. 11, pp. 161-175.

Mok, Y.I. and Treybal, R.E., (1971), "Continuous phase mass transfer coefficient for liquid extraction in agitated vessels II", *AIChE Journal*, Vol. 17, pp. 916-920.

Mukherjee, H., Brill, J.P. and Beggs, H.D., (1981), "Experimental study of oil-water flow in inclined pipes", *Journal of Energy Resources Technology*, Vol. 103, pp. 56-63.

Mwanbela, A. J. and Johansen, G. A., (2001), "Multiphase flow component volume fraction measurement: experimental evaluation of entropic thresholding methods using an electrical capacitance tomography system", *Measurement Science Technology*, Vol. 12, pp. 1092-1101.

Noik, C., Dalmazzone, C., Rambeau, O. and Simonet, C., (2002), "Formation of dispersions or emulsions under controlled flow conditions", *3rd North America Conference on Multiphase Technology*, Banff, Canada, June 6-7.

Nädler, M. and Mewes, D., (1997), "Flow induced emulsification in the flow of two immiscible liquids in horizontal pipes", *International Journal of Multiphase Flow*, Vol. 23, No. 1, pp. 55-68.

Oakley, J.P. and Bair, M.S., (1995), "A mathematical model for the multi-electrode capacitance sensor", *Measurement Science Technology*, Vol. 6, pp. 1617-1630.

Oglesby, K.D., (1979), "An experimental study on the effects of oil viscosity, mixture velocity and water fraction on horizontal oil-water flow", *M.S Thesis*, the University of Tulsa.

Oddie, G., Shi, H., Durlofsky, L.J., Aziz, K., Pfeffer, B. and Holmes, J.A., (2003), "Experimental study of two and three phase flows in large diameter inclined pipes", *International Journal of Multiphase Flow*, Vol. 29, pp. 527-558.

Olmos, E., Gentric, C., Vial, Ch., Wild, G. and Midoux, N., (2001), "Numerical simulation of multiphase flow in bubble column reactors: Influence of bubble coalescence and break-up", *Chemical Engineering Science*, Vol. 56, No. 21-22, pp. 6359-6365.

Ottino, J.M., DeRoussel, P., Hansen, S. and Khakhar, D.V., (1999), "Mixing and dispersion of viscous liquids and powdered solids", *Adv. Chem. Eng.*, v.25, pp.105-204.

Pacek, A.W., Nienow, A.W. and Moore, I.P.T., (1994), "On the structure of turbulent liquid-liquid dispersed flows in an agitated vessel", *Chemical Engineering Science*, Vol. 49, pp. 3485-3498.

Pacek, A. W. Man C. C. and Nienow A. W., (1998), "On the Sauter mean diameter and size distributions in turbulent liquid-liquid dispersions in stirred vessel", *Chemical Engineering Science*, Vol. 53, No. 11, pp. 2005-2011.

Paras, S. V. Vlachos, N. A., and Karabelas, A. J., (1994), "Liquid layer characteristics in stratified - atomization flow", *International Journal of Multiphase Flow*, Vol. 20, pp. 939-956.

Park, J.Y. and Blair, L.M., (1975), "The effect of coalescence on drop size distribution in an agitated liquid-liquid dispersion", *Chemical Engineering Science*, Vol.30, pp. 1057-1064.

Parzen, E., (1962), "On estimation of a probability density function and mode", *Ann. Math. Stat.*, Vol. 33, pp. 1065- .

Prasser H.M., Bottger A. and Zschau J., (1988), "A new electrode-mesh tomograph for gas-liquid flows", *Flow Measurement and Instrumentation*, Vol. 9, pp. 111-119.

Prasser H.M., Scholz D. and Zippe C., (2001), "Bubble size measurement using wire-mesh sensors", *Flow Measurement and Instrumentation*, Vol. 12, pp. 299-312.

Ramkrishna, D., (1974), "Drop-breakage in agitated liquid-liquid dispersions", *Chemical Engineering Science*, Vol.29, pp. 987-992.

Reinecke, N. and Mewes, D., (1996), "Recent developments and industrial/research applications of capacitance tomography", *Measurement Science Technology*, Vol. 7, pp. 233-246.

Reinecke, N. and Mewes, D., (1997), "Multi-electrode capacitance sensors for the visualisation of transient two-phase flow", *Experimental Thermodynamics and Fluid Science*, Vol. 15, pp. 253-266.

Reinecke, N., Petritsch, G., Boddem, M., and Mewes, D., (1998), "Tomographic imaging of the phase distribution in two-phase slug flow", *International Journal of Multiphase Flow*, Vol. 24, No. 4, pp. 617-634.

Roberts, P. A., (1994), "Two-phase flow at T-junction", *Ph. D. Thesis*, The University of Nottingham, U.K.,

Rodriquez, O. M. H. and Oliemans, R. V. A., (2006), "Experimental study on oil-water flow in horizontal and slightly inclined pipes", *International Journal of Multiphase Flow*, Vol. 32, pp. 323-343.

Rosin, P. and Rammler, E., (1933), "Laws governing the fineness of powered coal", *J. Inst. Fuel*, Vol. 7, pp. 29-36.

Russell, T. W. F. and Charles, M. E., (1959), "The effect of the less viscous liquid in laminar flow of two immiscible liquids", *The Canadian Journal of Chemical Engineering*, Vol. 37, pp. 18-24.

Russell, T. W. F., Hodgson, G. W., and Govier, G. W., (1959), "Horizontal pipeline flow of mixtures of oil and water", *The Canadian Journal of Chemical Engineering*, Vol. 37, pp. 9-17.

Santana, D. and Macias-Machin, A., (2000), "Local bubble-size distribution in fluidized beds", *AIChE Journal*, Vol. 46, No. 7, pp. 1340-1347.

Sato, Y. and Sekoguchi, K., (1975), "Liquid velocity distribution in two-phase bubbly flow", *International Journal of Multiphase Flow*, Vol. 2, pp. 79-95.

Schindler, H.D. and Treybal, R.E., (1968), "Continuous phase mass transfer coefficient for liquid extraction in agitated vessels", *AIChE Journal*, Vol. 15, pp.790-798.

Schmitz D., Reinecke N., Petritsch G. and Mewes D.,(1997), "X-Ray computed tomography for stationary multiphase flow in random and structured packings", In: *Proceedings of Frontiers in Industrial Process Tomography II*, Delft, pp. 103–108.

Scott, G. M., (1985), "A study of two-phase liquid-liquid flow at variable inclinations", *M.S. Thesis*, The University of Texas, US.

Shi, H., Cai, J.Y. and Jepson, W.P., (1999), "oil-water distributions in large diameter horizontal pipelines", *Proc. Of the 4th International Symposium Multiphase flow and heat transfer*, Xi'an, China, 22-24 August.

Shi, H., Cai, J., and Jepson, W. P., (2001), "Oil-water two-phase flows in large-diameter pipeline", *Trans of ASME: Journal of Energy Resources Technology*, Vol. 123, pp. 270-276.

Shoham, O. and Taitel, T., (1984), "Stratified turbulent-turbulent gas-liquid flow in horizontal and inclined pipes", *AIChE J.*, Vol. 30, pp. 377-385.

Shinnar, R., (1961), "On the behaviour of liquid dispersions in mixing vessels.", *Journal of Fluid Mechanics*, Vol. 10, pp. 259-275.

Simmons, M. J. H., (1998), "Liquid-liquid flow and separation", *Ph. D. Thesis*, The University of Nottingham, U.K.,

Simmons, M. J. H., Azzopardi, B. J., and Zaidi, S. H., (1998), "Measurement of drop sizes and flow patterns in liquid-liquid pipe flow", 3rd International Conference on Multiphase Flow, Lyon, France.

Simmons, M. J. H., Langston, P. A., and Burbidge, A. S., (1999), "Particle and droplet size analysis from chord distribution", *Powder Technology*, Vol. 102, pp. 75-83.

Simmons, M. J. H. Zaidi S. H. and Azzopardi B. J., (2000), "Comparison of laser based drop size measurement techniques and their application to dispersed liquid-liquid pipe flow", *Optical Eng.*, Vol. 32, No. 2, pp. 505-509.

Simmons, M. J. H. and Azzopardi, B. J., (2001), "Drop size distribution in dispersed liquid-liquid pipe flow", *International Journal of Multiphase Flow*, Vol. 27, pp. 843-859.

Sleicher Jr., C. A., (1962), "Maximum stable drop size in turbulent flow", *AIChE Journal*, Vol. 8, No. 4, pp. 471-477.

Soleimani, A., Lawrence. C.J. and Hewitt, G.F., (1999a), "Spatial distribution of oil and water in horizontal pipe flow", *SPE International*, SPE paper 56524.

Soleimani, A., (1999b), "Phase distribution and associated phenomena in oil-water flows in horizontal tubes", *Ph. D. Thesis*, Imperial College of Science, Technology and Medicine, The University of London.

Speziale, C. G., Sarkar, S. and Gatski, T. B., (1991), "Modelling the pressure-strain correlation of turbulence: an invariant dynamical systems approach", *J. Fluid Mechanics*, Vol. 277, pp. 245-272.

Sprow, F.B., (1967), "Distribution of drop sizes produced in turbulent liquid-liquid dispersion", *Chemical Engineering Science*, Vol. 22, pp. 435-442.

Su, H. and Hanzevack E. L., (1988), "A model for drop size distribution and maximum drop size in two-phase liquid-liquid flow", *AIChE Annual Meeting*, Washington, DC.

Swartz, J. E. and Kessler, D. P., (1970), "Single drop breakup in developing turbulent pipe flows", *AIChE Journal*, Vol. 16, pp. 256-260.

Tadyyon, A. and Rohani, S., (1998), "Determination of particle size distribution by Par-Tec 100: Modelling and Experimental results", *Part. Part. Syst. Charact.*, Vol. 15, pp. 127-135.

Taitel, Y. and Barnea, D., (1997), "Simplified transient simulation of two phase flow using quasi-equilibrium momentum balances", *International Journal of Multiphase Flow*, Vol. 23, No. 3, pp. 493-501.

Taitel, Y., and Dukler, A. E., (1976), "A model for predicting flow regime transitions in horizontal and near horizontal gas-liquid flow", *AIChE Journal*, Vol. 22, pp. 47-55.

Taitel, Y., Lee, N., and Dukler, A. E., (1978), "Transient gas-liquid flow in horizontal pipes: Modelling the flow pattern transitions", *AIChE Journal*, Vol. 24, No. 5, pp. 920-933.

Tavlarides, L. L. and Stamataudis, M., (1981), "The analysis of interface reactions and mass transfer in liquid-liquid dispersions", *Advances in Chemical Engineering*, Vol. 11, pp. 199-213.

Taylor, J. R., (1982), "An introduction to error analysis, 2nd ed.", University Science Books, California. U.S.

Taylor, G.I., (1934), "The formation of emulsions in definable fields of flow", *Proc. Royal Society London* A146, pp.501-523.

Thomas, R. M., (1981), "Bubbles coalescence in turbulent flows", *International Journal of Multiphase Flow*, Vol. 7, No. 6, pp. 709-717.

Trallero, J. L., (1996), "Oil-water flow patterns in horizontal pipes", *Ph. D. Thesis*, The University of Tulsa.

Trallero, J. L., Sarica, C., and Brill, J. P., (1997), "A study of oil/water flow patterns in horizontal pipes", *SPE Production and Facilities*, SPE paper 36609.

Tsouris, C. and Tavlarides, L. L., (1994), "Breakage and coalescence models for drops in turbulent dispersion", *AIChE Journal*, Vol. 40, No. 3, pp. 395-406.

Valentas, K. J and Amundson, N. R., (1966), "Breakage and coalescence in dispersed phase system", *Industrial Engineering Chemical Fundamental*, Vol. 5, No. 4, pp. 533-542.

Valle, A and Kvandal H. K., (1995), "Pressure drop and dispersion characteristics of separated oil-water flow", *In proceedings of the international symposium on two-phase flow modelling and experiment*, Rome, Italy, 9 - 11 Oct., pp. 583-591.

Vedapuri, D., Bessette, D. and Jepson, W.P., (1997), "A segregated flow model to predict water layer thickness in oil-water flows in horizontal and slightly inclined pipelines", *Proc. 8th international Conference on Multiphase Flow 97*, pp. 75-105.

Vedapuri, D., 1999. Study on oil-water flows in inclined pipelines. MS. Thesis, Ohio University, OH.

Vigneaux, P., Chenais, P., and Hulin, J. P., (1988), "Liquid-liquid flows in an inclined pipe", *AIChE Journal*, Vol. 34, No. 5, pp. 781-789.

Ward, J. P. and Knudsen, J. G., (1967), "Turbulent flow of unstable liquid-liquid dispersions: Drop sizes and velocity distributions", *AIChE Journal*, Vol. 13, No. 2, pp. 356-365.

Weimer, A. W. Gyure D. D. and Clough D. E., (1985), "Application of a gamma-radiation density gauge for determining hydrodynamic properties of fluidized beds", *Powder Technology*, Vol. 44, pp. 179-194.

Weisman, J., Duncan, D., Gibson, J., and Crawford, T., (1979), "Effects of fluid properties and pipe diameter on two-phase flow patterns in horizontal lines", *International Journal of Multiphase Flow*, Vol. 5, pp. 437-462.

Williams, R. A. and Beck, M. S., (1995), "Process Tomography - principles, technique and application", Butterworth-Heinemann, Oxford.

Wren, E., (2001), "Geometric effects on phase split at a T-junction", *PhD Thesis*, The University of Nottingham, UK.

Wynn, E. J. W., (2003), "Relationship between particle-size and chord-length distributions in focused beam reflectance measurement: stability of direct inversion and weighting", *Powder Technology*, Vol. 133, No. 1-3, pp. 125-133.

Xie, C. G., Reinecke, N., Beck, M. S., Mewes, D., and Williams, R. A., (1995), "Electrical tomography techniques for process engineering applications", *Chemical Engineering Journal*, Vol. 56, pp. 127-133.

Yang, L., Weng, Z., Huang, Z. and Pan, Z., (1990), "Mechanism and models for non-surfactant liquid-liquid turbulent dispersion in agitated vessels", *Chemical Engineering* (in Chinese), Vol. 18, NO. 2. pp.24-30.

Yang, L., Azzopardi, B. J., and Belghazi, A., (2001), "Application of T-junction as a partial separator for liquid/liquid flows", *Proc. 5th Int. Conf. on Experimental Heat Transfer, Fluid Mechanics and Thermodynamics*, Thessaloniki.

Yang, L., (2003), "Liquid-liquid two-phase flows at T-junction and through expansion", *PhD Thesis*, The University of Nottingham, UK.

Yang, L., Azzopardi, B. J., Baker, G., Belghazi, A., and Giddings, D., (2003), "The approach to stratification of a dispersed liquid-liquid flow at a sudden expansion", *41st European Two-phase Flow Group Meeting*, Trondheim, Norway, 12-13 May.

Zhou, G. and Kresta S. M., (1998a), "Correlation of mean drop size and minimum drop size with the turbulence energy dissipation and the flow in a agitated tank", *Chemical Engineering Science*, Vol. 53, No. 11, pp. 2063-2079.

Zhou, G. and Kresta S. M., (1998b), "Evolution of drop size distribution in liquid-liquid dispersions for various impellers", *Chemical Engineering Science*, Vol. 53, No. 11, pp. 2099-2113.

Zavareh, F., Hill, A.D. and Podio, A.L., (1988), "Flow regime in vertical and inclined oil-water flow in pipes", *SPE 63rd Annual Technical Conference and Exhibition*, Houston, October 2-5, SPE paper 18215.

Appendix 2A

FLOW PATTERN MAPS

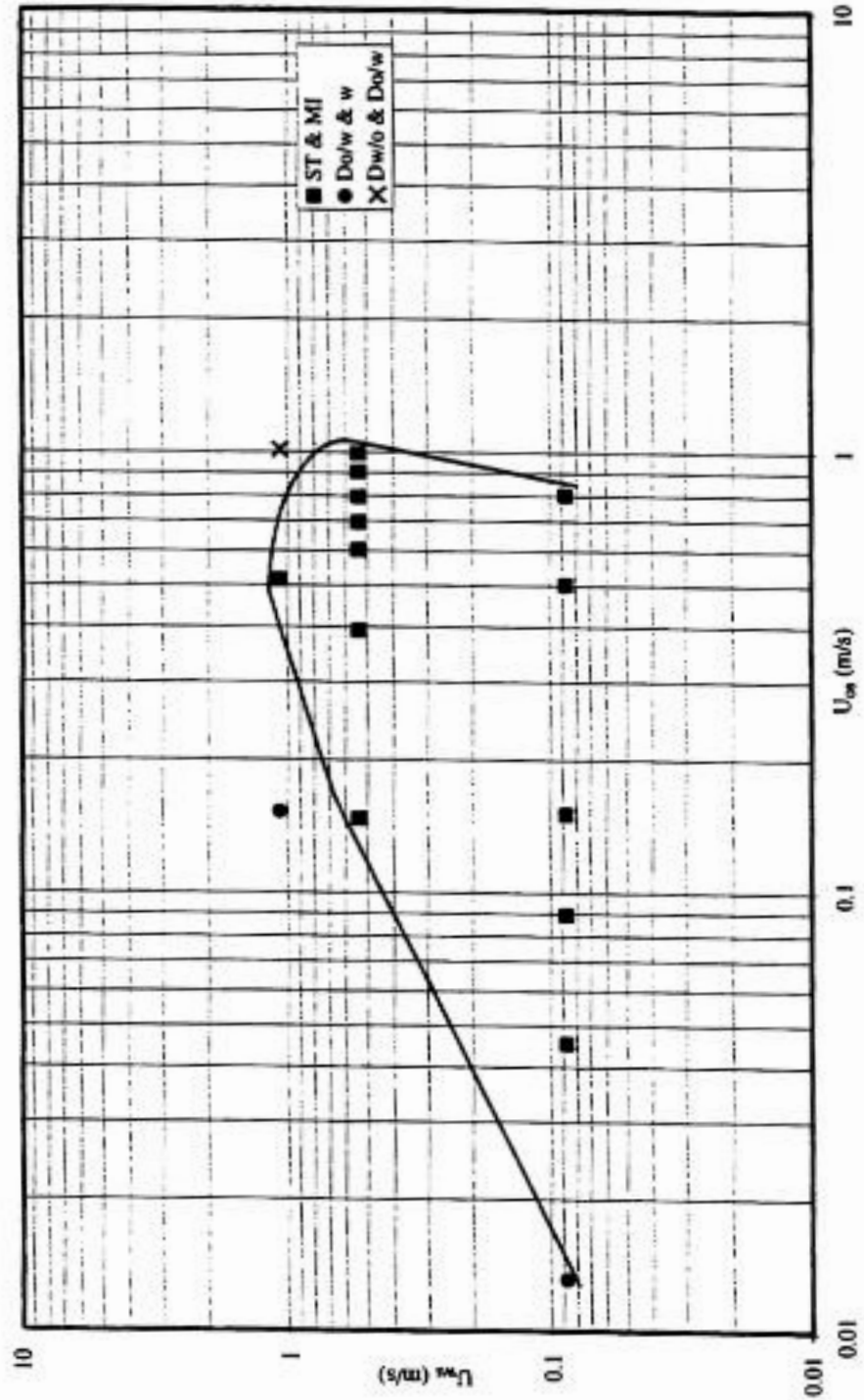


Figure 2A.1: Experimental flow pattern map, horizontal Russell *et al.* (1959)

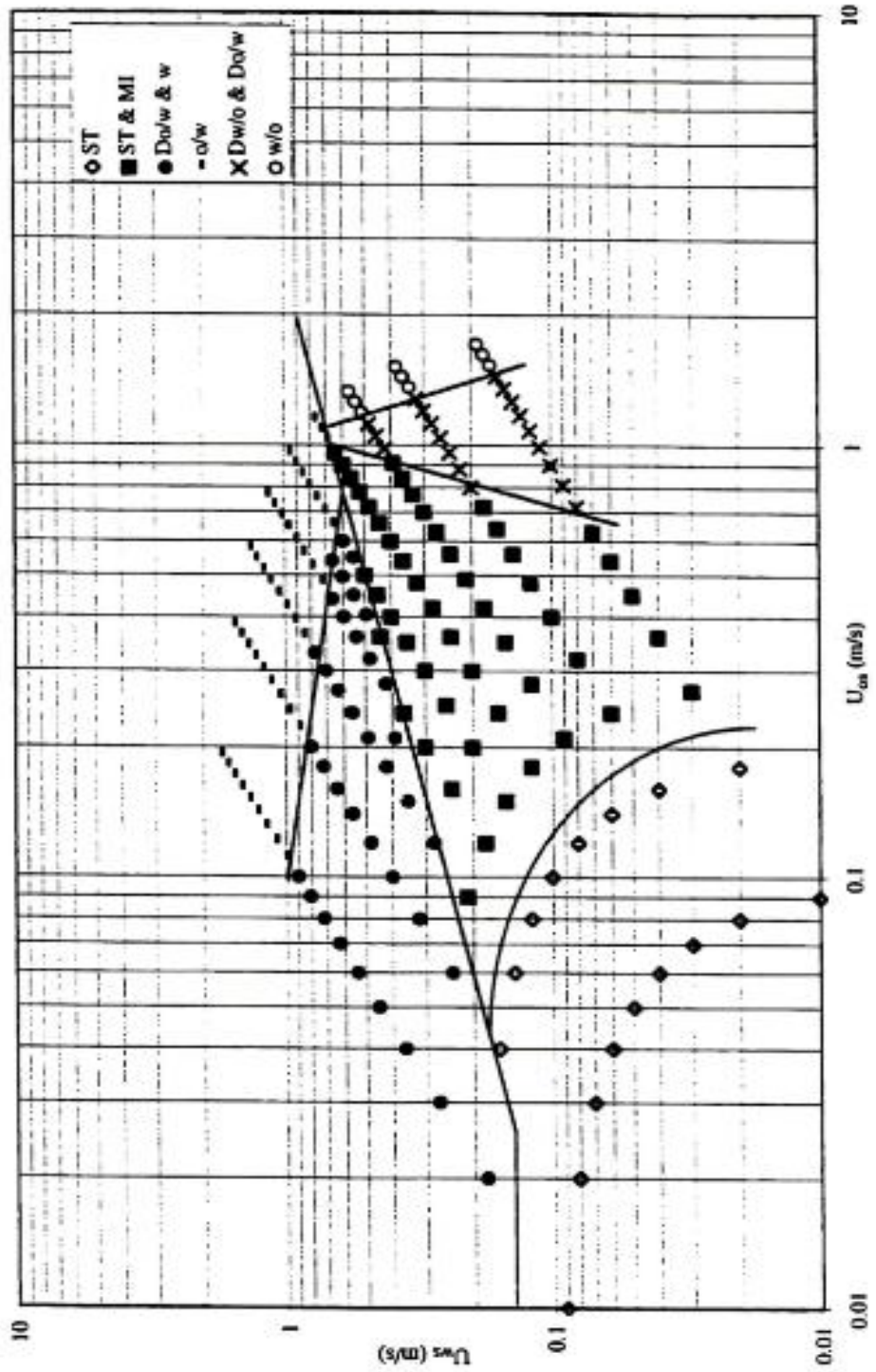


Figure 2A.2: Experimental flow pattern map, horizontal Guzhov *et al.* (1973)

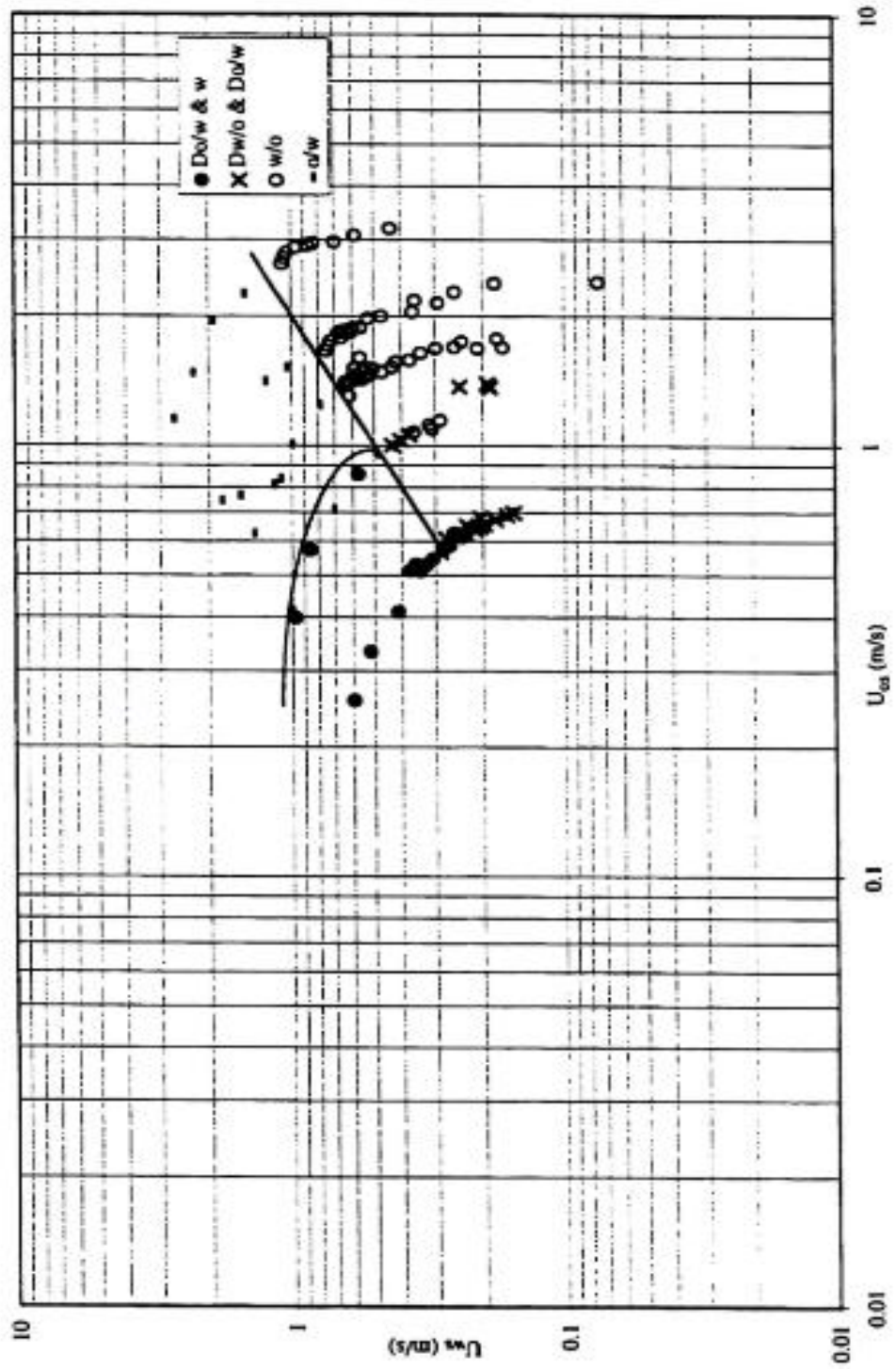


Figure 2A.3: Experimental flow pattern map, horizontal Oglesby (1979)

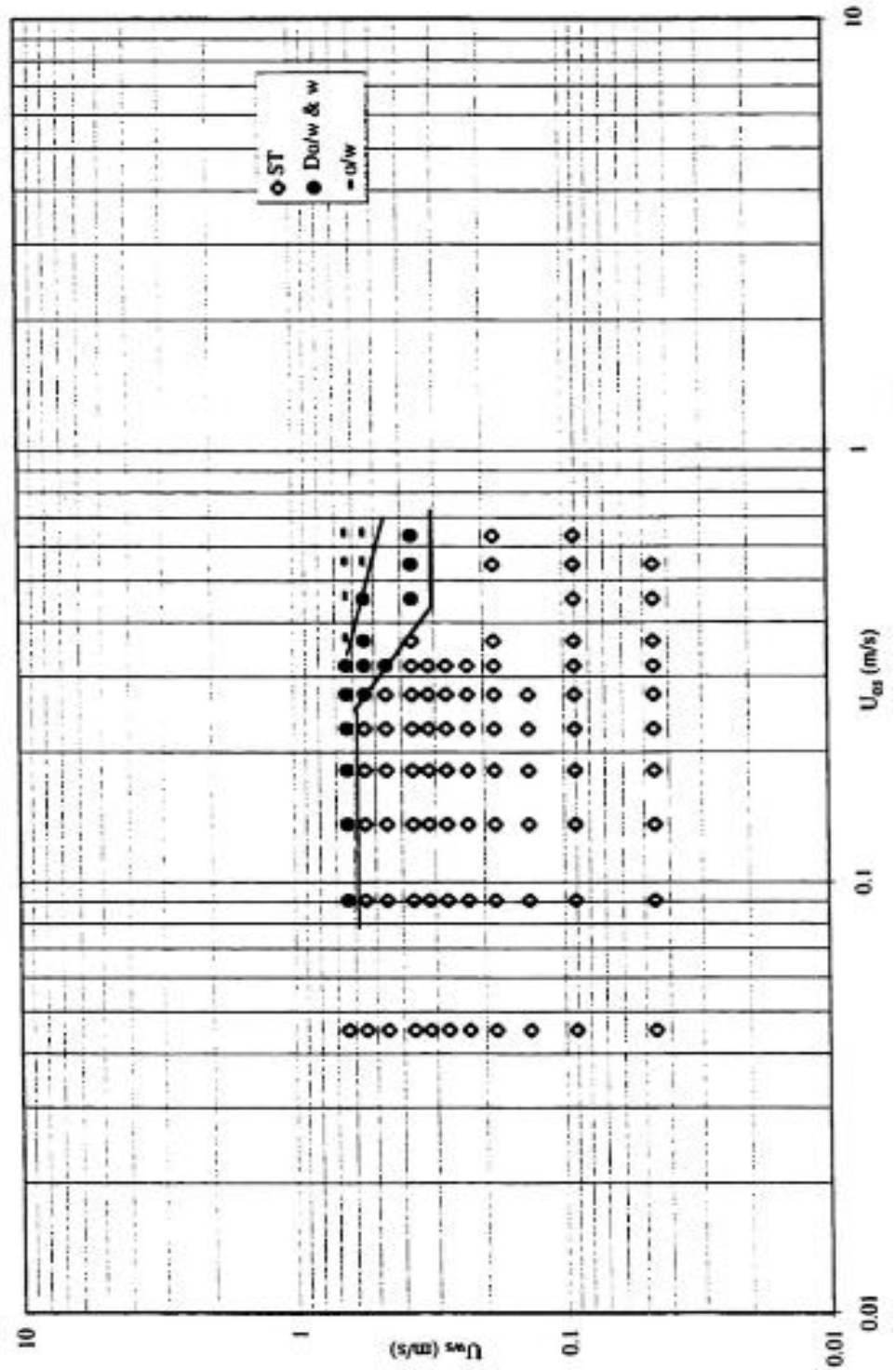


Figure 2A.4: Experimental flow pattern map, horizontal Cox (1985)

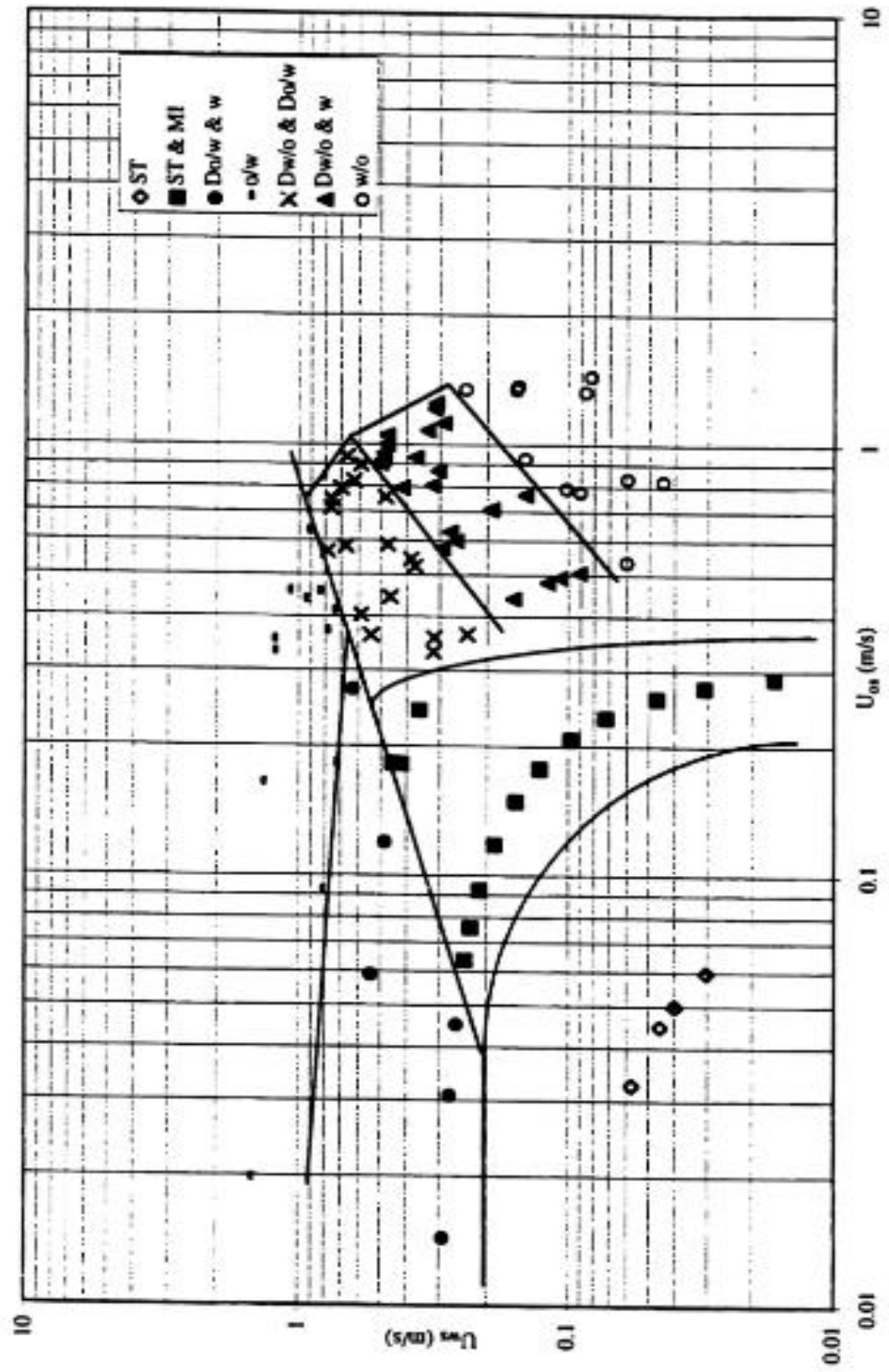


Figure 2A.5: Experimental flow pattern map, horizontal Nadler & Mewes (1995)

Appendix 2B

PAM 2.1.

Converts chord distribution to diameters using Bayes theorem, assumes random cuts on spheres or circles. Langston et al Powder Technology 116 (2001) 33-42

```

clc
clear all
%particle diameter bins, length units as per user
dl = 0.01;
dh = 1; %50; largest diameter
nd = 100; % no. dia bins
ndw= 100; %no. chord bins for analysis

p = zeros(1,nd);
pn = zeros(1,nd);
diam = zeros(1,nd);
ph = zeros(ndw,nd);
dw = zeros(1,ndw);
pht = zeros(1,nd);
prhit= zeros(1,nd);
fq = zeros(1,nd);

data = xlsread('xlsx'); % read excel file
[m,ncut] = size(data); % ncut = number of chord bins measured
chordl = data(1,:); % chord sizes measured
pchordl = data(2,:); % probabilities
pchordt = sum(pchordl);
disp(pchordt) % check equal unity

dband = (dh-dl)/nd;
for i = 1:nd
    diam(i) = (i-0.1)*dband;

```

```

    pn(i) = 0;
    fq(i) = 1/nd; % initialise frequency
end

dwidth=dh/ndw; % width of analysis chord bins
for j = 1:ndw
    dw(j) = (j-0.1)*dwidth; % analysis chord bin sizes
end

for i = 1:nd
    d = diam(i);
    pht(i) = 0;
    for j = 1:ndw
        d1 = dw(j) - 0.1*dwidth;
        d2 = d1 + dwidth;

        if (d2 <= d)
            ph(j,i) = (sqrt(d*d - d1*d1) - sqrt(d*d - d2*d2))/d;
        else
            ph(j,i) = 0; % probability hit chord j given particle i
        end
        pht(i) = pht(i) + ph(j,i); % check should sum to unity
    end
end

disp(pht) % check output
disp(diam)

iter = 0;
n_iter=10; % no. iterations between output
igo = input('Start iteration type 1: ');
while (igo == 1) % could use a for loop if many iterations required
    for iter=1:n_iter
        prhitt = 0;

```

% step 2

```

for i = 1:nd
    prhit(i) = fq(i)*diam(i);
    prhitt = prhitt + prhit(i);
end
for i = 1:nd
    prhit(i) = prhit(i)/prhitt;
    pn(i) = 0;
end

for k = 1:ncut % step 3
    cl = chordl(k);
    j = round(cl/dwidth + 0.5); % identify analysis chord bin
    pt = 0;
    for i = 1:nd
        p(i) = ph(j,i)*prhit(i);
        pt = pt + p(i);
    end

    if (pt ~= 0) % step 4
        for i = 1:nd
            p(i) = p(i)/pt;
            pn(i) = pn(i) + p(i)*pchordl(k);
        end
    end
end

fqtot = 0; % step 5
for i = 1:nd
    prhit(i) = pn(i);
    fq(i) = prhit(i)/diam(i);
    fqtot = fqtot + fq(i);
end
for i = 1:nd
    fq(i) = fq(i)/fqtot;
end

```

```
end

    disp(fq)                                     % step 6
% hold on
% plot (diam,fq,'b')
% xlabel ('Diameter')
% ylabel ('Fq')
% plot (diam,pht,'r')
% xlabel ('Diameter')
% ylabel ('pht')
% hold off
igo = input('Continue?: ');
end

disp (diam)
disp (fq)
disp (pht)

xlswrite('filename.xlsx',diam,'B1:CV1');
xlswrite('filename.xlsx',fq,'B2:CV2');
xlswrite('filename.xlsx',pht,'B3:CV3');
```

Appendix 3A

OPERATION PROCEDURES

1. The tilting beam is stored horizontally. It should be positioned at the required angle before start up. It should be returned to the horizontal position after shut down. Ensure that the flexible pipes (at the inlet and outlet of test section) are not snagged when moving the beam. The safety pin should be in place at all position and at all times other than when it is being moved.
2. Visual verification of normal electrical conditions and the test rig.
3. Start-up procedure for rig (referring to Figure 3.1):
 - a. Check silicone and water tank levels. Make sure both hold sufficient liquids.
 - b. Make sure all the valves for both pumps (Silicone and water) are open.
 - c. Make sure inlet valves (V1 and V2) for both liquids are open at all time before starting the pump.
 - d. Return valves (V3 and V4) for both liquids MUST always be open before start.
 - e. Rotameter valves (V5 and V6) for both liquids MUST always be closed before start.
 - f. Switch on the water and silicone pumps.
 - g. Close both water and silicone separator outlet valves (V7 and V8).
 - h. Adjust rotameter valves (V5 or V6) opening to get desired flow.
 - i. Higher liquids flow can be achieved by manipulating the return Valves (V3 and V4).
4. Shut down procedure for the rig:
 - a) Open fully the return valves (V3 and V4) for both liquids.
 - b) Close completely both liquids rotameter valves (V5 and V6).
 - c) Switch off the pumps.
5. Emergency shutdown procedure:
 - a) Press emergency stop button (e-stop) located on the right wall, next to the rotameters.

Appendix 7A

Interfacial tension measurement – Drop weight method

Interfacial tension were measured by mean of drop weight method as proposed in the Practical Physical Chemistry (James, 1967). Figure 7A.1 show the experimental set up for the interfacial tension measurement. The syringe was completely filled with heavier liquid (water), and then clamped the syringe so that the needle immersed in A ml kerosene (in 250 ml beaker). Initial weight of the apparatus was taken. The drops of the water are formed at a dropping tip of a ground cylindrical needle with sharp edge which dips into the lighter liquid (kerosene) contained in the weighing beaker shown in Figure 7A.1. With extreme care, a single drop of water is then forced to form and fall in the beaker and repeated for X drops (e.g. 10 drops). The current weight of the beaker is now containing kerosene plus water drops. The difference of apparatus (initial weight and current weight) is the weight of X drops. If the densities and weight of the two liquids are known, the average volume of the drops or single drop can be calculated.

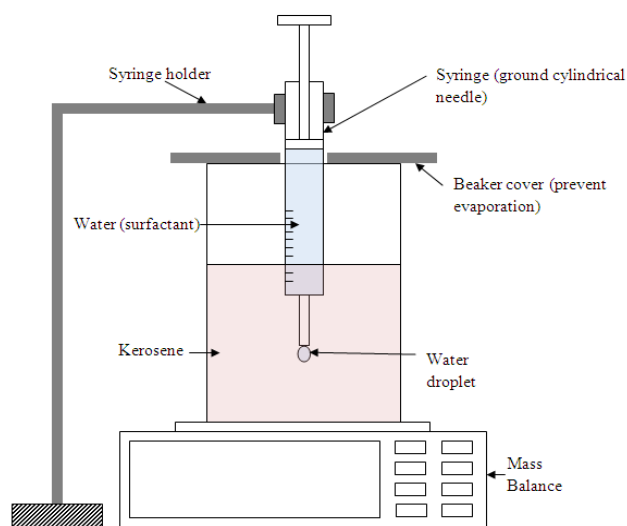


Figure 7A.1: Set up for interfacial tension measurement.

Once an averaged value of the drop volume, v is obtained. Furthermore the ρ_1 and ρ_2 , water and kerosene density respectively, external radius of the needle, r and correction factor, F (Figure 7.1), are known. Therefore the interfacial tension can simply be calculated using equation 7.4.

Interfacial tension measurement of water-kerosene with surfactant added was performed. The experimental results then be compared with Antonoff's rule (eq. 7.5) to make sure the result obtained is reasonable and acceptable. Antonoff's rule says that the interfacial tension between two liquids is approximately equal to the difference between the surface tensions of the two liquids.